NUCLEAR MAGNETIC RESONANCE STUDIES ON PHOSPHOLIPID MEMBRANES USING PARAMAGNETIC IONS

Z-E.M. MIRGHANI, B.Sc.

A DISSERTATION SUBMITTED TO THE COUNCIL FOR NATIONAL ACADEMIC AWARDS FOR THE DEGREE OF DOCTOR OF PHILOSOPHY

SCIENCE DEPARTMENT,
THE POLYTECHNIC OF WALES.

NOVEMBER, 1982.

DECLARATION

This dissertation has not been nor is being currently submitted for the award of any other degree or similar qualification.

Z.E.M. MIRGHANI

Z-E.M. MIRGHANI

TABLE OF CONTENTS

ACKNOWLEDGEMENT

I wish to thank my Director of Studies, Dr. G.R.A. Hunt for his helpful guidance and encouragemnent during the course of this investigation.

My thanks are also owing to Mr. J. McBride of the Computer Centre and Mr. M. Coundley of the Media Resources Unit, The Polytechnic of Wales. The support of all members of Staff of the Science Department is gratefully acknowledged.

Finally, my thanks go to Mrs. Stephanie Jones for the excellent typing of the manuscript.

LIST OF TABLES

LIST OF FIGURES

NUCLEAR MAGNETIC RESONANCE STUDIES ON PHOSPHOLIPID MEMBRANES USING PARAMAGNETIC IONS

Z-E. M. MIRGHANI

ABSTRACT

The aim of the following work was to develop the application of an nmr method, using lanthanide ions as probes, to the study of phospholipid vesicular membranes and their interactions with membrane active compounds.

Chapter I gives a general introduction to the field of biological and model membranes, nmr methods and the use of lanthanide ions. Chapter II illustrates and discusses the ^{1}H, ^{31}P and ^{13}C-nmr of small phospholipid vesicular membranes and the effect of interactions with lanthanide ions. Chapter III shows how ^{1}H-nmr and ^{31}P-nmr can be used to monitor ionophore mediated transport of lanthanide ions across sonicated vesicular membranes. The metal ion-ionophore stoichiometries and the activation energies of transport were measured. The transport of the charged ion-ionophore complexes into the vesicles was found to be accompanied by an efflux of protons. These observations are discussed in terms of a carrier mechanism.

Chapter IV describes and discusses experiments to investigate the result of introducing into phosphatidylcholine vesicles physiological concentrations of lipids known to stabilise non-bilayer phases. Rates of transbilayer transport, lipid exchange and vesicle-vesicle fusion and the effects of Ca^{++} on these were measured. The effect of temperature on liposomes composed of phospholipid extracted from *Micrococcus Cryophilus* and of lipid peroxidation were also examined in relation to changes in lipid organisation.

Chapter V extends the above methods to the study of the mechanism of action of calcium antagonist drugs. At low concentrations the antagonists were found to inhibit ionophore mediated transport of lanthanide ions, but at higher concentrations promotion occurred. A mechanism is proposed in terms of a membrane surface activity of these drugs.

The results show that in general the aim of the project has been justified in that a successful application of the lanthanide-ion-nmr method has been made and useful conclusions reached in each of the areas studied.

CHAPTER 1

GENERAL INTRODUCTION

SECTION 1 Structure and Organisation of Membranes

1.1 Composition of biological membranes.

1.2 Membrane Lipids.

- 1.2.1 Structure.
- 1.2.2 Phase transition.
- 1.2.3 Lipid polymorphism.

1.3 Membrane Proteins.

1.4 Structural Organisation of Membranes.

- 1.4.1 Davson-Danielli - Robertson model.
- 1.4.2 The Fluid mosaic model.
- 1.4.3 Shortcomings of these models.

1.5 Model Membranes. Why use models?

- 1.5.1 Liposomes.
- 1.5.2 Black Lipid membranes (BLM).
- 1.5.3 Vesicles.

GENERAL INTRODUCTION

SECTION 1 Structure and Organisation of Membranes

1.1 Composition of biological membranes:-

Overton in (1899) predicted a fatty barrier surrounding the protoplasm and suggested that Lecithin and Cholesterol may be involved [1]. The presence of proteins associated with membrane lipids was speculated on the basis of surface tension measurements, and on the spontaneous association of water soluble proteins with monolayers of lipid spread at an air-water interface [2]. It is now well established that all animal cell membranes consist mainly of an association of proteins and lipids (including cholesterol) - and a small amount of carbohydrates. The protein: lipid ratio varies from 80% by weight in "metabolicaly active membranes" such as the inner mitochondrial membranes to 20% by weight in the myelin where the main function of lipid is insulating the neurons from external pertubations [3]. The protein : lipid ratios of various membranes are shown in (Fig.1.1).

Fig. 1.1

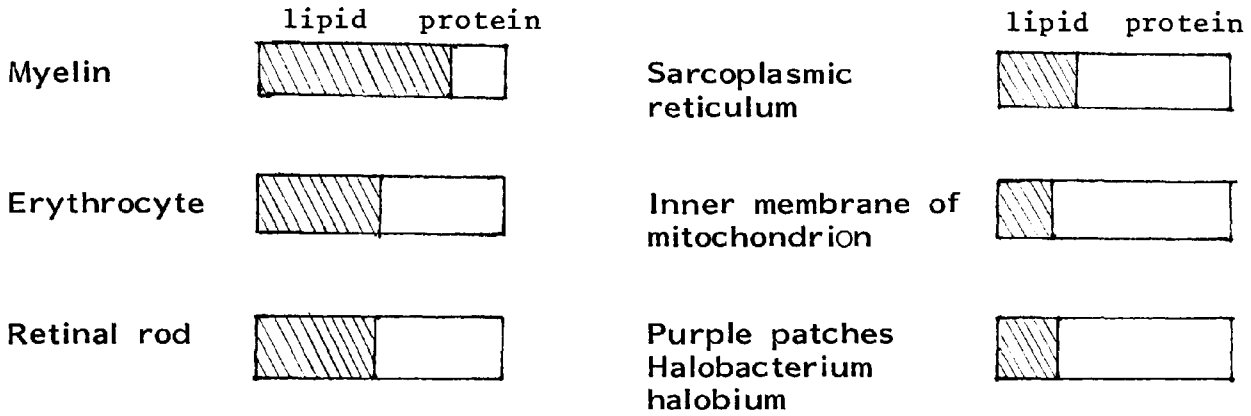

1.2 Membrane Lipids

1.2.1 Structure

Membrane lipids can be separated from non-lipid material by extraction with a mixture of chloroform-methanol and water. The lipids can then be separated into their various classes by chromatographic procedures. Membrane phospholipids are polar, also referred to as amphipathic meaning that they contain both a hydrophobic tail and a hydrophilic headgroup within the same molecule (Fig.I.2). The hydrophilic and hydrophobic regions can be bridged by a glycerol moiety, by a sphinganine derivitive or homologue or, finally, within a sterol molecule. The most abundant in the plasma membranes are the phospholipids and these contain two fatty acid chains esterified to the glycerol backbone in position 1 and position 2; the α and β positions respectively (Fig.I.2). The fatty acid chains have exclusively an even number of carbon atoms and they vary in length (between 12 and 24 carbon atoms); while R_1 is generally saturated, R_2 (depending on its length) is generally unsaturated. A single phospholipid isolated from a homogeneous source may contain variety of fatty acids, varying in both chain length and degree of unsaturation. This is illustrated by the gas-liquid Chromatographic analysis of egg yolk phosphatidylcholine (TableI.1).

Chain	% (w/w of total fatty acid)	Chain	% (w/w of total fatty acid)
16:0	26.2	20:2	2.8
16:1	2.0	20:4	5.4
18:0	15.1	20:5	2.8
18:1	31.9	22:5	2.8
18:2	12.2	22:6	4.4
18:4	2.8		

Fig. I.2

STRUCTURE OF GLYCEROL AND SPHINGOLIPIDS

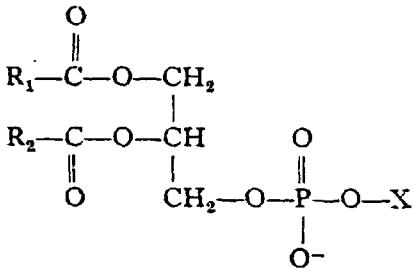

general structure of the
glycerol phospholipids

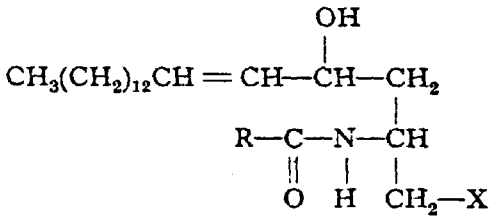

sphingolipids

X = —H ceremide

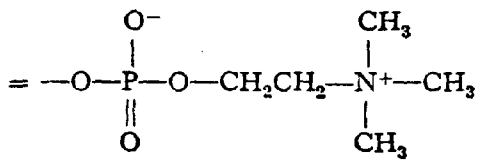

= —O—P(O⁻)(=O)—O—CH₂CH₂—N⁺(CH₃)₂—CH₃ sphingomyelin

= simple sugar of polysaccharide which may be N-acetylated — cerebroside

= polysaccharide containing N-acetylneuraminic acid (NANA, i.e. acetylated sialic acid) — ganglioside

The phosphoester headgroup of phospholipid is hydrophilic and varies in shape, size and it could be charged or neutral at physiological pH (Fig.I.3).

Fig. I.3

			net charge at neutral pH
X =	-H	phosphatidic acid	negative
=	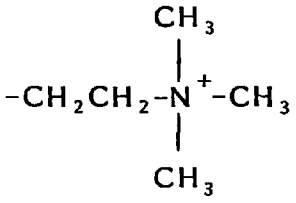	phosphatidyl choline (PC) (lecithin)	neutral
=	$-CH_2CH_2-N^+H_3$	phosphatidyl ethanolamine (PE)	neutral
=	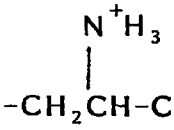	phosphatidyl serine (PS)	negative
=	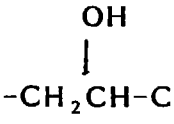	phosphatidyl glycerol (PG)	negative
cardiolipin is diphosphatidyl glycerol, and has phosphatidic acid esterified at the 1- and the 3- hydroxyl groups of glycerol			negative

The importance of the headgroup composition is seen in the variation of phospholipid headgroup composition in different systems and in specific lipid requirement of some membrane proteins.[4][5]

1.2.2 Phase transition (Tc):

This property of membrane lipids is not investigated in this study therefore it is mentioned only briefly.

Pure phospholipids have a characteristic melting point (Tc) at which the acyl chains show a free flowing phase called the liquid crystalline phase[6]. Using differential scanning calorimetry[6] and nuclear magnetic resonance[7] Chapman and coworkers have shown that in the liquid crystalline phase the lipid molecules show translational and rotational movements. The phase transition temperature of pure and mixed lipids was shown to depend upon several factors and some of these are listed below:

(a) The sharp Tc of pure lipids depend upon the length of the hydrocarbon chain, its degree of unsaturation, and the presence of cis or trans "kinks" in the chain .

(b) When different classes of lipids are mixed a considerable difference in the phase transition range occurs, and phase separation may take place

(c) Impurities in lipids, such as cholesterol, broadens the temperature range over which transition takes place .

(d) The size and charge of the lipid head group affect the packing of the lipid chains and consequently alters Tc .

(e) Electrostatic binding of proteins to phospholipids shifts the temperature of the gel-liquid transition of the lipid .

(f) The interaction of divalent cations with polar headgroups of the lipid raises the gel to liquid crystalline temperature .

Biological membranes contain a mixture of lipids (see above) such that a certain degree of fluidity is achieved, and this latter property was shown to influence a variety of physiologically important functions of biological membranes[8]. For comprehensive reviews on the thermal phase behaviour of lipids and its effects on the functions of membrane lipids and proteins (See Refs. 9,10).

1.2.3 Lipid polymorphism:

One property common to all lipids is the segregation of hydrophilic and hydrophobic moieties into distinct regions thus adopting a low energy state to satisfy thermodynamic requirements. In contrast, the polymorphic phase adopted by a particular lipid depends on the structure of that lipid[11] as well as other external parameters such as ionic strength, pH and. Using X-ray crystallography Luzzati et al.[12][13] observed a large number of phases in lipid-water systems, and classified the phases of lipids as a function of concentration and temperature. They found that phospholipids, at a given concentration, possess an order-disorder pattern depending on whether the temperature is lowered or raised respectively. The relative bulkiness of the hydrophilic and hydrophobic moieties was found to be the most important factor determining the adoption of a certain phase -; bulky hydrophilic group promote conformations with large surface-volume ratios, and vice versa. The nature of charge of the headgroup moiety the length of the acyl chain as well as their degree of unsaturation influences the range of existence of each phase.

Of particular interest in this study are the lamellar, the hexagonal (H_{II}) and the micellar phases - and these are shown in (Fig.1.4). The lamellar phase is adopted by lipids with similar headgroup size to their acyl chains

Fig. I.4

POLYMORPHIC PHASE OF PHOSPHOLIPIDS

AND ^{31}P-NMR LINE-SHAPES

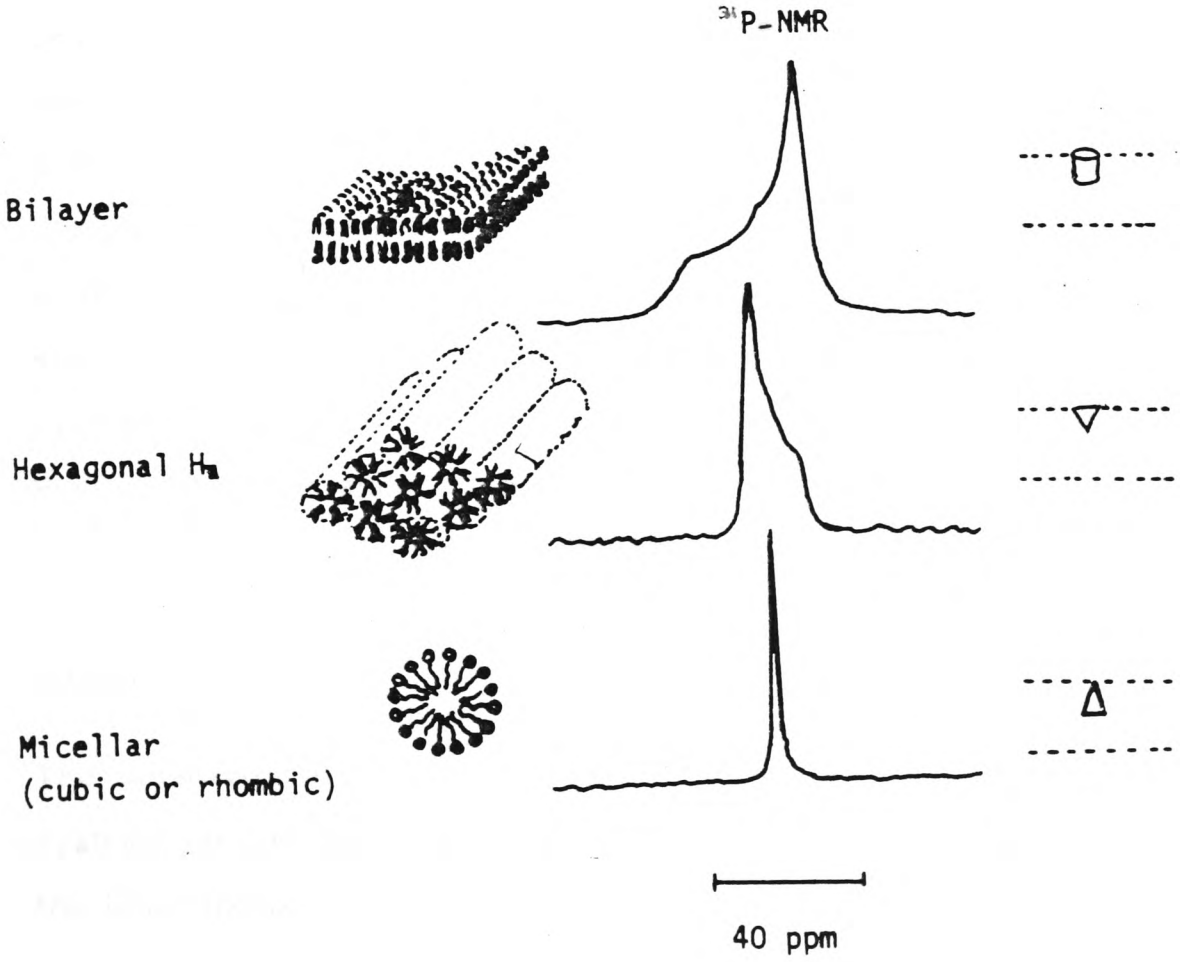

(i.e. cylindrical e.g PC) and the hexagonal phase is preferred by lipids with small headgroup size compared with their acyl chains (i.e. cone shaped e.g. unsaturated PE), and the micellar phase is adopted by lipids with bulky headgroup with reference to their acyl chains (i.e. inverted cone shaped compared to PE e.g. lysolecithin and detergents).

Lipid polymorphism was detected using DSC and X-ray diffraction by Harlos et al.[14], using high magnification electron microscopy by Tinker et al.[15] and Saha et al.[16] and using ^{31}P-nmr and freeze-fracture techniques by De-Kruijff et al.[17], Cullis et al.[11] and Verkleij et al.[18]. The latter techniques namely, freeze fracture and ^{31}P-nmr are being used extensively at present to study the different phases adopted by natural as well as synthetic lipids[19]. Freeze fracture evidence of the H_{II} phase have shown stacked parallel cylinders[20], and, the measured size and periodicity of the cylinders have given information about the water-filled hydrophil ic channel[20]. Furthermore, the appearance of particles and pits in the freeze fracture micrographs of lipids adopting the H_{II} phase have been interpreted as inverted micelles occurring within the bilayer matrix, or between bilayers of adjacent bilayer membranes[21][17].

The sensitivity of ^{31}P nmr technique to detect polymorphic phases of model systems (of radius >2000 Å) is due to the large chemical shift anisotropy of the lipid phosphrous $\Delta\sigma_{CSA}$ = -40 ppm which is only partially averaged out by the rapid rotation of the lipid moleculesabout their long axis and the lateral diffusion in the plane of the bilayer[22]. In the presence of broad band proton decoupling the ^{31}P-nmr spectrum of hand shaken liposomes in the liquid crystalline bilayer phase show a broad spectrum with a low field shoulder and a high field peak separated by $\sigma \frac{EFF}{CSA}$ = -40 ppm (Fig. 1.4)

In contrast, the hexagonal phase spectrum shows a low field peak and a highfield shoulder and a reduction in the chemical shift anisotropy of about 20 ppm due to the fast lateral diffusion of the lipid molecules around the small (20Å in diameter) aqueous Channel (Fig. I.4)

These ^{31}P-nmr properties and freeze fracture techniques were used by De-Kruijff and Cullis to show the presence of these phases in natural and synthetic lipids. Further discussion of non-bilayer phase effects which have particular relevance to the work in this thesis will be given in Chapter IV.

1.3 Membrane Proteins

Membrane proteins are divided into extrinsic (peripheral) and intrinsic (integral);- and in both the genetic sequence of amino acids determine the degree of hydrophobicity or hydrophilicity respectively [23]. The disposition of both types of proteins in the membrane must follow strict thermodynamic rules such that the whole system is at free energy minimum. Peripheral proteins require only mild treatment such as increasing the ionic strength of the medium to dissociate, free of lipids, from the membrane; and in the dissociated state they are relatively soluble in neutral aqueous buffers [3]. Integral proteins require more "drastic" treatment such as detergents or bile acids to dissociate from the membrane, and usually are associated with membrane lipids; and in the dissociated state these proteins are soluble in organic solvents [3]. The peripheral water soluble proteins show appreciable amount of α helical conformation while integral proteins are mainly globular in structure [3].

The disposition of membrane proteins with respect to the lipid bilayer, and the phenomenon of lipid-protein interactions have given motive to various research workers to study the mechanisms of the various processes carried out by these membrane constituents in model as well as in natural systems [24]. For these subjects see Refs. [25][26][27].

1.4 Structural Organisation of Membranes

The structure and topography of cellular membranes pose a fundamental unsolved problem in membrane biology [3]. To this end, many membrane models have been proposed, and in some cases improvements to the above models have been suggested. (See sections 1.4.1 and 1.4.2).
Some of these models were favoured by membrane biologists and biochemists, and were used to explain vital membrane processes [28]. However, the concept of structural organisation of lipids and proteins in cellular membranes awaits further research.

The following membrane models were cited to provide a general overview of the current understanding of membrane structure.

1.4.1 Davson-Danielli - Robertson model

Gorter and Grendel (in 1925) reported that lipid extracted from erythrocyte membranes spreads as a monolayer at an air-water interface (Fig.1.5). They calculated the surface area of the acetone extracted lipid as monolayer, and the surface area of the red cell in dried film preparation. Although the erythrocyte lipids were not completely extracted and the surface area of the erythrocyte was underestimated they obtained the correct ratio of 2:1 because the two errors cancelled each other [29]. They concluded that the erythrocyte membrane contains a membrane of lipid bilayer in which the hydrocarbon chains occupy the centre of the bilayer and the headgroup face outwards (Fig.1.5).

FIG. 1.5

Monolayer at an air/water interface

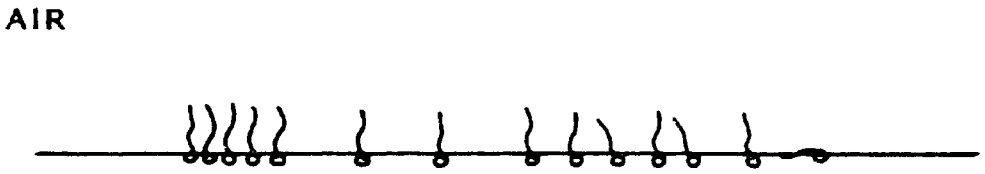

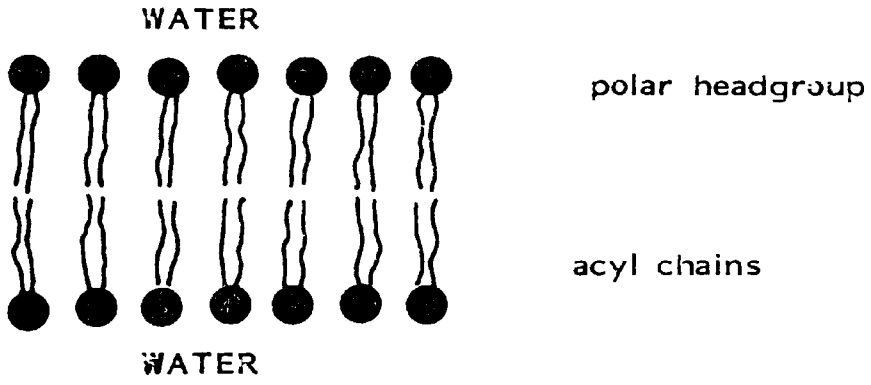

LIPID BILAYER

Apparently independantly, Danielli and Davson (1935) observed an anomalously low surface tension of biological membranes compared with lipid model systems and proposed a protein-lipid-protein sandwich model to explain their results. Evidence for this model was shown 30 years later with the discovery of the electron microscope which shows a typical three layered structure [1]. Based on the observations of Danielli and Davson, Robertson in the 1950's - 60's studied the myelin membrane and proposed his unit membrane model (Fig. 1.6) in which proteins are associated with the hydrophilic headgroups on both sides of the bilayer. He also proposed that the proteins coating the external surfaces of the phospholipids bilayer are in the β- structure and not globular; and therefore extensive hydrophobic interactions between protein and lipid are excluded (See 1.4.2).

1.4.2. The "fluid mosaic" model

The fluid mosaic model (Singer 1972) [23] (Fig. 1.7) suggests that integral globular proteins are amphipathic (c.f. lipid molecule) and are embedded to varying degrees into a lipid bilayer. This structural asymmetry allows the hydrophobic amino acids to interact with the lipid acyl chains, while the hydrophilic residues interact electrostatically with the polar headgroups on both sides of the bilayer. Peripheral proteins on the other hand seek the hydrophilic headgroups of the lipid, and do not submerge in the bilayer core; a thermodynamically forbidden process.

Further consideration of the "fluid mosaic" model reveals that the whole membrane is in a fluid state permitting lateral and rotational diffusion of membrane lipids

Fig. 1.6

DANIELLI-DAVIDSON MODEL

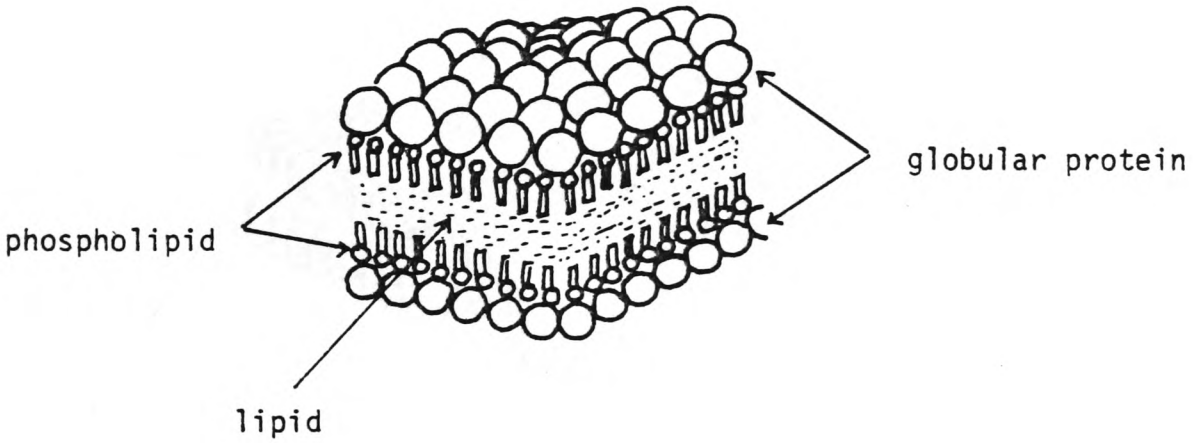

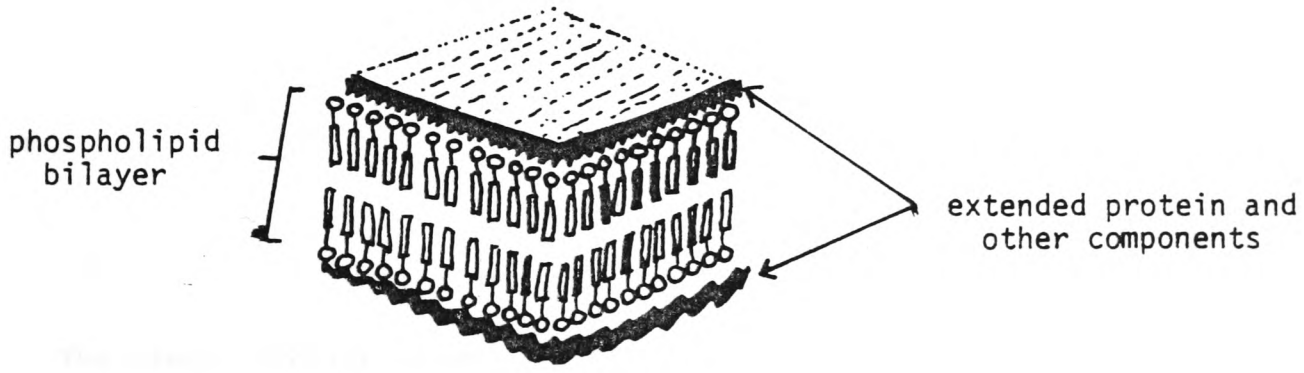

UNIT MEMBRANE MODEL OF ROBERTSON

Fig. 1.7

FLUID MOSAIC MODEL

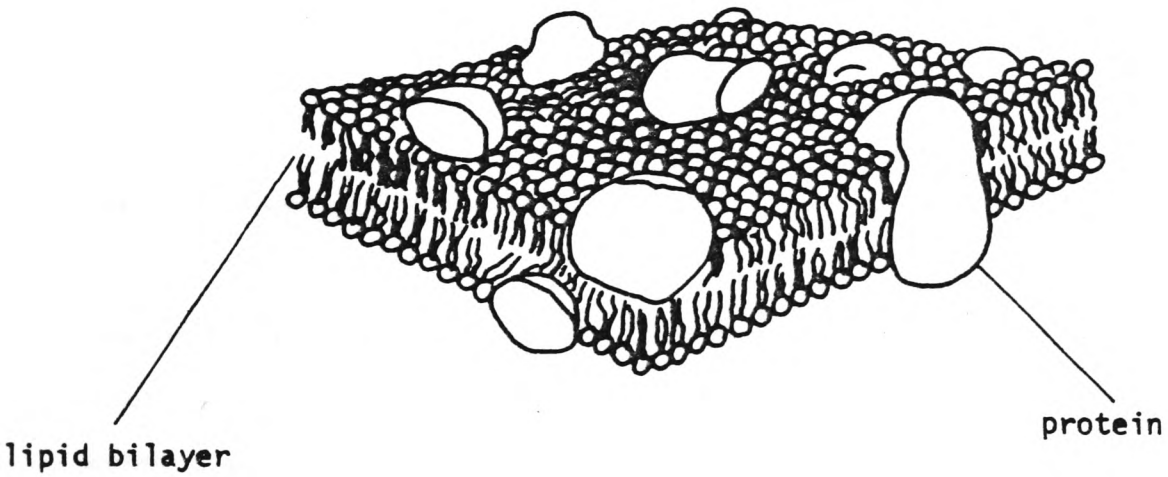

The Singer-Nicolson model for membrane structure. Proteins are predominantly globular and amphipathic, with their hydrophilic end protruding from the membrane and their hydrophobic ends embedded in the bilayer lipids. Proteins are embedded on one or the other side of the bilayer, others pass entirely through the bilayer. Some of the latter presumably contain transport pores.

and to a lesser extent membrane proteins, with the exception of lipids bound to proteins - the so called annulus lipid.

Probably the best evidence for this model came from freeze fracture studies which reveals the interior hydrophobic face of the membrane. Examination of the freeze fracture replica show particles attributed to integral proteins crossing the mid-plane of the membrane. Such proteins were thought to contain hydrophilic channels thus facilitating the transport of water soluble substances. Further evidence of this model using dsc, esr, and immunofluorescence were given in two published papers by Singer (Refs.[3][23]).

1.4.3 Shortcomings of these models

The unit membrane model ceased to function as a viable model when certain inconsistancies became apparent. Firstly, studies of other membranes than the mylein - particularly those containing high protein content such as the mitochondrial membranes show that there is insufficient lipid to form a continuous bilayer over the entire membrane[3]. Secondly, the unit membrane suggests that: only hydrophilic interactions between membrane proteins and lipid headgroups were present and hydrophobic interactions were excluded. The use of "drastic" solubilization methods to extract hydrophobic membrane proteins free of lipids is incompatible with such a suggestion.

The shortcomings of the "fluid mosiac" model are revealed when important membrane processes such as transbilayer transport, flipflop and membrane fusion are discussed. Within the framework of the "fluid mosiac" model a fraction of immobilized (annulus) lipid is supposed to be associated with

membrane proteins. The annulus lipid affects the microviscosity of the adjacent protein, or may affect certain conformational changes vital for the protein function. Although evidence of immobilized lipid was shown by esr studies, this was later reviewed because nmr techniques have shown that the "annulus lipid" is in rapid exchange with "bulk" phase lipid[30] and the esr data were argued on the basis of the 10^5 timescale difference between nmr and esr. The "mosaic" model proposed that certain lipids are required for the function of membrane proteins. But this was also disputed because some proteins e.g. Na^+/K^+ ATPase were shown to function when reconstituted in various types of lipids. However, the possibility of proteins requiring a certain degree of microviscosity for their function is not totally rejected.

1.5 Model membranes. Why use models?

1.5.1 Liposomes:

Shortly after Robertson proposed his universal unit membrane theory (1960s) Bangham reported that phospholipids of cellular origin spontaneously re-form, in the presence of water, into closed membrane systems. These so called liposomes can be prepared from a variety of lipids and lipid mixtures, with phospholipids being the most commonly used. The lipid is dissolved in an organic solvent which is subsequently evaporated thus leaving a dry film on the surface of the preparation flask. An aqueous phase is then added and the solution is shaken mechanically or by hand to disperse the larger lipid aggregates. The milky solution resulting contains liposomes of various sizes and shapes i.e. spherical or tubular, 0.1 to 5μm in diameter. However, regardless of their shapes and sizes these liposomes are organised as closed concentric "membranes" with aqueous compartments separating each "membrane" from its neighbour. The spacing between the membranes is determined by a balance of the Van der waals forces of attraction and the electrostatic and hydration repulsion forces between adjacent membranes. These can be varied by including charged molecules [31].

Since their discovery, liposomes have been extensively used in variety of practical fields of biochemistry and medicine. Their use in transport and fusion studies have shed light on the possible mechanisms operating in these processes. Their biodegradability offered a new type of carrier for many therapeutic substances [32]. Liposomes are used in enzyme replacement therapy, delivery of anti-cancer drugs which are highly toxic to normal tissue [32], chelation therapy using e.g. desferrioxamine [33], and as carriers for hormones

such as insulin for diabetics, cortisol esters for arthritic rabbits [32]. The above shows the potential of this model system, and the research in each of the above topics is at present carried out by many laboratories.

1.5.2 Black lipid Membrane (BLM)

Black lipid membranes are formed by dipping a metal, polyethylene, or hair loop of 1-2 mm diameter into the lipid solution, and then transferring it through air into a beaker containing 0.1 M Saline at 30-35°C. A more satisfactory alternative is to leave the loop under the saline solution and apply to it the lipid solution with a fine brush (approximately trimmed to avoid transferring an excess of lipid solution). For the study of electrical properties, the membrane is spread by brush on a 1.0 mm diameter hole in the side of a small polyethylene cup (5 ml Beckman PH cup) immersed in a glass petri dish. A heated needle held in a drill chuck is used to bore a polished hole after thinning the well of the pH - Cup to 0.2 mm. Both the cup and the dish are usually filled with histidine buffered 0.1 M NaCl at pH 7, and Calomel electrodes with small polyethylene tips are inserted into the cup and the dish.
The cup is held in place by a simple spring clip running to the edge of the petri dish. D.C. pulses or a.c. are applied through known resistors, and the potential across the membrane is recorded through a cathode follower with an oscilloscope. Substances to be tested for their effects on the membrane are injected into the saline on one or both sides of the membrane. The polyethylene cup must be thoroughly washed and rinsed in distilled water to avoid a conductance path over the rim. Temperature is maintained by a heating lamp, and evaporation is minimized by a cover over the petri dish.

The BLM was used by Neher etal [34] to demonstrate the ionic selectivity of the Gramicidin A channels. Negatively charged analogous of Gramicidin A were found to create an electrostatic effect of fixed negative charge localized near the mouth of the channel [35]. The permeability characteristics of BLMs to various anions and cations have been studied by many workers [36]. The research into functionally modified BLMs i.e. containing one of the various ATPases to demonstrate the induction of a pump mechanism was not very successful [37]. But a considerable amount of work has been devoted to characterize processes in which translocation of a solute or its acumlation accompanied by expenditure of energy [37].

1.5.3 Vesicles:

The classical procedure of sonicating a dispersion of phospholipids to form optically clear suspensions was initially introduced by Saunders [38] and Abramson and co-workers [39]. Subsequently, it was demonstrated by Papahadjopoulos et al. [40][41] that the structures formed by sonication were microvesicles of about 500 Å that enclosed an aqueous space. The preparation was rigorously characterised by Huang [42] who introduced gel filt ration chromatography to separate the residual larger multilamellar vesicles from the smaller unilamellar vesicles and who studied in detail their hydrodynamic properties. To briefly recapitulate, the usual multilamellar liposomes (see above) are subsequently sonicated either with a bath type sonicator[43] or a probe sonicator[39] under an inert atmosphere (usually nitrogen or argon). It is essential that the sonication to be performed at a temperature above the Tc of the highest melting lipid (if a mixture of lipid is used) because sonication below Tc was found to produce defects within the bilayer[44]. These allow rapid permeation of ions and when raised above Tc it permits

vesicle-vesicle fusion.

Due to the small radius of curvature in these vesicles there is higher percentage of phospholipid molecules in the outer monolayer (approximately 60%) compared to the inner monolayer. In mixtures of lipids this can lead to an asymmetric distribution of the components in the two bilayers. Thus when preparing small sonicated vesicles for studies relating lipid composition to some functional properties, the possibility for asymmetric distributions must be taken into account. The most important attribute of sonicated vesicles is the fact that they form a small homogeneous population of vesicles that can be separated from contaminating liposomes by simple techniques [45].

Sonicated vesicles have been extensively used in research and examples of such studies are given throughout this report. Their uses in biochemistry and medicine are covered by two recent reviews by Szoka and Papahadjopoulos [33] and Rhyman and Tyrrell [32].

Why use models?

The main motivation for working with model membranes is to obviate some of the uncertainties and difficulties inherent in the use of complex biological membranes. Clearly the basic requirement of a model membrane is the ability to define, and vary if necessary, the chemical composition and also to quantitatively characterise its morphology. It has been recognised for some time that many properties of biological membranes can be interpreted in terms of their physical chemistry and especially the interfacial properties of their constituent lipids. Such systems provide an opportunity to investigate the

characteristics of individual membrane constituents and to relate chemical structure and physical properties to physiological function.

Shortly after Robertson (1960) had postulated his universal unit membrane theory, Bangham reported that purified phospholipids of cellular origin spontaneously re-form, in the presence of water, into closed membrane systems (see above). It was suggested[1] that these liposomes resemble prebiotic membranous structures which first allowed the distinction to be made between inside and outside. For this reason it can be said that the approach of discussing model membranes is chronologically appropriate.

Our present day understanding of the structure and dynamics of natural and biomembranes owes a considerable amount to the development and study of model systems. Concepts which we now commonly accept when we discuss biomembranes such as membrane fluidity, phase transition, lipid and protein movement, trigger processes affected by metal ions or pH, and permeability processes for ions, have all emerged from model membrane studies.

SECTION 2 NMR OF MODEL AND BIOLOGICAL MEMBRANES

SECTION 2 NMR of Model and Biological Membranes

A remarkably short time after the discovery of the nmr phenomenon, studies were being initiated into organic molecules and molecules of biological interest. Indeed, one of the first molecules studied by Hahn (1950) using his spin echo technique was a solid paraffin. The first attempt to obtain motional information about lipids were the broad-line proton studies of Chapman and Salsbury [7] (1966), to be followed by many other studies by Chapman and co-workers.

Nuclear magnetic resonance should be ideally suited for investigating molecular dynamics in membranes, biological tissues, and biochemical model systems. The motional freedom of molecules in such systems may, in principle, be amenable to nmr line width, relaxation times, and self diffusion coefficient measurements. One of the chief features of using nmr for such studies is that the system need not be perturbed in any manner. Another feature is that the motion of various nuclei in the system may be monitored providing information about the motions of different molecules and, in fact, the motion of different parts of the same molecule. The various rotational and translational motions may, in principle, also be differentiated, although in practice it may be difficult to distinguish between them.

High resolution proton nmr spectra can be obtained from small vesicles resulting from sonicated liposomes (see above). There have been two reasons suggested for the appearance of a high resolution spectrum: (a) difference in Brownian tumbling rate for the different particle size (compare vesicles and liposomes), and (b) differences in molecular packing and thus molecular motion in the two types of dispersions. Horwitz et al. [46] Sheetz et al. [47] and Chapman et al. [48]

have conflicting views on relative contributions of the above given reasons to the difference in linewidths of sonicated and unsonicated lipids.

However, using such vesicles and variable temperature ^{1}H-nmr techniques Hunt et al. [49] studied the endothermic phase transitions of DPPC sonicated vesicles. They showed that as the temperature is dropped a progressive broadening of all the signals occurs as the system undergoes a liquid crystalline gel phase transition, and, the mobility of the protons in the bilayer (particularly $-CH_2-$ and $-CH_3$) is reduced. Although a plot of the linewidth of $N^+(CH_3)_3$ protons against temperature shows a sharp upward inflection as the temperature decreases through the transition point, it is evident from (Fig. II.3(b)) that the $N^+(CH_3)_3$ group retains considerable mobility, even when the aliphatic chains are 'frozen' in the gel phase.

Hunt [50] and Degani [51] used dynamic ^{1}H-nmr methods to examine how ionophores affect the transport of ions across membrane vesicles. Using DPPC vesicles and Lanthanide reagents (see later), Hunt found that Pr^{3+} caused a downfield shift of two-thirds of the choline methyl proton resonance intensity. He found that the nigericin - type ionophore A23187, causes the downfield shift of the inner choline signal. The rate of downfield shift and broadening of this signal yielded information about the transport rate. A plot of the rate against the ionophore concentration is shown to give information about the ionophore - metal ion stoichiometry.

Resolution of overlapping signals is a major problem in the application of proton nmr to lipid systems. Although this problem can be solved by using nmr instruments with large magnetic fields (e.g. 600 MHz)[52], studies of other nuclei have generally proved to be more fruitful. ^{13}C-nmr spectra have larger

chemical shifts and narrower lines, and they can be observed from the natural ^{13}C content of lipids if the sensitivity of the nmr spectrometer is enhanced by computer accumulation of repeated spectral scans. The scan time is reduced in practice by simultaneously exciting nuclei over the whole spectral range using a short intense radiofrequency pulse and converting the time dependant information, (Free Induction Decay (FID)) into a frequency dependant spectrum by a Fourier transform operation carried out by computer.

Employing this technique Levine (1972) [53] was able to resolve the acyl chain carbons, 2,3, 14,15 and 16, and the resonances of the glycerol and choline of DPPC sonicated dispersion in D_2O. ^{13}C-nmr has been used to measure the rate of molecular motion in different parts of the acyl chains (i.e. fluidity gradient). Metcalf and coworkers have measured the T_1 relaxation time (which is related to the correlation time of the various parts of the molecule [54] and they found that the rate of molecular motion increases from the carbon atom of the glycerol backbone to the ones at the end of the lipid chain.

Deuterium nmr is ideally suited to the measurement of anisotropic motion of deutrated fatty acyl chains. The deuterium nucleus possesses an electric moment which interacts with the local field gradient. The quadrupole interaction changes the absorption frequency of the deuterium nucleus and depends upon the orientation of the molecule with respect to the applied magnetic field. For a rapid isotropic motion (i.e. with equal possibilities in all directions) of the nucleus, these effects will average out and the ^2H-nmr spectrum will consist of a single line, whereas if the motion is anisotropic then the spectrum will appear as a doublet. This phenomenon was used by Seelig et al.[55] and Oldfield et al.[56] to study the "flexibility" of the headgroup of selectively deutrated lipids. The data obtained (order parameters - S_{MOL}) have been in agreement with two

aspects of the headgroup motion: (1) in the liquid crystalline phase there is rapid rotation about an axis perpendicular to the bilayer surface; (2) the bond torsion angles are neither completely fixed nor completely free to rotate.

Brown et al.[57] and Davies[58] have recently measured ^{2}H-nmr relaxation rates in deuterated DPPC bilayers. Brown et al. used selectively deuterated lipids and measured spin - lattice relaxation rates $1/T_1$ as a function of temperature and deuterated chain-segment position. Davies employed a perdeuterated sample and measured both spin-lattice and spin-spin ($1/T_2$) relaxation rates, as well as various moments of the spectra. The T_1 values of the two studies agree fairly well both in magnitude and dependance on chain position. The $1/T_1$ relaxation rates are found to be approximately constant over the first half of the acyl chains, then decreases rapidly towards the terminal methyl ends.

^{31}P-nmr has been particularly useful in studying unsonicated lipid bilayers and membrane systems of intact cells. De-Kruijff and co-workers[59] examined ^{31}P-nmr spectra of liver microsomes and suggested the presence of non-lamellar type lipids. Other biological membranes such as sarcoplasmic reticulum membranes,[60] the myelin sheath[61] and chloroplast membranes[62] have been studied by ^{31}P-nmr.

Very high field nmr instruments have been developed to detect phosphrous - containing tissue metabolites of whole muscle and to monitor changes in the concentrations of these metabolites with time. The first stage is to assign chemical shifts of metabolites such as inosine monophosphate, fructose - 1-6-diphosphate, inorganic phosphate, creatine phosphate and adenosine triphosphate by running their spectra both individually and in mixtures. A spectrum of intact freshly excised muscle from the hind leg of a rat is then obtained. The signals from this muscle, which are broader than those of the isolated metabolites

could be assigned, and the changes in them monitored as a function of time after excision. Many conclusions may be drawn from such results, for example that creatine kinase maintains the ATP levels constant at the expense of creatine phosphate until the later substance has been used up; demonstrating the ability of the kinase to buffer the muscle ATP concentration.[63]

SECTION 3 Uses of Lanthanide Reagents

3.1 Lanthanides as shift and Relaxation Reagents.

3.2 Lanthanides as Calcium Probes.

SECTION 3 Uses of Lanthanide Reagents

3.1 Lanthanides as shift and Relaxation Reagents

Proton nmr chemical shifts show low sensitivity to changes in chemical and stereochemical environment, and terms such as "methylene, methine envelope" are used frequently in connection with proton nmr of steroids and terpenes.[64] Lanthanide shift reagents (LSR) are used in nmr spectroscopy to reduce the equivalence of nuclei by altering their magnetic environment[65]. LSR function by co-ordinating to suitable donor atoms in the compound under study, thereby expanding their co-ordination shell and forming a new complex in solution as shown in equations (1) and (2):

$$L + S \xrightarrow{K_1} [LS] \quad \ldots\ldots\ldots\ldots (1)$$

$$[LS] + S \xrightarrow{K_2} [LS_2] \quad \ldots\ldots\ldots\ldots (2)$$

Where L and S are the concentrations of the LSR and substrate respectively, and [LS] the concentration of the complex formed in Solution; - the ratio of these species depends on K_1 and K_2 the binding constants. Owing to the magnetic interactions with the metal ion in the complexed substrate [LS], the nmr positions of associated nuclei in the substrate differ from those in the uncomplexed state[65]. Theequilibrium in solution between these species is rapid on the nmr time scale - so that only a single average signal is recorded for each nucleus in the different environment[64].

The lanthanide series is formed by the successive incorporation of electrons in the 4f inner shell. However, the 4f electrons are shielded by the 5s and 5p electrons and thus the chemical properties of elements in the lanthanide series are very similar. On the other hand, the magnetic properties of lanthanide ions vary sensitively with the number of 4f electrons, except the diamagnetic La^{3+} ($4f^{o}$) and Lu^{3+} ($4f^{14}$) ions. Amongst the lanthanide ions, Pr^{3+} ($4f^{2}$), Eu^{3+} ($4f^{6}$) and Yb^{3+}($4f^{13}$) ions, with short electron spin relaxation times ($\tau_s < 10^{-12}$s) induce shifts of nuclear magnetic resonance frequencies of substrates, without appreciable line broadening. On the other hand, Gd^{3+} ($4f^{7}$) and Eu^{2+} ($4f^{7}$) ions, with long electron spin relaxation times ($\tau_s > 10^{-10}$s) enhance nuclear magnetic relaxation rates, without inducing appreciable shifts. The ions Dy^{3+} ($4f^{9}$) and Ho^{3+} ($4f^{10}$), with intermediate electron spin relaxation times, induce shifts and also enhance relaxation rates. Thus, paramagnetic lanthanide ions may be utilized as shift probes and/or relaxation probes, depending on the lengths of electron spin relaxation times. In contrast to transition metal ions, the lanthanides form isomorphous complexes with a given substrate and induce shifts and relaxation rate enhancement of a substrate molecule which may be measured for isomorphous complexes with a variety of lanthanide ions.

The fractional shift (Δ L) of the nuclear magnetic resonance frequency (ν) induced by paramagnetic ions may be expressed as a sum of three terms including the complex formation shift (Δ_{CFS}), the contact shift(Δ_{CS}) and the pseudocontact shift (Δ_{PCS}):

$$\Delta L = \Delta\nu/\nu o = \Delta_{CFS} + \Delta_{CS} + \Delta_{PCS} \quad \ldots\ldots\ldots\ldots\ldots (3)$$

3.1.1 Complex formation shift:

On complex formation with a lanthanide ion, the electron cloud of a substrate molecule is polarized by the positive charge of the lanthanide ion and structural changes in the substrate molecule may also be induced. These changes affect the electronic state of the substrate molecule and thus induce shifts of nuclear magnetic resonance frequencies of nuclei in the substrate molecule. The shifts due to such diamagnetic effects are called complex formation shift (Δ_{CFS}). Accordingly, to obtain the contact shift (Δ_{CS}) and psudocontact shift (Δ_{PCS}) induced by the paramagnetic lanthanide ions, it is required to make corrections for complex formation shifts. Such corrections may be made by the measurement of the shift induced by the complex formation with the diamagnetic La^{3+} or Lu^{3+} ions.

3.1.2 Contact shift:

The hyperfine interactions of the delocalized unpaired electrons on the f atomic orbital of the lanthanide probe with the magnetic moment of the atomic nuclei in the substrate causes shifts of the magnetic nuclear frequencies (contact shift). The expression for the contact shifts is given by the following expression:

$$\Delta c = \Delta\nu/\nu o = (A/h)\langle S_z\rangle \mid (\gamma Bo/2\pi) \quad \ldots\ldots\ldots\ldots\ldots\ldots (4)$$

- where A/h is the hyperfine coupling constant (Hz), $\langle S_z \rangle$ is the thermal average of the component along the field of the electron spin magnetization of

the paramagnetic ion, γ is the magnetogyric ratio of the nucleus, and Bo is the applied magnetic field.

For lanthanide ions of value for $\langle S_z \rangle$ in the ground electronic state is given by:

$$\langle S_z \rangle_J = -\beta J (J + 1) g_J (g_J - 1) Bo \mid 3KT \quad \ldots\ldots\ldots\ldots\ldots\ldots (5)$$

- where K is the Boltzmann constant, T is absolute temperature, β is the Bohr magneton, J is the quantum number for the total angular momentum, and g_J is the Landé factor [66] and is given by:

$$g_J = [3J(J + 1) - L (L + 1) + S (S + 1)] \mid 2J (J + 1) \quad \ldots\ldots\ldots (6)$$

- where L and S are the quantum numbers for the orbital and angular momentum of the electron spin, respectively. Accordingly, the contact shift due to the J manifold of the ground electronic state of the lanthanide ion is given by:

$$\Delta c = -2 (A/h) \beta J (J + 1) g_J (g_J - 1) \mid 3KT\gamma \quad \ldots\ldots\ldots\ldots\ldots\ldots (7)$$

The unpaired electron spin in the atomic s orbital of the observed nucleus is induced through the chemical bond between the nucleus and the lanthanide ion. Therefore hyperfine coupling constants are usually larger for the magnetic nuclei in closer proximity (through the bond) to the lanthanide ion. In fact large contact shifts are observed for the ^{17}O, ^{14}N and ^{31}P nuclei at the co-ordination sites of lanthanide ions and for the ^{13}C nuclei near the co-ordination sites.

For Eu^{3+} ($4f^6$) and Sm ($4f^5$) ions, the excited electronic states are appreciably thermally populated and the contributions of the excited states to the average $< S_z >$ should also be taken into account. In particular for Eu^{3+} ion, the quantum number of the ground electronic state is J = o [$< S_z > = o, \Delta c = o$ for J = o, see equations (5) and (7)] and accordingly contact shifts arise only from the contributions of excited electronic states. The $< S_z >$ values of lanthanide ions, including the contributions of excited states as well as ground state have been treated by Golding and Halton[67].

However, the lanthanide induced contact shifts are proportional to T^{-1} [see equation (7)] which is different from the temperature dependence of lanthanide - induced pseudocontact shifts.

3.1.3 Pseudocontact shift:

The origin of pseudocontact shifts will be discussed here, primarily referring to the Bleaney theory[68]. For lanthanide ions, the spin-orbit interactions are much stronger than for transition metal ions, and the energy levels of the lanthanide ions are determined mainly by the total angular momentum (quantum number J). Since the 4f electrons are partially screened from ligands (see above), the energy differencies between the 2J + 1 sub-levels are not larger than KT at room temperature and thus these sub-levels are appreciably populated even at room temperature. The electronic relaxation times of the sub-levels are extremely short ($\tau_s < 10^{-11}$ s), except for the Gd^{3+} ion (f^7). These are characteristic for lanthanide ions, in contrast to transition metal ions.

The pseudocontact shifts from lanthanide ions are obtained from the local magnetic field induced by the magnetic moment of lanthanide ion. The magnetic moment is derived from the magnetic susceptibility, and the local magnetic field induced by such magnetic moment is averaged over all orientations of the lanthanide complex with respect to the external magnetic field. A Cartesian co-ordinate system may be set up (Fig. I.8) with the origin at the site of lanthanide ion and the x,y and z axes in the direction parallel to the three principle axes of the magnetic susceptibility tensor.

FIG_I·8

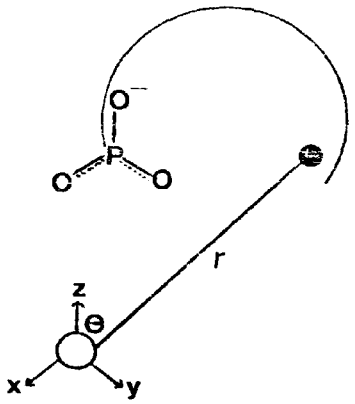

Then for a magnetic nucleus at the site (r, θ, ϕ) (Fig. I.8.), the pseudo-contact shift (Δ_{PCS}) induced by the lanthanide ion is given by:

$$\Delta_{PCS} = \Delta\nu/\nu_0 = (\chi_{zz} - \bar{\chi})\,(3\cos^2\theta - 1)/2r^3 + (\chi_{zz} - \chi_{yy})\,(\sin^2\theta \cos 2\phi)/2r^3 \quad \ldots\ldots (8)$$

- where χ_{xx}, χ_{yy} and χ_{zz} are the principle values of magnetic susceptibility tensor and $\bar{\chi} = (\chi_{xx} + \chi_{yy} + \chi_{zz})/3$. Thus, pseudocontact shifts arise

from the anisotropy of the magnetic susceptibility tensor of the lanthanide ion as bound to the ligand molecule. If the magnetic susceptibility tensor has axial symmetry, the pseudocontact shift is given by:

$$\Delta_{PCS} = \Delta\nu / \nu o = (\chi_{xx} - \bar{\chi}) (3\cos^2 \theta - 1) / 2r^3 \quad \ldots\ldots\ldots (9)$$

and becomes equal, in form, with the McConnell - Robertson equation[67] for the pseudocontact shift induced by transition metal ions. However, in the case of transition metal ions, pseudocontact shifts are due to the anisotropy of the g tensor.

3.1.4 Relaxation rate enhancement:

For the lanthanide complexes of small ligand molecules, the rotational correlation time (τ_R) is of the order 10^{-10} - 10^{-11} s, and the life-time (τ_M) will not be shorter than 10^{-8} s. For Gd^{3+} and Eu^{2+} ions the electron spin relaxation time (τ_s) is much larger than 10^{-10} s and accordingly the correlation time (τ_c) for the dipole-dipole interactions is primarily determined by τ_R. However, for the lanthanide shift probes (Pr^{3+}, Eu^{3+} and Yb^{3+}), τ_s is as short as 10^{-13} s and thus τ_c is primarily determined by τ_s. Moreover, the relaxation rates induced by "shift probes" are two or three orders of magnitude lower than those induced by "relaxation probes" (Gd^{3+} and Eu^{2+}). Thus, these shift probes induce contact and pseudocontact shifts without appreciable effect on relaxation rates. The lanthanide ions with intermediate τ_s values (for example Dy^{3+} and Ho^{3+} ions) induce shifts and enhance relaxation rates[69].

For the fast exchange case, the observed transverse relaxation rate of a ligand nucleus is given as,

$$\frac{1}{T_2}_{obs} = (1 - f)\ (1/T_{2_F}) + f\ (1/T_{2_M}) +$$

$$f\ (1 - f)^2\ \tau_M\ (2\pi\Delta\nu_M)^2 \quad \ldots\ldots\ldots\ldots\ldots\ldots (10)$$

- where f is the fraction of ligand molecules bound to lanthanide ions, T_{2F} is the transverse relaxation time of free ligand, and $\Delta\nu_M$ is the chemical shift difference between the bound ligand and free ligand molecules. Thus, the line widths of ligand resonances are affected by the third term in equation (10), and may not be directly used for structure studies, except for the Gd^{3+} complexes. However, there have been a number of examples where line width changes are readily explained as due to the effect of chemical exchange between the bound and free states of the ligand molecules in solution. But it must be remembered that the longitudinal relaxation rates are not affected by chemical exchange in the fast exchange conditions ($T_M >> \tau_M$).

3.1.5 Lanthanide shift reagents:

Lanthanide shift reagents suitable for nmr spectroscopy should show sufficient solubility in the medium under study and more importantly they must have co-ordinating ability for their substrate. (Fig. 1.9) shows some lanthanide shift reagents based on the β - diketone structure. The introduction of the fluorine atoms overcomes the solubility problem therefore leading to superior LSRs. One such complex, Fod (Fig.1.9), has improved solubility (of the order 400 mg/ml when complexed to the substrate) - and a

Fig. 1.9

LANTHANIDE SHIFT REAGENTS

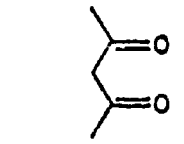

Acetylacetone (acac)

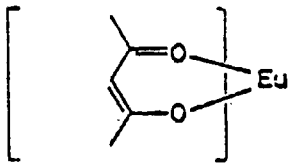

Tris(acetylacetonato) europium(III) [Eu(acac)$_3$]

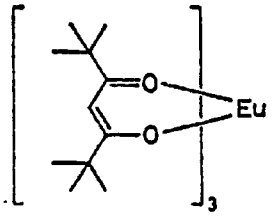

Tris(dipivaloylmethanato europium(III) [Eu(dpm)$_3$]

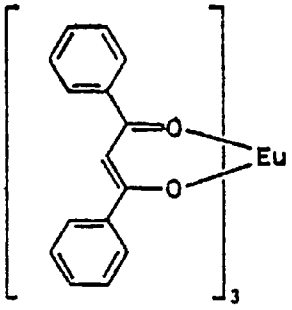

Tris(dibenzoylmethanato) europium(III) [Eu(dbm)$_3$]

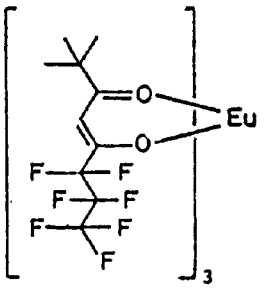

Tris-(1,1,1,2,2,3,3-heptafluoro -7,7-dimenthyloctane-4,6-dionato)europium(III) [Eu(fod)$_3$]

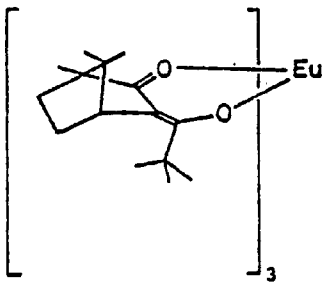

Tris-[3-(t-butylhydroxymethylene) -(+)-camphorato]europium(III)

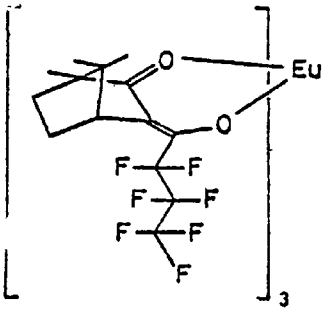

Tris-[3-(heptafluoro-n-propyl-hydroxymethylene)-(+)-camphorato]europium(III)

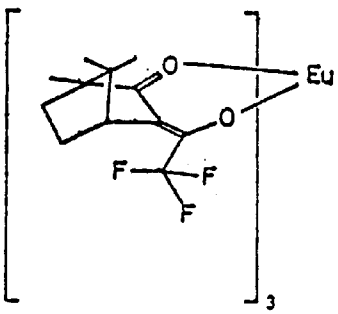

Tris-[3-(trifluoromethylhydroxy-methylene)-(+)-camphorato] europium(III)

more acidic metal ion owing to the electron withdrawing power of the fluorines. This fact attracted the attention of Hunt [50] who demonstrated that the sodium derivitive of Fod could act as an ionophore in sonicated lipid vesicles. Chapter III of this thesis expands on these observations with some comparisons of Nafod and other ionophores used in carrier mediated transport.

3.2 Lanthanides as Calcium Probes

Metal ions exert significant effects on the structural and functional properties of cell membranes[70]. Some of them e.g. the transition metal ions occur in trace quantities whereas others like sodium, potassium, magnesium and calcium are much more abundant[70]. The latter are ions with closed electronic shells and therefore devoid of spectroscopic properties suitable for studying their macromolecular environment. This statement is particularly true for calcium since nmr experiments with its only magnetic isotope, calcium 43, require sophisticated methods due to the low abundance (0.43%) and sensitivity (6.4% of that of an equal number of protons)[71].

The lanthanides are the series of atoms between atomic numbers 58 and 71 in which the 4f electronic shell is progressively filled. Thus the tripositive ions provide us with a remarkable multitude of spectroscopic and magnetic properties. On the other hand the 4f electrons are effectively shielded by the outer 5s and 5p orbitals and as a result complex formation is largely due to electrostatic attraction accompanied by little covalency. The chemical properties of the lanthanides show only a gradual variation along the series which results from the well known ionic radius contraction (See Table I.2). Although the lanthanides seem to be of little biological importance per se, their properties render them as important probes for studying biological systems[70].

The ionic radius of calcium (0.99 Å) is well with the range of the ionic radii of the lanthanides (See Table I.2); and the possibility of isomorphous replacement has been emphasized. The question of charge difference has been shown by Williams,[72] to be of less importance than size in isomorphous replacement.

Table I.2

The lanthanides and some properties of their trivalent ions

Atomic No.	Name	Symbol	f shell of Ln^{3+}	Ionic Radius [Å]
57	Lanthanum	La	$4f^0$	1.061
58	Cerium	Ce	$4f^1$	1.034
59	Praseodymium	Pr	$4f^2$	1.013
60	Xeodymium	Nd	$4f^3$	0.995
61	Promethium	Pm	$4f^4$	
62	Samarium	Sm	$4f^5$	0.964
63	Europium	Eu	$4f^6$	0.950
64	Gadolinium	Gd	$4f^7$	0.938
65	Terbium	Tb	$4f^8$	0.923
66	Dysprosium	Dy	$4f^9$	0.908
67	Holmium	Ho	$4f^{10}$	0.894
68	Erbium	Er	$4f^{11}$	0.881
69	Thulium	Tm	$4f^{12}$	0.869
70	Ytterbium	Yb	$4f^{13}$	0.858
71	Lutetium	Lu	$4f^{14}$	0.848

Further, the above author has shown that lanthanides have the same co-ordination number and the same sensitivity to steric effects as Calcium.

Already several observations have been made as to the effect of lanthanides in biochemical systems. Long and Mount[73] have demonstrated that 0.25 mM Ln^{3+} inhibits calcium binding by 75% in the presence of 100-fold excess of Ca in erythrocyte membranes. Takata et al.[74], Blaustein and Goldman[75] have shown La^{3+} to shift the membrane potential in excitable membranes in a similar fashion to high concentration of Ca^{2+}. Hagiwara and Takahshi[76] have shown La^{3+} inhibits the action potential in skeletal muscle. As with other membrane systems La^{3+} has been used to distinguish between the physiological role of intra and extracellular Ca^{2+} in smooth muscle preparations[77]. This has been of particular interest since smooth muscle does not contain an extensive S.R. to store the intracellular Ca^{2+}[77]. The significance of some of this work was concluded by the recent finding by Hodgson et al.[78] indicating that at least with rat myometrium, La^{3+} is transported across the plasma membrane. The use of lanthanide ions to differentiate between intra and extra cellular calcium is dependant on the lanthanide not being transported across the membrane.

Lanthanides can inhibit Ca^{2+}, Sr^{2+} and Mn^{2+} transport in mitochondria without inhibiting oxidative phosphorylation or K^{+} accumulation[79][80]. Approximately 50% inhibition is obtained at a 3000-fold molar excess Ca^{2+} over employed lanthanides. Al^{3+}, Zn^{2+}, Ba^{2+} and Se^{2+} are ineffective at the concentrations used with the lanthanides. These inhibition studies also indicate more than one site of action for the rare earth inhibition of Ca^{2+} accumulation.

SECTION 4 Ionophores and Mechanisms of transport

4.1 Carrier-type Ionophores.

4.2 Channel/Pore forming Ionophores.

SECTION 4 Ionophores and Mechanisms of transport

The transport of solutes across membranes involves processes other than simple diffusion [29]. Thus many compounds show much higher rate of passage than would be predic ted from a consideration of their concentration gradient, their oil-water partition coefficient and membrane potential ($\Delta\psi$) [29]. Furthermore, the activation energy is frequently lower than would be expected for passage of the molecules through the membranes by simple diffusion [29]. The major difference, however, is that Fick's law no longer holds [29], and the flux does not continue to increase with increasing solute concentration. Instead, the system shows saturation kinetics, i.e. increasing the concentration gradient increases the flux up to an asymptotic value [29].

There are two mechanistic models which are fundamentally different and which represent the two extremes of current view. The first of these is the mobile carrier able to diffuse rapidly from face to face of the membrane. It has specific high-affinity binding sites for the substrate which can be exposed at either face of the membrane [27]. Such a scheme is outlined diagrammatically in (Fig.I.10(a)).

The second interpretation which may be formed is the channel/pore hypothesis [81], sees the transport system as a specific pore or channel through the membrane. Fig.I.10(b). Unlike the "water filled pores" these pores are lined with hydrophilic groups of "permanent" structures [29]. Specificity may arise from pore diameters [29], charge distribution within the pore [29], the presence of specific binding sites at the pore entrance/exit [27], or indeed combinations of all these factors.

FIG.I.10

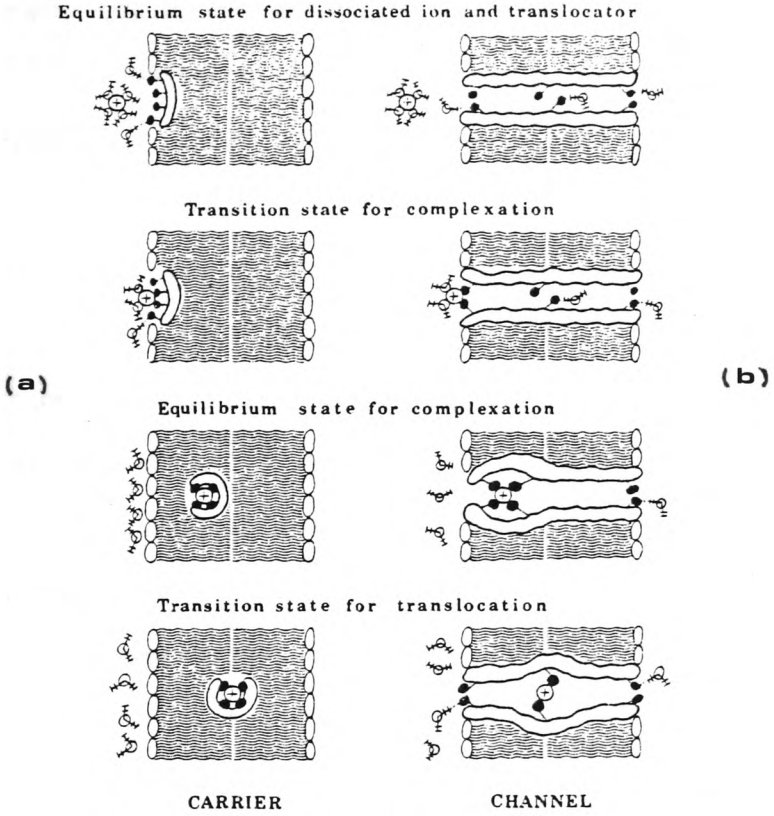

* Schematic representations of the ion, translocator, and membrane lipids corresponding to the different states in translocator-mediated ion permeation. These figures are schematic representations of the ion, translocator, and lipid molecules in the membrane associated with the different states of ion translocation, the left-hand figures representing carrier-mediated transport and the right-hand figures representing channel-mediated ion transport.

* FROM REF: ANDREOLI, T. E.; HOFFMAN, J. F. and FANESTIL, D. D. (eds.) (1978) "PHYSIOLOGY OF MEMBRANE DISORDERS" PLENUM. N.Y.

4.1 Carrier-type Ionophores

The naturally occurring antibiotic ionophore, valinomycin was discovered by Pressman[82] (1964) who demonstrated its specificity for transport of potassium into mitchondria. Since that time, other naturally - occurring antibiotics (e.g. A23187, ionomycin and X537A(Figs. I.11 (a), (b) and (c) respectively) have been found to function as mobile carriers for metal ions[83]. Other compounds such as NaFod (Fig. I. 11 (d)) were found to transport cations in bilayer membranes with efficiency equaling that of A23187 and X537A[50]. The advantages of using such an ionophore (NaFod) is its appreciable solubility in aqueous solvents[50], and its commercial availability since it can be synthesised chemically [50]. All these compounds are classified under the generic name ionophores. They are a heterogeneous group with respect to molecular structure, but these cation carriers have the common property of being folded in such a way to produce a hydrophobic exterior surrounding an interior cavity lined with critically - orientated oxygen or nitrogen atoms (Fig. I.11). These polar groups can bond with cations via ion-dipole interactions, in the same manner as a hydration shell forms around the ion in aqueous solution.

Some of the carriers form 1:1 complexes with their respective metal cation, and show marked discrimination between closely-related ions. Thus valinomycin shows a 10,000:1 preference for K^+ over Na^+[84] ; the difference in radius of the two ions is not great (K^+ being 0.133 nm and Na^+ 0.095 nm) which serves to emphasize the precision of fit of the ion into the polar oxygen lined cavity of the ionophore. There is unequivocal evidence that valinomycin (A23187 and Ionomycin) behave as mobile carriers[84], ferrying cations across

Fig. I.11

CARRIER IONOPHORES

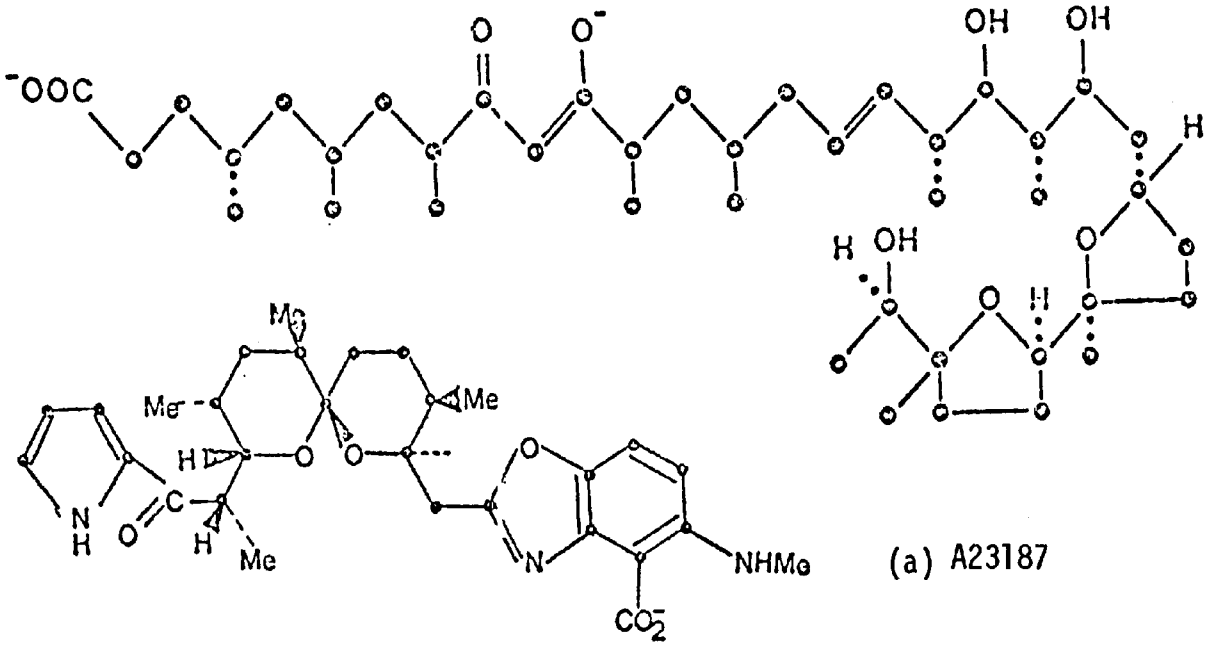

(b) IONOMYCIN

(a) A23187

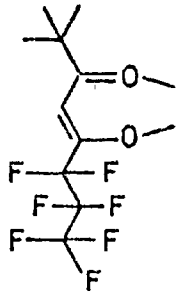

(d) FOD

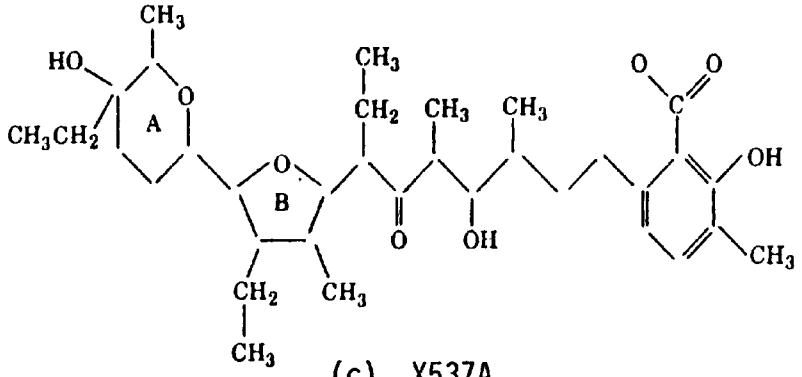

(c) X537A

the membrane. There is a linear relationship between ion flux and ion concentration up to a point where saturation occurs[29]. However, flux of ions drops if the temperature of the membrane is lowered below the phase transition of the acyl chains[37], indicating that a fluid membrane is a prerequisite to transport.

4.2 Channel/Pore forming ionophores:

These ionophores are equally clearly not mobile carriers. Gramicidin (A,B and C) (Fig. I.12 (b)) and alamethicin (Fig. I.12 (a)) are the two best characterised channel or pore-forming ionophores[27]. As in the case of mobile carriers, these molecules present a structure which is hydrophobic in exterior and an oxygen lined central channel. The peptide chain of gramicidin A appears to dimerise in the membrane, forming a helix X nm long with a hole 0.4 nm in diameter. Such a structure would span the hydrophobic region of the membrane and could provide a water-filled-ion-conduction channel (Fig. I.12 (c)). In general, the gramicidin allows the free passage of water and do not discriminate between ions to anything like the extent of the mobile carriers. Thus gramicidin can act as a facilitated diffusion system for a range of ions.

Alamethicin presents a more complex picture in that channel formation is seen to be dependant on membrane potential $\Delta\psi$[85]. As the voltage increases a point is reached when a water-filled ion conduction channel is formed[85]. Black lipid studies suggested that six molecules of a mixture of alamethicin 30 and alamethicin 50 are required to form the channel[37]. However, recent

Fig. 1.12 PORE/CHANNEL FORMING IONOPHORES

(a)

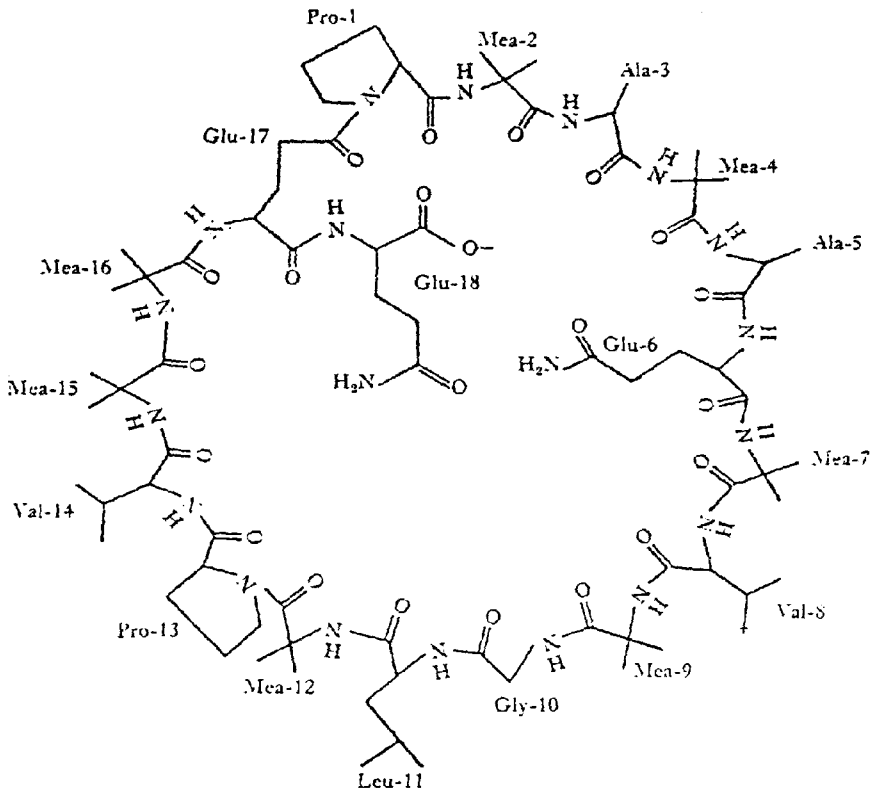

(c)

(b)

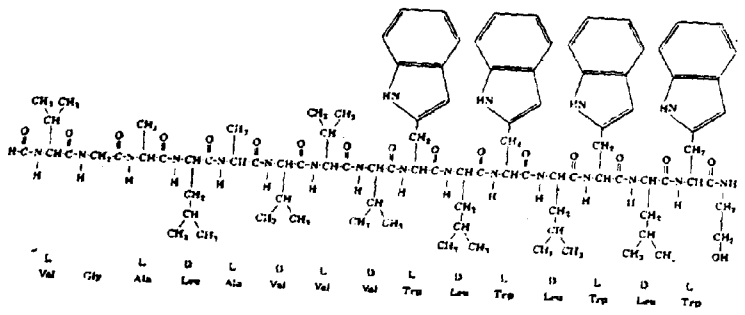

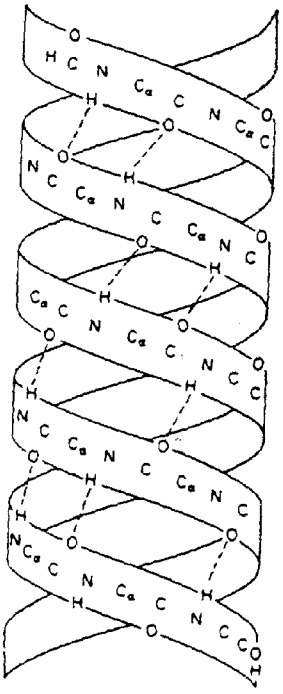

(a) The cyclic structure of alamethicin.

(b) The primary structure of gramicidin A.

(c) Structure of gramicidin channel: the antiparallel - β double helical dimer with seven residues per turn in the left handed configuration.

studies on alamethicin 30 - mediated transport on DPPC vesicles[86] have shown that aggregates of four alamethicin molecules are required to form an aggregate micelle (similar to staves in a barrel) enclosing a hydrophilic water filled channel. This finding is used in this thesis to interpret the results obtained with calcium antagonistic drugs (See Chapter V).

SECTION 5

NON-BILAYER PHASES

5.1 Recent advances in transport mechanisms.

5.1.1 Phospholipids as ionophores.

5.1.2 Non-bilayer phases (inverted micelles).

5.2 Lipid Peroxidation.

SECTION 5

5.1 Recent advances in transport mechanisms

5.1.1 Phospholipids as ionophores

Michell and co-workers[87] have postulated that the accumulation of phosphatidyl inositol (PI) is involved in the mechanism by which certain neurotransmitters and hormones activate membrane Ca-gates (PI-effect). However although Michell's observations are consistant with a phospholipid involvement probably somewhere between receptor occupation and Ca-gating, they do not suggest what the specific role of the phospholipid in Ca-gating mechanism might be. Recently Salmon and Honeyman[88] suggested that the critical event may be the net formation of phosphatidate (PA) following net break-down of PI which occurs in the pancreas[89], platelets[90] and smooth muscle[91][88]. PA has been shown to behave as a Ca^{2+} ionophore in a Pressman Chamber, and it is possible that an increase in PA concentration in cellular membranes might increase Ca-permeability of these membranes. However, this PI effect is Ca-independant and is not produced by the divalent cation ionophore A23187.

Putney et al.[92] reported that PA which is formed during the reaction sequence of the phosphatidate - effect may directly mediate the inward movement of Ca; and that results from activation of surface membrane receptors. Serhan et al.[93] tested the phospholipids phosphatidyl inositol and phosphatidic acid and the fatty acids linoleic and linolenic for thier ionophoretic activity in liposomes entrapping the metallochromic indicator arsenazoIII (specific for Ca^{2+}). They could not detect any ionophoretic properties for PI but PA and the fatty

acids translocated divalent cations selectively, demonstrating the same rank order as A23187 and ionomycin : Mg > Ca > Sr>> Mn. Tyson et al.[94] used the simple Pressman cell to compare the ionophoretic properties of thirteen different phospholipids including PA, CL, PS and SM and six different metal ions including Ca, Mn, Mg and Rb. Of all the phospholipids tested only CL and PA show activities comparable to that of X537A in respect to the translocation of divalent cations. And the rate of translocation by the two latter phospholipids was found to be independant of pH between pH 5.4 and 8.3. Further, these authors have demonstrated that mitochondrial lipids form complexes with reduced cytochrome C and such a complex enhances the ionophoretic capability of the phospholipid by one order of magnitude. The complex thus formed has the properties of polyionophore. This finding has enormous physiological significance especially in terms of the chemiosmotic hypothesis.

5.1.2 Non-bilayer phases (inverted micelles)

The existence of lipidic particles in freeze fracture replicas prepared from aqueous dispersions of cardiolipin/phosphatidyl choline mixtures containing Ca^{2+}, and in cardiolipin dispersions treated with Ca^{2+} or Mg^{2+}, were first reported by Verkleij et al.[95] and Vail and Stollery[96]. Subsequently a number of studies have shown "particle-like" structures in replicas prepared from dispersions of different phospholipids[21][17] and galactolipid mixtures[97]. In general these structures are observed in lipid mixtures containing at least one component which assumes an hexagonal configuration when dispersed in water; the other component(s) forming lamellar phase under such conditions. The molecular configuration associated with particle formation, however, is still

a matter of controversy [98].

De-Kruijff and Verkleij and their collaborators [99] have, on the basis of evidence obtained from freeze fracture and ^{31}P-nmr studies, proposed a number of possible molecular arrangements to account for the existence of such particles. Of these the most favoured arrangements involve inverted micelles present either inside the bilayer (Fig. I.13) or between the outer monolayers of two adjacent bilayers (Fig.I.13(a)). The former type of these inverted micelles mediates transbilayer transport and flipflop and the latter mediates membranes fusion.

However, since their discovery the nature of these particles (micelles) in freeze fracture replicas has been discussed by Sen etal [97] , Ken-Chun Lin etal [100], Hui etal [101] and Miller [98] . Their points of view are reflected in Chapter IV of this thesis.

5.2 Lipid Peroxidation

During the investigation of non-bilayer phase effects some lipid peroxidation was observed, therefore, the possible connection between these two phenomena was looked into.

Lipid peroxidation is a complex process known to occur in both plants and animals [102]. In addition biological membranes are filled with active catalysts of oxidation of fatty acids by oxygen with peroxide formation (lipoperoxidation) such as hemoproteins and nonheme iron, copper, and manganese complexes. The sequence of oxidation of even a small portion of unsaturated fatty acid

Fig I.13

Inverted lipid micelle inside the bilayer

Fig I.13.(a)

Inverted lipid micelle between two adjacent bilayers

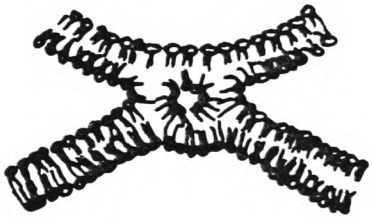

The bilayer thickness and the size of the inverted lipid micelle is drawn to scale.

in the phospholipid bilayer are obviously dramatic : deterioration of barrier and matrix function of the lipid bilayer, enzyme inactivation, toxic effect on cell division, [103]

The systematic study of the reaction kinetics of lipid peroxidation in isolated mitochondrial membranes[104] has shown that the process, being rather complicated, may, nevertheless be described by the reaction pattern shown in Scheme 1, in which XH is an initiator of the chain oxidation, X free radical of the initiator, LH, various lipid molecules undergoing peroxidation, L ,hydroperoxide molecule, InH, inhibitor (antioxidant) molecule, In, inhibitor free radical, P, LOH, molecular products, and MP, various unidentified molecular products not involved in further chain reactions.

According to scheme I.1 Lipoperoxidation is a branching chain reaction which can be considered as taking place in four main stages:

1. Chain initiation: The formation of primary radicals of polyunsaturated fatty acids L as the result of generation in the system of certain initial radicals X (Reaction O and 1).

2. Chain propogation, (Reaction 2 and 3): The rate of lipid peroxidation is obviously proportional to the concentration of L and LO_2 leading to chain reactions.

$$W = -\frac{d[LH]}{dt} = K_3 [LH][LO_2] = k_2[O_2][L]$$

- while the ratio of $[L]/[LO_2]$ is stationary state depends on the reaction rate constants k_2 and k_3 and the concentration of oxygen in the medium.

0. $XH \xrightarrow{k_0} X$

1. $X + LH \xrightarrow{k_1} p\,L$ (usually $p \ll 1$)

2. $L + O_2 \xrightarrow{k_2} LO_2$

3. $LO_2 + LH \xrightarrow{k_3} LOOH + L$

4. $LOOH + Fe^{2+} \xrightarrow{k_4} LO + OH^- + Fe^{3+}$

5. $LO + LH \xrightarrow{k_5} LOH + L$

6. $LO_2 + LO_2 \xrightarrow{k_6} P \quad P + \psi\, h\nu$ ($\psi \ll 1$)

7. $LO_2 + InH \xrightarrow{k_7} In + MP_1$

8. $In + LO_2 \xrightarrow{k_8} MP_2$

9. $LO_2 + Fe^{2+} \xrightarrow{k_9} Fe^{3+} + MP_3$

9. $L + Fe^{2+} \xrightarrow{k_9^1} Fe^{3+} + MP_4$

SCHEME 1.1. The pattern of main lipid peroxidation reactions: XH, an initiator of the chain oxidation; X , free radical of the initiator; LH, various lipid molecules undergoing peroxidation; L, LO, LO_2, free radicals produced from LH; LOOH, lipid hydroperoxide molecule; InH, inhibitor (antioxidant) molecule; In , inhibitor free radical; P, LOH, molecular products; MP_{1-4}, various unidentified molecular products not involved in further chain reactions.

3. Chain branching: There is much evidence that in biological membranes this reaction involves nonheme iron (Reaction 4).

4. Chain termination: At least three reactions are known to break the chains : interaction of two radicals leading the chain (Reaction 6), interaction of one radical with changing valency metal (Reactions 9 or 9^1), and reactions between such a radical and a molecule of "antioxidant", i.e. the compound whose radicals are unable to continue the chain reaction (Reaction 7). α - Tocopherol, some steroid hormones, and ubiquinone were shown to perform this function in membrane systems [103].

Three types of effects can be observed [103] in which lipid peroxidation proceeds: (i) shift in metabolism (ii) direct enzyme inactivation and (iii) the alteration of the physical properties of phospholipids in the membrane bilayer. And this third effect is of interest in this thesis.

The effects of lipid peroxidation on bilayer structure have been studied by Edwards and Quinn[105] using unsaturated lipid dispersions and Tween 80 . They found that large multibilayer dispersions are not accessible to free radicals generated in the bulk water, - hence multibilayer liposome dispersions can not be completely decomposed unless the dispersion structure is broken down or rearranged substantially so as to make it more accessible to radicals produced in the bulk water. Gast et al.[106] studied the effect of sonication in the presence or absence of air on the changes in size of vesicles due to peroxide formation. Their quasi-elastic light scattering (QELS) and electron microscopy methods show that PC vesicles fuse when the level of peroxides increases, and they emphasised the role of phosphatidyl choline

peroxides as fusogens.

Effects of lipid peroxidation on bilayer permeability of sonicated vesicles containing phosphatidylethanolamine and methods for detecting lipid peroxidation products are considered in Chapter IV , together with their relation to production of non-bilayer phases.

SECTION 6 Calcium Antagonists

6.1 Calcium and the Heart.

6.2 The calcium antagonists - their clinical use and side effects.

6.3 Their mode of action.

SECTION 6 Calcium Antagonists

6.1 Calcium and the Heart

It is now one hundred years ago since Ringer (1882) described the importance of Ca^{2+} in the maintenance of frog heart contractility[107]. The role of calcium in controlling both electrical and mechanical activity of the heart is now well established[108]. The important regulatory functions are affected when calcium moves across cellular membranes - including the sarcolemma and sarcoplasmic reticulum. These membranes are responsible for the non-equal distribution of calcium where extracellular calcium concentration exceeds that of the cytosol by a factor of 10^4[109]. The sarcolemma and the sarcoplasmic reticulum are composed of a hydrophobic bilayer which constitute a barrier to the flux of ions in which are embedded a number of intrinsic proteins. Some of the latter are involved in movement of calcium between different regions of the myocardial cell[109].

The "downhill" movement of calcium from regions of high Ca^{2+} activity in the extracellular space and the sarcoplasmic reticulum into the cytosol, where Ca^{2+} concentration is much lower, is mediated by "channels" that are probably lined by hydrophilic regions of the intrinsic proteins[107]. The sarcolemmal calcium channels which carry the slow inward current that is responsible for the plateau phase of the cardiac action potential is regulated by a voltage-sensitive gating mechanism that controls the access of ions to the channel[109]. The calcium permeability of the sarcoplasmic reticulum which controls the calcium release into the cytosol that initiates cardiac systol may be regulated by the calcium pump adenine triphosphatase

(ATPase) protein, also responsible for the active transport back into the sarcoplasmic reticulum during diastole[109]. Abnormal calcium movements may contribute to the depression of myocardial contractility seen in the failing heart[108].

Myocardial contraction is initiated by the delivery of calcium to the contractile proteins, where the binding of these ions to the troponin complex allows the thin (actin) filaments to interact with the thick (myosin) filaments in a manner that causes the heart to shorten and develop tension. Research development has revealed mechanisms of muscle contraction, but little is known of the mechanisms of excitation-contraction coupling and, whether the source of the activator calcium ions is from extracellular fluid, from internal stores within the sarcolemma, or both[110]. According to one theory[110]: the excitation contraction coupling - the process by which action potential at the cell surface initiates shortening and tension development in the myocardium - is initiated by the influx of a small amount of calcium across the sarcolemma triggering a larger calcium release in the sarcoplasmic reticulum ("calcium - triggered - calcium release") that provides sufficient calcium to bind to the contractile proteins and initiates cardiac systole.

Another dark area is the mechanisms of action of the 'slow calcium channel', and this has been discussed in a recent colloquium[111]. It is suggested that calcium ions are transported into cardiac mitochondria in exchange for Na^+ ions, and the latter are exchanged with H^+ via the Na^+/H^+ antiporter.Fig.I.14.

The entry of Na^+ does not decrease the membrane potential because the "slow calcium channel" is more selective for calcium ions and therefore transports Na^+ more slowly. Also as shown overleaf Na^+ is exchanged for H^+ via the Na^+/H^+ antiporter. However, the elucidation of the properties and mechanisms

FIG. I.14. Na^+/H^+ ANTIPORTER OF CARDIAC MITOCHONDRIA

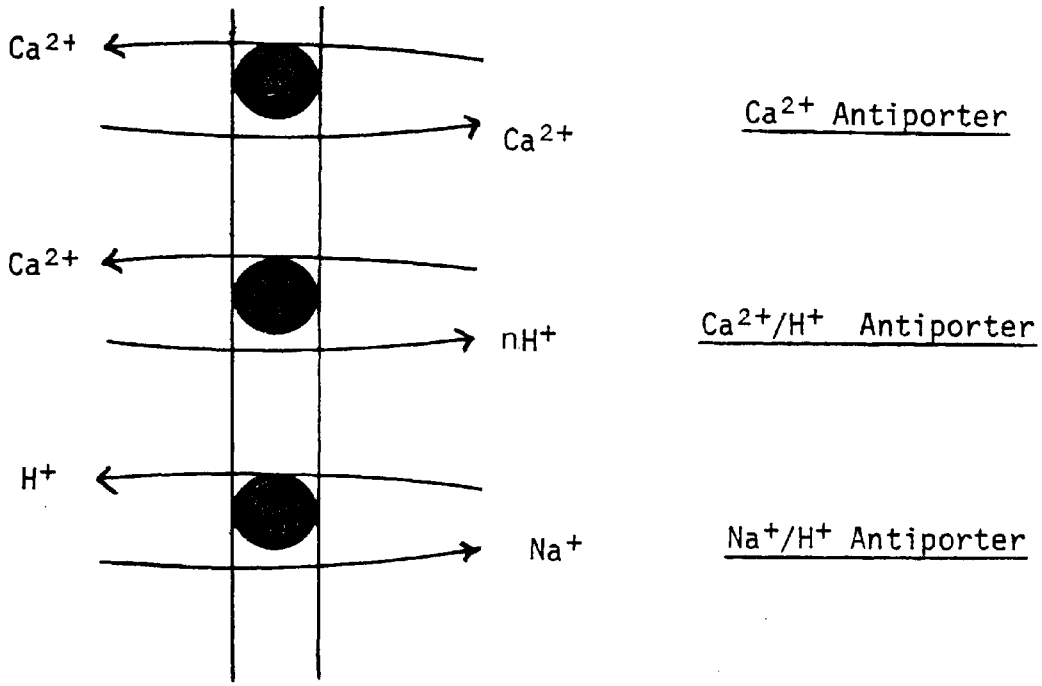

of calcium transport through the "slow calcium channel", and the mechanisms of excitation-contraction coupling are far from complete[112]. But the link between pertubation in calcium concentration in cardiac tissue and the possible heart mal-function is well proven.

Recent publications[113] discuss the involvement of the newly discovered protein (calmodulin) as calcium binding proteins in the Ca^{2+}-ATPase present in cellular membranes. It has been shown that calmodulin-free Ca^{2+} pump ATPase show activity and Ca^{2+}-sensitivity that are similar to those of the calmodulin-activated intact protein. These results show that the transport protein Ca^{2+}-ATPase contains binding sites to calmodulin which are hydrolysed by trypsin. Research involving calmodulin is still in its infancy and details of mechanisms of binding calcium is not yet available.

6.2 The calcium antagonists - their clinical use and side effects:

A group of drugs that dialate the coronary vessels have been grouped under "Calcium antagonistic drugs" by Fleckenstien[114]. Since their discovery 20 years ago by Linder[17] these antagonists have been used in isolated smooth muscle, in the rat and guinea pig myocardia, and in patients suffering from heart diseases.

Most of the clinical studies are concerned with the use of calcium antagonists in patients with angina pectoris[115]. The fact that these drugs increase coronary blood flow, decrease arterial pressure, and have an antiarrhyth mic effect would suggest their value as anti-anginal agents[118]. Furthermore, these drugs were found to reduce the number of daily attacks in patients with

bronchospasm which reduces the necessity for nitro glycerin[112]. Some of the properties of these drugs and their therapeutic uses are listed in Table I.3.

Side effects, mostly headache and dizziness were reported[112] in patients treated with verapamil. Side effects with Nephédipine were encountered but they were usually minor occurrences such as headaches, heat sensation, vomiting or nausea. Perhexiline was found to cause side effects quite frequently.

6.3 Their mode of action

The basic mechanism of action of coronary dilator drugs through which the smooth muscle of the vessels is relaxed is not fully understood. Nevertheless it is possible to formulate some broad hypothesis on the basis of the evidence that is available.

The contractile mechanism of smooth muscle, like that of skeletal and cardiac muscle is dependant on a Ca^{2+} activated myosin ATPase. However, unlike the situation in skeletal muscle, the intracellular stores of Ca^{2+} in smooth muscle are relatively sparse[110]. Consequently, much of the Ca^{2+} necessary to activate the contractile mechanism enters during the cell during the action potential. Many smooth muscle relaxants, including most, and possibly all, coronary dilator drugs appear to act by depriving the contractile mechanism of calcium [110].

The precise mechanism of action of these drugs has been studied by many

Some drugs that dilate normal coronary vessels

Drug	Vasodilator properties	Therapeutic uses
Chromonar (carbocromen)	Prolonged intense dilator effect on coronary arterioles. Very little effect on systemic vessels or on other smooth muscle.	Angina pectoris, but efficacy not proven and rarely used.
Fendilinum	Dilates coronary arterioles in doses only slightly below those that produce systemic vasodilation and hypotension. (Chemically resembles prenylamine.)	Angina pectoris in some countries including Germany and Switzerland.
Verapamil	Dilates peripheral as well as coronary arterioles.	Angina pectoris and cardiac dysrhythmias.
D600	Similar to verapamil.	Experimental drug.
Nifédipine	Dilates peripheral arterioles (especially in skin and skeletal muscle) as well as coronary arterioles.	Angina pectoris and antihypertensive.
SKF 24260	Similar to nifédipine.	Experimental drug.
MG 8926	Similar to prenylamine.	Experimental anti-anginal and antidysrhythmic drug.
Lidoflazine	Enhances and prolongs cardiac reactive hyperaemia in doses below those that produce general coronary arteriolar dilation. Lowers peripheral resistance in slightly larger doses.	Angina pectoris.
Perhexilene	Produces a fall in peripheral resistance as well as dilating coronary arterioles. Blood flow through coronaries is increased despite fall in perfusion pressure.	Anti-anginal and antidysrhythmic drug.
L 8040	Similar to amiodarone.	Experimental anti-anginal and antidysrhythmic drug.

workers, and a summary of their suggested mechanisms is outlined. Fleckenstein[117] suggested that these drugs antagonise calcium by inhibiting its influx (i.e. from extracellular pools) through the cell membrane. Church and Zsoter[118] studied the mechanism of action of three calcium antagonists, diltiazem, nephidipine and verapamil by investigating their effect on Ca^{2+} uptake and efflux in rat heart and aorta in rabbit vesicles. They suggested that calcium antagonistic drugs may act by other mechanisms than the inhibition of transmembrane Ca^{2+} flux; probably on the mechanisms of release and binding of Ca^{2+} in intracellular pools. Mas-oliva et al.[119] studied the effect of verapamil on sarcolemmal membranes and found that it interferes with the ATPase dependant Ca^{2+} transporting activities of the sarcolemma, and inhibits ATP hydrolysis. This would imply that 'active' transport of calcium involving ATP is inhibited and calcium would not be released for the next action potential.

Malaisse et al.[120] used solvent extraction (Pressman cell) techniques involving calcium ionophores and $^{45}Ca^{2+}$. They suggested that the antagonists bind to the complexing sites of the ionophore molecule (which mimics the "inherent" ionophore in the plasma membrane) and therefore antagonise calcium binding to the ionophore molecule.

Katz et al.[110] studied sarcolemmal calcium channels and suggested that the calcium antagonists may modify ion fluxes through the membrane channel by an interaction with functionally important membrane lipids surrounding the hydrophobic region of the "channel proteins". An interesting report by Opie[121] compared the antiarrhyth mic effects of nephidipine, verapamil and perhexiline in patients with angina pectoris. He found clinical differences between these drugs which suggests that there may be more than one type of calcium channel for calcium antagonists to act on. Alternatively, the calcium channels

in different tissues may differ in sensitivity to various antagonists, with the atrio-ventricular node channel most sensitive to verapamil and nephidipine, and the myocardial channel possibly sensitive to perhexilene.

The understanding of the mechanism of antagonism by these drugs clearly depends on further investigations of the nature and mechanism of the calcium channel in various membranes, and the effect of these drugs on calcium movement through these membranes.

Chapter V of this thesis describes experiments in which NMR methods are used to investigate the effect of the calcium antagonists on ionophore mediated transport of lanthanide ions. Sufficient background on the above section has been given in order to appreciate how successful the attempt has been to investigate these areas using the novel method of NMR in conjunction with lanthanide probe ions.

CHAPTER II

PARAMAGNETIC ION-BINDING TO PHOSPHOLIPID VESICULAR MEMBRANE SURFACES

CHAPTER II

PARAMAGNETIC ION-BINDING TO PHOSPHOLIPID VESICULAR MEMBRANE SURFACES

II.1 Introduction

Bergelson et al.[122] and Bystrov et al.[123] have shown that the "inner" and "outer" choline ^{1}H-nmr signals of sonicated vesicles can be separated by salts of paramagnetic ions such as lanthanides and manganese added extra-vesicularly. The appealing advantage of this finding is that it enables the investigator to monitor separately perturbations of the "inner" and "outer" shells of the bilayer; thus adding a new dimension to nmr studies of membrane systems. The above authors suggest that the lanthanide - ion - interactions with outer headgroups of the lipid (bilayer impermeable to Ln^{3+}) is responsible for the observed shifts.

Generally, the interactions of metal ions, particularly calcium, has been a subject of interest for some time due to the well known regulatory role played by calcium in biological phenomena, as well as the ability to induce aggregation and fusion in phospholipid vesicular dispersion[124]. The problem in hand however, is the nature of the interaction of these metal ions with the surface binding sites, how this binding is altered (if any) in the presence of other cations, and/or anions and also the stoichiometry of binding of metal ions to phosphate headgroups of the lipid.

Hauser et al.[125] used surface chemical and nmr methods to study the

interactions of calcium and lanthanide PC sonicated vesicles. Their ^{1}H and ^{31}P-nmr spectra have shown that there is only weak interactions between Ca^{2+} and the phospholipid, and using spin lattice relaxation times and line broadening using Gd^{3+} they concluded that these cations bind to the phosphate group and that this is the only binding site. They suggest that the weak interaction between Ca^{2+} and lecithin means that the packing of egg lecithin molecules in the bilayer does not change up to calcium concentration of about 0.1 M. Increasing the ionic strength by adding NaCl enhances the binding of the lanthanide to lecithin headgroups. Grasdalen et al.[126] suggest that the binding efficiency is controlled by electrostatic potential produced by the bound cation of the membrane surface. This potential is slightly modified by the weak chloride binding. They used computer simulations and ^{31}P-nmr to find a value for the stoichiometry factor n. Amongst the values of n tested they favour n = 3 for the lanthanide used, Tb^{3+} . This is different from that calculated by Hauser et al. and suggests that further investigation will be necessary to settle this point. However, their application of the theory of diffuse double layer to membrane phenomena indicates that calcium and the lanthanide show similar interactions, except that in the case of calcium the interaction is approximately two orders of magnitude smaller. The surface chemical methods of Hauser et al.[127] suggest that lanthanide binding is up to 10 times greater than calcium.

Both Hauser et al.[125] and Grasdalen et al.[126] report that the absorption of cations to bilayer surfaces is accompanied by anion binding. Westman et al.[128] applied the theory of diffuse double layer (Gouy-Chapman-Grahame) and suggest that the binding of the anion depends on the nature of absorbed cation. They also find that the ^{31}P-nmr shift enhanced in the presence of

anions in the order $Cl^- < Br^- < NO_3^-$. The specific anion binding has been questioned by McLaughlin et al.[129]. But contrary to Barsukov et al.[130], they claim that anions (chlorides) do not influence the electrophoretic properties of the liposomes. However Westman et al. claim to have demonstrated an intimate synergism between the cation and the anion promoted by surface potential effects.

The Springer group[131] used dimethyl phosphonate anion (DMP^-) as an internal monitor for studying the lanthanide ion binding to bilayer membranes and they calculated the binding stoichiometry to be two DPPCs per Pr^{3+} . They have also emphasized that headgroup conformation changes brought about by lanthanide binding only involves the choline moiety.

Cohen and Cohen[132] derived a generalized expression of the Stern theory to study the absorption of monovalent and divalent cations by phospholipid membranes of phosphatidylserine[132]. Their treatment of the theoretical data is complicated by the consideration of competitive and non-competitive binding of monovalent and divalent cations. For example they show a stoichiometry of 2:1 for divalent cation binding for noncompetitive binding and 1:1 for competitive binding by monovalent cations. Further, their analysis of isotherm plots shows evidence for simultaneous 1:1 and 2:1 binding for cations when stability constants are measured in a solution containing a mixture of monovalent and divalent cations.

Hunt et al.[133], in a recent publication have demonstrated that the binding of paramagnetic lanthanide ion to the outer headgroup of the vesicles can set up an additional magnetic field inside the vesicle causing upfield shifts of inside choline signal. They explain these results in terms of the Bleaney theory[68] and the anisotropic susceptability effect and conclude that the

application of the Bleaney theory and the added feature of the intravesicular field conservation would together explain the nature of pseudocontact shift resulting from the binding of lanthanide ions to the outer headgroups.

Finally, recent reports[134] involving the transport of biologically important cations (e.g. Na) was shown to be monitored by nmr methods. ^{23}Na-nmr spectra were presented and the Gramicidin-mediated transport of this metal both out of and into sonicated vesicles was observed. The development of these techniques should enable the study of reconstituted vesicle preparations involving e.g. Na^+ - ATPase to be made, - and details of such studies may reveal the nature of binding and transport of these metal ions in model and biological systems.

For the most part of this work unilamellar vesicles have been used to study transmembrane transport, phospholipid exchange and vesicle-vesicle fusion. In this chapter the ^{1}H, ^{13}C and ^{31}P-nmr spectra of these vesicles are described; their interaction with divalent and trivalent cations is discussed in the light of published work; and the effect of sonication of pre-formed vesicles with extra-vesicularly added lanthanides is examined. Calculations of the physical details of the vesicles are made including their numbers and mean diameter.

II.2 Materials and Methods

Chemicals

Egg phosphatidylcholine (Egg PC) and DL-α Dipalmitoylphosphatidyl-choline (DPPC) were obtained from Lipid Products (S. Nutfield, England). Stock solutions in chloroform-methanol of DPPC (10 mg/ml) and egg PC (50 mg/ml) were prepared and stored at -5°C. The chloroform methanol used was purified by passing the chloroform through a preactivated (500°C overnight) 10 x 50 cm alumina column and distilled in all glass apparatus. 1% analar methanol was added to stop fosgene formation.

The lanthanides, $GdCl_3.6H_2O$, $PrCl_3.6H_2O$, $DyCl_3.XH_2O$ and $YbCl_3.6H_2O$ were obtained from Koch light (Berks, England) - all at 99.9% purity. Solutions of these lanthanides were prepared in D_2O (99.8% D-atom, Aldrich, U.S.A.) such that 5-10 µl per 0.5 ml vesicle solution gives the required concentration.

Experimental:

II.2.1 Preparation of vesicles

(a) Sonicating Method

The vesicles were prepared by pipetting a known volume of the stock PC solution into a glass sonicating tube, and the chloroform solution was evaporated by passing a stream of nitrogen. Traces of methanol were removed by evacuation for 20 minutes at 2 mm Hg pressure using an electric

pump. The dry lipid was hydrated in a known volume of D_2O (usually 1 ml per 40 mg lipid) and the contents were shaken for 2-3 minutes using a vortex mixer to produce homogeneous milky liposomes. The sonicating tube was placed on an ice bath, a stream of nitrogen passed over the liposomes and were sonicated for 10 minutes using a DAWE soni-probe Type 7532A fitted with a Ti-microtip, at a delivery approximately 25 W. The sonicator probe tip was repolished after every few sonications, a procedure which avoids contamination by Ti particles from the microtip. The sonicate was spun for 10 minutes in a bench centrifuge at maximum speed to remove large vesicles and unsonicated liposomes. The homogeneous vesicle solution in the supernatant was clear and typically bluish. 0.5 ml of the vesicle dispersion was pipetted into 5 mm nmr tubes and placed in a thermostated water bath set at the required temperature before nmr spectra were recorded.

(b) Ether evaporation method

Large volume vesicles were prepared by drying a known volume of the chloroform solution of egg PC, and subsequently re-dissolving the lipid in a known amount of ether, giving a concentration of 1μ mole ml^{-1}. The lipid solution was injected (at a rate of 0.2 ml min^{-1}) from a glass syringe (Fig. II.1) into a preheated (55°C) aqueous phase (4 ml D_2O) through a fine-gauge needle (18 gauge). The needle tip barely penetrated the aqueous phase and the latter is thermally protected along its length by a Teflon plug to prevent evaporation of the ether in the needle shaft. The aqueous phase was heated by a water jacket in a Leibig condenser, with the jacket of the condenser connected to a hot water circulator. The

Fig. II.1. DIAGRAM OF ETHER INJECTION APPARATUS

(SEE BELOW FOR DETAILS.)

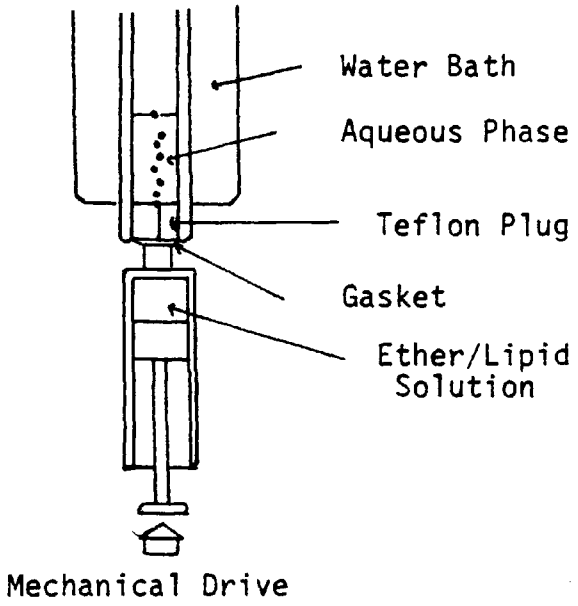

Fig. II.2. ^{31}P NMR SPECTRUM OF LARGE VESICLES PREPARED BY THE ETHER INJECTION METHOD

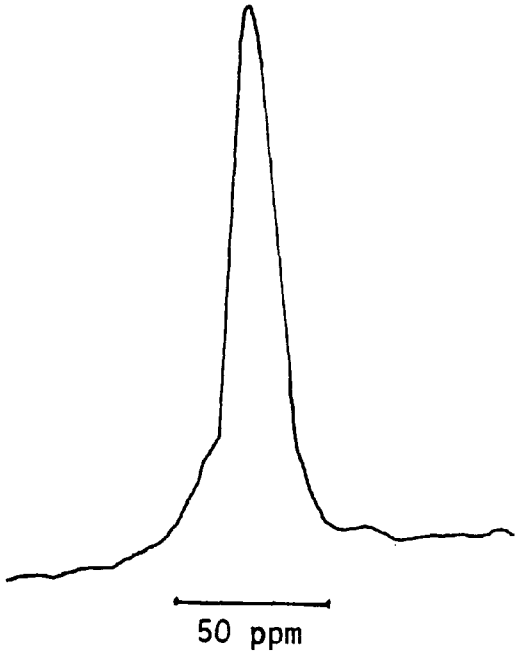

Lipid concentration in ether was 2μ mol/ml, the rate of injection was 0.2 ml/min, the volume of aqueous phase was 4 ml and the temperature of the aqueous phase was 55°C.

syringe plunger was driven upwards by a mechanical drive, similar to an infusion pump. As the ether came into contact with the aqueous phase, a steady stream of ether vapour rose to the surface, producing an unstable foam which filled but did not overflow the vessel. However, in practice it was found useful to join an extension glass tube to the top of the condenser to avoid over-flowing of foam. It is also found that one of the drawbacks of using this method is the limited solubility of lipid in ether. This is directly proportional to the size of vesicles obtained, hence ^{31}P-nmr spectra (Fig. II.2) of these vesicles show a broad spectrum indicating that the size of these vesicles is greater than sonicated vesicles (i.e.>250Å) but less than 2000 Å .

II.2.2 NMR Spectroscopy:

^{1}H-nmr spectra were usually recorded in a JEOL-C60HL high resolution continuous wave instrument, fitted with calibrated variable temperature accessories. The resolution in the nmr oscilloscope was adjusted using the HOD peak which is subsequently shifted such that it does not appear in the spectrum.

^{13}C and ^{31}P-nmr spectra were recorded using a JEOL-FX60Q F.T. nmr also fitted with temperature control accessories. ^{13}C spectra were recorded using 10 μs (90°) pulse, 4500 Hz spectral width, 4K data or 8K data and up to 500 transients depending on the concentration of the lipid. ^{31}P-nmr spectra were recorded using 13 μs (90°) pulse, 4K data, 6666 Hz sweep width, 0.5s pulse delay, and up to 1200 transients.

II.2.3 Sizing of Sonicated Vesicles:

The size of sonicated vesicles was determined using electron microscopy and ^{1}H-nmr.

(a) Electron microscopy:

Since model membranes do not contain proteins they cannot be "Fixed" with conventional cross linking reagents such as glutaraldehyde and osmium tetroxide. Alternatively, negative staining was carried out using ammonium molybdate or phosphotungstate.

The vesicle solution (40 mg/ml) was diluted to 1-5 mg/ml in distilled water and a drop of the resultant solution was applied to a 200 mesh grid coated with parlodin sprayed with a thin film of carbon. After 30 seconds the excess lipid was blotted out, and the grid washed successively with three drops of the staining solution (2% phosphotungstic acid (PTA) at pH 7.4) the grid tilted at an angle ~60° to the horizontal. With the grid held horizontal an additional drop of PTA solution was applied for 30 seconds. The excess liquid was blotted off by a piece of fine filter paper and the grid was allowed to air dry prior to observation under the electron microscope. A preferred staining method involved the mixing of 1% ammonium molybdate (pH 7.0 with 10mM NaOH) in the ratio 1% w/v with respect to the vesicle solution.

The resultant solution was applied to a collodian and carbon coated grid, the excess liquid blotted off and the grid allowed to air dry.

Grids prepared according to the above procedures were observed on a Philips EM300.

(b) NMR

The size of sonicated vesicles was determined from the integral ratio of the outer:inner choline headgroup signal. This is done assuming that the vesicle is spherical and has a bilayer thickness of 4 nm [47]. For actual calculation of physical dimensions of the vesicles see the results and discussion section.

II.3. Results and Discussion

II.3.1 Interpretation of ^{1}H-nmr data

The proton nmr spectrum of sonicated egg PC vesicles (Fig.II.3.(a)) reveals sharp well resolved signals corresponding to the choline (C), methylene (H) and methyl group (M). In contrast to this high resolution spectrum, unsonicated liposomes exhibit sharp resonances superimposed on a broad featureless spectrum (Fig.II.3.(b)). The reason for the appearance of a high resolution spectrum from sonicated vesicles is interpreted as being due to two possible reasons: (a) the fast Brownian rate for small particle size; and (b) the molecular packing and thus the molecular motion of phospholipid molecules along the horizontal plane of the membrane.

In the unsonicated lipid there is already considerable internal motion [135], but this motion is very anisotropic consisting largely of oscillations and rotation about the long axis of the lipid with respect to the long axis. There are therefore residual static dipolar interactions. However, due to the motion about the C-C bonds higher up the chain, the motion at the terminal methyl end of the chain will be more isotropic than the motion near the glycerol backbone [135]. Static dipolar interactions will therefore be important at the glycerol backbone end of the chain than at the terminal methyl ends. The effect of Brownian movements occurring in sonicated vesicles will be to cause a rapid re-orientation of the long axis of the lipid molecule, so that the static dipolar interactions are reduced [136].

Fig. II.3.

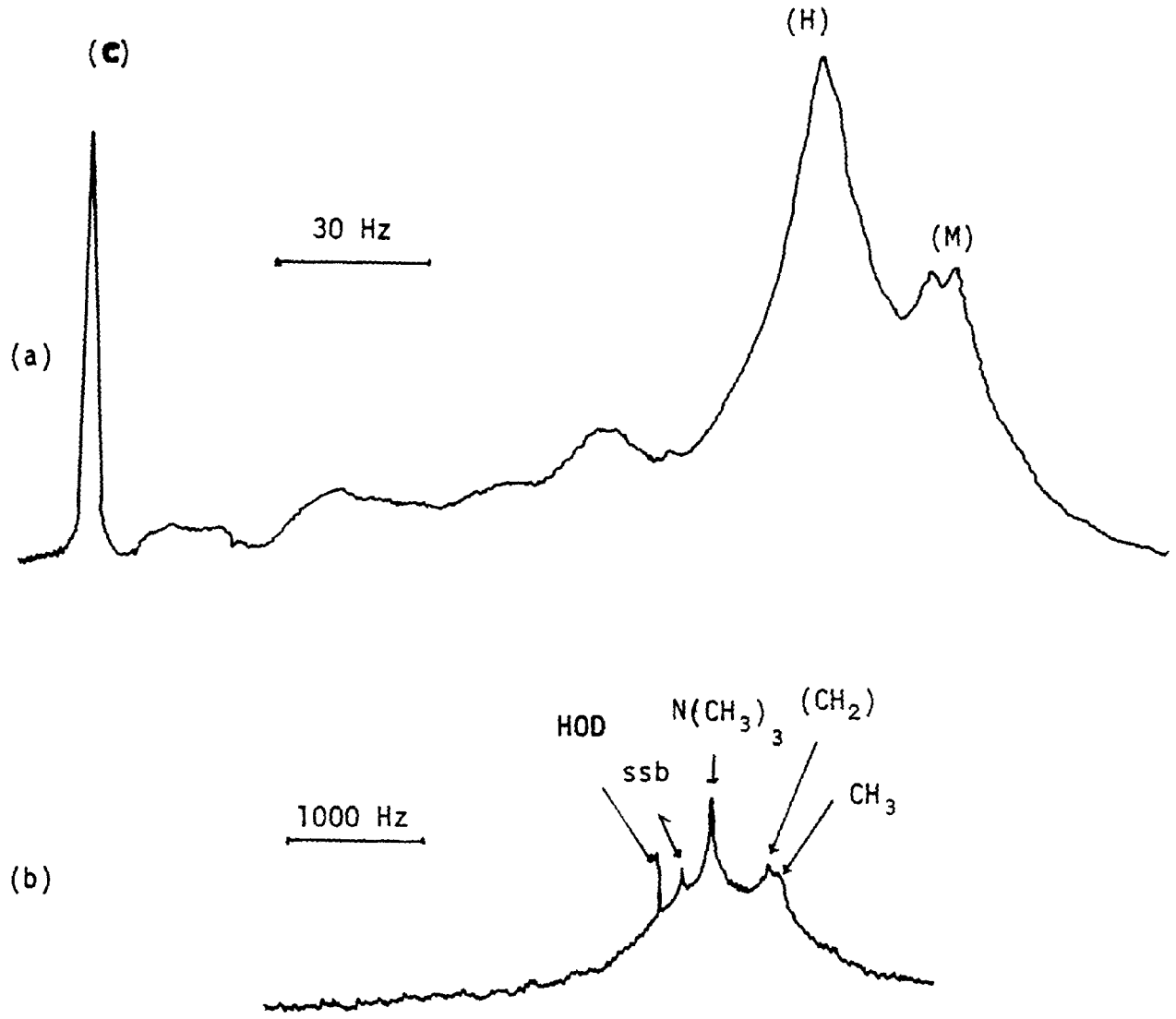

PROTON NMR SPECTRA OF EGG PC

LIPOSOMES AND SONICATED VESICLES (b) & (a)

II.3.2 ^{31}P-nmr

The 24.15 MHz (note this refers to the actual ^{31}P resonance frequency) nmr spectrum of egg PC vesicle dispersion (Fig. II.4) show a single line of width ca: 30 Hz. At 24.15 MHz the resonances of the inner and outer headgroups are not separated due to the fact that the chemical shift (and line broadening) of the ^{31}P-nmr signals is dependant on the external magnetic field [137]. Berden et al.[137] reported that their 129 MHz nmr linewidths of sonicated vesicles under proton coupling conditions have shown an increase by a factor of five compared to the linewidths measured at 36.4 MHz.

The field dependance of the line width has several important consequences. First of all, it implies that the sensitivity for ^{31}P will be optimum at ~ 50 MHz[137] and will decrease as the field is raised. This is in contrast with the situation in proton NMR, where the sensitivity continues to increase as the field is raised. Also, it implies that the resolution of chemically shifted lines from different phospholipids will be optimum at ~ 50 MHz, since the frequency of the linewidth begins to increase as the square of the field, while the separation between the lines increase only linearly with the field.

The vesicles prepared by the ether injection method are larger (>2000Å outer diameter) compared to sonicated vesicles, hence the contribution to the linewidth from the chemical shift anisotropy is greater (Fig. II.2), therefore the optimum frequency for resolution will be lower. However, Brunell et al.[138] pointed out the positive aspects of the chemical shift anisotropy, and discussed the lineshapes of different size vesicles (up to

5000 Å in diameter) in relation to the theory of motional narrowing. The results of such studies have been used in this work to interpret the ^{31}P-nmr spectra of unsonicated liposomes, and to discuss the different polymorphic phases adopted by the different phospholipids. Such interpretation depended upon the observations that phospholipids in the bilayer configuration e.g. PC exhibit a broad (50 ppm wide) asymmetric spectrum with a high field shoulder and a low field peak (Fig. I.4),while those phospholipids in the hexagonal H_{II} configuration e.g. $_{\wedge}^{unsat.}$PE,exhibit a ^{31}P-nmr spectrum with reversed asymmetry with respect to the bilayer spectrum (Fig. I.4) and the width is narrower by a factor of two due to the fast tumbling of the phospholipids around the small aqueous channel (Fig. I.4).

II.3.3 ^{13}C-nmr

In spite of the low natural abundance (1.1% with respect to ^{1}H), and low sensitivity (1.6% with respect to proton detection) ^{13}C-nmr of sonicated vesicles (Fig.II.5) has been useful in determining the longitudinal relaxation rates (Fluidity gradient) of phospholipid acyl chains. The sharp signals observed in the spectrum show that ^{13}C-nmr avoids much of the problem of dipolar broadening which is important in ^{1}H-nmr (Fig.II.3.(a)). In particular, the ^{13}C-nmr signals due to the choline headgroup, the majority of the acyl chain carbons, as well as the glycerol backbone are quite well resolved. The problem of ^{13}C-nmr sensitivity can be overcome by the use of longer accumulation times, or by ^{13}C enrichment [139]; the first of these is used in this work.

Fig. II.4. ^{31}P-NMR SPECTRUM OF EGG PC VESICLES

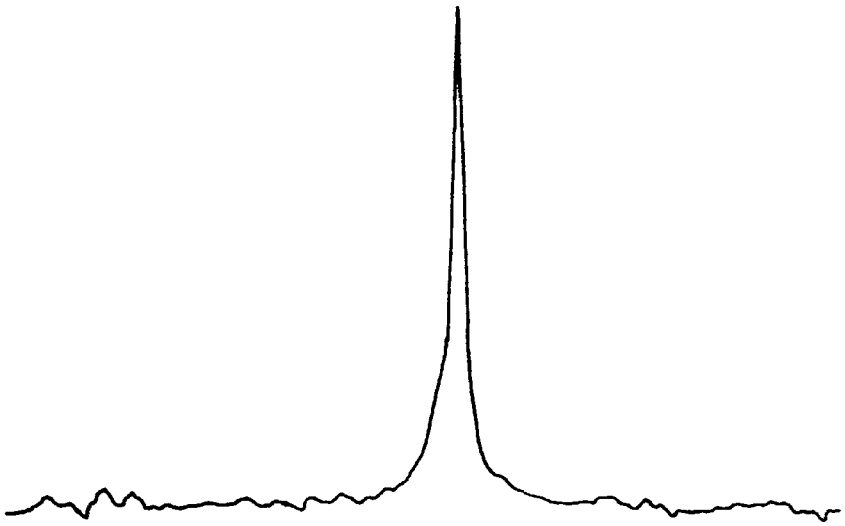

The concentration of the lipid was 45 mg/ml and the spectrum recorded at R.T. The spectral width was 6666 Hz, 13 μs (90^{o}) pulse angle, and 500 pulses were accumulated.

Fig. II.5. ^{13}C-NMR SPECTRUM OF EGG PC VESICLES IN THE PRESENCE OF 0.2 M Pr^{3+}

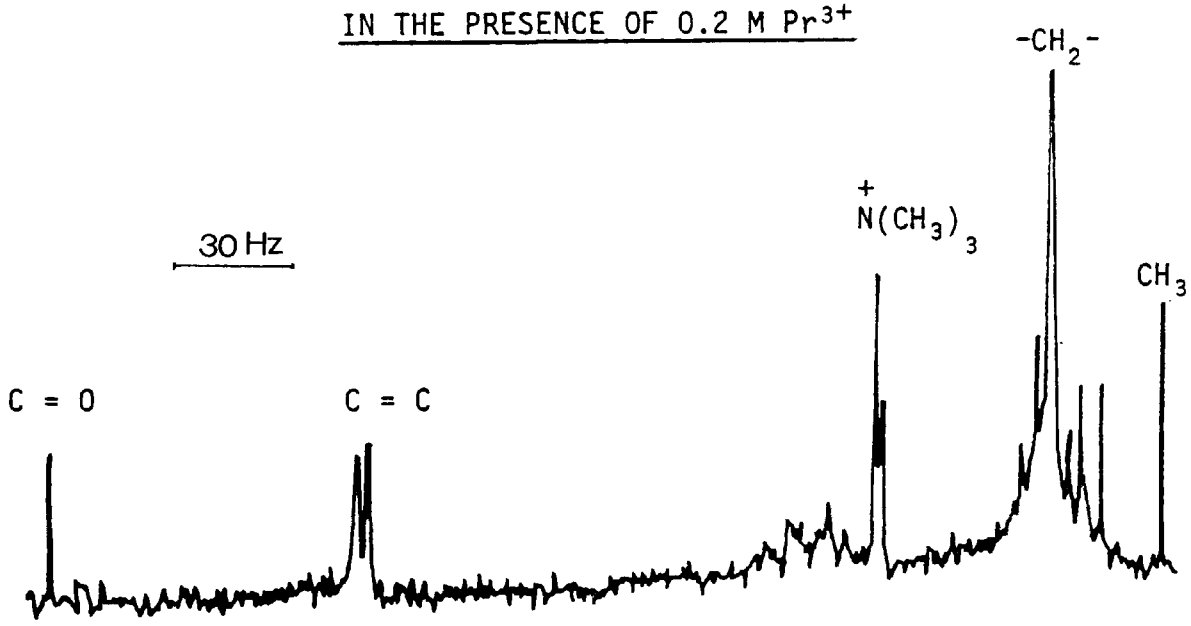

The concentration of the lipid was 30 mg/ml and the spectrum was recorded at R.T. Other conditions were 8 μs (72^{o}) pulse angle, 5 KHz spectral width and 3000 pulses were accumulated.

II.3.4 Cation binding to the surface of vesicles

Although phosphatidylcholine is electrically neutral at physiological pH values it can bind di - and trivalent cations at the phosphate or carboxyl groups of the membrane surface. In this context Ca^{2+} is of importance due to its many physiological functions [140]. However Ln^{3+} can mimic the properties of Ca^{2+} and therefore competes with the latter in biological systems [70] [71]. The co-ordination chemistry of Ca^{2+} and Ln^{3+} are similar [72], and Ln^{3+} as a probe will reflect the general scheme for the absorption of cations to the membrane surface. Lanthanide ions, for example Pr^{3+} cause the separation of the inner and outer headgroups signals of egg PC sonicated vesicles suggesting that the paramagnetic lanthanides interact with the nuclei on the outer surface of the vesicles, and thus produce an upfield shift of the outer choline signal. It is now widely recognised that the addition of metal cations such as Pr^{3+} and Ca^{2+} reduces the surface potential hence causing a shift of the conductance - voltage curves of biomembranes by essentially a screening mechanism providing that the charge density is sufficiently high [141].

The equation most frequently used to express the effects of electrostatic interactions on the binding of charged species to macroscopic membrane surfaces is the Stern equation [131]; a Debye-Hückel-like solution for an infinite plane with uniform smeared surface-charge density σ (charge/area). The binding isotherm is given in the following equation where the amount of

$$K_s = \frac{\sigma}{(\sigma_{max}-\sigma)\{[M]_\infty \exp(-ze\psi_0/KT)\}}$$

bound Ln^{3+} is related to the charge density σ, produced by the binding; σ_{max} is given by $ze/(A_h n)$ (where z is the signed charge of Ln^{3+}, e is the unsigned magnitude of the electronic charge, and A_h is the area per head-

group), $[M]_\infty$ is the concentration of free Ln^{3+} in the bulk (i.e. at a relatively great distance from the membrane surface) and ψ_o is the surface electrical potential (relative to the potential of the bulk aqueous phase).

However, for this theory to be applied to cation binding to the surface of biomembranes the following assumptions haveto be made: (a) the charge on the membrane is assumed to be uniformally distributed over the surface; (b) the dielectric constant in the aqueous phase is assumed to be constant equal to its bulk value; (c) the ions are assumed to be point charges.

Eriksson[128]
Westman and ^ suggested that, in spite of the above assumptions, the Gouy - Chapman - Graham equations applied to cation-binding predicts correctly the change in the surface potential resulting from binding.
The Graham equation giving the relations between the charge on the surface created by the ions bound, the surface potential and the ionic composition in the bulk solution is given by:

$$\sigma = \pm\left(2\varepsilon\varepsilon_o RT \sum_i [i]_b\right) \exp\left(-\frac{z_i F \psi}{RT} - 1\right)^{\frac{1}{2}}$$

where σ is the surface charge in electronic charges $/\mathring{A}^2$, $[i]_b$ is the bulk concentration of the i'th ionic species in mol/l, z_i is its charge, ψ is the surface potential in mV, $F/RT = 26.1$ mV and $(2\varepsilon\varepsilon_o RT)^{-\frac{1}{2}} = 274.0$ at 30°C.

This group reported that for divalent cations at a concentration greater than 10^{-3} M, the magnitude of the surface potential decreases by about 27 mV for a 10-fold increase in divalent ion concentration which agrees with the theoretical value obtained from the Gouy expression for divalent cations alone:

$$\text{Sinh}\ F\psi(0)/RT \cong -1/2 \exp - F\psi(0)/RT = 136\sigma/\sqrt{C^{++}}$$

Furthermore this theory describes the screening effects of both monovalent and divalent cations on the surface potential of charged phospholipid bilayers.

An interesting confirmation of the surface potential effects was obtained by Mc Laughlin et al.[129] who made an independant determination of the zeta - potential caused by Co^{++} binding; and by Westman and Eriksson who studied Ca^{++} and Ln^{3+} binding and determined the relative contribution of contact and pseudocontact to the measured chemical shift. The total chemical shift induced by a Ln^{3+} (j) for the ^{31}P nucleus studied can be expressed as:

$$\delta j^{tot} = \delta j^{dia} + \delta j^{para}$$

However, it has been claimed [128] that this latter study is complicated by the conformational changes occurring due to lanthanide binding. According to Barsukov et al.[142] the conformation is independant of the presence of lanthanide ions, hence the average motional rate of the phosphate region should be unaffected by ions[143].

In order to distinguish between the contact and pseudocontact shifts due to the intra - as well as intermolecular vectors, Hunt and Tipping[133] and Westman and Eriksson studied the effects of several different lanthanides, on the ^{1}H and ^{31}P-nmr spectra of sonicated PC vesicles. Hunt and Tipping described the binding in terms of the Bleaney theory[68], and suggested that the change in magnetic field susceptibility explains the pseudocontact shifts; while Westman and Eriksson suggested that the binding curves (F - curves)

describing the contact contribution to the binding are complicated due to the fact that conformational changes occurred at low ion binding, and made it difficult to determine the precise intrinsic binding constants.

The results obtained in the present study (Chapter III, Fig. III.2) demonstrates that the lanthanide induced shift increases with increasing extravesicular Cl^- ion concentration suggesting that the binding of the metal cations is accompanied by the co-binding of Cl^- anions. This suggestion agrees with that of Barsukov et al.[130] and Westman and Eriksson[128] who independently have shown that the binding of Cl^- to PC membranes is weak in absence of absorbed cations, but enhanced binding occurs in the presence of absorbing cations.

Thus it is reasonable to describe the binding of both lanthanide ions to the phosphate sites and a weaker binding of chloride ions to the quaternary nitrogen as a cooperative effect. The diagram below indicates clearly that the Cl^- will shield the Ln^{3+} from the repulsion of the positively charged $N^+(CH_3)_3$. This can also be discussed in terms of a lowering of the zeta potential on the membrane surface.

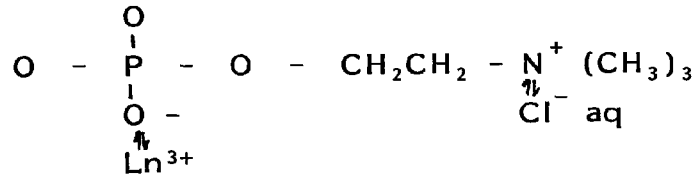

Support for this model of binding should be found in calculations of intrinsic binding constants but this is made difficult by the fact that charge distribution along the surface is not constant (see assumptions made above, and references 144, 125, 126).

Finally, problems also exist in determining the stoichiometry of the lanthanide to head group binding. A result of one Ln^{3+} to two phosphate (head groups) was reported by Hauser et al.[125] [145]. However, Mc Laughlin et al.[129] and Grasdalan et al.[181] reported stoichiometry of 1:1 and 3:1 respectively. According to recent reports by the Springer group[131] who used an independent method based on the perturbation of the ^{31}P-nmr spectrum by the dimethylphosphonate anion (DMP^-), Pr^{3+} binds to DPPC vesicles and produces a hyperfine splitting corresponding to 181.6 ppm; thus showing that the binding stoichiometry is two DPPC's per Pr^{3+}. This group also confirmed previous findings[133] that the relative affinity binding of Ln^{3+} to the "inner" and "outer" headgroups is different, with Ln^{3+} favouring higher affinity binding for the inner monolayer.

II.3.5 Determination of the sizes and number of sonicated vesicles

(a) Vesicle sizes

Apart from opening the possibility of monitoring the changes occurring in the "inner" and "outer" monolayers of vesicles, the use of paramagnetic ions gives an independant method for measuring the average diameter of sonicated vesicles[143]. Fig. II.6.(a) shows that the ratio of the outer:inner choline signals is equal to 1.80, therefore;

$$\frac{4\pi r_o^2}{4\pi r_i^2} = \frac{\text{Area of signal O}}{\text{Area of signal I}} = 1.8 \quad \ldots\ldots\ldots \text{(i)}$$

Fig. II.6

'H-NMR SPECTRUM OF EGG PC VESICLES CONTAINING 5 mM Pr^{3+}

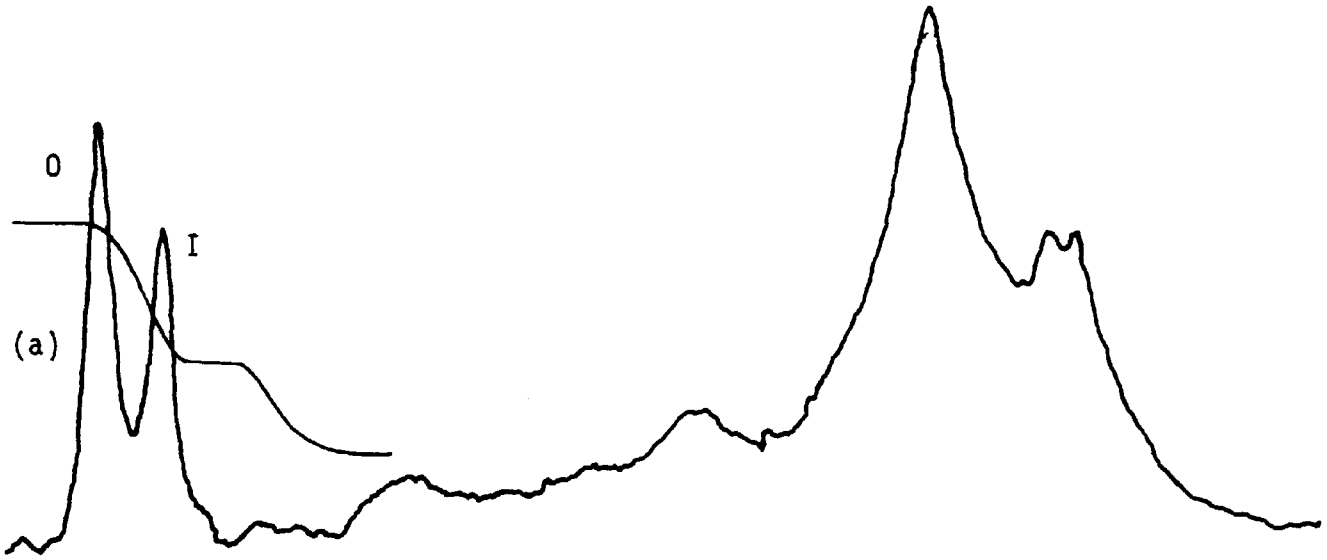

The integral ratio $\frac{O}{I}$ equals 1.8.

Recording the spectrum several hours later did not show any variation.

DIMENSIONS OF SINGLE BILAYER VESICLE

(b)

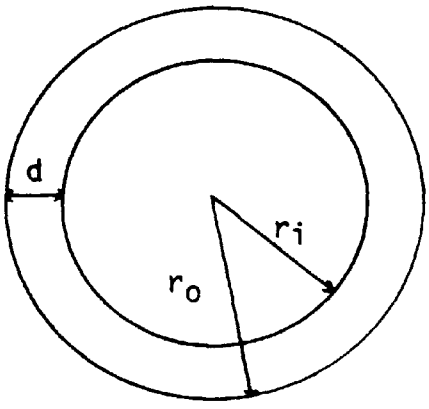

r_i and r_o are the internal and external radii of the vesicles, and d is the bilayer thickness.

where r_o and r_i are the outer and inner radii of the vesicles, respectively (Fig. II.6.(b)).

Assuming a bilayer thickness of 4 nm (from X-ray crystallography [47]), e.g. (i) can be written in the form:

$$\frac{r_o^2}{(r_o - 4)^2} = 1.8$$

i.e. $$r_o = \frac{14.40 \pm [(14.40)^2 - 4(0.80)(28.80)]^{\frac{1}{2}}}{2 \times 0.80}$$

i.e. r_o = 2.30 nm or r_o = 15.70 nm ... (ii)

The first of these values for r_o is ignored as it is smaller than the bilayer thickness. Hence the vesicle has an outer radius of 15.70 nm.

Determination of the outer diameter of the same population vesicles by electron microscopy (negative staining) (Fig. II.7) gave an average outer diameter of 30 nm which agrees with that determined by the nmr method. Furthermore, the E.M. micrographs show that the vesicles are unilamellar and free of contamination with large multilayer structures. This suggests that preparing small vesicles by the sonication method gives uniform size vesicles, and virtually all larger structures are reduced to small single bilayer vesicles [146] .

Various workers reported an outer:inner phospholipid ratio of approximately 2.0, including the results reported by this laboratory (Table II.1) which gives confidence to the validity of the nmr method; especially when it is considered that these workers have used different sonication times;

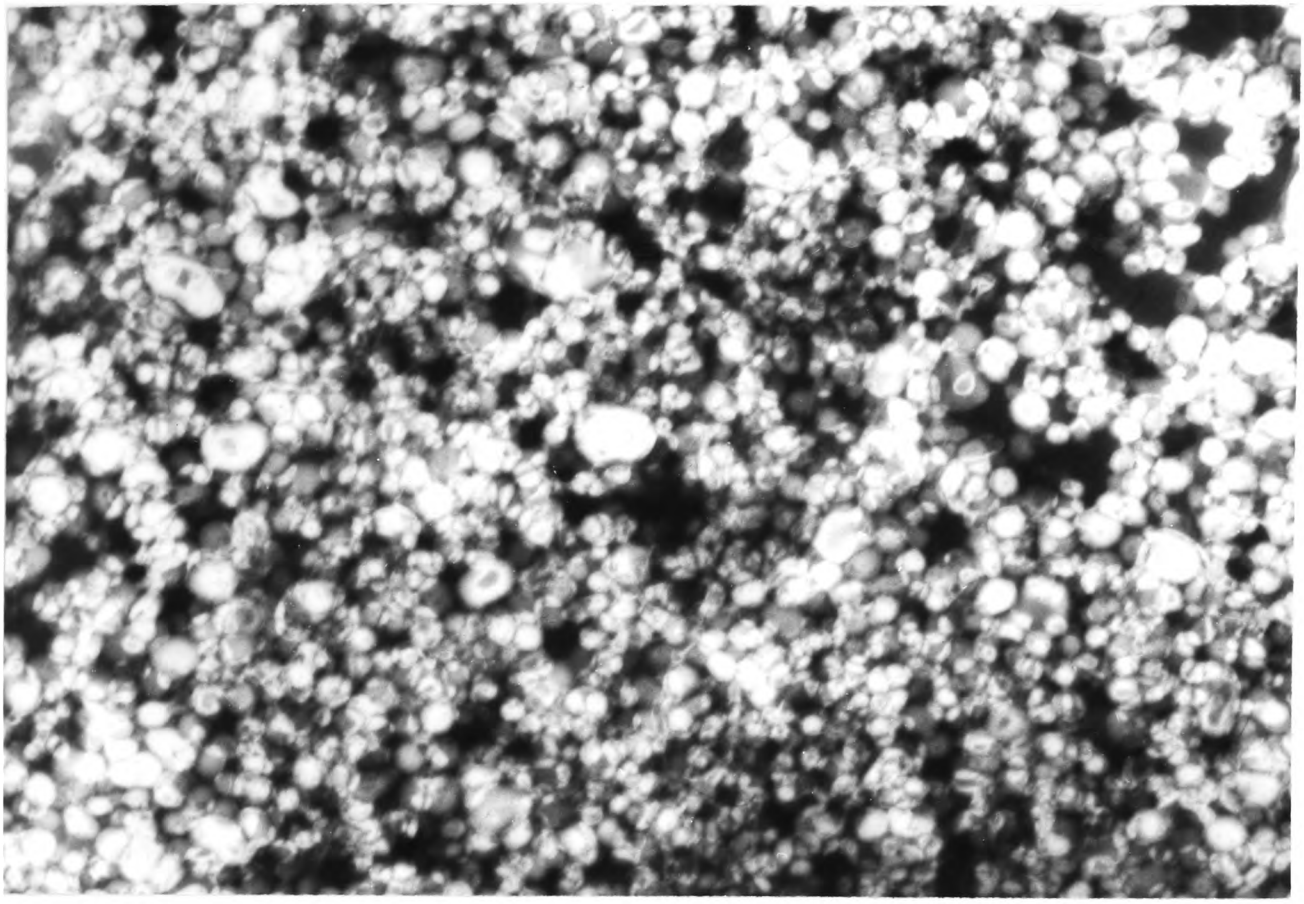

FIG.II.7. Electron micrograph of negatively stained sonicated Egg PC vesicles. The vesicles are uniform in size and free of multibilayer structures. The total magnification is X25000. The average diameter of these vesicles is 30 nm.

Table II-I

Summary of outer/inner phospholipid ratios in egg PC vesicles

Metal ion	O/I	Reference		Comments
		Proton (^{1}H) NMR		
$MnSO_4$	1.7	Michaelson et al.	[147]	Area determined from broadening.
$EuCl_3$	1.7	Michaelson et al.	[147]	
$Fe(CN)_6^{3-}$	2.0	Berden et al.	[146]	Ratio unchanged after 24 hours.
$Fe(CN)_6^{3-}$	1.9	Berden et al.	[146]	Metal trapped in vesicle interior.
$Fe(CN)_6^{3-}$	1.8	Berden et al.	[146]	Unfractionated vesicles.
$Fe(CN)_6^{3-}$	1.9	Berden et al.	[146]	Fractionated vesicles.
$Pr(NO_3)$	2.0	Barsukov et al.	[148]	
$MnSO_4$	1.5	Bystrov et al.	[149]	Sonicated for 10 min. determined from broadening.
$Pr(NO_3)_3$	2.1	Andrews et al.	[150]	$-N-CH_2-$protons.
$Pr(NO_3)_3$	2.1	Andrews et al.	[150]	$-O-CH_2-$protons.
$Tm(NO_3)_3$	2.1	Andrews et al.	[150]	
$Dy(NO_3)$	2.1	Andrews et al.	[150]	
$Tb(NO_3)_3$	2.1	Andrews et al.	[150]	
$MnSO_4$	1.7	Michaelson et al.	[151]	Determined from broadening.
$Eu(NO_3)_3$	1.7	Michaelson et al.	[151]	
$MnSO_4$	1.8	Kostelnik and Castellano	[152]	Determined from broadening.
$MnSO_4$	2.3	Hauser and Barnett	[153]	Determined from broadening.
$Nd(NO_3)_3$	2.3	Huaser and Barnett	[153]	
$PrCl_3$	1.8	Hunt	[154]	
		Carbon (^{13}C) NMR		
$YbCl_3$	2.1	Sears et al.	[155]	Synthetic PC, mono *N*-methyl enriched.
$PrCl_3$	2.1	Sears et al.	[155]	Synthetic PC, mono *N*-methyl enriched.
$PrCl_3$	1.75	Shapiro et al.	[156]	
$YbCl_3$	2.2	Yeagle et al.	[157]	Synthetic PC, mono *N*-methyl enriched.
		Phosphorus (^{31}P) NMR		
$Pr(NO_3)_3$	1.8	Bystrov et al.	[123]	NOE not considered.
$Pr(NO_3)_3$	2.0	Bystrov et al.	[123]	KNO_3 added, NOE not considered.
None	2.0	Hauser et al.	[125]	
$Nd(NO_3)_3$	2.0	DeKruijff et al.	[158]	NOE considered.
$PrCl_3$	2.1	Yeagle et al.	[157]	NOE suppressed.

different salt concentrations; and three different measured nuclei. In order for the NMR - paramagnetic ion technique to give accurate ratios of the outer to inner phospholipids in the vesicles the following nine conditions must be met:

1. Exchange between free and bound metal ions must be fast on the nmr time scale;

2. At low site occupancy metal ion binding sites are independant so that the shift reagent interacts similarly with all phospholipids on the vesicle surface;

3. Shift reagents do not alter the phospholipid chemically;

4. Metal ions do not penetrate the bilayer;

5. The vesicle preparation is homogeneous or the observed value will be a weighted average over all sizes present;

6. All phospholipids contribute to the NMR signal intensity;

7. Shift reagent is used at a concentration which does not cause significant aggregation, precipitation, or disruption of the vesicles;

8. The NMR spectrometer is operated so that the observed peak intensities accurately reflect the number of nuclei on the vesicle surface.

9. Shift reagent is used in sufficient concentration to allow separation of the inner and outer resonances and any overlap with other resonances is taken into account.

The assumption of fast exchange between metal ion and phospholipid has been accepted in the literature [144] . A minimum limit for the exchange rate is the chemical shift separation, ca.30 Hz (Fig. II.6), for the bound and free phospholipid. Since separation is complete with lipid/metal ratio as low as 0.05 [159] , the exchange rate is probably quite fast on the nmr time scale.

The NMR spectrum of the vesicles (Fig. II.3) recorded several hours after the addition of the paramagnetic lanthanide (Pr^{3+}) does not show any spectral changes which suggests that the vesicle dispersion is quite stable, and these are impermeable to the lanthanide cations. Undesired results can sometimes be obtained if gross variation in the [155] vesicle size occurred perhaps due to incomplete sonication. Non-homogeneous vesicle preparations will give outside/inside ratios that are weighted average of the ratios for the individual vesicle sizes. When the vesicles being studied are of sufficiently small size (see EM micrograph Fig. II.7) it is safe to assume that all of the phospholipids present contribute to the NMR signal. This assumption has been confirmed experimentally [158] .

However, using the lanthanide/NMR method the bilayer values of the vesicle can be calculated:

Bilayer volume = Total vesicle volume - Internal volume ..... (iii)

$$= \frac{4}{3}\pi r_o^3 - \frac{4}{3}\pi (r_o - 4)^3$$

$$= 1.62 \times 10^{-17} cm^3 - 6.73 \times 10^{-18} cm^3.$$

$$= \underline{9.47 \times 10^{-18} cm^3.}$$

(b) Vesicle Numbers

The gas chromatographic analysis of position 1 and position 2 of the acyl choline chains of egg PC (Table 1.1.) gives an average molecular weight of 767 g [160].

For the majority of the experiments performed the lipid concentration was 40 mg/ml. Therefore;

$$40 \times 10^{-3} g \text{ of lipid contain} = \frac{40 \times 10^{-3} \times N_A}{767}$$

$$= \underline{3.14 \times 10^{19} \text{ molecules}}.$$

where $N_A = 6.023 \times 10^{23}$, Avagadro's number.

However, since only 0.5 ml of the sonicated was pipetted in each 5 mm nmr tube, then the number of molecules present equals $\underline{1.57 \times 10^{19} \text{molecules}}$ .. (iv)

Now the No. of phospholipid molecules present in the outer monolayer of each vesicle = $\frac{\text{Total surface area of one vesicle}}{\text{Area occupied by one molecule}}$ ..... (v)

Assuming the area occupied by each molecule is $96 \times 10^{-16} cm^2$ (from X-ray studies [252]), equation (v) yields:

$$\frac{4\pi(15.71 \times 10^{-7})^2}{96 \times 10^{-16}} = \underline{3,231} \text{ molecules in the outer monolayer.}$$

and from the nmr integration (see above), the phospholipid molecules present in the inner monolayer equals:

$$\frac{3,231 \times 1}{1.8} = \underline{1795} \text{ molecules.}$$

Therefore total number of molecules (inner and outer) which are present per vesicle = 3,231 + 1795 = 5026 molecules.

These values are in close agreement with previously published results[1]. From equations (iv) and (iii), the number of vesicles present in 0.5 ml of sonicate =

$$\frac{\text{Total no. of molecules in 0.5 ml}}{\text{No. of lipid molecules present in 1 vesicle.}}$$

$$= \frac{1.57 \times 10^{19}}{5026} = \underline{3.12 \times 10^{15} \text{ vesicles}} \quad \ldots\ldots\ldots\ldots\ldots \quad \text{(vi)}$$

The internal volume of all vesicles present in 0.5 cm^3 of sonicate = Internal volume of one vesicle x total no. of vesicles,

i.e. from equations (vi) and (iii):

$= 6.73 \times 10^{-18} \times 3.12 \times 10^{15}$

$= \underline{2.09976 \times 10^{-12} \text{ cm}^3}$ ..... (vii)

- this represents $\frac{2.09976 \times 10^{-12}}{0.5} = \underline{4\%}$ of the total volume.

The total volume occupied by the vesicles =

Internal volume of all the vesicles + Bilayer volume of all the vesicles.

$= 2.09976 \times 10^{-12} + (9.47 \times 10^{-18} \times 3.12 \times 10^{15})$

$= \underline{2.9546 \times 10^{-2} \text{ cm}^3}$

Hence the remaining outer volume $= 0.5 - 2.9546 \times 10^{-2}$

$= \underline{0.47 \text{ cm}^3}$ .....(viii)

(c) Equilibrium number of ions inside the vesicles:

The extravesicular Pr^{3+} concentration = 5mM.

Therefore the No. of Pr^{3+} ions per 1 cm^3 $= 5 \times 10^{-6} \times N_A$

$= \underline{3.0 \times 10^{18}}$ Pr^{3+} ions outside.

Therefore the No. of Pr^{3+} ions which have to be transported inside each vesicle to achieve 5 mM Pr^{3+} inside $= \frac{\left(\frac{3.0 \times 10^{18}}{2}\right)}{3.12 \times 10^{15}} \times \frac{4}{100} = \underline{19.0 \ Pr^{3+} \text{ ions}}$

The No. of Pr^{3+} ions in 1 cm^3 x Internal volume of each vesicle

$$= 3.0 \times 10^{18} \times 6.73 \times 10^{-18}$$

$$= \underline{20.0\ Pr^{3+}\ \text{ions}} \quad \ldots\ldots\ldots\ldots\ldots\ldots \quad \text{(ix)}$$

Recently the Springer group [134] calculated the number of Na^+ ions transported inside the larger 240 nm vesicles prepared by the detergent - removal (dialysis) method [161]. They found that 39 x 10^3 Na^+ ions were transported per vesicle, and this concentration represents 10 mM inside.

The internal volume of the above vesicles =

$$\frac{4}{3}\ \pi\ r^3 = \frac{4}{3}\ \pi\ (120 - 4.0) \times 10^{-7\ \ 3}\ cm^3$$

$$= 6.50 \times 10^{-15}\ cm^3 \ldots\ldots\ldots\ldots\ldots\ldots\ldots\ldots \quad \text{(x)}$$

Therefore $\underline{\text{The internal volume of the vesicles prepared by dialysis method}}$
The internal volume of the vesicles prepared by sonication

$$= \frac{\underline{6.5 \times 10^{-15}}}{6.73 \times 10^{-18}}$$

$$= \underline{0.97 \times 10^3} \quad \ldots\ldots\ldots\ldots\ldots\ldots\ldots\ldots\ldots\ldots\ldots\ldots\ldots\ldots\ldots\ldots\ldots\ldots \text{(xi)}$$

Also, the concentration of Na^+ ions inside these large vesicles (10 mM) is greater by a factor of 2 compared with the concentration of Pr^{3+} (5 mM) inside sonicated vesicles.

Hence, comparing the experimental conditions used by the Springer group and by us gives:

$$\frac{39 \times 10^3}{0.97 \times 10^3 \times 2} = \frac{20.0}{} \; Na^+ \text{ ions} \quad \ldots\ldots\ldots\ldots\ldots\ldots\ldots\ldots (xii)$$

this agrees with the number of Pr^{3+} ions calculated in the present study (See Equation (IX)).

This result is significant since it indicates that using small unilamellar vesicles discrete (small) number of ions will cross the membrane during an approach to equilibrium.

Thus, valuable mechanistic information can be obtained from an NMR study of ion transport when the resonance frequency of an inside peak depends on the number of ions that have entered the vesicles[162]. Pike et al.[161] used computor simulated curves to analyse their NMR data which showed a distinction between processes by which the ions enter the vesicles one or a few at a time (such as via a diffusive carrier) and those by which the ions enter in large bursts (such as by pore activation). Further consideration of these factors are considered in the next chapter.

(d) Change in extravesicular ion-concentration during transport:

Now assuming that Pr^{3+} transport occurs to give an equilibrium concentration inside all the vesicles, then the total number of Pr^{3+} ions transported

= 20.0 x total number of vesicles in 0.5 ml

= $\underline{7.16 \times 10^{16}}$ Pr^{3+}

Therefore no. of Pr^{3+} ions left outside = initial Pr^{3+} ions outside - Total no. of Pr^{3+} transported.

= $1.50575 \times 10^{18} - 7.16 \times 10^{16}$

= 1.43415×10^{18} Pr^{3+} ions remaining outside.

- this still corresponds to 5 mM extravesicularly i.e. after complete transport of Pr^{3+} the extravesicularly concentration of Pr^{3+} remains effectively constant.

In fact the % of Pr^{3+} ions transported = $\frac{7.16 \times 10^{16}}{1.50575 \times 10^{18}}$ = 4.76%

= $\underline{4.76\%}$.

This corresponds to change in molar ity outside the vesicle equal to only

= $5 \times \frac{4.76}{100}$ = $\underline{0.238 \text{ mM}}$

II.3.6 Effect of sonicating Ln^{3+} with the vesicles:

In order to investigate the effect of lanthanide ions on the ^1H-nmr spectrum of sonicated vesicles the effect of sonicating lanthanide ions Pr^{3+} and Dy^{3+}

with preformed vesicles was briefly examined. 1 mM Dy^{3+} was added to sonicated egg PC vesicles, and the dispersion was re-sonicated for various length of time, and the ^{1}H-nmr spectra were recorded at the various time intervals between sonications. The changes in the spectra (Fig. II.8) are: the downfield shift and the broadening of signal I, and the simultaneous increase of the $\frac{o}{T}$ ratio. This indicates that the vesicles are opening and closing during the sonication process, thus equilibriating 1 mM Dy^{3+} inside. Note that Fig. II.8.(e), shows that a fraction of the signal remains "sharp" suggesting that a fraction of the vesicles remained intact. However, the broadening of a fraction of the signal while the rest of the signal remained unaffected can result from using inhomogeneous population of the vesicles [47]. The electron microscopy data presented in (Fig. II.7) shows that the sonication method used in this work produce vesicles which are homogeneous in size. This led to the conclusion that the sonication is a random process, and sufficient length of time is required to achieve reproducable results.

Hunt [154] reported that the transport of lanthanide ions (Pr^{3+}) inside sonicated vesicles leads to the shift and broadening of signal I.

The broadening of signal I is interesting because if the transport of ions inside the vesicles results in instantaneous equilibr ation of 5 mM Pr^{3+} inside (equal to extravesicular concentration) the "inner" choline headgroup signal would be shifted under the "outer" headgroup signal. Because this does not occur the transport of ions is thought to take place in successive "bursts" of metal ions to the inside of the vesicles which eventually reaches 5 mM Pr^{3+} . This result is similar to that obtained after successive sonications (Fig. II.8.(d)) where the inner choline resonance indicate that

Fig. II.8. EFFECT OF ADDING 0.15 mM Dy^{3+} TO PREFORMED VESICLES THEN SONICATING FOR VARIOUS LENGTHS OF TIME

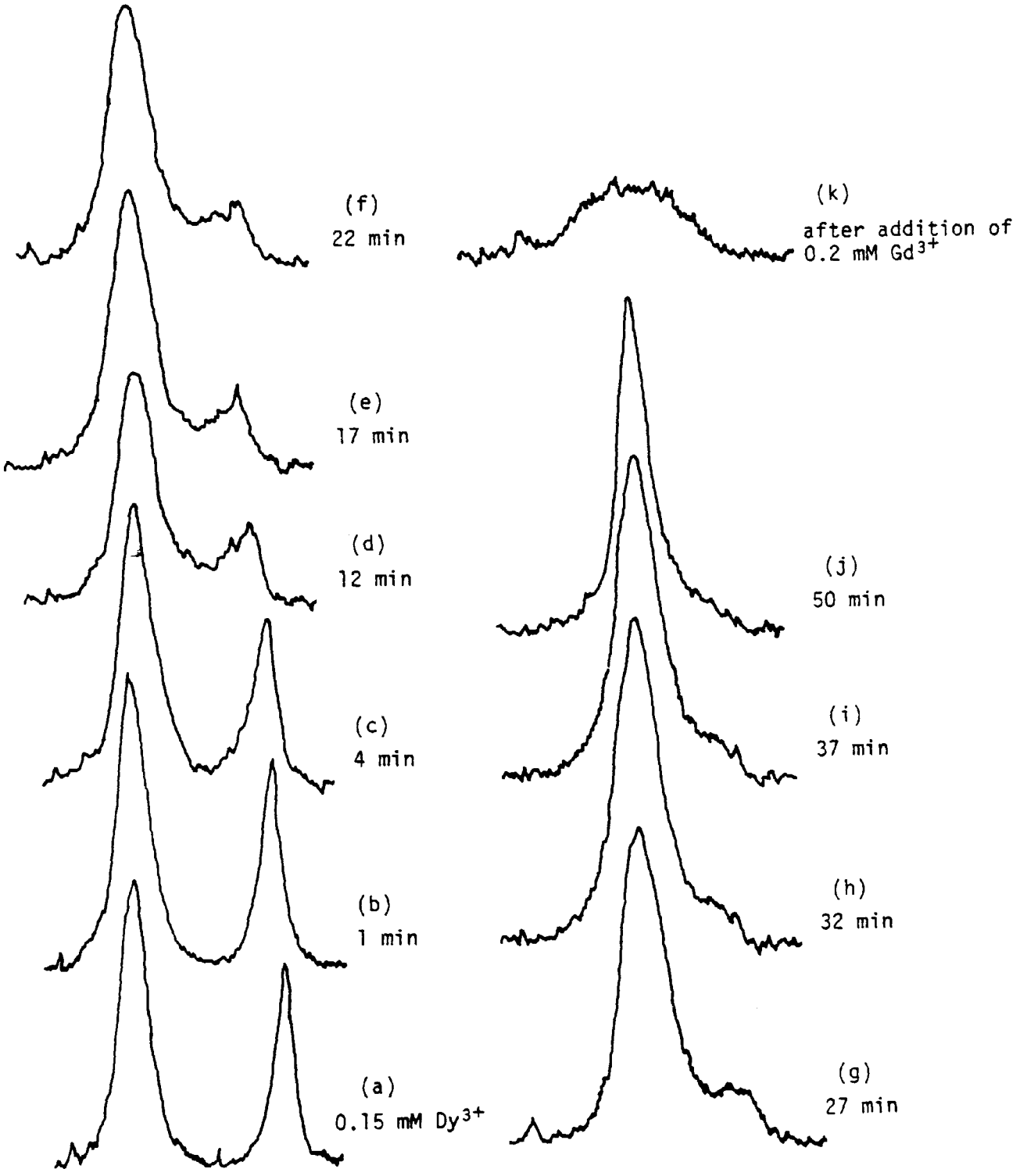

vesicle population contain various concentrations of Dy^{3+} . Repeated sonication causes all the inner choline signal to shift under the outer choline resonance (Fig. II.8.(j)).

It can be seen (Fig. II.8.(k)) that the addition of 0.2 mM Gd^{3+} to the vesicle dispersion containing 1 mM Dy^{3+} inside (by sonication) reveals a broad signal due to inner choline resonance. Hence, if the transport of lanthanide inside the vesicles causes the broadening of signal I, the transport of ions from inside to outside would be expected to cause the sharpening up of signal I. This hypothesis was tested by sonicating egg PC liposomes containing Dy^{3+} followed by the removal of the outside Dy^{3+} ions with ligand XE*. The inside to outside transport was achieved by adding the diamagnetic lanthanum to the outside of the vesicles such that it binds to the ionophore and thus diffusing to the inside. This experiment was unsuccessful because it was realised that the vesicles leaked as soon as the outside Dy^{3+} was removed by ligand XE, i.e. suggesting that the internal osmotic pressure caused the partial lysis of the vesicles.

Finally, (Fig. II.8)shows that the sonication of insufficient concentration of Dy^{3+} with the vesicles (i.e. less than one Dy^{3+} ion per vesicle) causes the downfield shift of signal I; but signal O moves upfield suggesting that the extravesicular concentration of Dy^{3+} is affected. Therefore, it may be important to mention that when lanthanide transport is followed by the nmr method sufficient concentration of the metal ions should be employed (e.g. 5 mM Pr^{3+}) such that the extravesicular concentration remains effectively constant after transport is completed.

* Ligandex "E". REANAL. BUDAPEST. HUNGARY.

CHAPTER III

IONOPHORES AND MECHANISMS OF TRANSPORT

CHAPTER III

IONOPHORES AND MECHANISMS OF TRANSPORT

III.1 Introduction

In order to investigate the problem of biological membrane transport mechanisms, the reconstitution of functionally active transporting substances is essential. Reconstitution has been successful in a growing number of membrane bound proteins and enzymes[27]. Only in a few cases e.g. ATPases can the protein be identified as a metal ion transporter, with successful reconstitution into lipid bilayers[27]. Even allowing for the difficulties in extraction, purification and reconstitution[163], restoration of functional behaviour in a pure bilayer system does not demonstrate the mechanism by which the protein operates, e.g. whether it acts as a channel or 'pore' or whether conformation changes result in a carrier type process. The possible mechanisms have been discussed many times and the evidence for them given[27]. However it has recently been admitted that the mechanisms will only be elucidated when physicochemical methods of sufficient power have been developed[163]. As indicated in chapter 1, NMR spectroscopy is one such method which has the potential for making a major contribution to the solution of transport mechanisms.

Because of the difficulties encountered in working with whole membranes and with reconstituted systems a large research effort has been made to study the mechanisms by which certain small molecules (known as "ionophores") render lipid bilayers permeable to metal ions[154][27][83]. In this way it was hoped that some understanding of the in vivo biological systems

would emerge from the model membrane studies. However the use of ionophores has had considerable application outside that of membrane permeability mechanisms, so that their study has become an important field of research [83]. The work described in this chapter aims to be a contribution to this study and in particular to the development of methods using NMR spectroscopy and the lanthanide ions. It is hoped that this work will lead to a better understanding of ionophore-mediated transport and to give insight on how improvements in these methods will allow them to be applied to reconstituted and whole membrane mechanisms.

The first evidence of a "carrier mechanism" of transport was provided by Pressman [164] who isolated the low mol. weight streptomyces metabolite valinomycin and demonstrated its ionophoretic "carrier" properties in a two phase (organic and aqueous) systems. Valinomycin, enniatins and polyethers are a group of neutral ionophores which have a group of oxygen atoms orientated towards the interior of the molecule. X-ray studies have shown these ionophores, on complexing with the metal ion, adopt a cyclic or cage-like structure with hydrophobic groups outwards that is essential for the solubilization in lipid media [164].

The second group of carrier type ionophores is the carboxylic acid or nigericin type and these include A23187, X537A which are non-cyclic but similarly to the first group of ionophores contain a variable number of oxygen atoms (Fig. I.11). The carboxylate group dissociates at pH ~ 7 and on complexing these ionophores adopt a cyclic structure [1]. The "carrier" properties of these ionophores was demonstrated by Hunt [50] using single bilayer sonicated vesicles and high resolution NMR technique. The synthetic ionophore NaFod and the naturally occurring antibiotic ionophore ionomycin

both contain a β- diketone group (Fig. I.11). The carrier properties of NaFod was demonstrated using the lanthanide probe ion Pr^{3+} [50], and its efficiency was compared with that of A23187 and X537A. The potential of synthetic ionophores such as NaFod in the development of medical and pharmacological research has encouraged other laboratories to study some of its ionophoretic properties. Gomperts et al.[165] have shown that NaFod stimulates the Ca^{2+} dependant K^+ efflux from human red blood cells and the Ca^{2+} dependant histamine release from peritoneal mast cells. Bulman, R.A. (personal communication) found that NaFod extracts Pu^{IV} which suggests its potential as a detoxicant. Recently, this laboratory developed interest in introducing extra functional groups in order to improve NaFod specificity for a given metal, its ionophoretic action and its antibiotic activity.

Further investigations using carrier ionophores and sonicated vesicles revealed that in transporting charged complexes (metal ion - ionophores) across the polar/non-polar interface work must be done to cross the acyl chain region. Theoretical analysis showed that the diffusion over this so called "image potential barrier" is the rate determining step, and the calculation of the height of this barrier for the non-equilibrium state gives results which agree well with the experimentally determined activation energy[166].

A second class of ionophores was demonstrated in black lipid membranes [167](BLM) and were shown to translocate substances via a membrane "channel" or "pore". BLM is an artificial membrane first developed by Mueller[36] and involves the application of a small amount of lipid dissolved in a solvent over a tephlon diaphragm immersed in aqueous solution. The lamellaethen formed gradually becomes thinner and after an intermediate stage a "black" lipid membrane forms. Electrical conductivity measurements using Alamethicin or

Gramicidin have shown these ionophores translocate ions through discrete channels or pores in the BLM[37][34]. There was a considerable confusion in the literature with respect to alamethicin primary structure, its interaction with lipid bilayer and the mechanism of pore formation[307]; e.g. alamethicin was believed to be a ring peptide with 18 amino acids until Martin and Williams[168] showed (in 1976) that the molecule is linear and consists of 19 amino acid residues. And although the amino acid sequence suggests hydrophobic character, the NMR data of Lau and Chan suggests a predominant hydrophilic interaction[85]. The development of the NMR technique enabled Hunt et al.[86] to study the molecular mechanisms of channel formation. They suggested that four alamethicin aggregates stacked like staves in a barrel form the aqueous channel[86].

Generally ionophores have been a powerful tool in the study of the properties of mitochondria, chloroplast and chromatophores[27]. They have also been used to trigger certain metabolic processes that depend on the flux of Ca^{2+} across membranes[70]. The research on the possibility of incorporating carriers such as A23187 in liposomes in the treatment of metal storage diseases has shown increased Fe excretion in mice[83]. Monensins are used in a large scale as a feed addition for livestock and the rationaleis that carboxylic ionophores control endemic coccidiosis in poultry gut and promote a more favourable fermentation of cellulose in the Bovine rumen[83].

Until recently the physiological relevance of the NMR method of following ionophore mediated transport was severely limited because ion transport was too rapid to monitor by the nmr method[169]. Recently, Hunt[50] developed an ^{1}H-nmr method for studying transmembrane transport of paramagnetic ions across sonicated vesicles, and suggested that useful

information regarding the transport rate can be obtained providing that lanthanide shift probes (as in contrast with broadening probes) are used in combination with low concentrations of the ionophore i.e. such that instantaneous equilibr ation of the probe ion in the interior of the vesicles doesn't occur. In the present study the above ^{1}H-nmr method is used to study the molecular mechanisms of ionophore mediated transport occurring in egg PC vesicles. The metal ion-ionophore stoichiometries are determined, and the activation energies are calculated. The effect of varying chloride ion concentration and varying the extravesicular pH is discussed in relation with the transport rate obtained.

III.2 Materials and Methods

Chemicals

The calcium ionophores 8 - [1-(ethyl-1-carboxy-pyrrole-2)]-4-carboxy-5-methylamino-benzoazole)-spiro (5,5) hendecan-3, 9, 11 - trimethyl - 6, 7 - dioxane (A23187) as the free acid and 3 - methyl-5-bromo-6- 7 - ethyl-4-hyroxy-3,5-diethyl-6-oxo-7-[5-ethyl-3-methyl-5-(ethyl-5-hydroxy-6-methyl-2-tetrahydropyranyl)-2-tetrahydrofuryl]heptyl salicylic acid (X537A) were gifts from Lilly Research Laboratories (Indianqpolis - USA) and Roche Products Limited (Welwyn Garden City - Herts. England) respectively. Stock solutions of these ionophores (2 to 5 mg/ml) were prepared in chloroform-methanol and stored at room temperature in the dark. The calcium ionophore ionomycin was obtained as the calcium salt from Squibb Institute (Princeton. N.J.). The free acid was obtained by extracting the calcium salt three times with a (2:1 v/v) of spectroscopic hexane/4 N HCl mixture. Complete extraction of the free acid was determined using UV spectrophotometry unicam (SP1800). The absorption maximum of the calcium salt is at 300 nm while that of the free acid is at 280 nm (Fig.III.1).The free acid in the hexane fraction did not show absorption at 300nm(Fig.III.1)and this was consequently diluted to 25 mls hexane giving a stock solution of 10 mg/25 ml which was stored at -5°C.

The synthetic ionophore 1,1,1,2,2,3,3-heptafluoro-7,7-dimethyloctane-4,6-dione (known as Fod) was obtained as the sodium salt from Lancaster Synthesis (Lancaster, England). Stock solutions were prepared either in D_2O (1 mg/1ml) or in chloroform-methanol (1mg/2ml) and stored at room temperature.

FIG.III.1. UV SPECTRA OF IONOMYCIN AS THE FREE ACID[b] AND AS THE Ca^{2+} SALT[a]

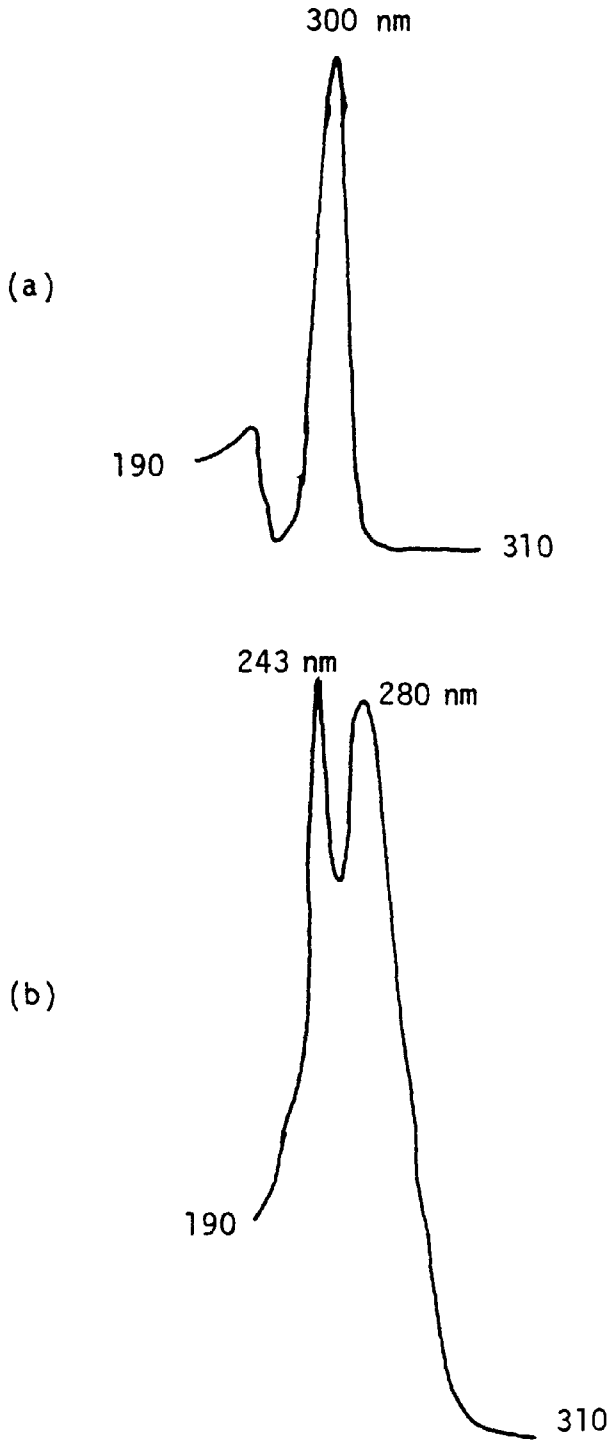

The calcium salt of Ionomycin displays a single absorption at 300 nm (a) while the free acid displays two absorption maxima at 243 nm and 280 nm (b).

Experimental Methods

III.2.1 Ionophore mediated transport of paramagnetic lanthanide ions monitored by ^{1}H-nmr

An ^{1}H-nmr method developed by Hunt [50] allows the monitoring of ion diffusion into single bilayer vesicles. Fig. II.3.a. shows the ^{1}H-nmr spectrum of egg PC vesicles at 50°C, i.e. above the gel to liquid-crystal phase transition temperature of the lipid, so that the high resolution signals are seen from the acyl chains (H), the terminal methyl group of the acyl chains (M) and the headgroup choline methyls (C). As first shown by Bergelson [144] the extravesicular addition of paramagnetic lanthanide ions separates the extravesicular head-group signal (O), and the intravesicular head-group signal (I) (Fig. II.6.(a)). Such shifts are now well documented (See Chapter I) and are caused by a pseudocontact, dipolar interaction of the lanthanide ions (which are in rapid exchange between the D_2O and the phosphate sites on the extravesicular lipid head-groups) with the neighbouring protons. The separation of the signals "O" and "I" thus results principally from the downfield shift of the extravesicular head-group signal "O", but a small upfield shift at signal "I" is also observed [50] .

When the lanthanide ions diffuse or are carried across the lipid bilayer into the intravesicular region, the rise in intravesicular concentration of probe ions causes signal "I" to move downfield towards signal "O". By measuring the decreasing shift difference $\Delta\nu$(I-O) between "O" and "I" as a function of time, the rate of diffusion or transport can be obtained.

III.2.2 Method of addition of the ionophores

There were two extravesicular and two intravesicular methods used to introduce the ionophores into the nmr tube containing the vesicle dispersion. The first extravesicular method involved pipetting a chloroform solution of the ionophore into an empty nmr tube and removal of the solvent with N_2 followed by evacuation for 10 minutes. 0.5 ml of the sonicated vesicles were then added to the nmr tube containing the solid ionophore, and the tube was placed in a thermostated water bath for 30 minutes. The tube was occasionally shaken by hand to aid partitioning of the ionophore into the bilayer. The second extravesicular method involved the addition of small amounts (5-6 µl) of the D_2O solution of the ionophore (e.g. Nafod) to 0.5 ml of vesicles in the nmr tube.

The first intravesicular method involved mixing of the chloroform solutions of the lipid and the ionophore in the sonicating tube followed by evacuation and then sonication as described in Chapter II. This method sites the ionophore in the lipid bilayer itself. The second intravesicular method involved the addition of a D_2O solution of the ionophore to the dry lipid in the sonicating tube followed by shaking for 90 minutes in a flask shaker, then sonication of the liposomes. This method allows the distribution of the ionophore in the D_2O regions outside and inside the vesicles.

Transport experiments were initiated by the addition of small amounts (5 - 10µl) of the D_2O solution of the lanthanide (to achieve 5 mM outside) or in the case of Nafod, the addition of the D_2O solution of the ionophore to the vesicles containing lanthanide ions and a timer was started as soon as mixing was achieved.

III.2.3 Calibration graph

A calibration graph is required to calculate the concentration of the lanthanide ions transported into the vesicles by the ionophore.

A small volume (3-5 µl) of $PrCl_3$ stock solution was dissolved in the required volume of D_2O giving a 0.5 mM Pr^{3+} solution. This was added to the dry lipid in the sonicating tube and the contents were shaken for 90 minutes using a flask shaker. The liposomes formed were sonicated as in Chapter II. The sonicated vesicles will then contain equal concentrations of Pr^{3+} in the intra and extravesicular spaces. 0.5 ml of these vesicles were pipetted into a 5 mm nmr tube. The extravesicular concentration was adjusted to 5 mM Pr^{3+} using the stock solution of the metal. 0.5 µl methyl cyanide was added as the internal standard. After shaking the nmr tube the ^1H-nmr spectrum was recorded and the chemical shift of the inside peak (Signal I) was measured with reference to the standard. Various concentrations (0-150 mM) saline (NaCl in D_2O) was added extravesicularly to the same tube and the chemical shift was measured after each addition. The above method for preparing the vesicles was repeated for various Pr^{3+} concentrations between 0.5 mM and 4.5 mM. A graph of the measured shifts against intravesicular concentration of Pr^{3+} (mM) was plotted (Fig. III.2).

III.2.4 Transport of gadolinium into sonicated vesicles monitored by ^1H-nmr

Calculation of results:

In the cases of Pr^{3+} and Dy^{3+} the rate of ionophore-mediated transport of the

PLOT OF INTRAVESICULAR [Pr^{3+}] V SHIFT OF PEAK I

FIG. III. 2

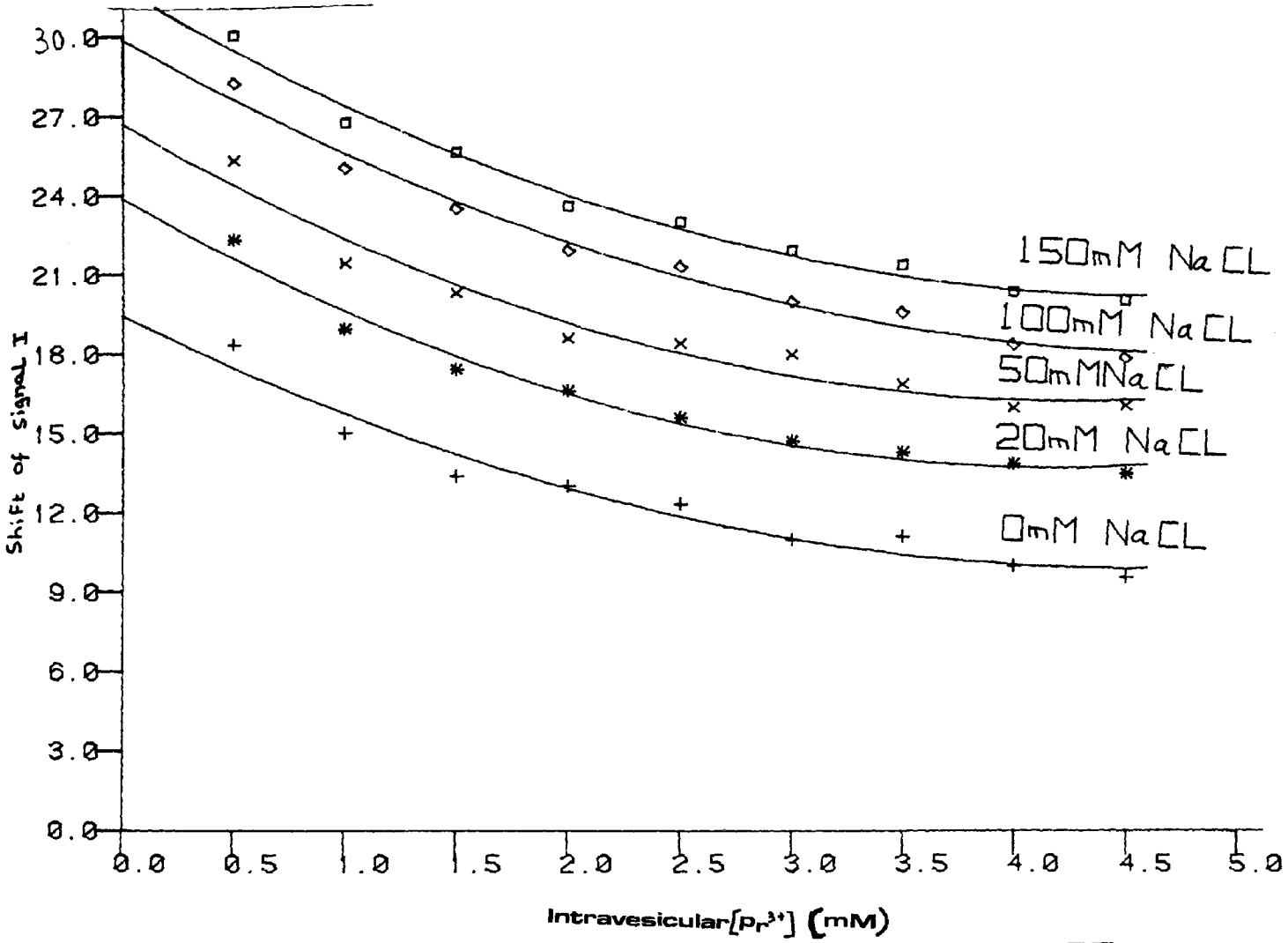

FIG. III. 2 SHOWS A CALIBRATION GRAPH OF EGG PC VESICLES AT VARIOUS CONCENTRATIONS OF Cl^-. THE SHIFT OF SIGNAL I REPRESENTS THE ACTUAL ION CONCENTRATION INSIDE THE VESICLES.

ions can be measured in terms of shift differences between signals O and I. However, in the case of gadolinium this is not possible as the transport of one gadolinium ion inside the vesicle causes the complete loss of the ^{1}H-nmr internal head-group signal (Fig. III.12) and therefore the observed signal I arises from those vesicles without gadolinium ions inside. Thus, as gadolinium is transported into the vesicles the observed signal decreases in intensity but does not broaden [170] . The rate of transport can therefore be calculated as follows:

The diffusion of gadolinium through the vesicle can be described by the equation:

$$\frac{d\bar{c}_i}{dt} = K_1 C_o - K_1 \bar{c}_i \quad \ldots\ldots\ldots\ldots\ldots\ldots\ldots\ldots \quad (1)$$

where C_o is the gadolinium concentration in the extravesicular medium and $\bar{c}_i$ is the average concentration of gadolinium inside the vesicle. The appropriate boundary conditions are: at t = o, $\bar{c}_i$ = o; at t = oo, $\bar{c}_i = C_o$. The solution to equation (1) satisfying these conditions is:

$$\bar{c}_i\ (t) = C_o\ (1 - e^{-kt}) \quad \ldots\ldots\ldots\ldots\ldots\ldots\ldots\ldots \quad (2)$$

where $K = K_1 = K_{-1}$

The observed intensity of the ^{1}H-nmr signal from the inner head-group signal I, $S_{(t)}$, is thus proportional to the probability that a particular vesicle contains no gadolinium ions inside, P(O,t) ; thus following ref[170]:

$$P(O,t) = \exp(\bar{n}(t)) \quad \ldots\ldots\ldots \text{[from ref. 170]}$$

where $\bar{n}(t)$ is the average number of gadolinium ions per vesicle at time t, $\bar{n}(t)$ is given by:

$$\bar{n}(t) = V.\bar{c}_i(t).N \quad \ldots\ldots\ldots\ldots\ldots\ldots\ldots\ldots\ldots\ldots \quad (3)$$

where N is Avagadro's number, V is the intravesicular volume and $\bar{c}_i(t)$ is the average gadolinium concentration in the extravesicular space at time t, $S_{(t)}$ is given by the expression:

$$S_{(t)} = S_{(o)} \exp\left\{ - VC_oN\ (1-e^{-kt}) \right\} \quad \ldots\ldots\ldots\ldots\ldots\ldots \quad (4)$$

where $S_{(o)}$ is the signal intensity at t=0.
when $K_t \ll 1$ equation (4) simplifies to:

$$S_{(t)} = S_{(o)} \exp\left\{ - VC_oNK_t \right\} \quad \ldots\ldots\ldots\ldots\ldots\ldots\ldots \quad (5)$$

and this equation may be used to analyse the data in the initial time period.

Using equation (5), the slope of the semilogarithmic plot of the height of signal I against time gives the product VC_oNK and not simply the intrinsic rate constant K_1.
We define an observed rate constant K', where

$$K' = VC_oNK \quad \ldots\ldots\ldots\ldots\ldots\ldots\ldots\ldots\ldots\ldots\ldots\ldots\ldots \quad (6)$$

The observed rate K' is simply the probability per unit time for the transport

of a gadolinium ion from the extravesicular to the intravesicular space. The intrinsic rate constant K_1 can then be calculated from K using equation (6), where V is the known vesicular volume and C_o is the initial external gadolinium concentration.

Thus using equation (6) the rate of gadolinium transport by the ionophore is calculated from the slope of the semilogarithmic plot of signal I against transport rate.

III.2.5 pH measurements

After the extravesicular addition of 5 mM Pr^{3+} the initial pH of the vesicle dispersion was measured at 25°C using a pre-calibrated pH meter (Orion Research, model 701A). The final pH of the vesicles was measured after the ion transport inside the vesicles was completed. The effect of the ionophore on the final pH was ignored since only a few microgrammes were used.

III.3 Experimental Results

III.3.1 Ionophore mediated transport of paramagnetic ions across single bilayer vesicles monitored by the ^{1}H-nmr method:

In the following experiments 20 µg A23187 was allowed to equilibriate with 0.5 ml of egg PC vesicles, followed by the extravesicular addition of 5 mM Pr^{3+}. The time dependant changes of the ^{1}H-nmr spectrum of the vesicles is shown in Fig. III.3 . The difference in signal O and I can be seen to decrease with time as the intravesicular concentration of praseodymium $[Pr^{3+}]_i$ rises. The extravesicular concentration $[Pr^{3+}]_o$, remains effectively constant since the internal volume of the vesicles is only a few per cent of the total volume of the sonicate (See Chapter II). Fig. III.4.(a). shows a plot of the shift of signal I with respect to the unshifted outside signal δ (O-I) against time. Note that at t = several hours, peak "I" is found under peak "O", i.e. equilibration of 5 mM Pr^{3+}has taken place between outside and inside the vesicles. Since a reading of the initial separation, i.e. at zero-time can not be obtained due to the time taken to add the metal ions and the ionophore, and the time spent to record the spectrum, a zero-time reading giving the initial separation of the peaks is obtained by extrapolating the graph in Fig.III.4.(a). to intersect with the Y-axis. A plot of the difference between the initial separation and $\Delta\delta$ (O-I) against time is shown in Fig. III.4.(b). In order to convert these experimental values into an intravesicular concentration of Pr^{3+} in mM the calibration graph described in the methods section and shown in Fig. III.2. was used. Fig. III.5. depicts the results obtained during the transport of Pr^{3+} by A23187 and shows the linear increase of the intravesicular concentration of Pr^{3+} with time, and

FIG.III.3. ^{1}H-NMR SPECTRA OF EGG PC VESICLES AT 50°C IN THE PRESENCE OF 5mM Pr^{3+}

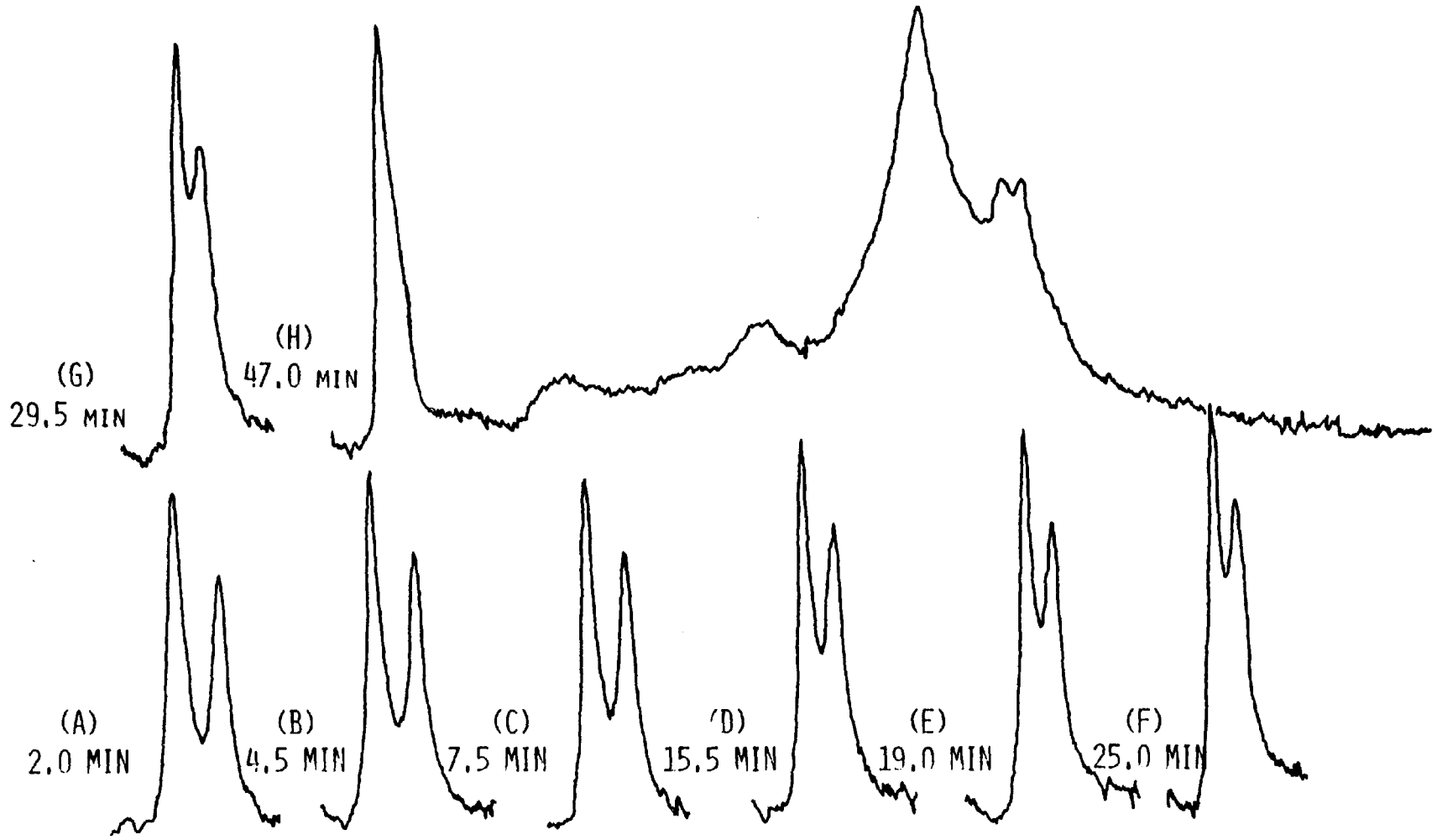

THE TRANSPORT OF Pr^{3+} BY THE IONOPHORE A23187 (20 µg PER 0.5 ml OF VESICLES) CAUSES THE TIME DEPENDENT DOWNFIELD SHIFT OF SIGNAL "1" ((A)-(H)). AT TIME t=47 MIN...SIGNAL 1 IS SHIFTED UNDER SIGNAL "0" INDICATING THAT THE INNER AND OUTER $[Pr^{3+}]$ EQUALS 5 mM.

FIG. III. 4(A)

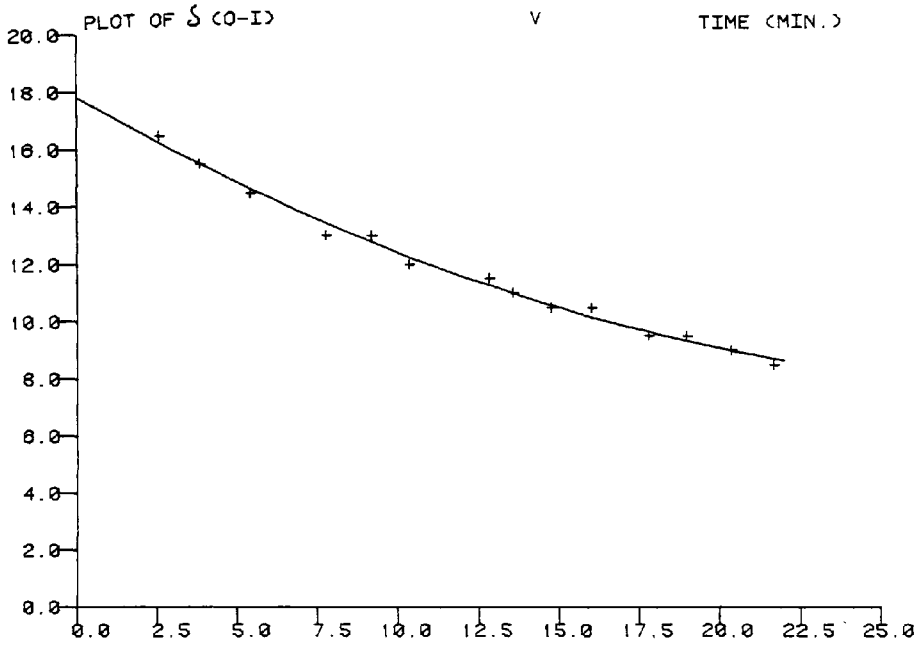

FIG. III. 4(B)

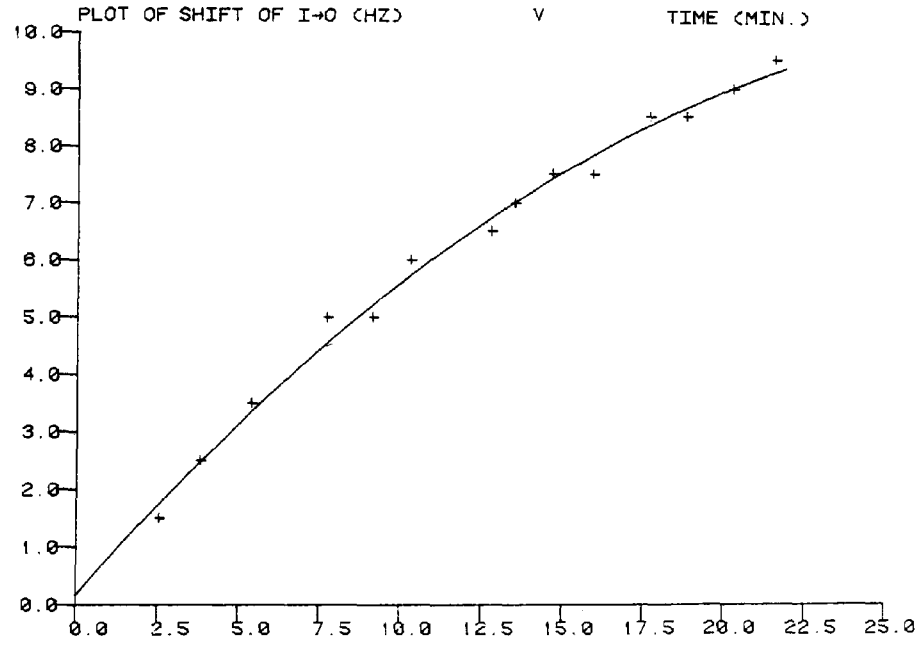

FIG. III. 4 (A) SHOWS THE DOWNFIELD SHIFT OF SIGNAL I TOWARDS SIGNAL O. NOTE THAT THE INITIAL SEPARATION INTERCEPT WITH THE Y AXIS EQUALS 17.8
FIG. III. 4(B) SHOWS THE SHIFT OF SIGNAL I IN HERTZ AGAINST TIME IN MINS.

FIG. III. 5

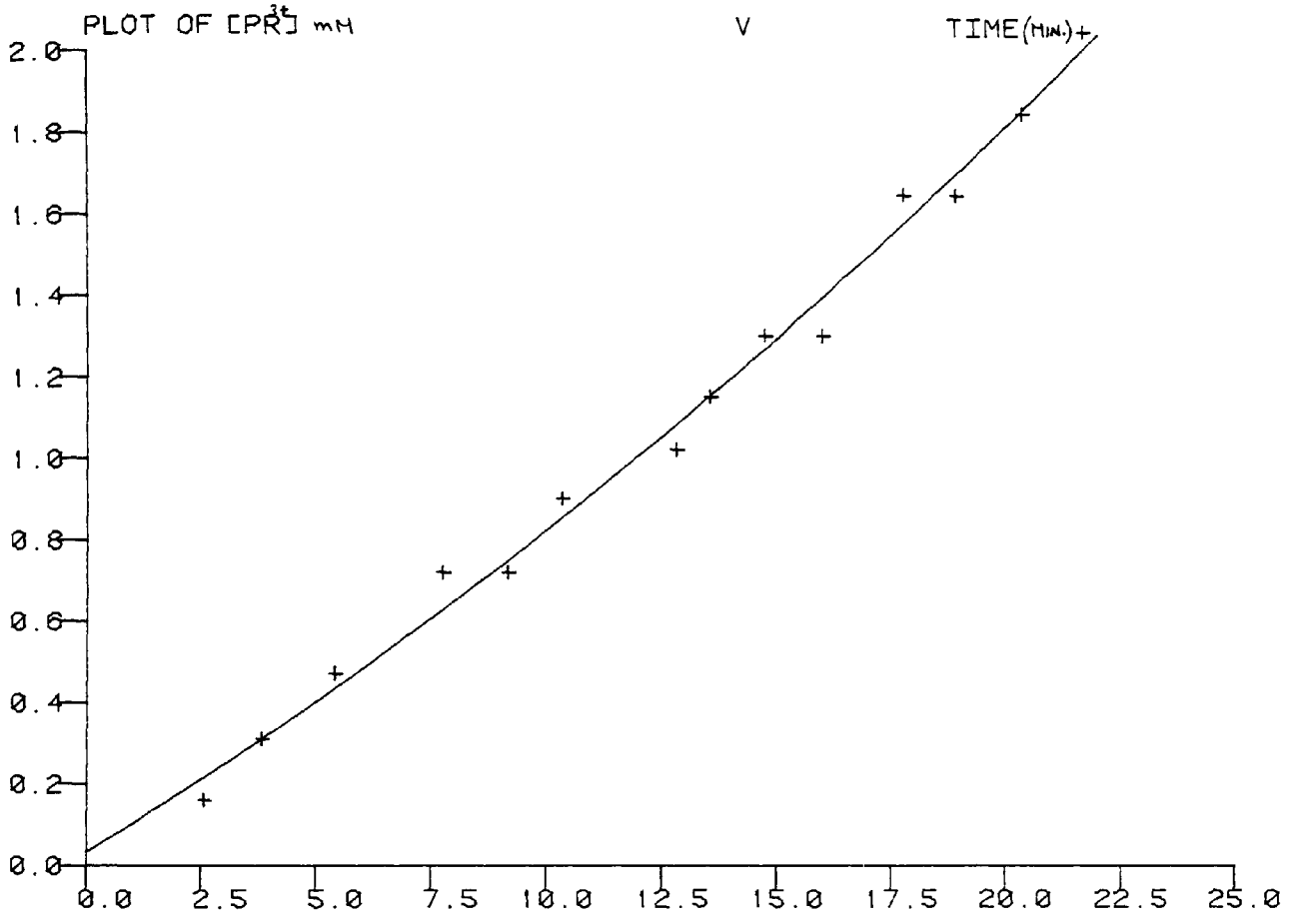

FIG. III. 5 SHOWS THAT THE TRNSPORT OF Pr^{3+} BY A23187 FOLLOWS A FIRST ORDER KINETICS. THE SLOPE OF THE ABOVE GRAPH SHOWS THAT THE RATE EQUALS 9×10^{-2} mM/MIN.

indicates that the transport rate is zero order with respect to $[Pr^{3+}]_i$. That is, the rate at which Pr^{3+} ions arrive in the intravesicular space = $d[Pr^{3+}]_i/dt = K_o$, the zero order rate constant. The slope of the line in Fig.III.5 then gives the value of K_o for this concentration (30 µg per 0.5 ml) of A23187.

III.3.2 Comparison of the rate of lanthanide ion transport across sonicated vesicles mediated by carrier ionophores:

Equimolar concentrations of NaFod (12.5 µg), A23187 (20.0 µg) and ionomycin (27.0µg) were used to transport the lanthanide probe Pr^{3+}. The results presented in Fig. III.6 shows that the rates of transport (the slopes) are 5.8×10^{-2}mM/min, 15.6×10^{-2}mM/min and 16.3×10^{-2}mM/min for NaFod, A23187 and ionomycin, respectively. Therefore, the transport activity of these ionophores is in the order ionomycin > A23187 > NaFod (III.6.).

However, during the transport of Pr^{3+} by the above ionophores the ^{1}H-nmr spectrum (Fig. III.3) show that the linewidth of the inside choline resonance undergo a time dependant broadening. Hunt[154] in the initial report on these methods used the time-dependant increase in line-width of signal "I" as a measure of the lanthanide transport. Later the time-dependant shifts of signal I were used[166]. In order to evaluate the two methods the increase in line-width caused by ionophore mediated transport is investigated in the following section.

FIG. III. b

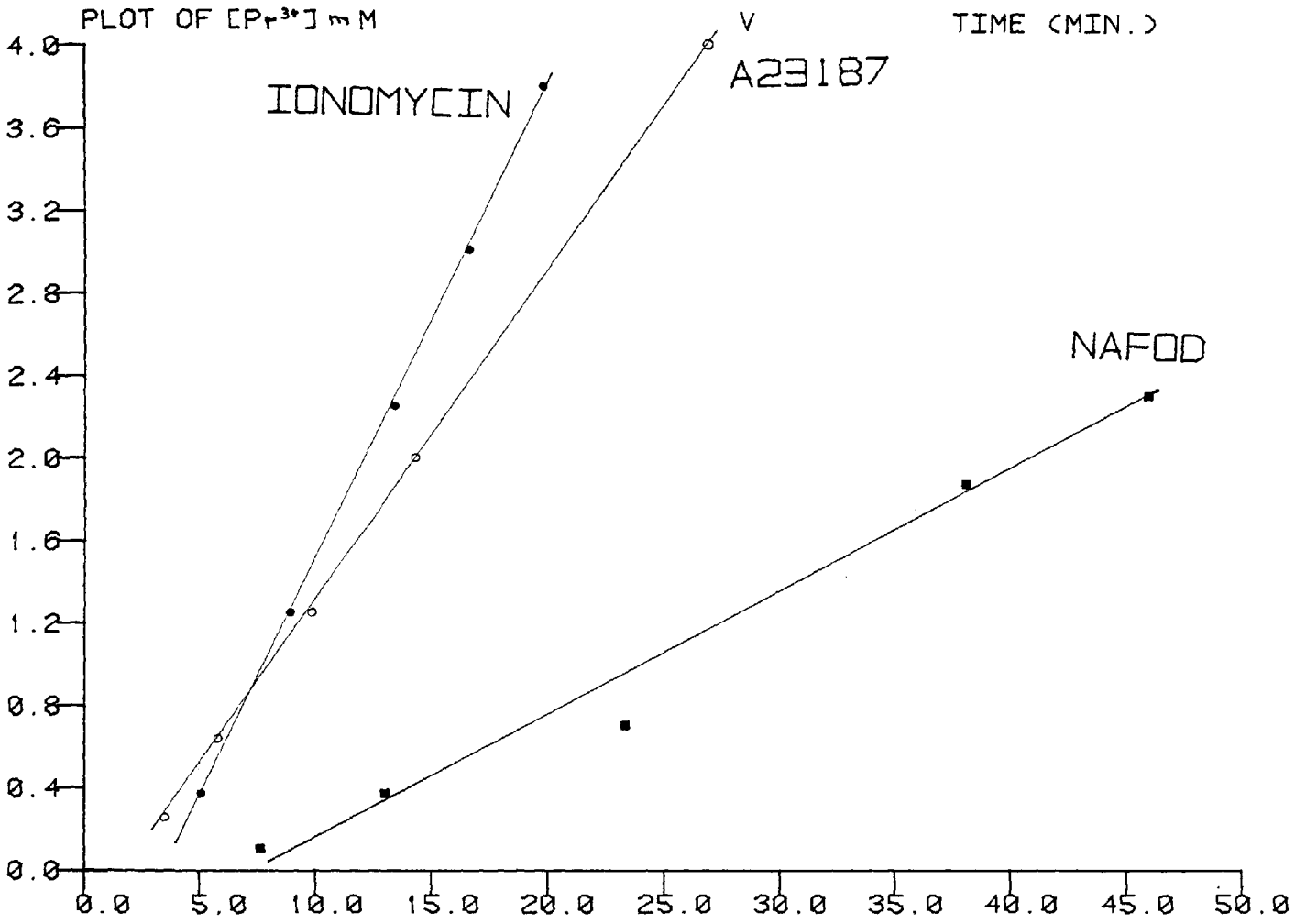

FIG. III. b SHOWS THAT IONOMYCIN IS MORE EFFICIENT THAN A23187 OR NAFOD IN TRANSPORTING Pr^{3+} INTO SONICATED VESICLES.

III.3.3 Broadening of Signal I:

The following experiments investigate the factors causing line broadening of the inner choline signal I. Fig. III.7 shows the results of two experiments where the same concentration of ionophore (60 µg NaFod) but different probe ions (Pr^{3+} and Dy^{3+}) were used for transport. The increase in linewidth of signal I is shown to be greater with Dy^{3+} compared with Pr^{3+} as expected from the value of the electronic relaxation times of these metals. However, using the same concentration of the probe ion (5 mM Pr^{3+}) the increase in linewidth of signal I is greater with NaFod than with ionomycin or A23187 (Fig. III.8). Therefore, the broadening of signal I is a function of the probe ion used as well as the metal-ionophore complex present.

The reason for the differences in signal "I" broadening caused by the ionophore mediated transport was investigated using X537A, A23187, ionomycin and NaFod; and the lanthanide probes Dy^{3+} and Pr^{3+} . The rate of transport of Dy^{3+} and Pr^{3+} by each of these ionophores was measured using the time-dependant downfield shift of the inner choline signal; and the results obtained were related to the rate of broadening of signal I caused during Dy^{3+} and Pr^{3+} transport (Tables III.1 (a) and (b)). These show that vast differences in the rate of cation transport and the rate of signal broadening occur.

Using Pr^{3+} (Table III.1. (a)) the rate of transport by any of the three ionophores as measured by the downfield shift of signal I is consistently greater than the rate of transport obtained by the time dependent broadening of signal I. However, using X537A and A23187 gives the closest agreement

FIG.III.7 'H NMR SPECTRA SHOWING Dy^{3+} AND Pr^{3+} TRANSPORT BY EQUAL CONCENTRATION OF NaFod

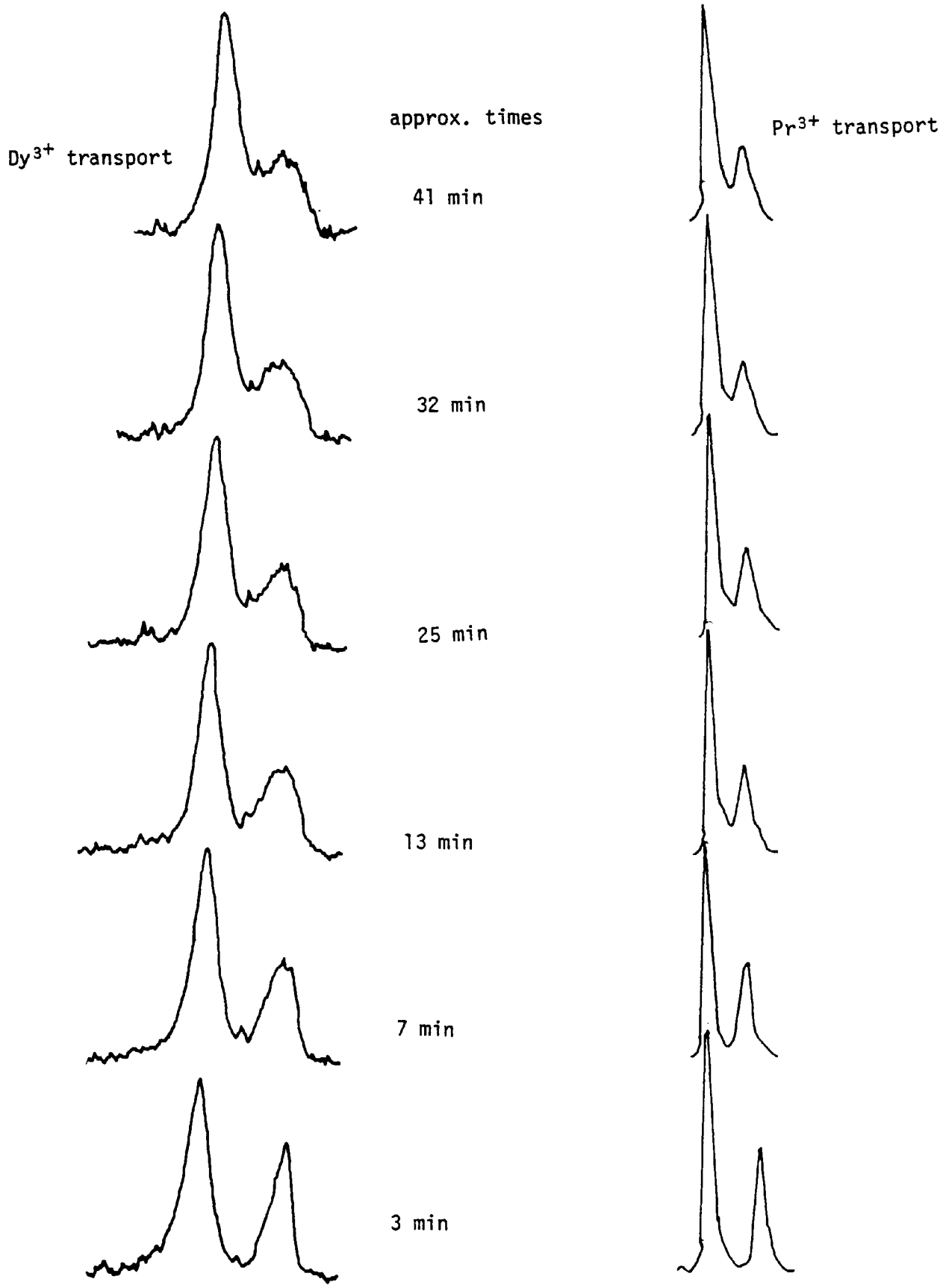

Dy^{3} transport causes extensive broadening of the 'H NMR signals compared with Pr^{3} transport. This is to be expected due to the difference in the electronic relaxation times between Dy^{3+} and Pr^{3+}.

FIG. III. 8

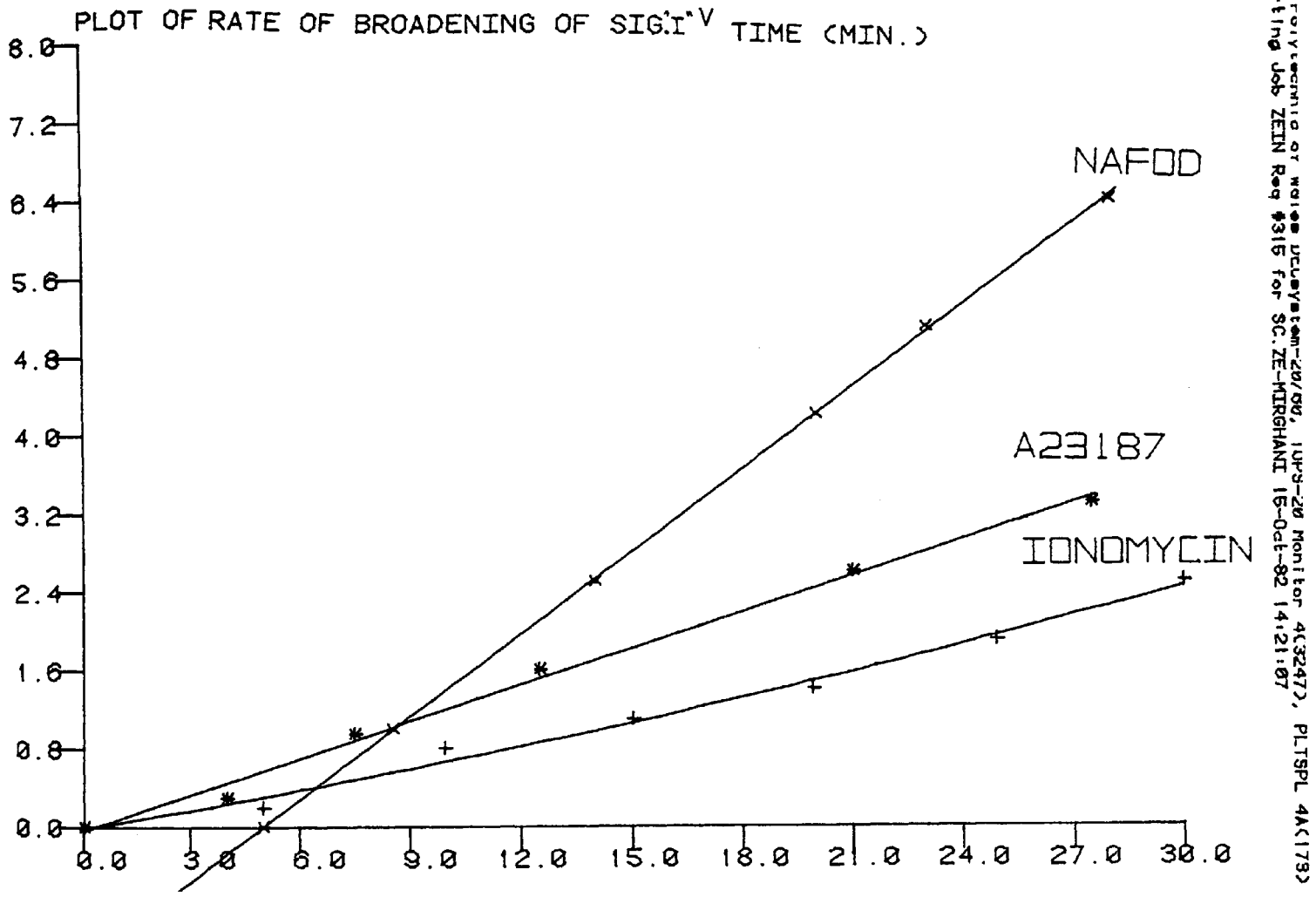

FIG. III. 8. SHOWS THAT THE BROADENING OF SIGNAL "I" CAUSED BY THE IONOPHORS IS GREATER WITH NAFOD THAN WITH A23187 OR IONOMYCIN

Table III.1

Summary of the Rates of Transport of Pr^{3+} and Dy^{3+} by Selected Ionophores through the Phospholipid Bilayer

(a)

Ionophore	Rate of Transport of Pr^{3+} determined from the shift of I → O $\Delta\delta$ (O-I) mm/min.	Rate of Transport of Pr^{3+} determined from the Broadening of signal I. $\Delta\nu_{\frac{1}{2}}$ mm/min.
40 mg Ionomycin	0.400	0.0787
60 mg NaFod	0.254	0.0889
40 mg A23187	0.0857	0.0526
40 mg X537A	0.0641	0.0453

(b)

Ionophore	Rate of Transport of Dy^{3+} determined from the shift of I → O $\Delta\delta$ (O-I) mm/min.	Rate of Transport of Dy^{3+} determined from the Broadening of signal I. $\Delta\nu_{\frac{1}{2}}$ mm/min.
40 mg Ionomycin	1.07	0.73
20 mg NaFod	0.31	0.30
40 mg A23187	1.21	0.57
40 mg X537A	0.074	0.070

between the two methods of measurement. NaFod and X537A show that (Table III.1.(b)) the rate of Dy^{3+} transport measured by the downfield shift of signal I is much greater than the time dependent broadening of signal I. These results suggest that the use of inefficient ionophores X537A and NaFod causes greater broadening than that shown by ionomycin and A23187 (see the transport results of Dy^{3+} table III.1.(b)). They further demonstrate that the rate of broadening is dependent upon the electronic relaxation time of the transported metal ion.

However, if the transport of lanthanide ions inside the vesicles causes the broadening of signal I, the transport of ions from inside to outside would be expected to cause the sharpening up of signal I. This hypothesis was investigated by sonicating egg PC liposomes containing Dy^{3} followed by the removal of the outside Dy^{3+} ions with ligand XE. To help the ionophore to diffuse inside the vesicles, 5 mM of Lanthanum (Diamagnetic) was added extravesicularly, and the inside to outside transport of Dy^{3+} was followed by observing the sharpening up of signal I. This experiment was unsuccessful because it was discovered that the vesicles leak as soon as Dy^{3+} ions were complexed with ligand XE* due to osmotic lysis. Similar experiments using Fe^{3+} have produced identical results, plus the effect of Fe^{3+} on phospholipid oxidation which is known to cause leaky vesicles [103]. It is shown in Fig. III.2 of this thesis that chloride ions cause an increase in lanthanide induced shift of the ^{1}H-nmr choline signals of egg PC. Fig. III.9 depicts the results of the effect of chloride ions on the time depend nt broadening of signal I occurred during transport initiated by 40 µg A23187 and 5 mM Pr^{3+}. The broadening of signal I is shown to be in the order: 150 mM NaCl inside and outside > 150 mM NaCl outside > 0 mM NaCl. This is consistent with the

* See page 103

FIG. III. 9

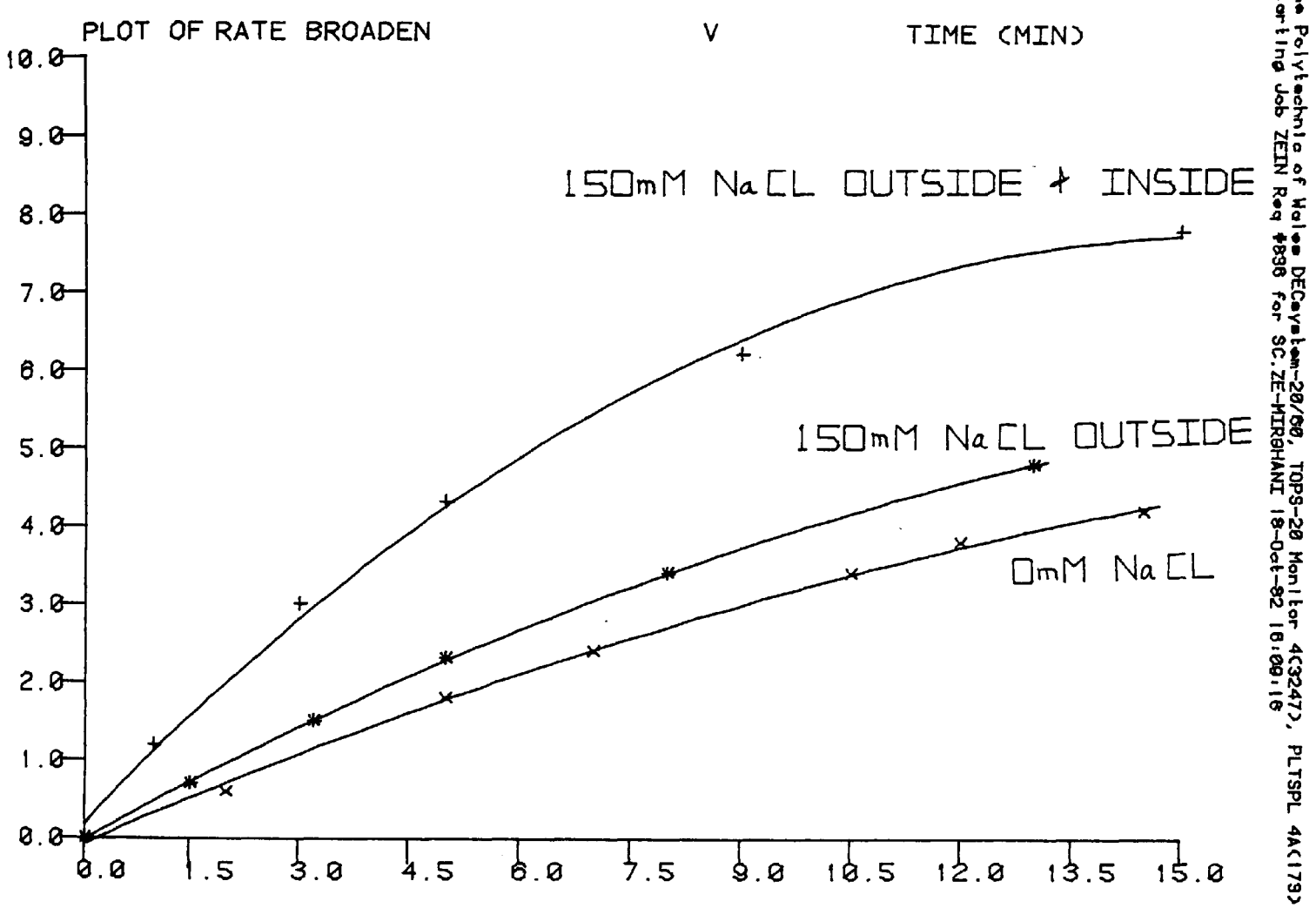

FIG. III. 9. SHOWS THAT USING THE SAME IONOPHORE (NAFOD) THE RATE OF BROADENING OF SIGNAL "I" INCREASES IN THE PRESENCE OF CL^-. CHLORIDE IONS INSIDE THE VESICLES CAUSE EXTENSIVE BROADENING.

fact that chloride ions interact with the lipid headgroups thus lowering the zeta potential and enhancing the binding of the metal ions (See Chapter II).

III.3.4 Metal ion - ionophore stoichiometries:

The experiments carried out to investigate the nature of the transported complex involved the measuring of Pr^{3+} transport by various concentrations of the ionophores. Fig. III.10 (a) show a plot of the log of the transport rate against the log of ionophore (NaFod) concentration. The slope yields a stoichiometry of 2.9 which shows that three ionophore molecules are involved in complexing a single Pr^{3+} ion. Similar plots using A23187 (Fig. III.10 (b)) and ionomycin (Fig. III.10 (c)) yield slopes equals to 1.85 and 1.1 showing that the stoichiometries are 2.0 and 1.0 respectively. These measured stoichiometries show that ionomycin and A23187 form charged complexes with the metal ion, $[Pr\ (ionomycin)\ ]^{+}$ and $[Pr\ (A23187)_2]^{+}$, whilst NaFod forms neutral complexes, $[Pr(NaFod)_3]$.

III.3.5 Activation energies:

The transport of Pr^{3+} across egg PC vesicles was measured at various temperatures but constant ionophore concentration. The Arrhenius plot (Fig. III.11) shows the measured rate of transport against $\frac{1}{T}$, where T is the absolute temperature. The slope is equivalent to $\frac{E^*}{R}$ where E^* is the activation energy and R is the universal gas constant. From Fig.

(a)
NaFod

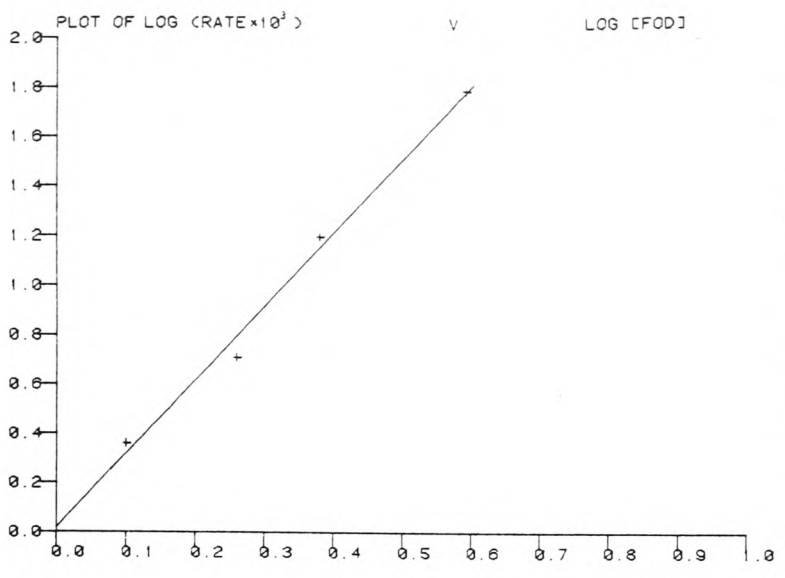

(b)
A23187

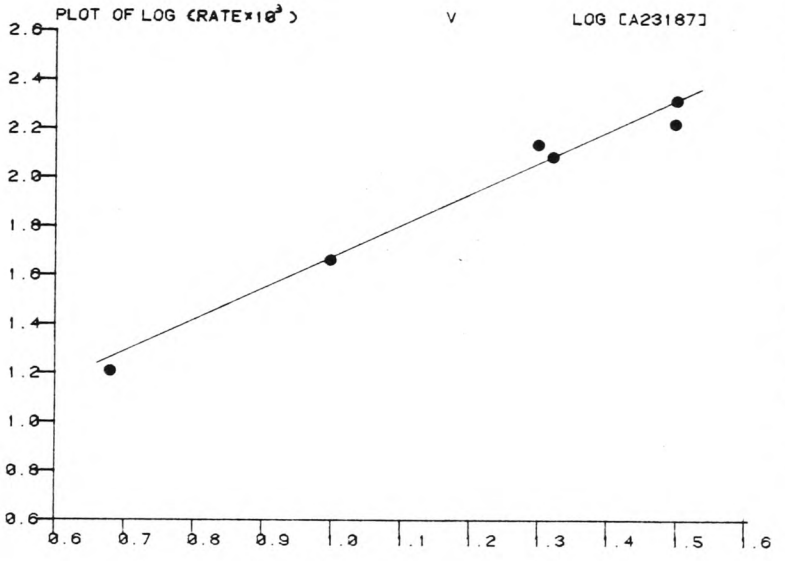

(c)
Ionomycin

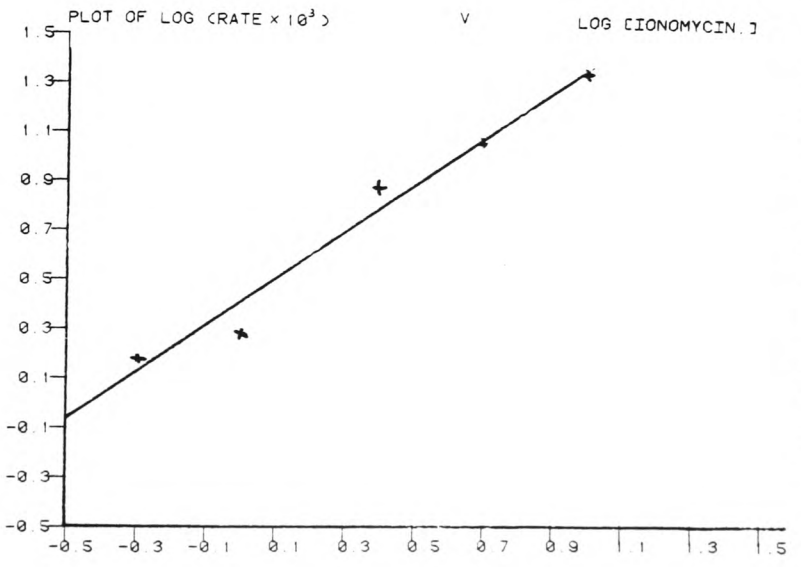

Fig.III.10. The slopes of the stoichiometric plots are 2.9, 1.85 and 1.1 for NaFod, A23187 and Ionomycin respectively.

III.11 (a) (b) and (c) E* is calculated to be 57.4 kJ/mole for NaFod, 102.92 kJ/mole for A23187 and 96.0 kJ/mole for ionomycin.

III.3.6 Transport of Gd^{3+} across the vesicles by carrier ionophores:

The lanthanide probe Gd^{3+} belongs to the second group of paramagnetic ions that have long relaxation times causing relaxation effects resulting in extensive line broadening (Chapter II). The addition of 0.2 mM Gd^{3+} to egg PC vesicles in the presence of 5 mM Pr^{3+} causes the complete broadening of the outer choline resonance. The addition of 0.2 mM Gd^{3+} alone to the egg PC vesicles can be seen to cause the complete loss in the intensity of the outer head group signal. Hence, the sharp signal remaining is attributed to the internal headgroup resonance (Fig. III.12 (b)). The transport of Gd^{3+} by 5 μg NaFod (Fig. III.12) causes the time dependant, loss of the inner choline signal. It has been shown by Degani et al.[170] that the arrival of a single Mn^{2+} ion inside the vesicle causes the complete loss of the inside choline signal (by broadening into the base line) originating from that vesicle. The above experiment shows that the use of lanthanide broadening probes results in a similar broadening to that shown by transition metal ions, and further demonstrates that the vesicles without Gd^{3+} ions inside exhibit sharp "inner" choline resonance (Fig. III.12). However, from measuring the time dependent loss of the inner choline signal intensity, the transport rate of Gd^{3+} by NaFod can be calculated (see Calculation of results section III.2.4). A plot of the log of signal intensity against time (Fig. III.13) is seen to be linear, which shows that the arrival of a single Gd^{3+} ion inside the vesicle

(a)
NaFod

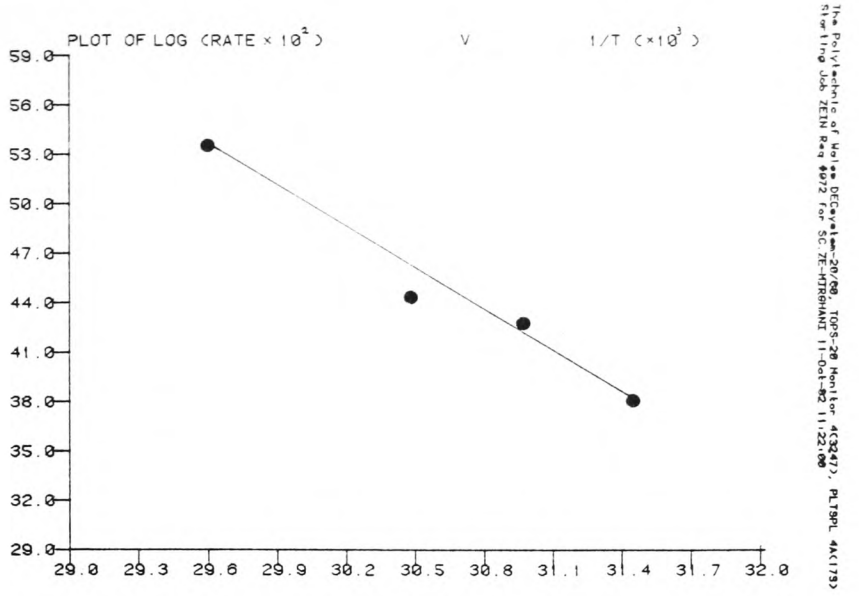

(b)
A23187

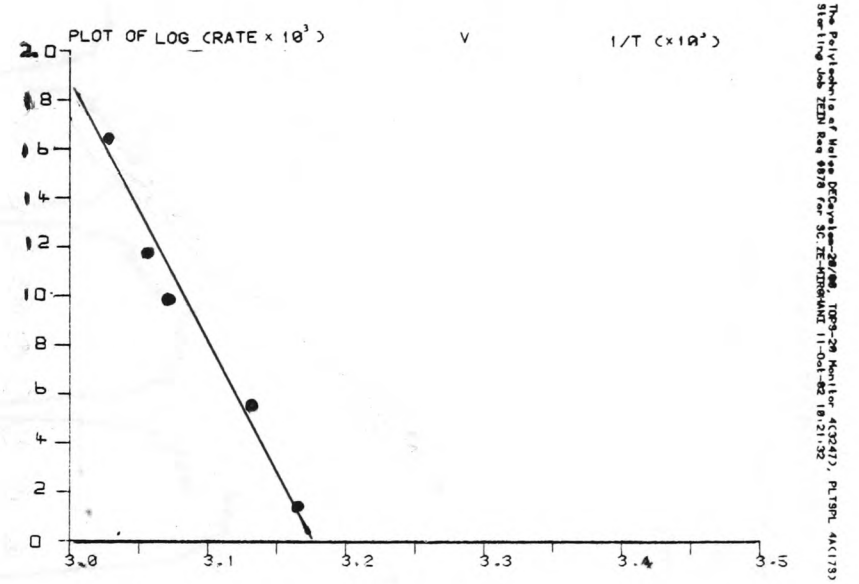

(c)
Ionomycin

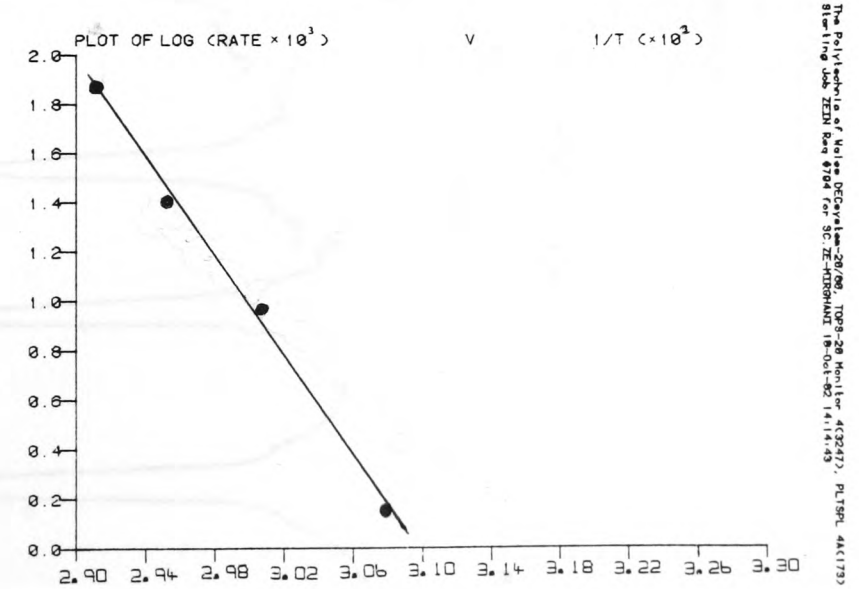

Fig.III.11 shows that Arrhenius plots give the activation energies 57.4 kJ/mole, 102.92 kJ/mole and 96.0 kJ/mole for the transport mediated by NaFod, A23187 and Ionomycin respectively.

FIG. III.12 ^1H NMR SPECTRUM OF EGG PC VESICLES SHOWING THE TIME DEPENDANT LOSS OF INTERNAL CHOLINE SIGNAL

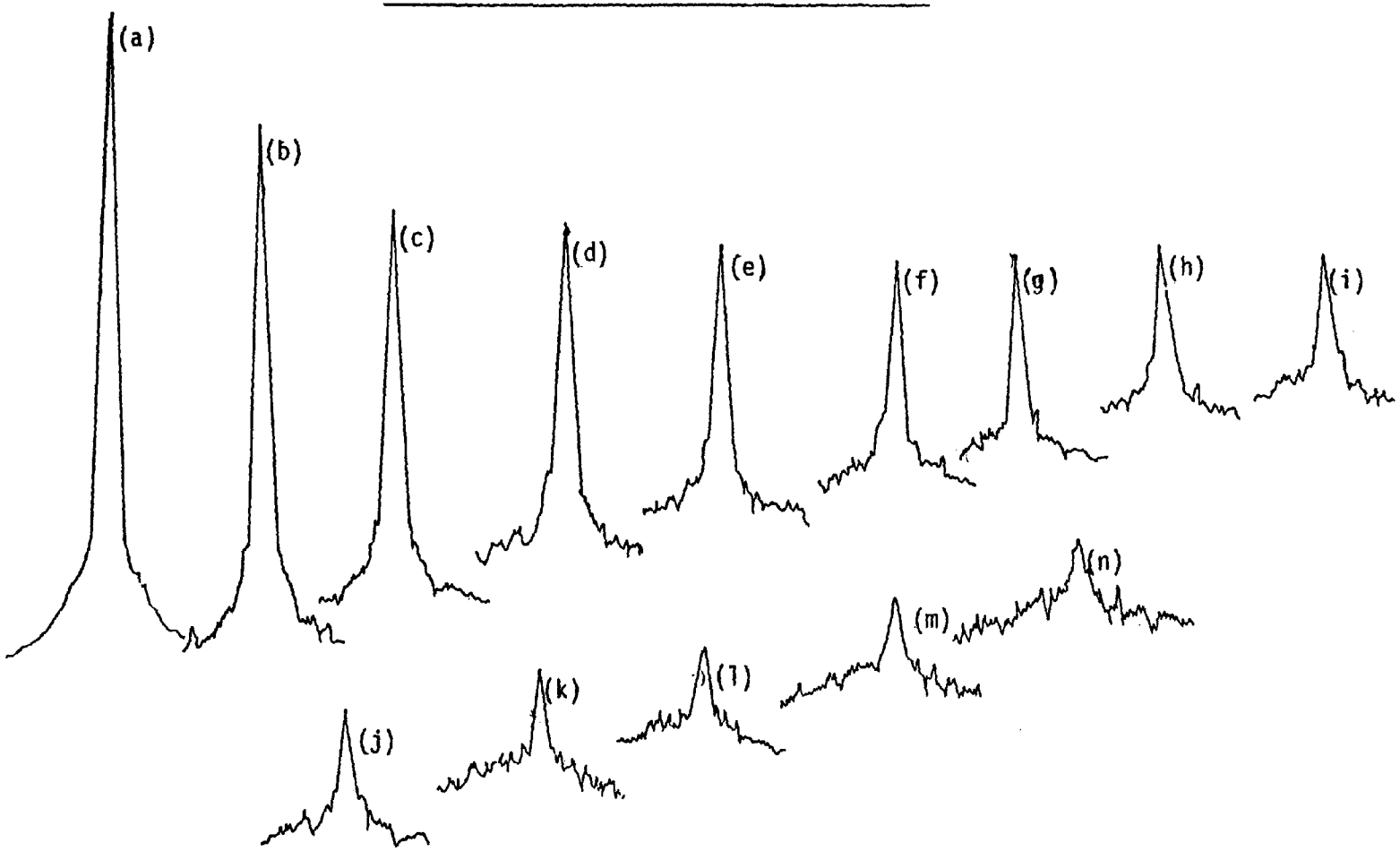

The transport of Gd^{3+} inside the vesicles causes the complete broadening of the inner choline signal. The spectra showing head group signals (O + I) before adding Gd^{3+} (a); after adding Gd^{3+} (b); after adding Na Fod (c); and at measured time intervals [(d) - (n)].

FIG. III.13. PLOT OF LOG OF SIGNAL I AGAINST TIME (MIN)

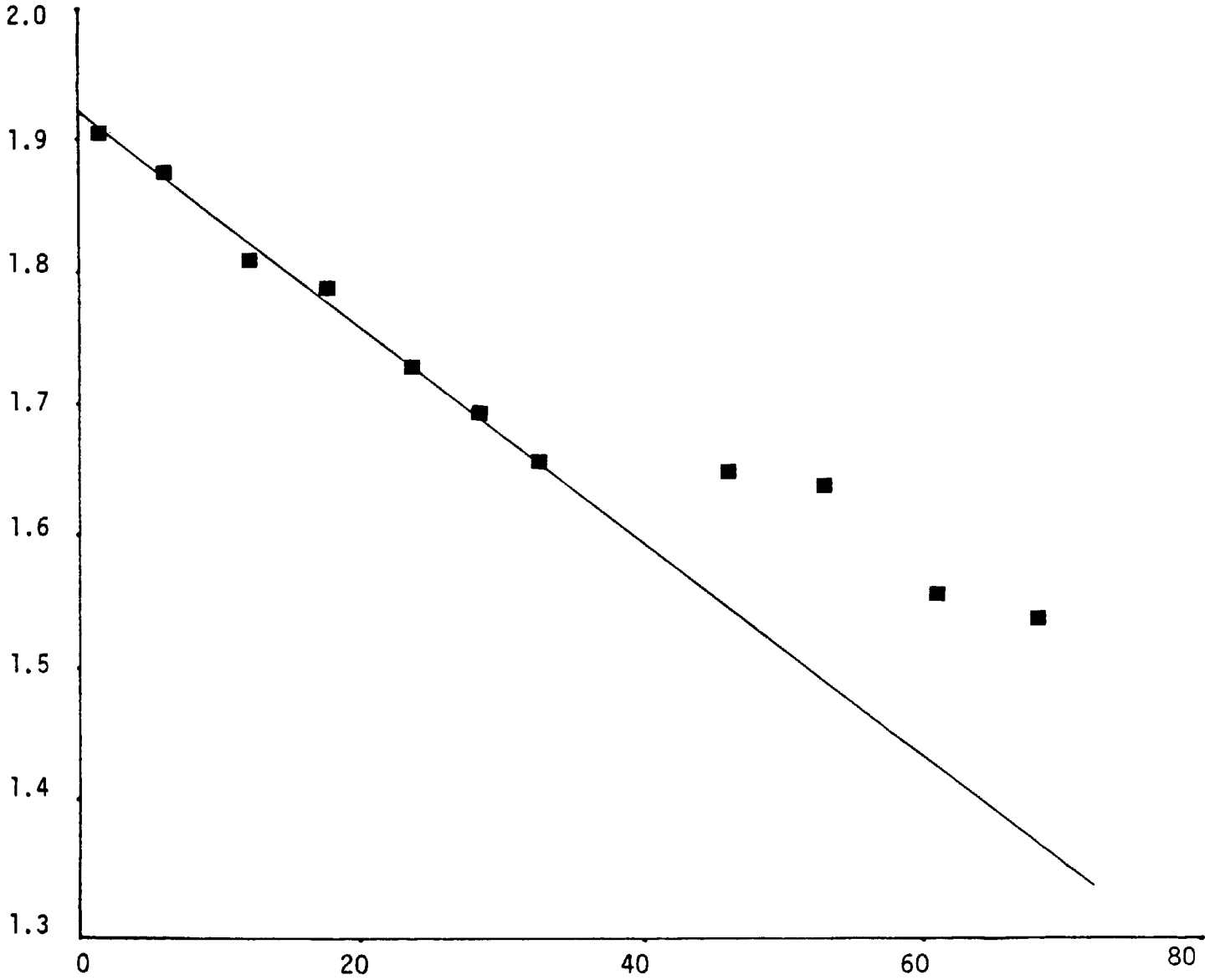

The transport of Gd^{3+} (0.2 mM) by NaFod (5 μg/ml) causes the loss of signal I intensity. The rate of transport is calculated to be (slope) = 5.52×10^{-3} mM/min.

results in the complete broadening of the "inner" choline signal originating from those vesicles. This was further supported by the results of an experiment where insufficient concentration of Gd^{3+} (0.02 mM, i.e. less than one Gd^{3+} ion per vesicle - See Chapter II) was used. The results of this experiment (Fig. III.14) show that after an initial transport of Gd^{3+} an equilibrium is reached where the number of Gd^{3+} ion transported to the inside of the vesicles equals those transported in the opposite direction into the extravesicular space.

Table III.2 shows the results of an experiment where 0.1 mM Gd^{3+} was transported by various concentrations of NaFod at 50°C. Increasing the ionophore concentration would normally increase the transport rate but it is clear from Table III.2 that the extravesicular Gd^{3+} concentration is rate limiting. The results presented in Fig. III.15 show the opposite effect where the transport rate increases with increasing extravesicular concentration of the probe ion (Pr^{3+}), however, the transport reaches a plateau when the complexing sites of the ionophore are saturated with metal ions (40 mM Pr^{3+}).

III.3.7 Following lanthanide ion transport by ^{31}P-nmr:

Transport of Pr^{3+} ions was also followed using ^{31}P-nmr, though this technique produces large chemical shifts (^{1}H-nmr) and very broad signals during the transport process. A further difficulty in using ^{31}P-nmr is the longer sampling time (ca.1 hour) due to the large number of pulses required. For these reasons the above technique was rejected by others [169] as a useful method for following transport rates.

FIG. III.14 PLOT OF LOG OF SIGNAL I AGAINST TIME (MIN.)

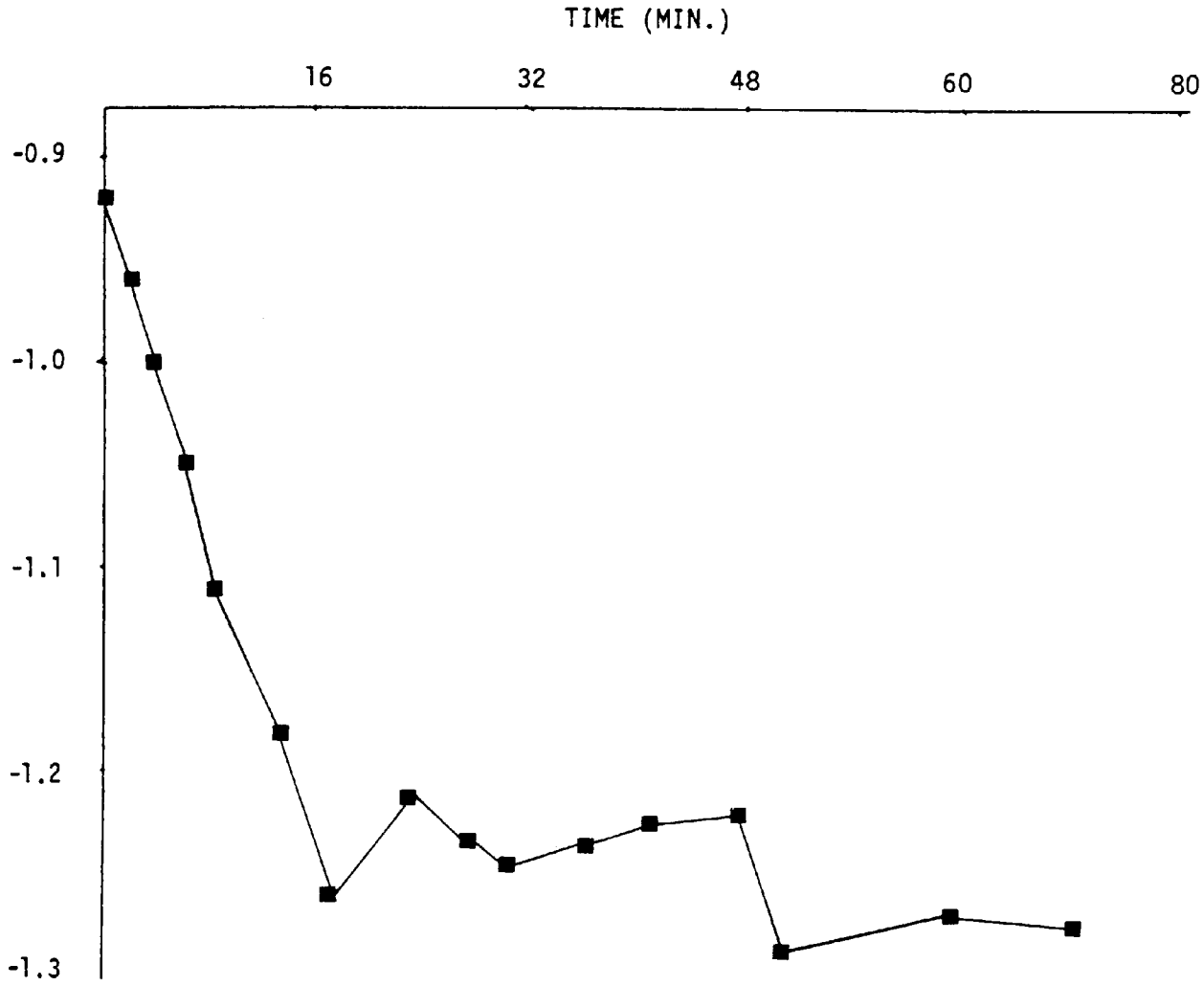

Initial extravesicular concentration of Gd^{3+} was 0.02 mM. Gd^{3+} transport reaches an equilibrium where the back-diffusion rate equals the rate of transport.

Table III.2

NaFod dependence on the observed rate of transport of Gadolinium inside P.C. vesicles (10 mg/ml) at 50°C

Na (FOD) (μg)	[NaFod]/ [vesicle]	K' mM/min	K-intrinsic rate constant $X10^{-6}$
5.0	1.52	5.519	9.30
10.0	3.04	6.351	10.70
40.0	12.14	5.323	8.97

FIG. III. 15

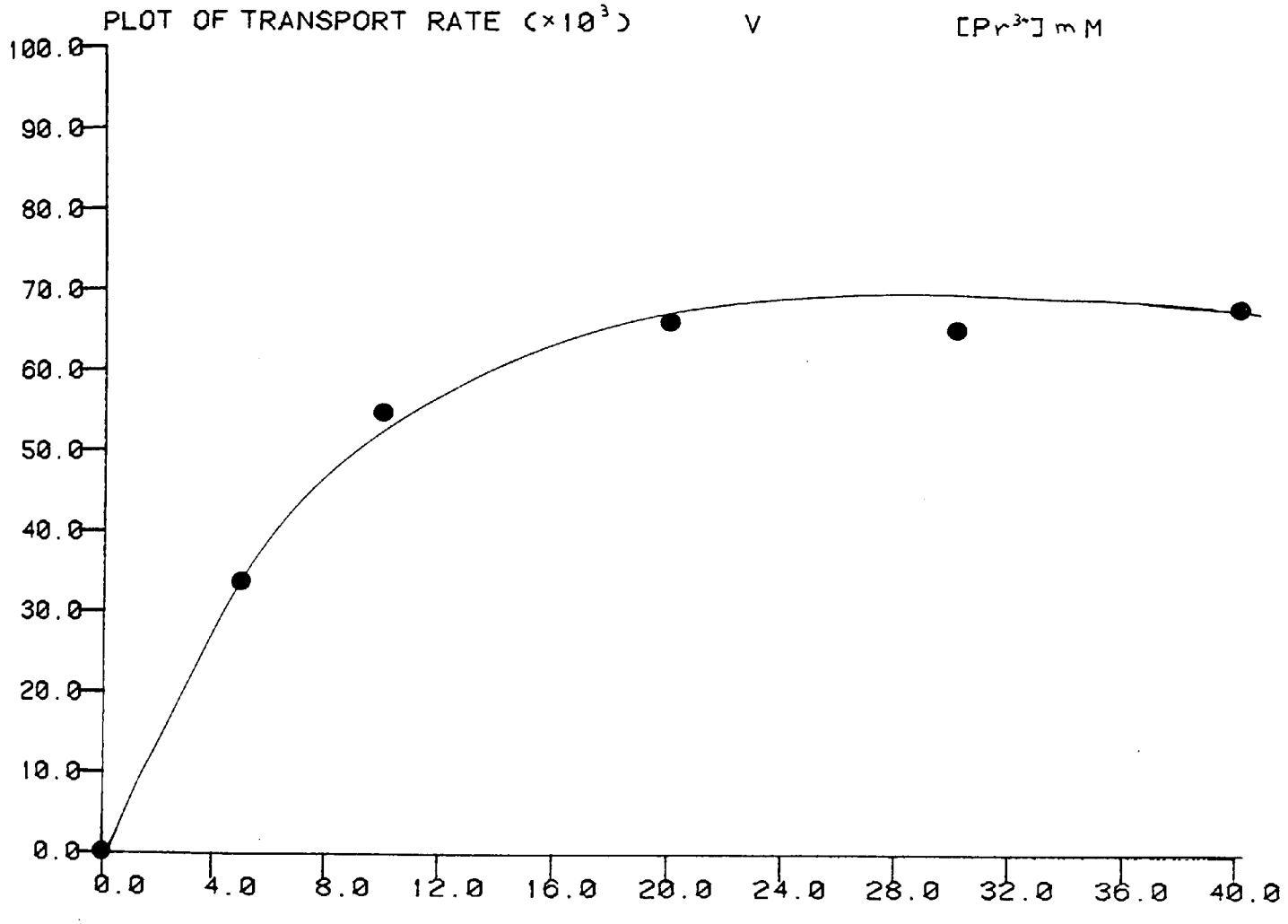

FIG. III. 15. SHOWS THAT INCREASING THE EXTRAVESICULAR CONCENTRATION OF Pr^{3+} INCREASES THE TRANSPORT RATE.

However the use of lanthanide ions with short relaxation times and little effect on T_2 (See P35), and the use of small concentrations of ionophore overcome the above difficulties. Fig. III.16 shows the ^{31}P-nmr spectra obtained during the transport of 0.32 mM Pr^{3+} by 10 µg NaFod at 30°C. Other conditions are given in the spectrum. Fig. III.17 shows a plot of $\delta\nu(0-1)$ against time for the above experiment. As discussed before, a calibration graph using ^{31}P-nmr is required to convert these experimental results into concentrations of Pr^{3+} inside the vesicles. Such a graph was not constructed but the results of using such a graph would be expected to give a linear plot for the transport rate.

III.3.8 Effect of pH and NaCl on transmembrane potential of sonicated vesicles:

It was claimed by Chen[169] that ionophore mediated transport of paramagnetic ions across salt-free vesicles should result in a build up of a transmembrane potential which would hinder and finally halt the transport process. However, since complete equilibration of the transported lanthanide ions was observed (Figs. III.2 and III.3) whether salt is included or not, experiments were set up to explain the above discrepancy.

The possibility of co-transport of the monovalent negatively charged chloride ions with the trivalent positively charged lanthanide was investigated. Fig. III.18 is a log-log plot of transbilayer transport by A23187 against variable extravesicular concentrations of NaCl. Increasing the extravesicular concentration of NaCl is seen to increase the rate of transport of Pr^{3+} .

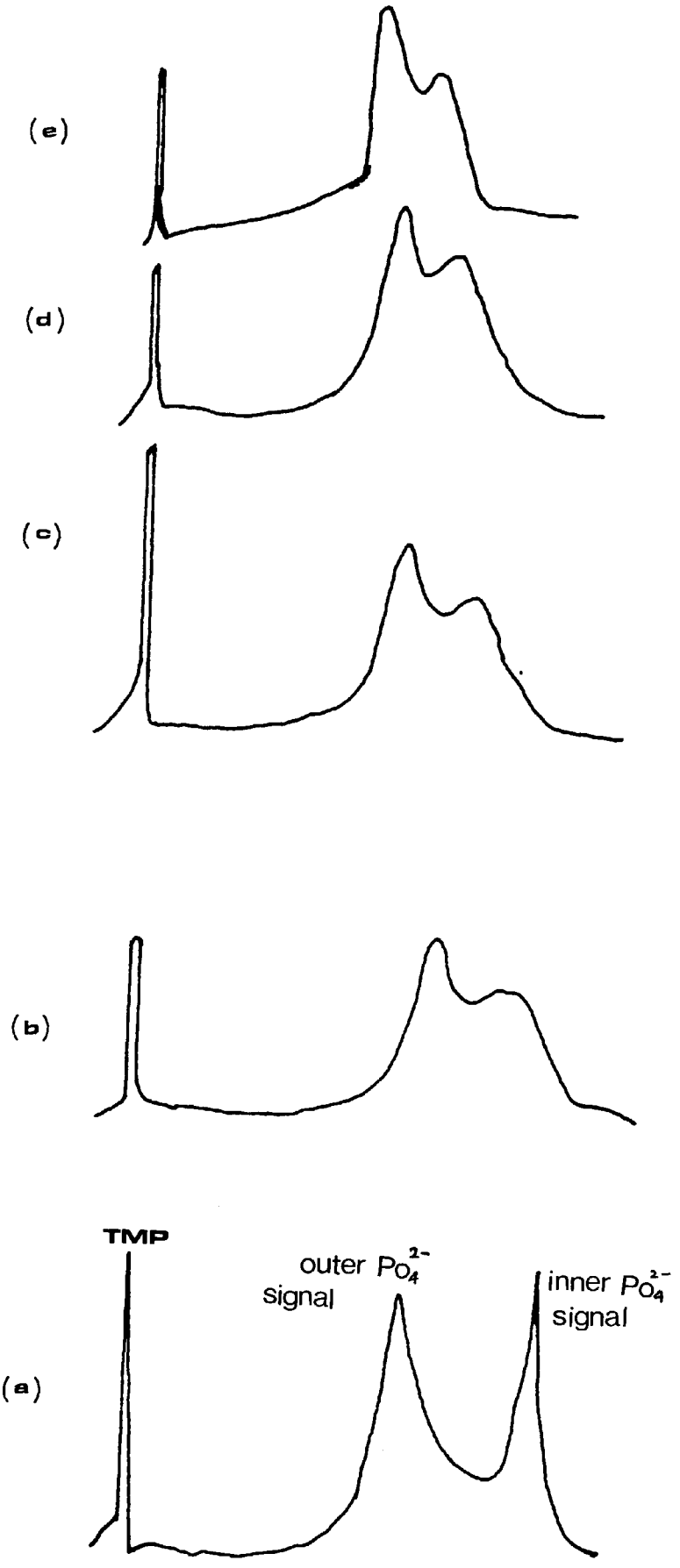

Fig.III.16. ^{31}P-nmr spectra of egg PC vesicles containing 0.32 mM Pr^{3+} The spectra [(a)-(e)] were recorded every half hour. The concentration of lipid was 30 mg/ml and the temperature was 30°C.

FIG. III. 17

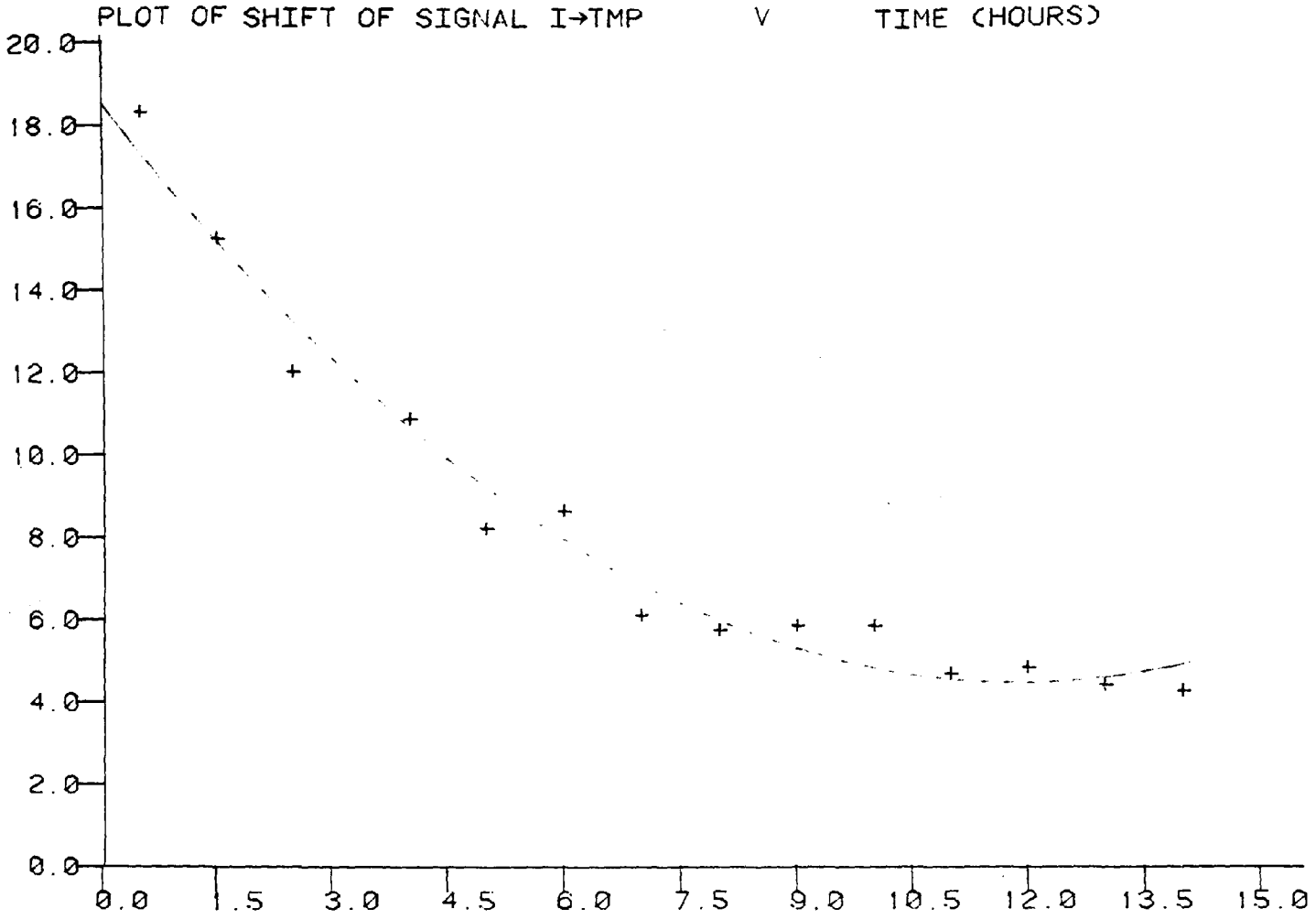

FIG. III. 17. IS A PLOT OF THE MOVEMENT OF PEAK "I" IN HERTZ WITH RESPECT TO THE INTERNAL STANDARD, (TMP). THE LIPID CONCENTRATION IS 40 MG PER ML; Pr^{3+} CONCECTRTION IS 0.32 M. THE SPECTRA WERE RECORDED EVERY HALF HOUR AND STORED ON TAPE.

FIG. III. 18

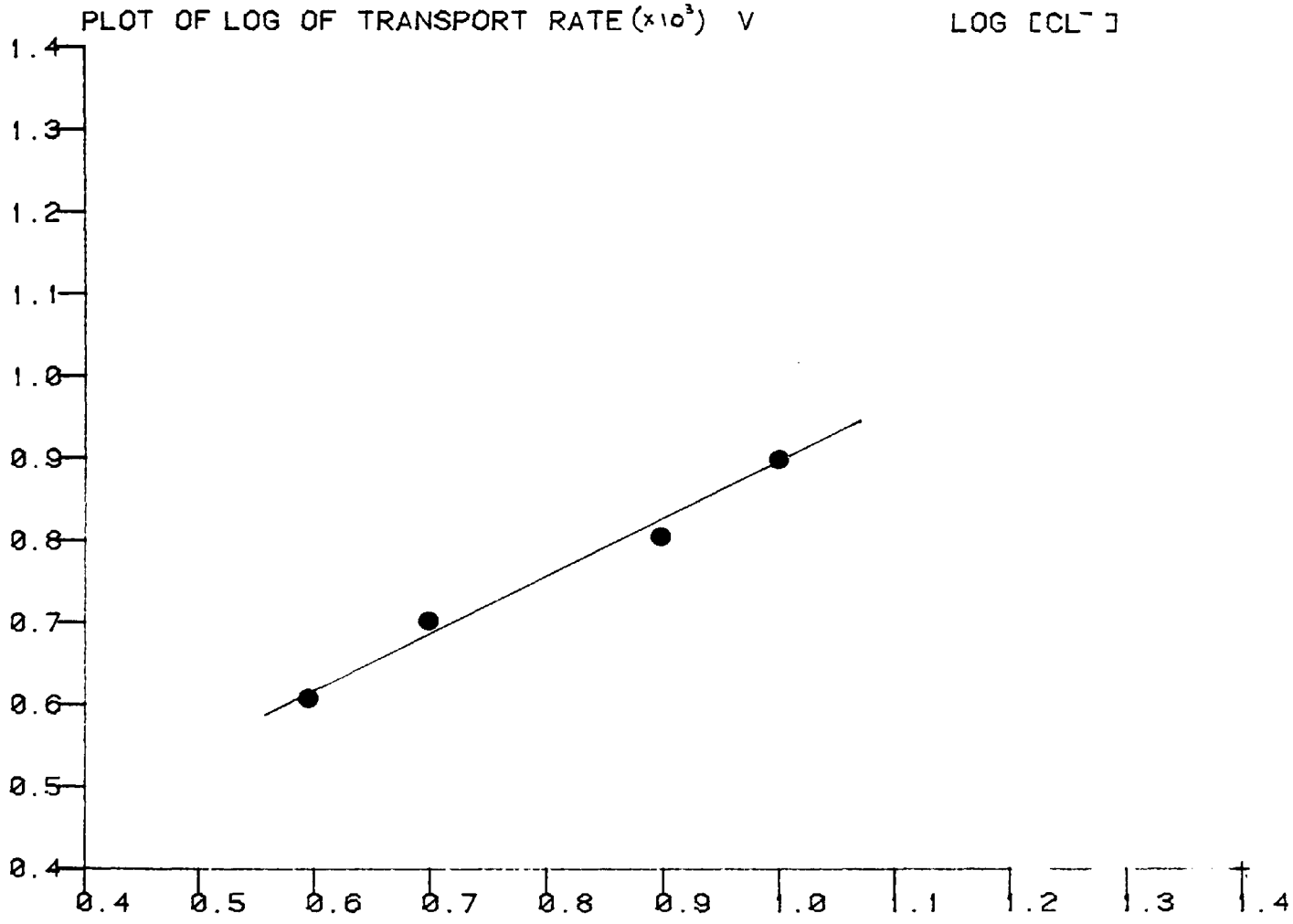

FIG. III. 18 THE SLOPE OF THE STOICHIOMETRIC PLOT EQUALS 0.45. THIS INDICATES THAT Cl^- IS NOT CO-TRANSPORTED WITH THE METAL. CHLORIDE IONS HOWEVER INCREASE THE BINDING OF OF THE METAL TO THE VESICLE SURFACE THUS INCREASING THE RATE OF TRANSPORT.

The slope (i.e. the stoichoimetry of the above graph is equal to 0.45.

Fig. III.19 is a plot of ionophore mediated transport (A23187 and Fod) against various values of the extravesicular pH. A distinct feature of this plot is the fact that both ionophores are most active near neutral pH. If the pH is raised to 7.5 or lowered to 5.5 the transport rate is lowered considerably. Another difference between the two ionophores is in the final pH of the vesicles, see table III.3. When A23187 is used to transport the probe ion the final pH of the vesicles is between 1 and 1.5 pH units lower than the initial pH. The final pH when NaFod is used remains unaltered. This would indicate that in the case of A23187 protons are transported from the inside of the vesicles.

FIG.III.19

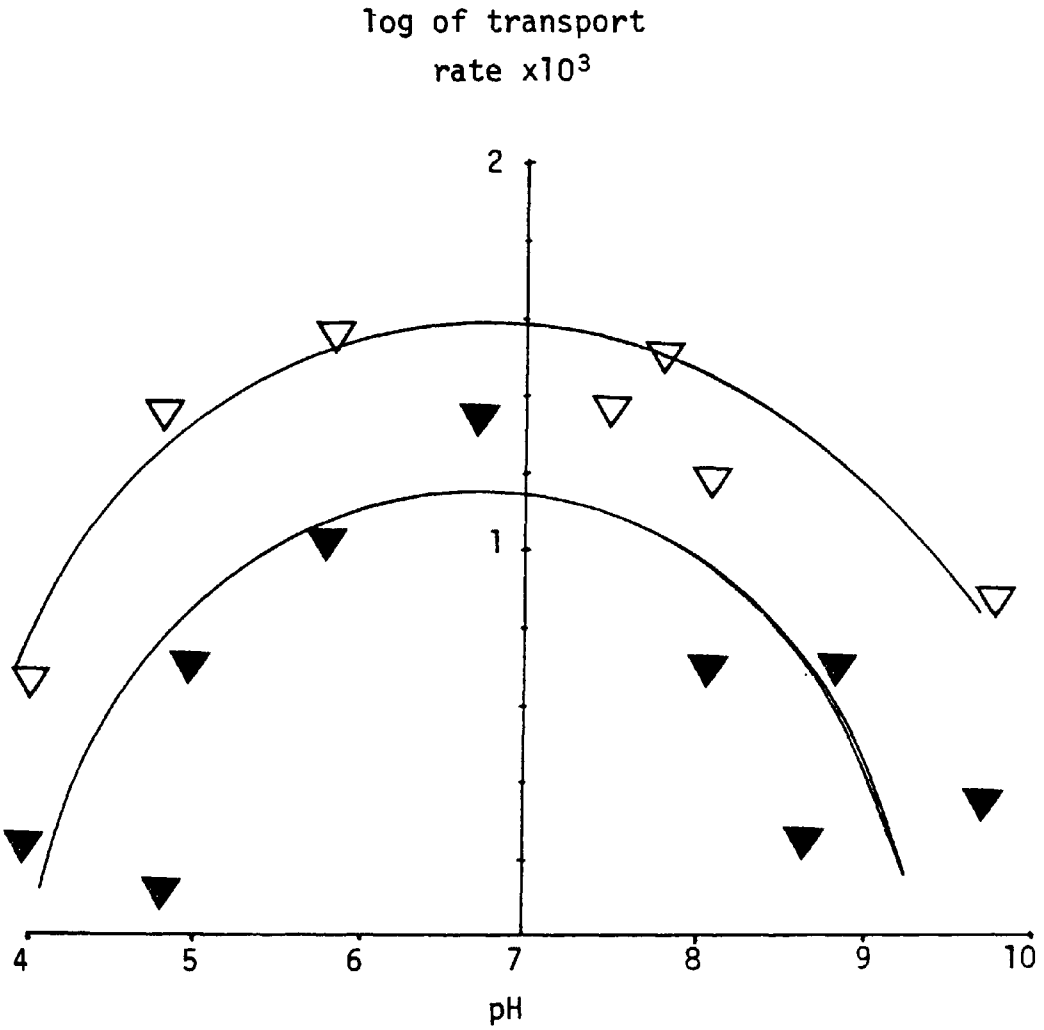

PLOT OF LOG OF Pr^{3+} TRANSPORT ($x10^3$) AGAINST EXTRAVESICULAR pH

Both A23187 (Top) and NaFod (Bottom) are most active near neutral pH. Increasing the extravesicular pH above 8.5 or decreasing it below 4.5 decreases the transport rate substantially.

Table III.3

Ionophore	Initial pH	Final pH
A23187	9.3 8.1 5.5 4.6	8.1 7.0 4.2 4.0
NaFod	9.3 8.1 5.5 4.6	9.1 8.0 5.5 4.7

III.4 Discussion

III.4.1 Ionophore mediated transport of lanthanide ions monitored by the ^{1}H-nmr method:

The experimental results presented in (Fig. III.5) shows the first report where A23187 mediated cation transport is demonstrated in egg PC sonicated vesicles. The transport data obtained at this concentration of ionophore (20 μg/0.5 ml) is compared with that of equimolar concentrations of the synthetic ionophore NaFod and the newly discovered ionophore ionomycin (Fig. III.6). Previous reports[50] compared the efficiency of transport by A23187 and by NaFod using DPPC vesicles and discussed the similarity of the carrier properties of these ionophores. The carrier mechanism of ionomycin, on the other hand is demonstrated in biological membranes by Bennett et al.[172] who reported that this ionophore stimulates histamine secretion from mast cells, apparently by forming an ionomycin - Ca^{2+} complex which is lipid soluble. The results obtained in (Figs.III.6) shows that the efficiency of these carrier ionophores is in the order ionomycin>A23187>NaFod. The efficiency of ionomycin shown to occur in this system is in agreement with the results of Massini & Naf[173], who reported that platelet activation is linked to an increase in cytoplasmic Ca^{2+} concentration, which can be induced by ionomycin mobilizing Ca^{2+} from intracellular sites or by transporting it through the plasma membrane. The above group investigated eight substances including A23187, and X537A, and of these only ionomycin seemed to act on platelet exclusively as a Ca^{2+} ionophore in the sense that all observed effects (i.e. platelet aggregation, shape transformation and serotonin secretion) can be explained by its ability to transport Ca^{2+} through the membrane.

The interesting observations regarding ionomycin and NaFod transport is the common presence of a β- diketone group in both ionophores suggesting that the enolate (or "diketonate") ion forms lipid soluble complexes with the trivalent lanthanide. The presence of the $-CF_3$ - and - CF_2 - groups [50] in NaFod increases the lipophilicity, and this has been suggested to form the basis of pharmacological activity of drug type molecules by facilitating their lipid permeability. The other diketone (ionomycin) contains a carboxyl group which is common to nigericin type ionophores e.g. A23187 and X537A which suggests that a similar carrier mechanism operates in these ionophores.

Comparing the ^{1}H-nmr spectra obtained during the transport by these ionophores indicated that major differences in the rate of broadening of signal I occurred. When NaFod is used to transport Pr^{3+} extensive line broadening of the inner headgroup signal occurred (Fig. III.8 (a)), and this is in contrast with the small degree of broadening caused by A23187 (Fig. III.8.(b)) and ionomycin (Fig. III.8.(c)). The differences in the degree of broadening of signal I caused by these ionophores is investigated in more detail in the following section.

III.4.2 The rate of broadening of signal I during transport:

Lanthanide ion binding to the choline headgroups on the inner surface of the vesicles causes a concentration dependent decrease in the transverse relaxation time (T_2); T_2 is inversly related to the linewidth of the nmr signal ($\nu_{\frac{1}{2}} = \frac{1}{\pi T_2}$). Therefore, a small degree of broadening of the inner choline resonance due to lanthanide ion binding is to be expected.

This, however, does not explain the vast differences in linewidth occurring during NaFod transport as compared with that of A23187 and ionomycin transport. Furthermore, this difference in linewidth is not a consequence of transporting Pr^{3+} through an inhomogenous population of vesicles because negative staining electron microscopy has shown that the sonication method employed in this work gives a uniform population of small vesicles (Chapter II). The possibility that the method used to introduce the ionophore causes an unequal distribution of the ionophore between the vesicles, and hence differences in intravesicular concentration of Pr^{3+} leading to line broadening is thought not to be responsible for the differences in broadening because the ionophore which causes most broadening (NaFod) was introduced as a D_2O solution.

The results presented in (Figs. III.7 and III.8) suggest that the degree of broadening depends upon the metal ion and ionophore employed. In order to investigate this further the range of ionophores was extended to include X537A, and, the lanthanide ion Dy^{3+} was employed. The rate of broadening of signal I caused by lanthanide ion transport was measured, and the transport data obtained by this method are compared with the rate of transport as measured by the downfield shift of signal I. The results of these experiments are summarized in (Tables III.1. (a) and (b)) show that these two methods produced vastly different results.

For X537A the rate of transport of Dy^{3+} is independent of the method of measurement; this is also true for Pr^{3+} transport by X537A. However, vast differences occurred with ionomycin and A23187-mediated transport of both Dy^{3+} and Pr^{3+} ; and also with Pr^{3+} transport mediated by NaFod.

In general, when Dy^{3+} transport is considered, NaFod and X537A produce

broader lines compared with A23187 and ionomycin.

The single peak observed due to the inner or outer choline head groups in the presence of the lanthanide ion implies that the exchange rate of the Ln^{3+} ion on the phosphate binding sites is fast on the nmr time-scale (i.e. $> 10^5$ Hz). If this exchange rate is slowed then the band due to the choline head group will broaden due to well established exchange effects on the spin-spin relaxation time [174]. Since there already exists good evidence (see Chapter II) that the inner phosphate groups bind ions more strongly on this inner surface of the vesicle, a lower exchange rate is possible and hence the broadened inner head group signal observed. Similarly if the ionophore molecules remain on the inner surface long enough to provide additional binding sites then the exchange rate will be lowered. The least efficient ionophores (NaFod and X537A) will be expected to have the greatest effect since they exchange across the bilayer less rapidly.

Clearly further work is required to investigate other possible causes of broadening. It should be noted that studies on lanthanide binding to vesicular membranes are also important because the variations observed in the nmr bandwidths could be related to headgroup conformation differences on the inner vesicle surface and changes in the conformation on binding the lanthanide ion.

III.4.3 Metal ion-ionophore stoichiometry:

In a number of studies of ion transport across lipid bilayers using ionophores [175], and surface active materials such as detergents[176] difficulties have been experienced in establishing the stoichiometry of the transported species. Bangham and Lea[176] have recently studied the surfactant-mediated conductance changes in lipid membranes and presented theoretical objections against the relevance of the monomer concentration to form the conductance unit. Furthermore, these workers experienced difficulties in obtaining integral stoichiometries using planar lipid membranes. In contrast, the use of phosphatidylcholine vesicular membranes and the NMR techniques have made it possible to gather information on the stoichiometries of synthetic and naturally occurring ionophores. The experimental results (Fig. III.10), using the ionophores NaFod, A23187 and ionomycin yield the metal ion - ionophore stoichiometries 2.9, 1.85 and 1.1 for the expected stoichiometries of 3, 2 and 1, for the above ionophores, respectively. Examination of chemical structures of these ionophores (Fig. I.11) reveal that NaFod forms neutral complexes with the metal ion $[Pr(Fod)_3]$, whilst A23187 and ionomycin form charged complexes $[Pr(A23187)_2]^+$ and [Pr (ionomycin)]$^+$.

III.4.4 Activation energies:

It would be useful to compare the effect of transporting a charged complex with that of a neutral complex on the energy of activation required for the transport process; and to try to relate the data obtained to the mechanism of ionophore mediated transport. The activation energy can be obtained from

constructing Arrhenius plots (Fig. III.11) giving 57.4 kg/mole^{-1} to transport the neutral [Pr(Fod)$_3$] complex, this is in contrast to the substantially larger energies of activation(102.92kJ mole^{-1} and 96.0 kJ mole^{-1}) required to transport the charged [Pr(A23187)$_2$]$^+$ and [Pr(ionomycin)]$^+$ complexes respectively. This suggests that the transport of a charged complex across the "image potential barrier" is accompanied by higher energies of activation compared with that required to transport neutral complexes [166].

Comparison of the transport rates mediated by charged and neutral ionophores (Fig. III.6) shows that A23187 and ionomycin are more efficient than NaFod in transporting the lanthanide ion Pr^{3+} . Although the value of activation energy seems to suggest that the overall charge of the transported complex is important in determining the kinetics of the ionophore transport, the results in (Fig. III.6), suggest that other factors are also important. The rate of ionophore mediated transport is related to an enthalpy of activation term and an entropy of activation term by the Arrhenius equation[177] :

$$k_2 = \frac{kT}{h} e^{+(\Delta S^\circ)^{\ddagger}/R} e^{-(\Delta H^\circ)^{\ddagger}/RT}$$

where k_2 is the rate constant, k and T are Boltzman constant and absolute temperature respectively, h is Planck's constant, ΔS and ΔH are the entropy and enthalpy changes, respectively.

The above equation shows that a decrease in enthalpy, or an increase in entropy of the system increases the transport rate. Therefore it could be that the aggregation of three Fod molecules to form a complex with the transported metal ion which is accompanied by large decrease in entropy

controls the transport rate using this ionophore. This high entropy change is in contrast with that occurring in ionomycin and A23187 mediated transport because these ionophores require less degree of order to form the 1:1 and 2:1 complexes, respectively. It is suggested therefore that the transport of charged complexes $[Pr(A23187)_2]^+$, $[Pr(ionomycin)]^+$ is accompanied with high enthalpy of activation, whilst the transport of neutral complexes $[Pr(Fod)_3]$ is accompanied with high entropy changes; and both may influence the transport rate.

III.4.5 Following ion transport using ^{31}P-nmr:

In principle one can expect to follow Ln^{3+} transport across phospholipid vesicles lacking choline using ^{31}P-nmr. The major problems in practice, however, are the extensive line broadening which results from contact contribution of the binding (See Chapter II) and the long sampling time required to achieve a reasonable signal to noise ratio. The inherent advantage of this technique, however, is the large contact shift which results from adding very small concentrations of Ln^{3+} , this in turn, minimizes the resultant broadening. This is particularly true when lanthanides with short relaxation times are employed. Furthermore, the use of low concentrations of ionophore enables the transport of cations to be followed over several hours. The advantage of slowing down the transport rate is that sufficient transients can be collected before the nmr resonance positions change substantially. In fact using such conditions the transport of Pr^{3+} (0.3 mM) by NaFod (5μg/ml) was followed using ^{31}P-nmr (Fig. III.17). The recorded spectra (Fig. III.16) shows that a reasonable signal to noise ratio

can be obtained in about 30 minutes for this concentration of lipid (20 μg/ml). Hence, contrary to previous reports[169] the broadening of the inner headgroup signal in ^{31}P-nmr does not limit this technique for monitoring cation transport. Using the ^{31}P-nmr method Donis et al.[178] have recently demonstrated the synergistic effects produced when a mixture of ionophores was employed to transport the lanthanide probe ion Pr^{3+} .

Particular adaptations of this method can be applied to monitor transbilayer transport using ^{13}C-nmr. Although ^{13}C-nmr (like ^{31}P-nmr) requires long acquisition times to obtain a reasonable signal to noise ratio, the particular advantage of this technique is the sharper lines produced compared with those observed in ^{1}H and ^{31}P-nmr. However, relatively high concentrations of the lanthanide are required to separate the headgroup signals which suggests that vesicle aggregation[140] or fusion[179] may be facilitated in these systems. This implies that the use of lanthanides which produce large shifts such as Yb^{3+} and Dy^{3+} would be particularly useful in ^{13}C-nmr. Finally, the relatively high concentration of the lanthanide will cause the rate of transport to increase (Fig.III.15) which would require that even lower concentrations of the ionophore should be used to achieve a reasonable transport rate, and at the same time accumluate a reasonable nmr signal.

III.4.6 ^{1}H-nmr method for measuring Gd^{3+} transport:

The transport of Gd^{3+} across sonicated vesicles was followed by monitoring the paramagnetic effect of the lanthanide on the ^{1}H-nmr signal of the inner choline headgroup (Fig. III.12). The addition of 0.2 mM Gd^{3+} to the vesicles

caused the complete broadening of the outer choline resonance thus revealing the sharp resonance due to the inner headgroup (Fig. III.12. (b)). The transport of Gd^{3+} initiated by adding small concentrations of NaFod (5μg/0.5ml) caused the time dependant loss of the inner headgroup signal intensity (Fig. III. 12). Degani et al.[170] studied X537A mediated Mn^{2+} transport across DPPC vesicles, and suggested that the time dependant loss of signal I intensity can be used to obtain a rate of transport. The analysis of data shown in the materials and methods section of this chapter shows that a plot of the log of signal intensity (Peak I) against time should be linear. Using such a plot (Fig. III.13) the transport rate can be calculated (k_o= 8.08 x 10^{-3} mM/min.).

The complete broadening of the inner choline signal originating from all the vesicles by such low concentration of Gd^{3+} (0.2 mM) suggests that the transport of a single Gd^{3+} inside the vesicle is sufficient to completely broaden the signal originating from the inside headgroup of that vesicle. Further investigations involved the use of lower concentration of Gd^{3+} (0.02 mM). An analogous calculation to that done in Chapter II show that at this concentration insufficient Gd^{3+} ions are present to transport one Gd^{3+} ion per vesicle. Therefore, the results of this experiment (Fig. III.14) show that appreciable transport of Gd^{3+} occurs; but soon Gd^{3+} concentration outside the vesicles becomes depleted and an equilibrium is reached when the transport of ions inside equals the back diffusion of cations. This can account for the "beating" effect shown in (Fig. III.14) and suggests that a single Gd^{3+} ion inside the vesicle causes the complete broadening of the ^{1}H-nmr signal originating from the inside of that vesicle. Furthermore, the efficient transport of Gd^{3+} by such low concentration of ionophore (5 mg/ml) is not related to the "specificity" of NaFod for Gd^{3+} but is a consequence of

the efficiency of the cation relaxation mechanisms for example Gd^{3+} and Mn^{2+}

These results support previous reports which suggest that since the nmr method is sensitive to single ion conduction, valuable information on the kinetics and mechanisms of transport can be obtained from monitoring the changes of the inner headgroup signal. Recently, the nmr method has been used to monitor the transport of biologically important cations such as sodium using aqueous complexes of the shift reagents to separate the headgroup signals[134]. The scope of utilizing the nmr method and single bilayer vesicles can now be extended to monitor the transport of biologically relevant cations and essential metabolites using reconstituted systems e.g. the ATPases.

III.4.7 Transmembrane Potential:

The transfer of charged species across the bilayer of sonicated vesicles would be expected to give rise to an electrochemical potential (positive inside), a situation which would hinder and finally halt the transport process. Chen[169] suggested that such a problem may occur when ionophore mediated transport of lanthanide ion across salt free sonicated vesicles is considered. It has also been pointed out that the transport of charged species across the image potential barrier is accompanied by high energy of activation. However, in contrast to the point of view of Chen, the ionomycin and A23187 mediated transport of Pr^{3+} across salt free egg PC sonicated vesicles show that the inner choline signal is shifted under the outer choline signal indicating that the "inner and "outer" Praseodymium concentrations is at equilibrium. It must be remembered, however, that on the transport of charged species it is mandatory that charge balance is

maintained, therefore, two lines of investigation which may account for the observed transport were followed. The first possibility is that of co-transport of anions (Cl^-), and experiments were carried out to monitor the Ln^{3+} transport under various extravesicular concentrations of NaCl (between 0.0 and 150 mM). The second possibility investigated was nH^+/Ln^{3+} counter - transport mechanism, and compares the transport mechanisms of neutral and charged complexes at various pH values (between 3.5 and 8.5), also the change in the final pH.

Increasing the extravesicular Cl^- concentration seems to cause Pr^{3+} transport to increase (Fig. III.18). However, if the monovalent chloride is co-transported with the trivalent lanthanide then (in order to maintain charge balance on the inside of the vesicles) the log-log plot of the rate of Pr^{3+} transport against the extravesicular Cl^- concentration should give a slope equal to three. Such a plot (Fig. III.18) yields a slope $<<1$ which suggests that chloride ion co-transport does not occur. Such a mechanism is therefore unlikely to be responsible for reducing the transmembrane potential.

The increase in the transport rate of Pr^{3+} with increasing Cl^- concentration (Fig. III.18) could be due to the enhancement of lanthanide binding caused by chloride ion co-binding. The latter has the effect of increasing the effective concentration of the lanthanide on the surface of the vesicle leading to enhanced permeability. The suggestion of enhanced cation binding due to chloride ion co-binding agrees with the results of Bergelson[144] who showed that the Pr^{3+} induced shift by anions increases in the order $Cl^- < NO_3^- < CNS^-$ due to the lowering of the zeta potential on the surface of the bilayer (See Chapter II.) and not due to changes in co-ordination of the metal [144].

The effect of varying the extravesicular pH on the rate of A23187 mediated and NaFod mediated transport is shown in (Fig. III.19). A distinct feature of this plot is the fact that both ionophores are most active near neutral pH. If the extravesicular pH is raised to 7.5 or lowered to 5.5 the transport of Pr^{3+} is lowered considerably. However, the striking difference between the two ionophores is in the final pH of the vesicles. When A23187 is used to transport the probe ion the final pH is between 1.0 and 1.5 pH units lower than the initial pH (Table III.3). In contrast, when NaFod is used to transport the probe ion the initial pH remains unchanged.

The lower rate at pH >7.5 is probably due to an increased tendency to hydrolysis of the Pr^{3+} . At low pH protons will compete for Ln^{3+} on the ionophore and hence lower the rate. The extravesicular fall in pH using A23187 is consistant with Ln^{3+} /H^+ exchange as discussed above, which assumes that A23187H carries the protons out. The failure of fod^- to recycle across the membrane would explain the lack of change in pH. There is sound evidence from the excessive broadening of signal I discussed previously (section III.4.2) that fod^- does remain on the inner surface.

Such counter - transport mechanisms facilitating the movement of cations (Ca^{2+}) in one direction and protons in the opposite direction was demonstrated in mitochondria[80] where it is shown that the extramitochondrial pH does not become acidic due to proton efflux because H^+ are exchanged with Na^+ via the Na^+/H^+ antiporter[181] see Scheme 1.14. Furthermore, the counter-transport mechanism agrees with the Mitchell's Chemiosmotic theory. According to this theory [182] [183] the mitochondrial membrane contains a number of enzyme complexes that catalyse (reversibly) the coupled movement of electrons from low to high potential redox components

and of H^+ ions from inside to outside. One way to utilise the latter is by the dehydration of ADP and Pi to form ATP coupled to the influx of H^+ ions; a reaction that is catalysed (reversibly) by the H^+ - ATPase complex. This transmembrane proton gradient is an intermediate in transduction of free energy of oxidation into free energy of hydrolysis (of ATP).

Recently Carafoli's group[184] reported that the purified human erythrocyte Ca^{2+} - ATPase reconstituted in asolectin containing liposomes can be stimulated by A23187 which indicates the tight coupling between Ca^{2+} transport and ATP hydrolysis. However, the number of protons produced in the medium exceeded the ratio of 2 H^+ per ATP hydrolysed which indicates that the ATP - linked Ca^{2+} uptake induces the ejection of protons from the vesicles. In the presence of the protonophore carbonyl cyanide-m-chlorophenyl hydrazone and of valinomycin, the proton ejection is decreased by about 50%, indicating that a transmembrane proton gradient is indeed formed during Ca^{2+} transport. Waisman et al.[185][186] have postulated that Ca^{2+} transport in inside-out resealed ghosts is electrogenic, resulting in the creation of a positive membrane potential inside the vesicles, which would be the driving force for anion uptake. But, no direct evidence for the generation of a membrane potential has been provided by these authors. However in the light of Carafoli's results and the results obtained in this chapter it seems that cation transport can be coupled to proton efflux. Perhaps anion transport in inside-out ghosts studied by Waisman et al. occur via the known anion transporter band 3.

In summary, the transport of charged complexes across the vesicles is not accompanied by large transmembrane potential because such potential is

discouraged from building up by the counter transport of protons to the outside of the vesicles.

Conclusion

The NMR/Ln^{3+} method has been successfully applied to the study of carrier mediated transport of metal ions in vesicular membranes. The experiments demonstrate how both shift and relaxation probes can be used to follow transport. The results give information on the kinetics stoichiometries, mechanisms and thermodynamics of the processes involved.

CHAPTER IV

NON-BILAYER PHASES

CHAPTER IV

NON-BILAYER PHASES

IV.1 Introduction

The reason for the great variety of lipids found in biological membranes, and the relations between composition and membrane function pose major unsolved problems in membrane biology. The observations that biological membranes contain regions of bilayer structure, and that model systems consisting of naturally occurring and synthetic phospholipids often spontaneously adopt such a configuration on hydration provide strong evidence that the lipid component is responsible for basic membrane structure. The fact remains however, that a single phospholipid such as phosphatidylcholine could satisfy such structural requirements. In this context, the observation that a typical mammalian cell membrane contains one hundred or more distinctly different lipids implicity suggests that lipids play other functional roles.

This point in question was recognised by Luzzati et al.[13] in 1966. They employed X-ray diffraction techniques to study crystal symmetry and dimension and hence the various polymorphic phases of lipid-water systems. They reported that a large number of phases (e.g. bilayer, H_I , H_{II} etc.,) were observed, but more importantly, they pointed out that their experimental conditions (concentration and temperature) under which these polymorphic transitions were observed are not too different from those that exist in living cells; therefore, it is not unreasonable to assume that analogous reversible structural changes may take place in vivo, under the

action of other parameters of more direct biological significance. Luzzati's observations were overshadowed and largely ignored because of the emergence of the Singer "fluid mosiac" model (Fig. I.7) which dominated the thinking of cell biologists and biochemists during the 1970's [23].

The Singer model (February, 1972) suggests that membrane lipids are organised in a bilayer structure and membrane proteins are globular, and these are embeded at various depths in the bilayer matrix resembling ice-bergs in a sea of lipid. Within the framework of this model the molecular mechanisms of important membrane processes such as transbilayer transport and membrane fusion could not be fully explained, a fact which inspired (or motivated) other workers to search for alternative models for the membrane structure.

Van Deenen's group were re-alerted to the importance of non-bilayer phases during their study of flip-flop mechanisms. De-Kruijff et al.[187] showed that conversion of PC to PA during phospholipase attack on the external headgroups of unilamellar small vesicles gives rise to rapid transbilayer exchange of the PA formed with intravesicular PC. The ^{31}P-nmr techniques used in conjunction with paramagnetic ions also showed that the vesicular membranes remained impermeable under these conditions. Such flipflop of lipids clearly requires specific molecular mechanisms since the energetic requirements are against movement of polar head-groups across the bilayer. The role of PA in this mechanism was clearly central and such experiments drew attention to the need to re-examine the structural effects of such lipids.

So in 1978 De-Kruijff and Cullis[188] began to use ^{31}P-nmr line shapes to study the polymorphic phase behaviour of extracted phospholipids in model systems.

They found that phospholipids with head-group diameter comparable with their acyl chains (i.e. cylindrical in shape e.g. PC) adopt the bilayer phase, and their ^{31}P-nmr spectrum (Fig. I.4) shows a broad spectrum with a low field shoulder and a high field peak, which are separated by

$\Delta \sigma^{EFF}_{CSA}$ = -40 ppm (See Appendix 1.)

In contrast, phospholipids with small head-group diameter compared to their acyl chains (i.e. cone-shaped e.g. PE) adopt the hexagonal (H_{II}) phase, and their ^{31}P-nmr spectrum (Fig. I.4) has reversed symmetry compared to the bilayer spectrum - and narrower by a factor of two due to the lateral diffusion around the small (~ 20A° in diameter) aqueous channel.

Based on these observations and freeze fracture studies which show the co-existence of bilayer and hexagonal H_{II} phases (Section IV.4) Van Deenen's and Cullis's laboratories in a series of publications have shown that[189] cardiolipin and phosphatidate exhibit bilayer $\rightarrow H_{II}$ transitions on addition of calcium; Soya PE[11] and egg PE[190] show similar polymorphic behaviour when the temperature is raised above 8°C and 25°C respectively. Perhaps more importantly, they suggested that the enhanced permeability and fusion observed during these polymorphic (bilayer $\rightarrow H_{II}$) transitions are mediated by two types of inverted micelles[11]. The first type occurs inside the bilayer and this mediates transmembrane transport and flipflop (Fig. I.13). The second type occurs between the outer monolayers of two bilayers and this mediates membranes fusion (Fig. I.13.(a)).

The occurrence of such micelles would be expected to give isotropic ^{31}P-nmr signals due to the fast tumbling rates, and this feature is frequently observed in many of their recorded spectra[191].

Supporting evidence for the presence of these inverted micelles comes from

the freeze fracture studies of Van Venetie and Verkleij[20] which show particles and pits of comparable size to those of inverted micelles. Further, these electron micrographs suggest that bilayer $\rightarrow H_{II}$ transitions occur via an intermediate phase involving inverted micelles[18].

Most of the above work on non-bilayer phases in model membranes has been done with relative concentrations of mixed lipids which are not related to physiological systems. Experiments described in the present study were designed to investigate the effects of physiologically relevant concentrations of PA, PE and CL using nmr/lanthanide ion probe methods described in the previous Chapters. Particular adaptations of these methods are given below (See Materials and Methods).

Recently, research to determine the functional roles of lipids was extended to biological membranes by Quinn and co-workers[192], who examined the polymorphic phase behaviour of mono and di-galactosyldiacyl glycerol (MGDG and DGDG) extracted from chloroplast membranes. Their freeze fracture replicas have shown lipidic particles (10-12 nm in diameter) corresponding to inverted lipid micelles sandwiched within lipid bilayers.

In the field of microbiological membranes, Ferguson et al.[193] investigated the phase behaviour of the major lipids of Tetrahymena ciliary membranes using X Ray diffraction, ^{31}P-nmr and freeze fracture electron microscopy. Phosphatidyl-ethanolamine and amino-ethyl phosphonate which amount to 60% and 10% of the total lipid of the ciliary membranes were shown to adopt the hexagonal H_{II} phase at 10°C and 20°C respectively. However, ^{31}P-nmr of intact cilia exhibited the bilayer phase which suggests that phosphatidyl choline (amout to 10%) is responsible for stabilizing the bilayer structure.

The phase behaviour of the total phospholipids extracted from *Micrococcus cryophilus* is examined by ^{31}P-nmr as part of this work, and interesting observations were made regarding the different lipid phases exhibited at various experimental conditions. The physical state of the membrane of this microorganism and the activity of its membrane bound enzyme ($\Delta 9$ - desaturase) is being studied at present.

A major development of De-Kruijff's and Cullis's work has been achieved when model systems containing "functional" proteins of the inner mitochondrial membrane and the plasma membrane were studied by ^{31}P-nmr and freeze fracture electron microscopy [35]. Cytochrome c was found to induce non-bilayer structures in cardiolipin containing model membranes, and freeze fracture studies have shown that this cytochrome crosses to the opposite side of the bilayer via an inverted micelle (c.f. Mitchell's hypothesis).

Research to determine the functional roles of lipids in biomembranes laid the foundation for the suggestion of a unified model which extends the fluid mosaic model of membrane structure (Fig. IV.1). This model (proposed by Cullis [19]) suggests that non-bilayer phase mediated processes such as transbilayer transport, flipflop, membrane fusion, exocytosis, endocytosis .. are mediated by the two types of inverted micelle and also accounts for some functional roles of membrane proteins.

An important problem associated with the use of unsaturated lipids (e.g. PE, CL and PA) is acyl chain oxidation. The peroxidation of biological membranes, though known to occur readily and to be associated with many pathological diseases such as cellular aging, atherosclerosis and oxygen toxicity [103]; quantitative information regarding reaction mechanisms, changes in the

Fig.IV.1. DYNAMIC MODEL OF MEMBRANE STRUCTURE PROPOSED BY CULLIS ET AL.

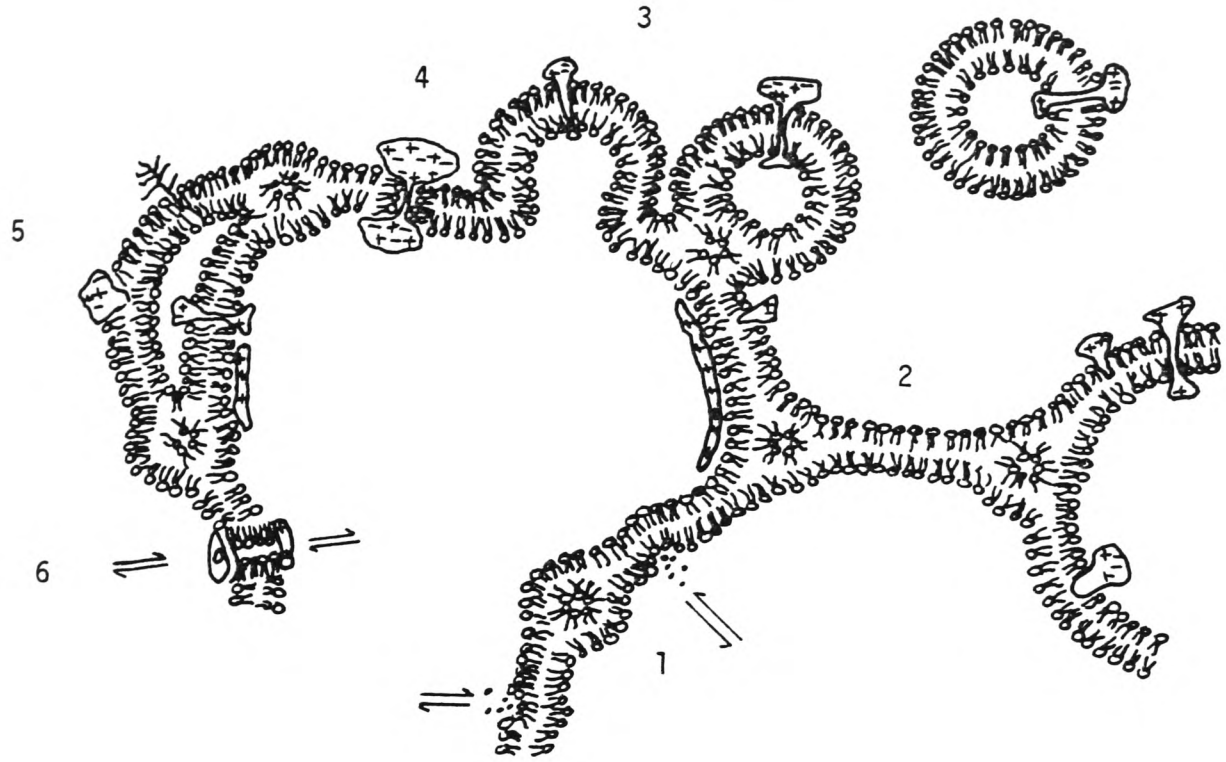

A metamorphic mosaic model of biological membranes illustrating various structures and processes suggested by the ability of lipids to assume nonbilayer configurations. In part 1 transbilayer transport of polar molecules (e.g., divalent cations) is facilitated by intermediary formation of inverted micelles, whereas part 2 indicates membrane continuity between membrane bound compartments. In section 3 a process of budding off of a membrane bound vesicle is illustrated,
The protein in region 4 is shown to assume a transmembrane configuration without the requirement for an apolar sequence of amino acids. The protein penetrates the membrane through a (short) cylinder of phospholipid. In the region 5 compartmentalization is depicted within a continuous membrane system, whereas part 6 indicates possibilities of transmembrane transmembrane transport where hexagonal (H_{II}) phase lipids form an aqueous pore through the membrane. This lipid configuration is stabilized in an orientation perpendicular to the plane of the surrounding bilayer by doughnut shaped proteins with hydrophilic and hydrophobic sides, which could also serve as selectivity filters.

bilayer properties and the nature of breakdown products is still lacking[194]. This is not surprising since the peroxidation of linoleic acid alone results in the formation of at least 20 degradation products[102]. A number of reports claim alterations in the physical properties of biomembranes as a result of lipid peroxidation. Increased permeability[195], decreased fluidity[196], cell swelling[197] and increases in the rate of flipflop[198] are only some of the reported bilayer changes associated with increased peroxidation. Clearly more information regarding each and every of these important topics is needed.

The work described in the present study is divided into two main areas of investigation:

(a) The effect of non-bilayer preferring lipids (e.g. PE, CL and PA) on the rate of transbilayer transport, flipflop and vesicle-vesicle fusion.

(b) The polymorphic phases adopted by *Micrococcus Cryophilus* extracted phospholipids at various temperatures.

The effect of lipid peroxidation on membrane permeability was also briefly examined.

IV.2 Materials and Methods

IV.2.1 Preparation of mixed lipid vesicles:

Egg phosphatidylethanolamine (PE), Bovine Cardiolipin (CL,DPG) and egg phosphatidic acid (PA) were purchased from lipid products (S. Nutfield England). Egg PC/10 mole% PA vesicles, egg PC/10 mole% CL vesicles and egg PC/40 mole% PE vesicles were prepared by pipetting the required volumes of the chloroform solutions of these lipids in the glass sonicating tube. The contents of the tube were briefly mixed and the solvent was evaporated with nitrogen followed by evacuation at low pressure. The required volume of D_2O was added to the dry lipid and the liposomes formed by shaking were sonicated and centrifuged as described previously. Egg PC/1 mole% PA vesicles and egg PC/1 mole% CL vesicles were also prepared at the initial stages of this work.

IV.2.2 Methods for triggering non-bilayer phases:

0.5 ml of the mixed lipid vesicles was pipetted into 5 mm nmr tubes. In some cases 0.2 µl CH_3CN was added (as internal standard) and the transport was initiated by the addition of known concentrations of the required lanthanide. When required, non-bilayer phases were triggered either by adding microlitre amounts of stock solution of calcium to the nmr tube (Egg PC/10 mole% PA or egg PC/10 mole% CL vesicles) or by incubating the nmr tube containing the vesicles (egg PC/40 mole% PE vesicles) at various temperatures between 25°C and 57°C.

The first transport experiments attempted were initiated by the addition of 5 mM Pr^{3+}, but the transport rates were found to be appreciable even in the absence of calcium which suggested that this concentration of Pr^{3+} (5 mM) was sufficient to trigger non-bilayer phases (hence inverted micelles - see Introduction) and therefore one could not distinguish between the effect of Pr^{3+} alone and that of subsequent addition of calcium. In later experiments this lanthanide (5 mM Pr^{3+}) was substituted with another lanthanide ion (Dy^{3+}) at much lower concentration (0.15 mM) which enabled the complete separation of the choline headgroups signal without causing the enhanced permeability observed with 5 mM Pr^{3+} . On the other hand, the choice of Pr^{3+} to study transbilayer transport in egg PC/40 mole% PE vesicles is still appropriate since non-bilayer phases in these vesicles is triggered by increasing the temperature and not by calcium (See Introduction). Ionophores were not added at any stage during these experiments.

IV.2.3 Measurement of transbilayer transport, flipflop and vesicle-vesicle fusion :-

Transbilayer transport of Dy^{3+} and Pr^{3+} and flipflop across the mixed lipid vesicles was measured by monitoring the time dependant changes in the ^{1}H and ^{31}P-nmr signals. Transbilayer transport occurring in egg PC/10 mole% CL vesicles and egg PC/40 mole% PE vesicles was measured by the time dependant downfield shift of signal I with respect to the internal standard. Transmembrane flipflop occurring in egg PC/10 mole% PA vesicles was monitored by measuring the time dependant upfield shift of signal O with respect to the internal standard.

During transbilayer transport occurring in the former vesicles signal O remained unshifted; whilst during transbilayer flipflop occurring in the latter signal I remains unshifted.

Vesicle-vesicle fusion occurring in all the vesicles was measured by the increase in linewidth at half height ($\nu\frac{1}{2}$) of the hydrocarbon acyl chain signal (H) i.e. according to the method Liao and Prestegard[199].

IV.2.4 ^{31}P-nmr:

^{31}P-nmr measurements were performed at 24.15 MHz on a JEOL FX60Q FT spectrometer fitted with variable temperature accessories. Transbilayer flipflop in egg PC/10 mole% PA vesicles was measured using broad band proton decoupling employing 600 Hz_1 spectral width, 7 μs (45°) pulse angle, 2.5 seconds pulse delay and up to 300 scans were accumulated. TMP was used as internal standard.

^{31}P-nmr spectra of *Micrococcus cryophilus* liposomes, were recorded using 4K data, 6666 Hz spectral width, 7 μs (45°) pulse angle, 0.17 s pulse delay, and up to 10,000 scans were accumulated. All scans were multiplied by an exponential window to improve the S/N ratio resulting in 33 Hz line broadening.

IV.2.5 Treatment of Results:

It is mentioned earlier (See Chapter III) that in order to convert the measured

shifts of the inside signal I into lanthanide ion concentrations inside the vesicles a calibration graph is required. The calibration graph obtained with pure egg PC vesicles (Fig. III.2) can not be applied here since the binding of the probe ions to mixed lipid vesicles is different and therefore the shift of signal O will be different. The results of transbilayer transport and flip-flop observed in mixed lipid vesicles are therefore presented as the measured shifts of signal I and signal O respectively in hertz against time. The results of vesicle-vesicle fusion are presented as the measured increase in line-width of signal H in hertz against time.

IV.2.6 Preparation of liposomes from *Micrococcus cryophilus* extracted phospholipids

Micrococcus cryophilus extracted phospholipids were a gift from Dr. N.J. Russell (Department of Biochemistry, University College, Cardiff). Analysis of the lipid mixture gave 45% PG, 45% PE and 10% CL. 60 mgs of the chloroform solution of the lipid mixture was pipetted into 500 ml round bottom flask and the solvent was evaporated with nitrogen. Traces of the solvent were removed by evacuation for 20 minutes at 2 mm Hg. 1.2 ml D_2O containing 150 mM NaCl and a few glass beads were added to the dry lipid and the flask filled with nitrogen and sealed with parafilm. The contents of the flask were shaken for 60 minutes using a flask-shaker. A warm water bath at 30°C was sometimes required to free the lipid from the sides of the flask. The milky liposomes formed were pipetted into 10 mm nmr tube and the tube was filled with nitrogen and capped. ^{31}P-nmr spectra were recorded using a JEOL. FX60Q as described above.

IV.2.7 Lipid Peroxidation:-

A yellow colour was observed during the transport experiment involving egg PC/40 mole% PE vesicles, particularly those incubated at 47°C and 57°C. Since the development of the yellow colour was associated with lipid peroxidation [200], further experiments were set up to investigate the effect of lipid peroxidation on bilayer permeability of the vesicles.

To 0.5 ml of egg PC/40 mole% PE vesicles, 5 mM Pr^{3+} was added and the nmr tube was filled with oxygen free nitrogen and capped to avoid oxidation by air. The vesicle solution at this stage was clear and typically bluish. Lipid oxidation was initiated either by introducing 2 µl of (30 volume) hydrogen peroxide, or by uncapping the nmr tube so that oxidation by air takes place. Lipid oxidation and transbilayer transport were followed simultaneously. Progress of peroxidation was followed by removing known microlitre amounts of the vesicle solution and dissolving the vesicles in 2 ml spectroscopic ethanol. The peroxidation index $\frac{A\ 215}{A\ 233}$ [200] was measured using the Beckman (Model 26) UV spectrophotometer. A cell of 1 cm path length was used. Transbilayer transport of Pr^{3+} across the vesicles was followed by ^1H nmr as described previously.

IV.3 Experimental Results

IV.3.1 The effect of calcium ions on transbilayer transport of lanthanides across egg PC/10 mole%CL vesicles monitored by ^{1}H-nmr:

The effect of various concentrations of calcium on transmembrane transport of Dy^{3+} across egg PC/10 mole% CL vesicles is shown in (Fig. IV.2). In the absence of calcium ions it can be seen that slow but appreciable amount of transport occurs. The addition of 5 mM Ca^{2+} to the vesicles caused an increase in the rate of Dy^{3+} transport by approximately one order of magnitude i.e. from 3.8 Hz/min to 8.4 Hz/min.

However, more important is the rapid increase in transport occurring during the initial 10 minutes of transport which is in contrast to the gradual increase observed when Ca^{2+} is excluded from the mixture. The addition of higher concentrations of calcium (10 mM and 20 mM) gives rise to further increases in permeability. However, all concentrations of Ca^{2+} (5, 10 and 20 mM) cause similar transport behaviour, that is, substantial increase in the rate of Dy^{3+} transport, and this reaches a plateau after approximately 30 minutes. It is important to mention that the transport of calcium itself is possible since this metal is diamagnetic and can not be detected by nmr.

In the preliminary experiments carried out in this work the transport of Dy^{3+} occurring in sonicated vesicles containing very low concentrations of cardiolipin (1 mole%) was compared with the Dy^{3+} transport occurring in the control i.e. vesicles containing pure egg PC. Fig. IV.3 shows that the effect of added Ca^{2+} is detectable even at this concentration of negatively charged lipid. Extravesicularly added calcium is seen to cause appreciable

FIG. IV. 2

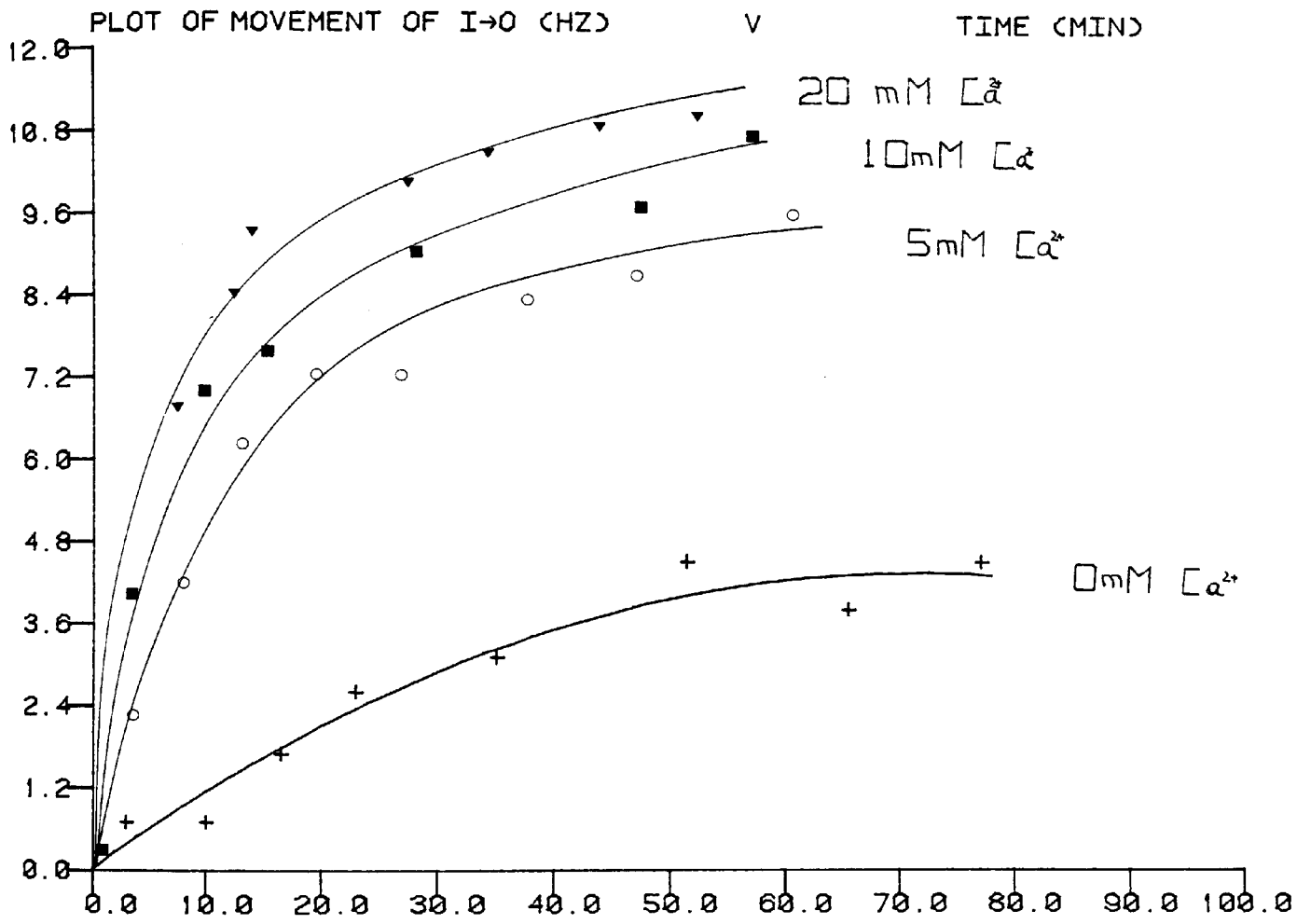

FIG. IV. 2 SHOWS THAT IN THE ABSENCE OF CALCIUM AN APPRECIABLE AMOUNT OF TRANSPORT OCCURS. THE EXTRAVESICULAR ADDITION OF CALCIUM IONS TO EGG PC/10 MOLE% CL VESICLES CAUSE THE RATE OF DY^{3+} TO INCREASE

Fig.IV.3 EFFECT OF CALCIUM IONS ON THE TRANSPORT OF Pr^{3+} ACROSS EGG PC/1 MOLE % CL VESICLES COMPARED WITH THAT OCCURRING IN PURE EGG PC VESICLES (CONTROL)

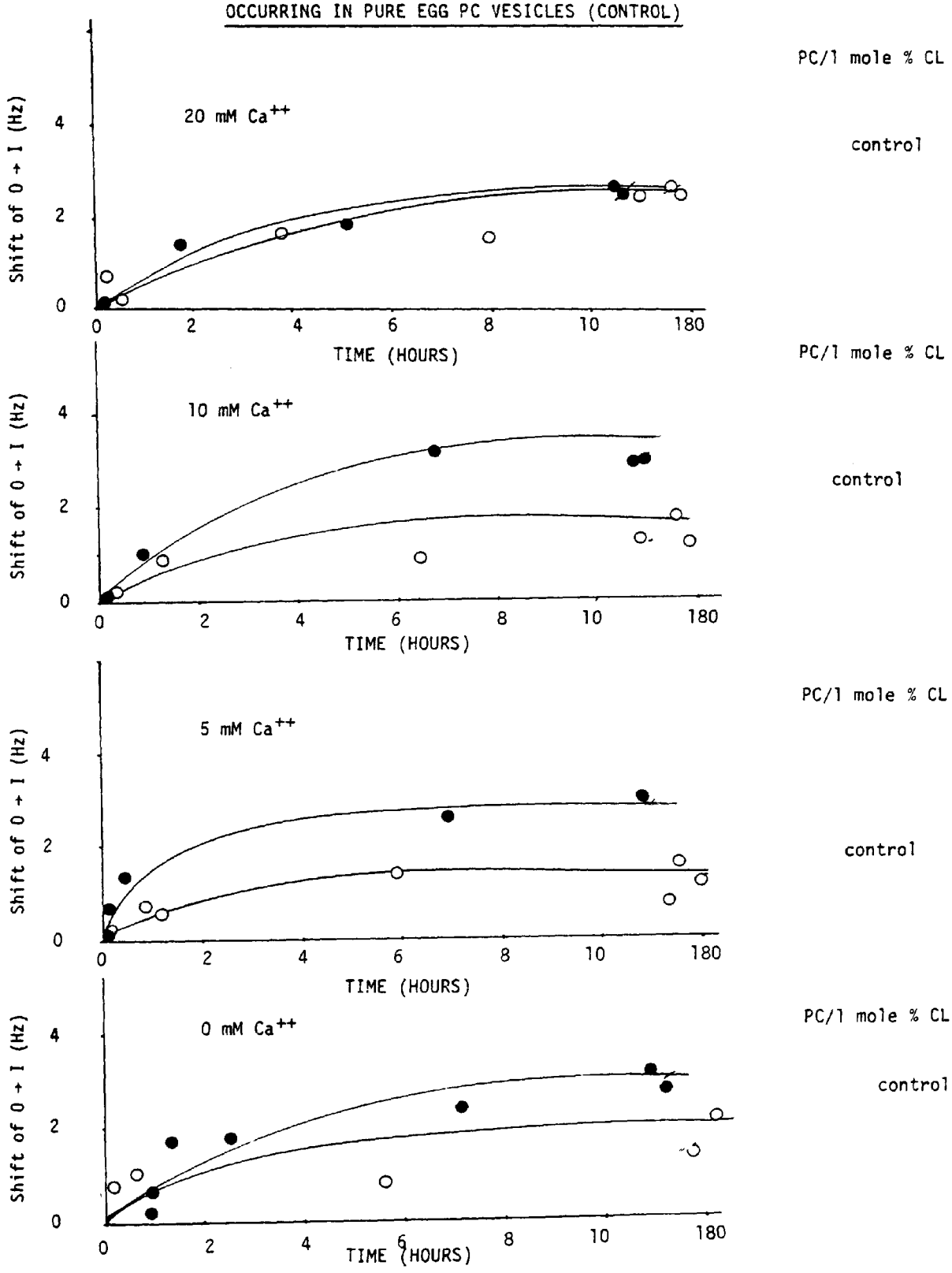

increase in the rate of transport which is considerably higher than the transport occurring in pure egg PC vesicles. In agreement with the transport results obtained with egg PC/10 mole% CL vesicles, Fig. IV.3 shows that calcium causes a rapid increase in the initial rate of transport across egg PC/1 mole% CL vesicles, and this rapid transport soon reaches a plateau.

IV.3.2 Transmembrane "flipflop" monitored in sonicated vesicles containing physiological concentrations of PA:

The addition of 0.15 mM Dy^{3+} to egg PC/10 mole% PA vesicles revealed that the outer choline signal is asymmetric; the shoulder on the lowfield side of signal "O" probably being caused by the adjacence of phosphatidate molecules to phosphatidyl-choline headgroups. The negative charge of PA enhances the binding of the Ln^{3+} to the adjacent PC molecules, hence causing greater downfield shift of the cholines. The unshifted inner choline resonance (Fig. IV.4) is symmetric and sharp indicating that the vesicles are stable, and Ln^{3+} diffusion inside the vesicles does not occur. Recording the ^{1}H-nmr spectrum of these vesicles at measured time intervals (Fig. IV.4) shows that the lowfield shoulder of signal "O" gradually disappears, signal "O" enhances in intensity and shifts upfield, whilst signal "I" decreases in intensity but remains unshifted. The rate of occurrence of these events is slightly increased by extravesicularly adding calcium (Fig. IV.5).

The addition of the lanthanide (and calcium) to these vesicles causes the partial neutralization of PA negative charge which encourages the formation of inverted micelles [11].

Fig.IV.4 'H-NMR SPECTRUM OF EGG PC/10 MOLE % PA

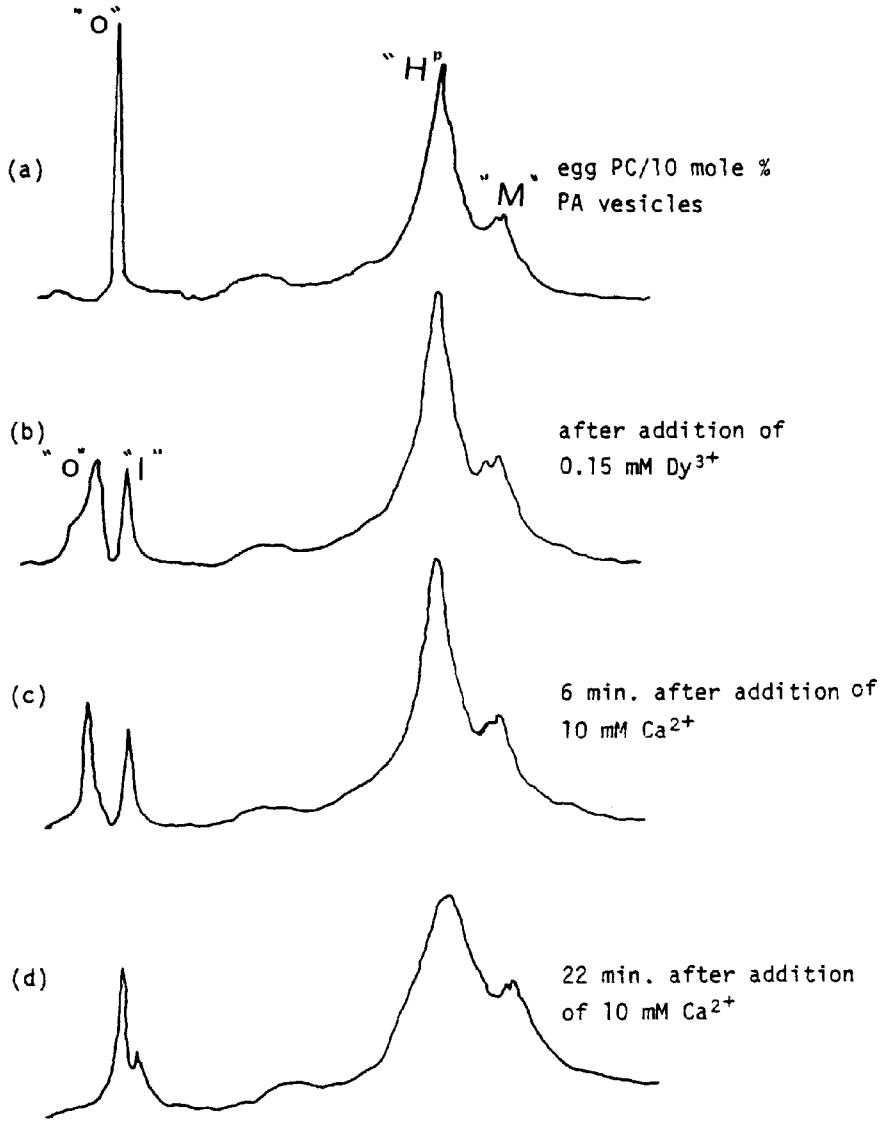

Adding 0.15 mM Dy^{3+} to the vesicles results in an asymmetric outside choline signal (b) which becomes more symmetrical with time (c). Signal "I" remains unshifted whilst signal "O" shifts upfield (c) and (d). Signal "O" enhances in intensity whilst signal "I" decreases in intensity (c) and (d).

FIG. IV. 5

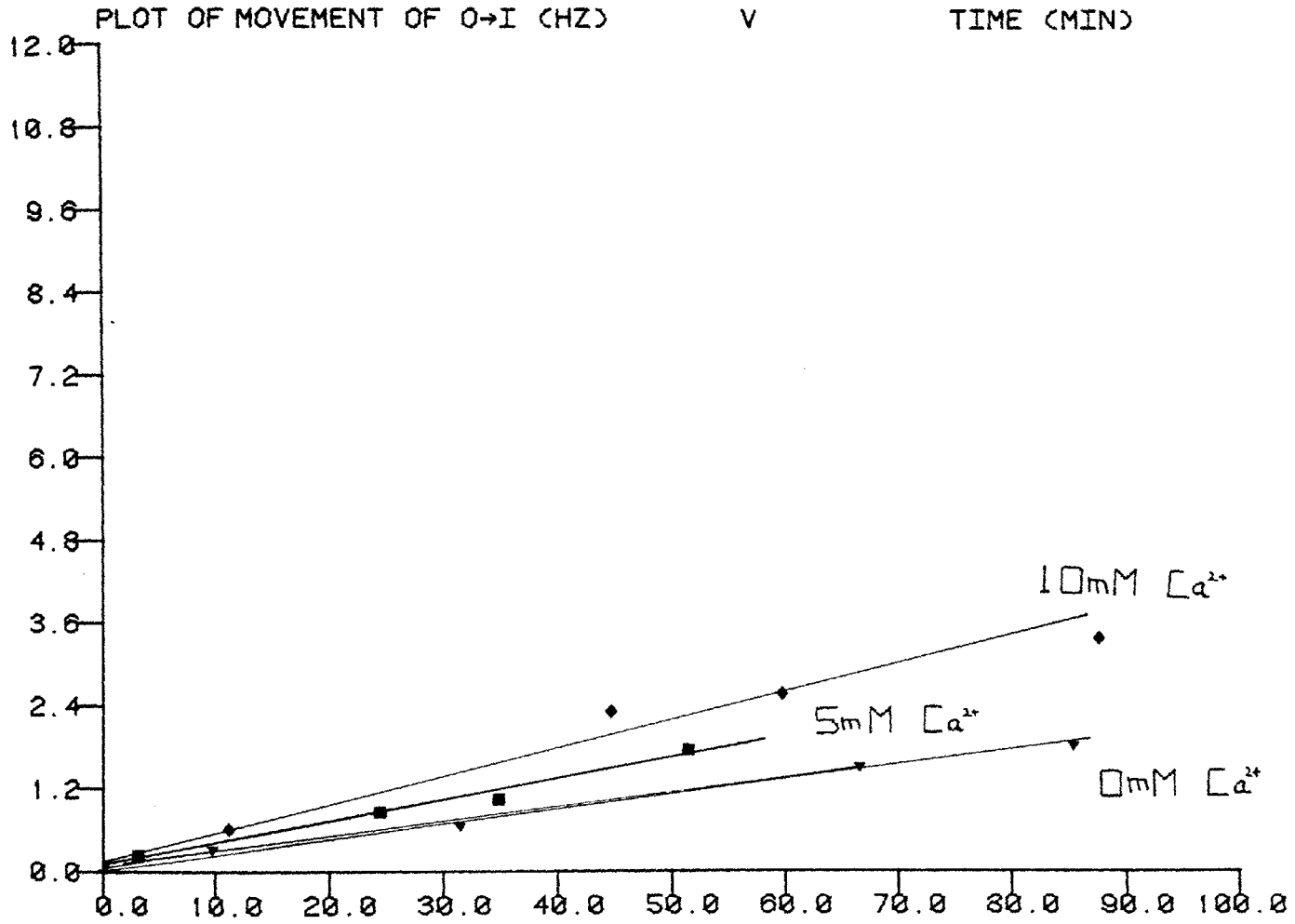

FIG. IV. 5 SHOWS THAT PHOSPHOLIPID FLIPFLOP OCCURSIN EGG PC/10 MOLE% PA VESICLES. EXTRAVESICULARLY ADDED CALCIUM INCREASES THE FLIPFLOP RATE.

These micelles mediate transmembrane movement of PA from the "outer" to the "inner" monlayer; hence the gradual disappearance of the lowfield shoulder, and this migration of PA is accompanied by a fast exchange of PC which migrates from the inner to the outer leaflet; hence the decrease in the intensity of signal "I" and the simultaneous increase in the intensity of signal "O". The disappearance of PA from the outer monolayer lowers Ln^{3+} binding to this monolayer hence causing signal "O" to shift upfield. Signal "I" remains unshifted suggesting that Ln^{3+} transport inside the vesicles does not occur. The non shifting of signal "I" also suggests that the inverted micelles mediating transbilayer flipflop are different from those mediating transbilayer transport in that the former do not open into the aqueous space inside the vesicles, i.e. these micelles remain in lateral diffusion along the horizontal plane of the bilayer.

The effect of extravesicular calcium ions (5 and 10 mM) is much more noticeable in transbilayer transport occurring in egg PC/10 mole% CL vesicles (Fig. IV.2) as compared with transbilayer flipflop occurring in egg PC/10 mole% PA vesicles (Fig. IV.5). This is probably due to the difference in negative charge between phosphatidate and cardiolipin; the addition of lanthanide and calcium ions to PA and CL containing vesicles causes subtantial neutralization of the negative charge of PA compared with CL.

IV.3.3 Asymmetric distribution of phospholipids detected by ^{31}P-nmr:

^{31}P-nmr is a useful technique for the investigation of transbilayer asymmetry in phospholipid vesicles containing phosphatidyl choline and negatively charged

lipids. The usual approach is to compare the intensities of the "inner"and "outer" signals for a given phospholipid component separated by lanthanide ions added from the outside or the inside of the vesicles [201]. The ^{31}P-nmr spectrum of egg PC/10 mole% PA vesicles without paramagnetic ions is shown in Fig. IV.6.(a) . The three phosphorus resonances are assigned to external PA, external PC and internal PC (Fig.IV.6.(a)). The titration of paramagnetic ions (0.3 mM Pr^{3+}) results in the downfield shift of the external PC signal and the complete broadening of external PA signal (Fig.IV.6.(c)). The disposition of the internal PA resonance is then revealed to be under the unshifted external PC resonance (Fig.IV.6.(c)) therefore, the two unshifted signals in Fig.IV.6.(c) belong to the internal PC and PA appearing at low and high field respectively. A schematic representation of the distribution of PC and PA before and after the addition of paramagnetic ions is shown in Fig. IV.7.

The following observations can be made on the ^{31}P-nmr spectra shown above:

(a) Comparing the intensities of the "inner" and "outer" PA resonances (Fig. IV.6) shows that PA favours the inside monolayer of the vesicles. This is to be expected since the comparatively smaller head-group of phosphatidate (c.f. bulky choline head-group), and the small radius of curveture of the vesicle enables PA molecules to pack much closer in the inner monolayer.

(b) The separation of outside and inside PC resonances without paramagnetic ions is 11.9 Hz (Fig.IV.6.(b)). This is considerably larger than that observed in pure egg PC vesicles (4Hz) at 36.4 MHz [202]. This is due to the effective shielding of the external magnetic field caused by the unequal distribution of negative charge of phosphatidate (See point (a)).

Fig.IV.6 ^{31}P-NMR SPECTRUM OF EGG PC/10 MOLE % PA VESICLES SHOWING TRANSBILAYER FLIP FLOP

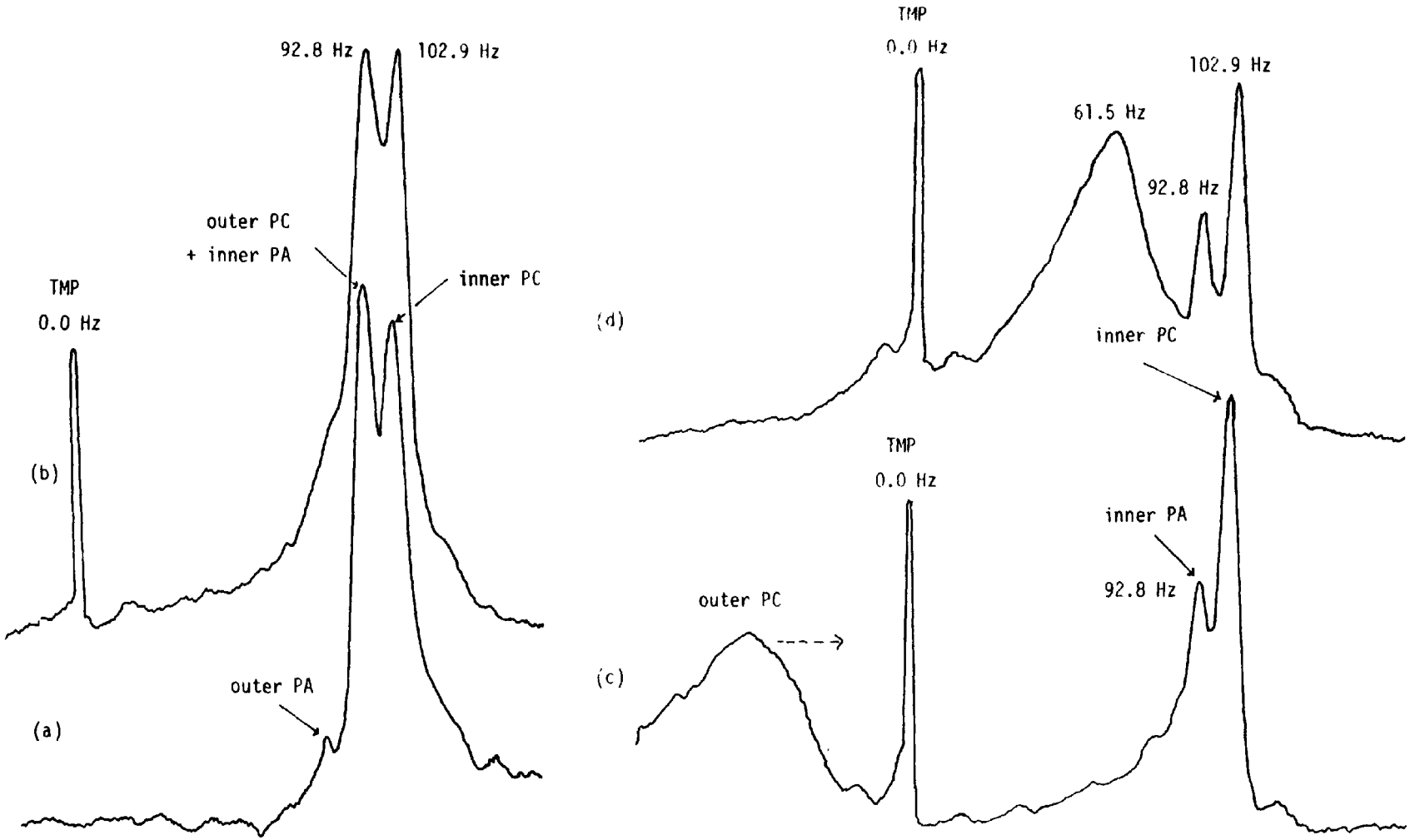

NOTE THAT IN (a) THE OUTER PC AND INNER PA SIGNALS OVERLAP. THE SMALL OUTER PA SIGNAL (SHOWN IN (A)) BROADENS TO THE BASE-LINE UPON ADDITION OF 0.3mM Pr^{3+} (c). ADDING Pr^{3+} SHIFTS THE OUTER PC RESONANCE DOWNFIELD (c) WHICH REVEALS THAT THE POSITION OF THE INNER PA IS UNDER THE UNSHIFTED OUTER PC. 30 MINUTES AFTER ADDING 5 mM Ca^{2+} THE OUTER PC SIGNAL IS SHIFTED UPFIELD (d), WHILST THE INNER PA AND INNER PC SIGNALS REMAIN UNSHIFTED (d).

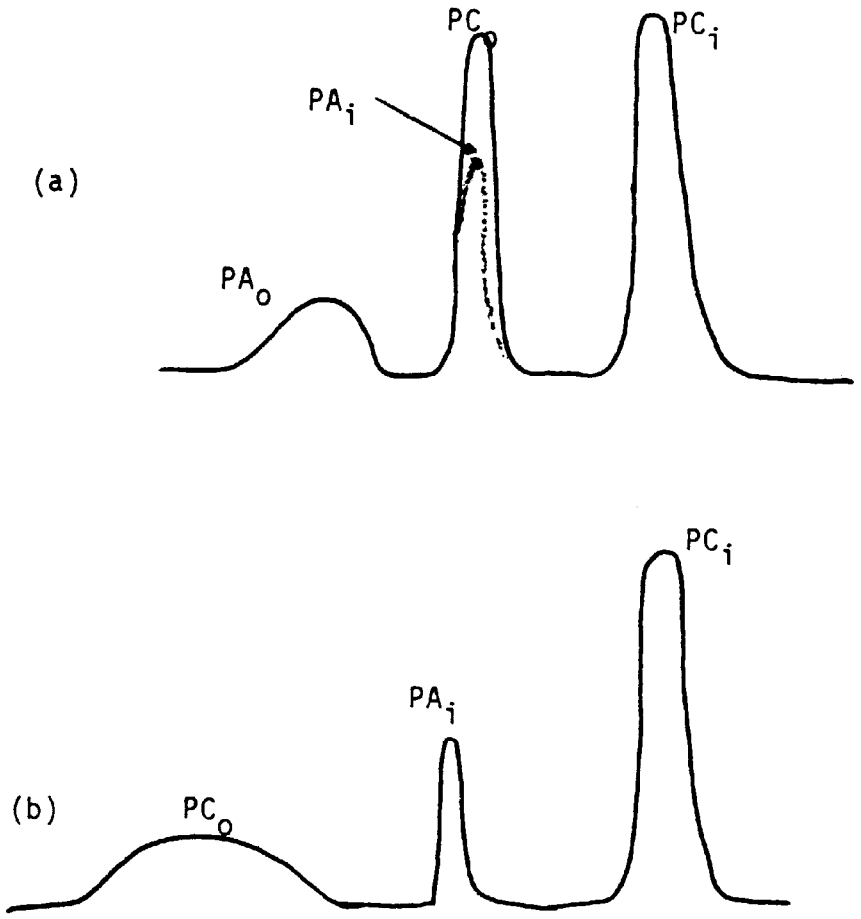

FIG.IV.7. Schematic representation of ^{31}P nmr spectrum of Egg PC/10 mole % PA vesicles before and after the addition of the lanthanide. The position of internal PA is under the unshifted outer PC, and the outer PA signal broadens completely after the addition of Ln^{3+}.

(c) The addition of 0.3 mM Pr^{3+} to the vesicles causes the external PA signal to broaden completely due to the stronger binding of this metal to the negative charge of phosphatidate. Also it should be remembered that the binding of the Ln^{3+} takes place to the phosphate oxygen, hence the shifts produced in the outer head-group signal are a combination of both contact (through bond) and pseudocontact (through space) effects, the former predominating.

(d) Fig. IV.6.(a) shows that the internal PA signal is approximately one fifth that of internal PC although the total phosphatidate per vesicle is 10% of the total phospholipid present. This shows that PA favours the inside monolayer. If PA is equally distributed in both halves of the bilayer the ratio of internal PA to internal PC would be one tenth.

IV.3.4 Transbilayer flipflop monitored by ^{31}P-nmr:-

The effect of adding calcium ions to egg PC/10 mole% PA vesicles containing 0.3 mM Pr^{3+} is shown in Fig. IV.8 . The external PC signal increases in intensity and shifts slightly upfield with respect to the internal standard (TMP). The time dependent changes occurring in the external PA signal can not be monitored because this signal broadens completely upon adding the lanthanide (Fig. IV.6). Internal PA signal intensity decreases perhaps due to the removal of PA from this monolayer to form inverted micelles inside the hydrocarbon region of the bilayer. The upfield shift of external PC signal indicates that perhaps PA is removed from this monolayer hence causing lanthanide ion binding to decrease (Fig. IV.8).

Fig.IV.8 ^{31}P-NMR SPECTRUM OF EGG PC/10 MOLE % PA VESICLES

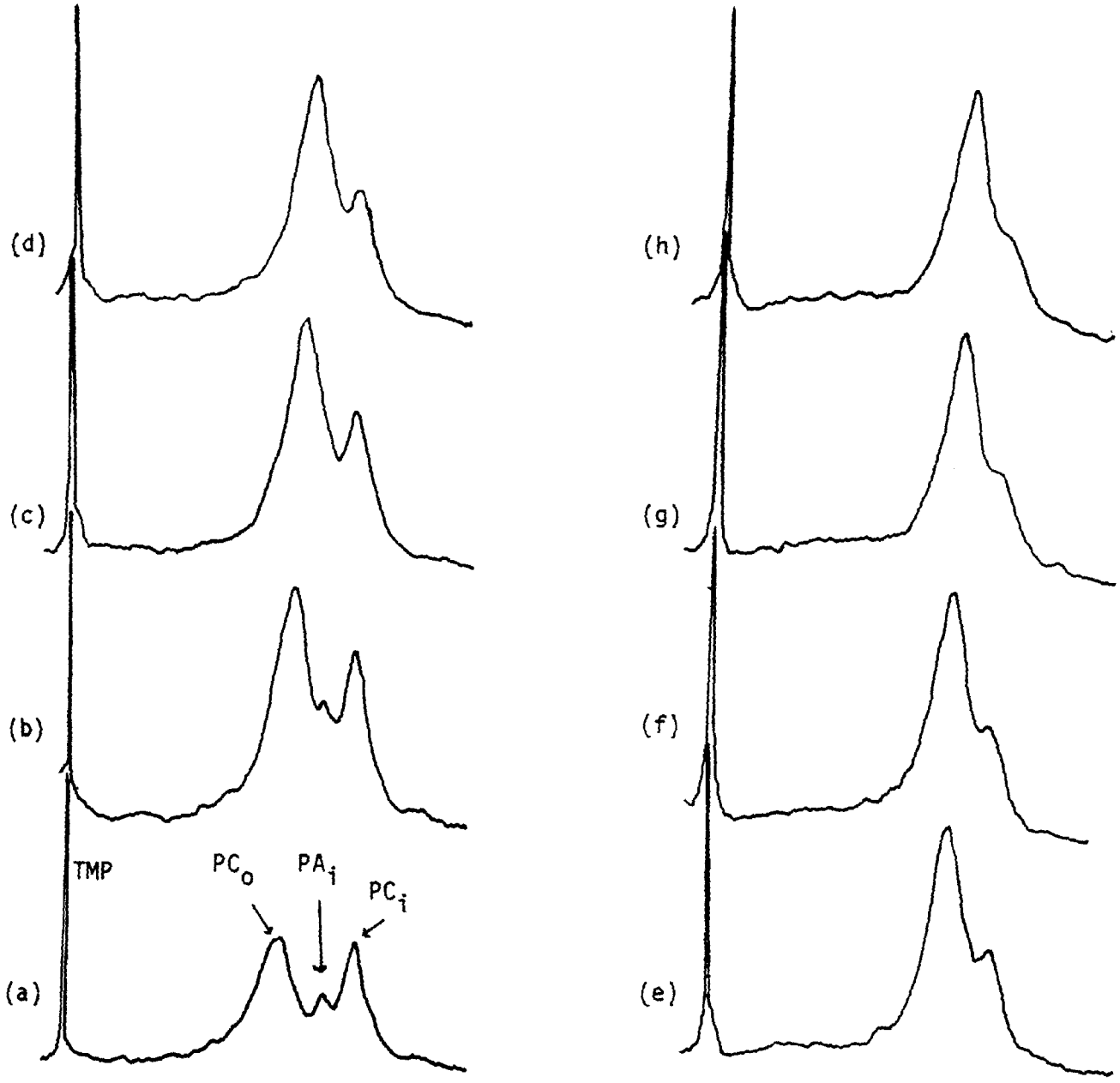

External PC signal enhances in intensity and internal PA signal decreases in intensity. External PC signal remains unshifted whilst internal PC signal shifts downfield. Internal PA signal gradually disappears.

The spectra were collected every 30 minutes.

IV.3.5 Polymorphic phases adopted by phosphatidylethanolamine:

The effect of increasing the temperature on transbilayer transport of Pr^{3+} across egg PC/40 mole% PE is shown in Fig. IV.9 . At 25°C and 37°C very slow transport is seen to occur. This is in contrast to the enhanced permeability occurring at 47°C and 57°C. A distinct feature of Fig. IV.9 is the sudden increase in permeability occurring at 47°C and 57°C compared with at 37°C and 25°C. This indicates that the temperature induced bilayer changes causing enhanced permeability are triggered at a temperature above 37°C. These bilayer modifications are suggested to be inverted micelles occurring inside the hydrocarbon region of the bilayer (Fig. I.13)

During the time course of the above experiment the vesicles incubated at the higher temperatures (37°C upwards) developed a yellowish colour indicating that slight peroxidation took place. Lipid peroxidation has been associated with increased bilayer permeability[103] . Therefore, in order to distinguish between the cation permeability occurring due to the formation of inverted micelles and the increased permeability occurring due to lipid peroxidation, experiments were set up to follow these two processes simultaneously (See Section IV.3.8).

IV.3.6 Vesicle-Vesicle fusion:

The effect of calcium ions on the ^{1}H-nmr acyl chain resonance of egg PC/ 10 mole% CL vesicles is shown in Fig. IV.10. The time dependent increase in the line width of this signal indicates that vesicle-vesicle fusion is taking place[203]. Similar effects were observed on the ^{1}H-nmr spectra of egg PC

FIG. IV. 9

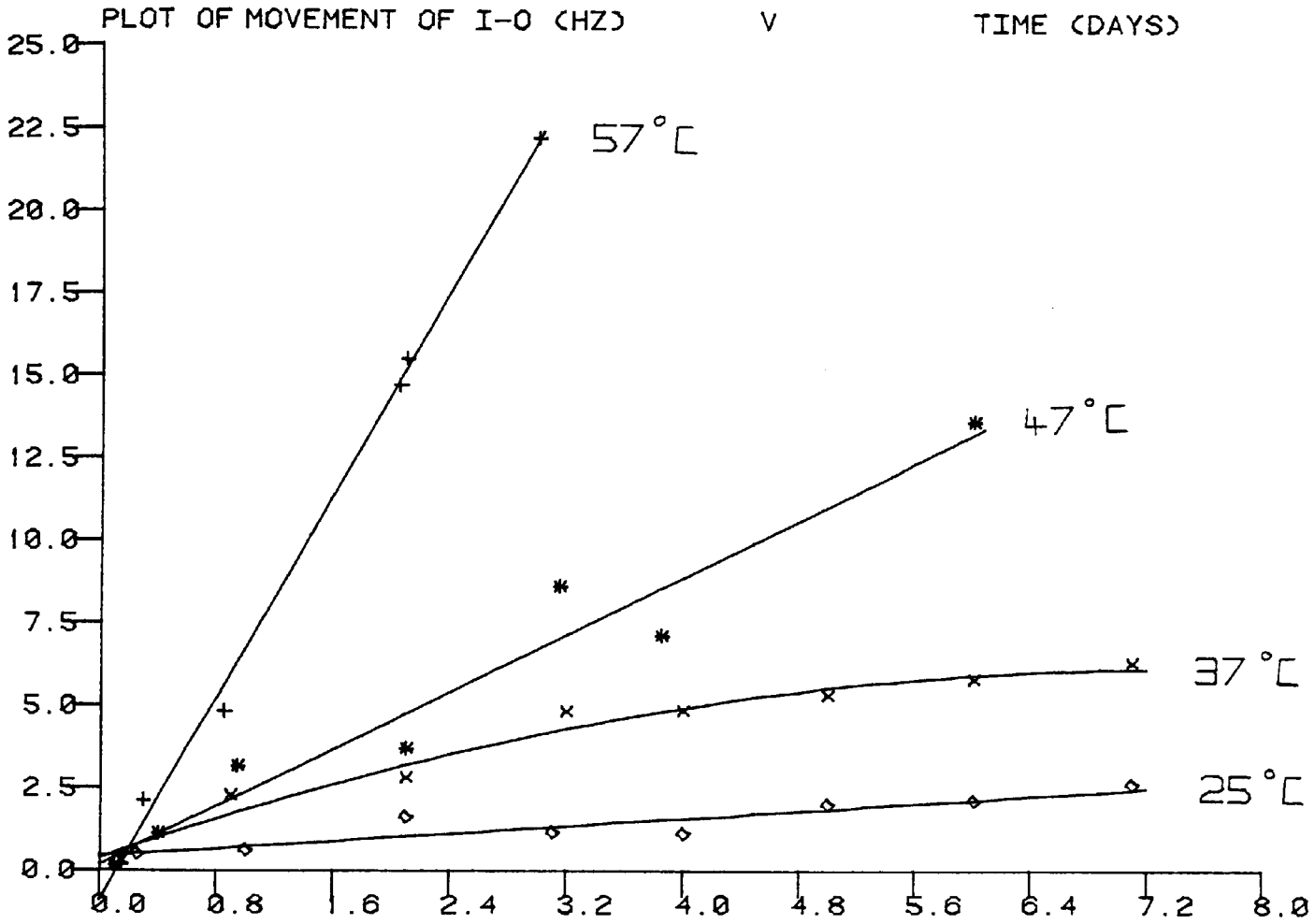

FIG. 9 SHOWS THAT AT 25°C AND 37°C THE TRANSPORT OF Pr^{3+} ACROSS EGG PC/40 MOLE% PE VESICLES IS SLOW. INCREASING THE TEMPERATURE TO 47°C OR 57°C INCREASES THE TRANSPORT RATE SUBSTANTIALLY.

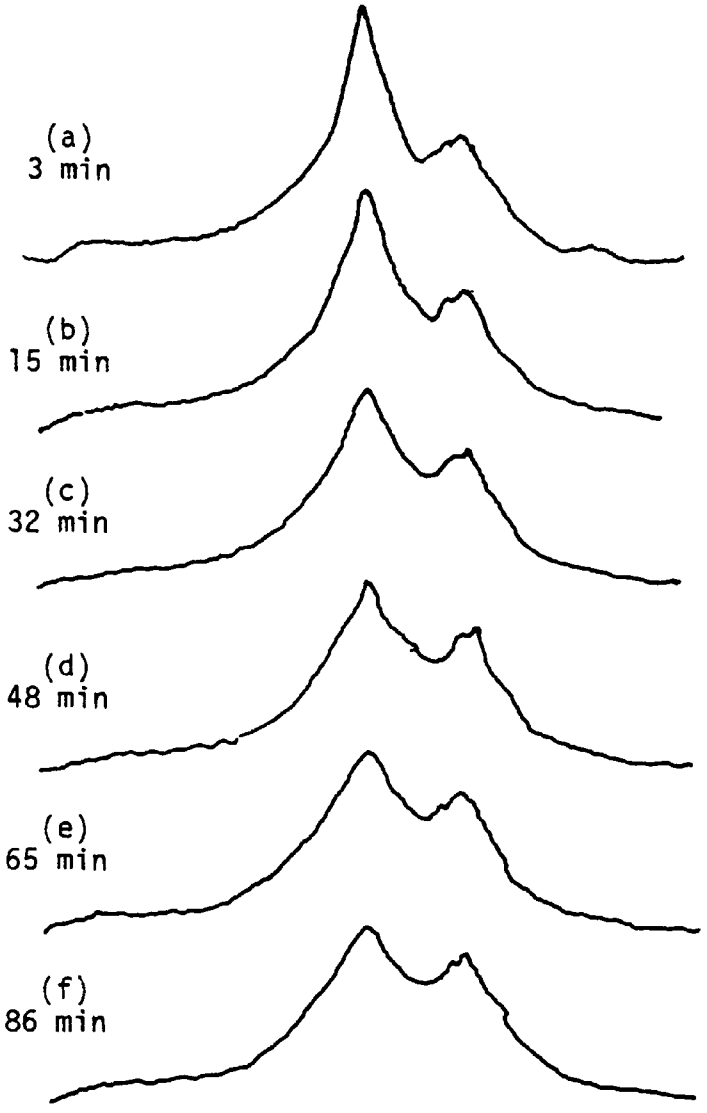

FIG.IV.10 shows the time-dependent increase in line-width of the acyl chain resonance (signal H) which indicates that vesicle-vesicle fusion occurred.

1 mole% CL vesicles, egg PC/10 mole% PA vesicles and egg PC/40 mole% PE vesicles (Results not shown).

The results in Fig. IV.11 show that egg PC/10 mole% CL vesicles do not fuse in the absence of calcium. However, in the presence of 5, 10 and 20 mM Ca^{2+} a concentration dependent increase in the rate of fusion takes place. Fig. IV.12 , shows that the rate of vesicle-vesicle fusion occurring in the vesicles containing low concentrations of cardiolipin (1 mole%) is higher than that occurring in the control (i.e. vesicles containing pure egg PC). This is consistent with the suggestion that negatively charged phospholipids under certain conditions exhibit configurations which facilitate bilayer fusion [11]. Egg PC/10 mole% PA vesicles fuse even in the absence of calcium (Fig. IV.13) probably due to the partial neutralization of PA by the lanthanide. The rate of fusion occurring in these vesicles is higher than that occurring in egg PC/ 10 mole% CL vesicles (Fig. IV.11). This may be related to the molecular shape of PA (smaller headgroup compared to CL (Fig. I.3)) favouring closer packing of PA hence increasing the surface concentration of this phospholipid.

Egg PC/40 mole% PE vesicles exhibit (Fig. IV.14) very high rates of fusion at 47°C and 57°C compared with that at 37°C and 25°C. This suggests that the enhanced rate of fusion occurring above 37°C is probably due to the formation of inverted micelles (Fig. I.13) induced by the higher temperatures. Finally, the fusion rates occurring in PE containing vesicles are higher than that shown by PA or CL containing vesicles which suggests that the higher molar concentration of PE is responsible for the enhanced fusion occurring in the former vesicles.

FIG. IV. 11

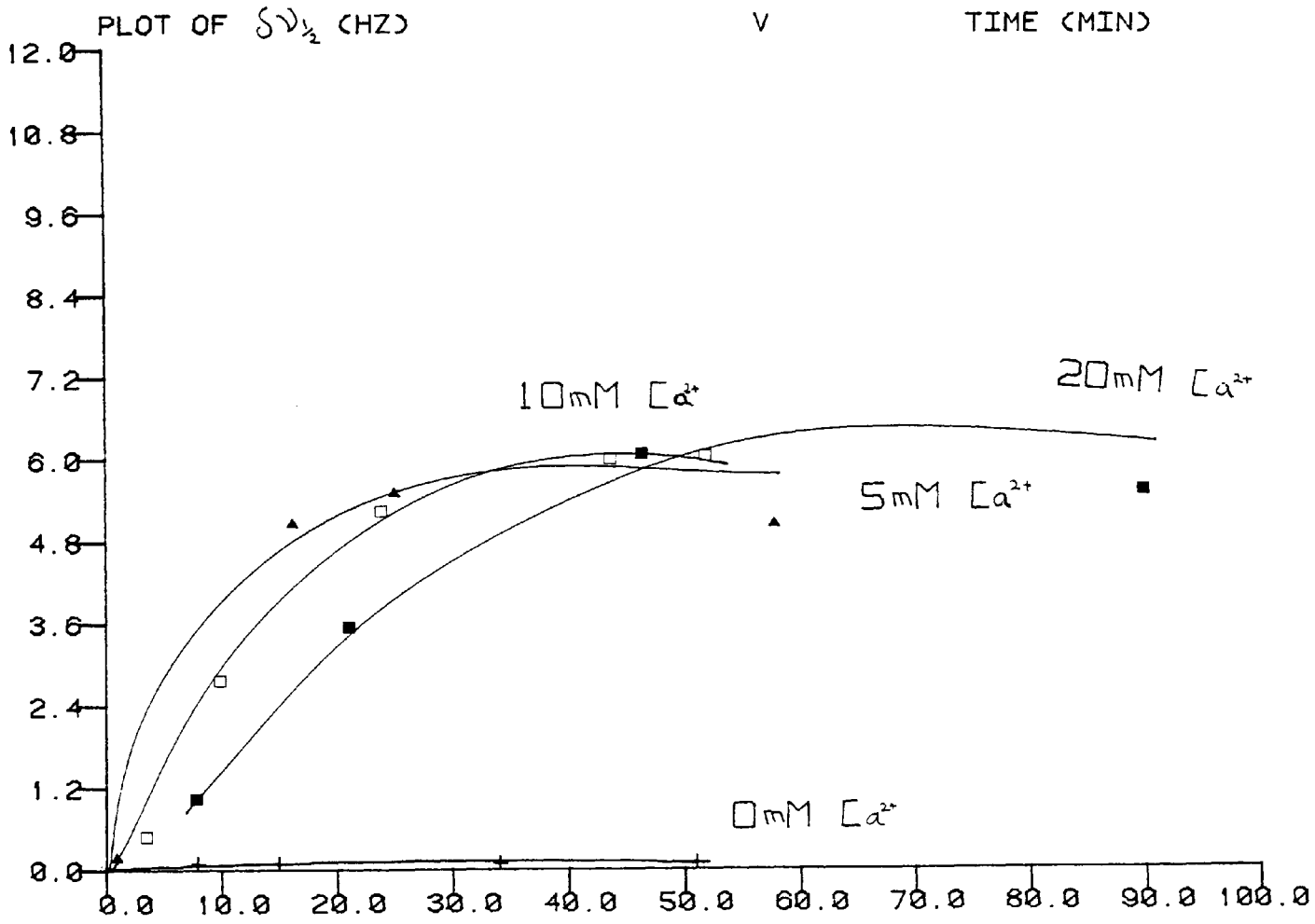

FIG. IV. 11 SHOWS THAT EGG PC/10 MOLE % CL VESICLES DONOT FUSE IN THE ABSENCE OF CALCIUM. THE EXTRAVESICULAR ADDITION OF 5, 10 AND 20 mM CALCIUM INITIATES VESICLE-VESICLE FUSION. THE MECHANISM OF FUSION IS DISCUSSED IN THE TEXT.

Fig.IV.12 EFFECT OF CALCIUM IONS ON FUSION RATES OF EGG PC/1 MOLE % CL VESICLES COMPARED WITH THAT OCCURRING IN PURE EGG PC VESICLES (CONTROL)

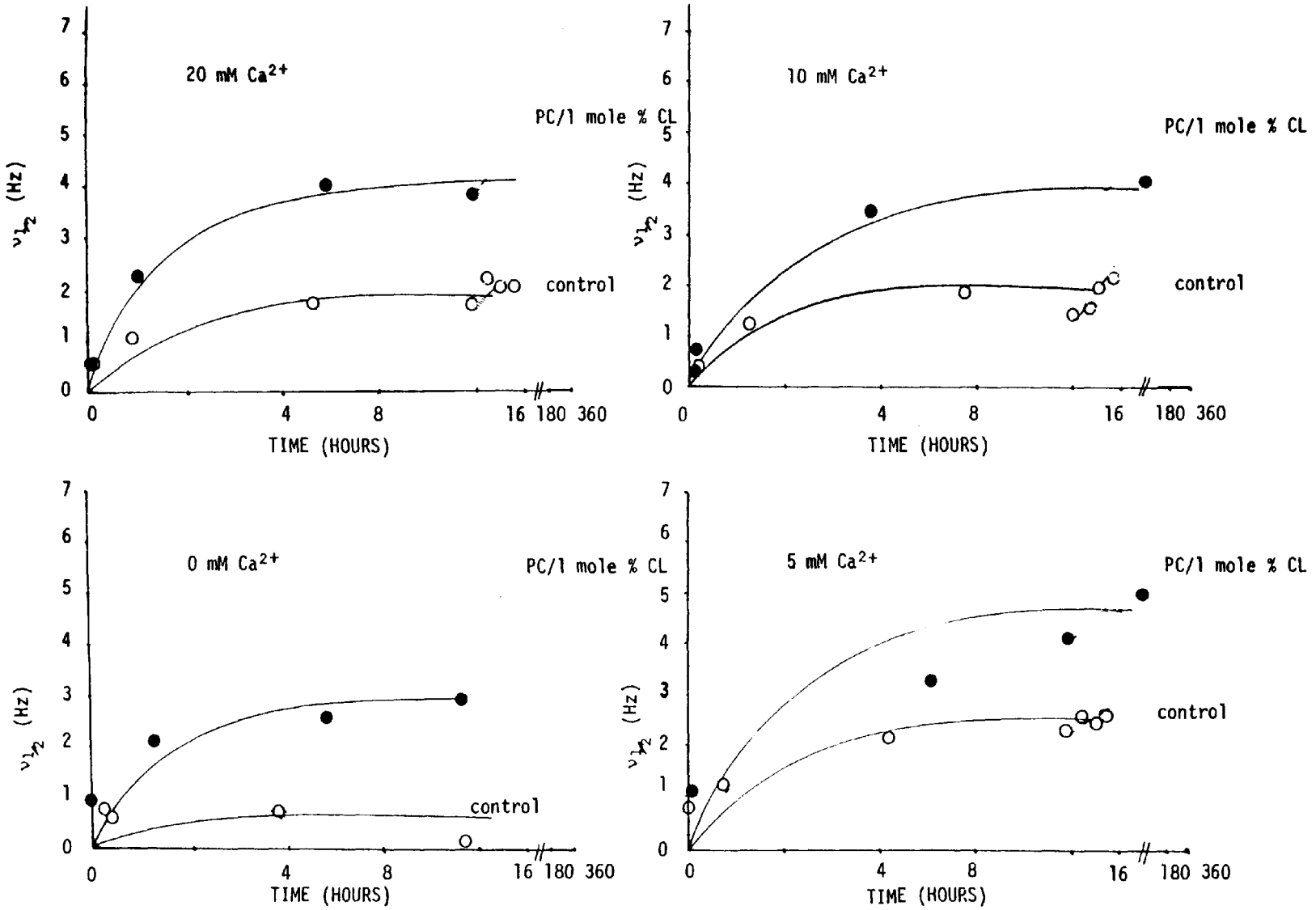

FIG. IV. 13

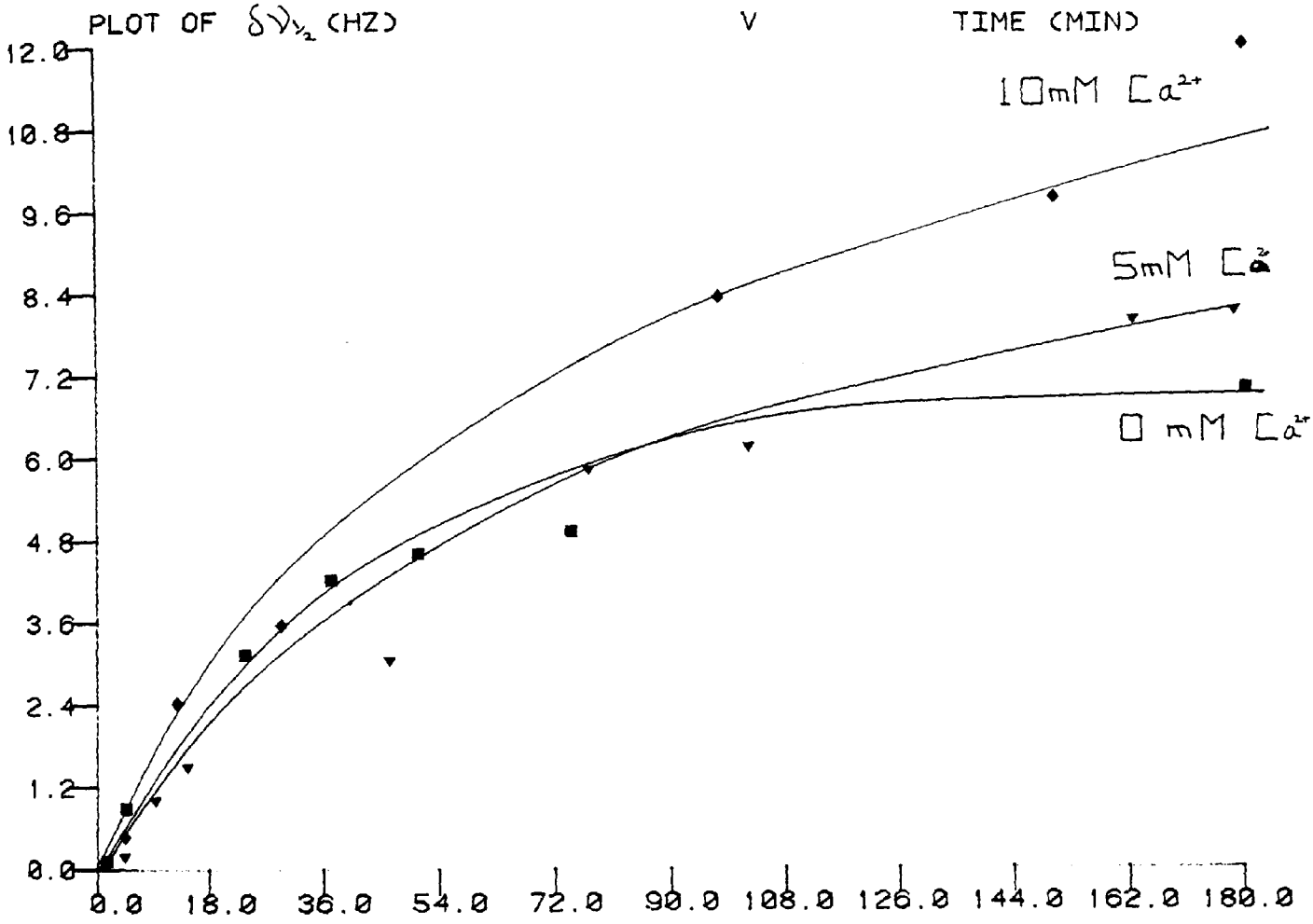

FIG. IV. 13 SHOWS THAT EGG PC/10 MOLE% PA VESICLES FUSE IN THE ABSENCE OF ADDED CALCIUM. 5 AND 10 mM CALCIUM CAUSE A SLIGHT INCREASE IN THE FUSION RATE.

FIG. IV. 14

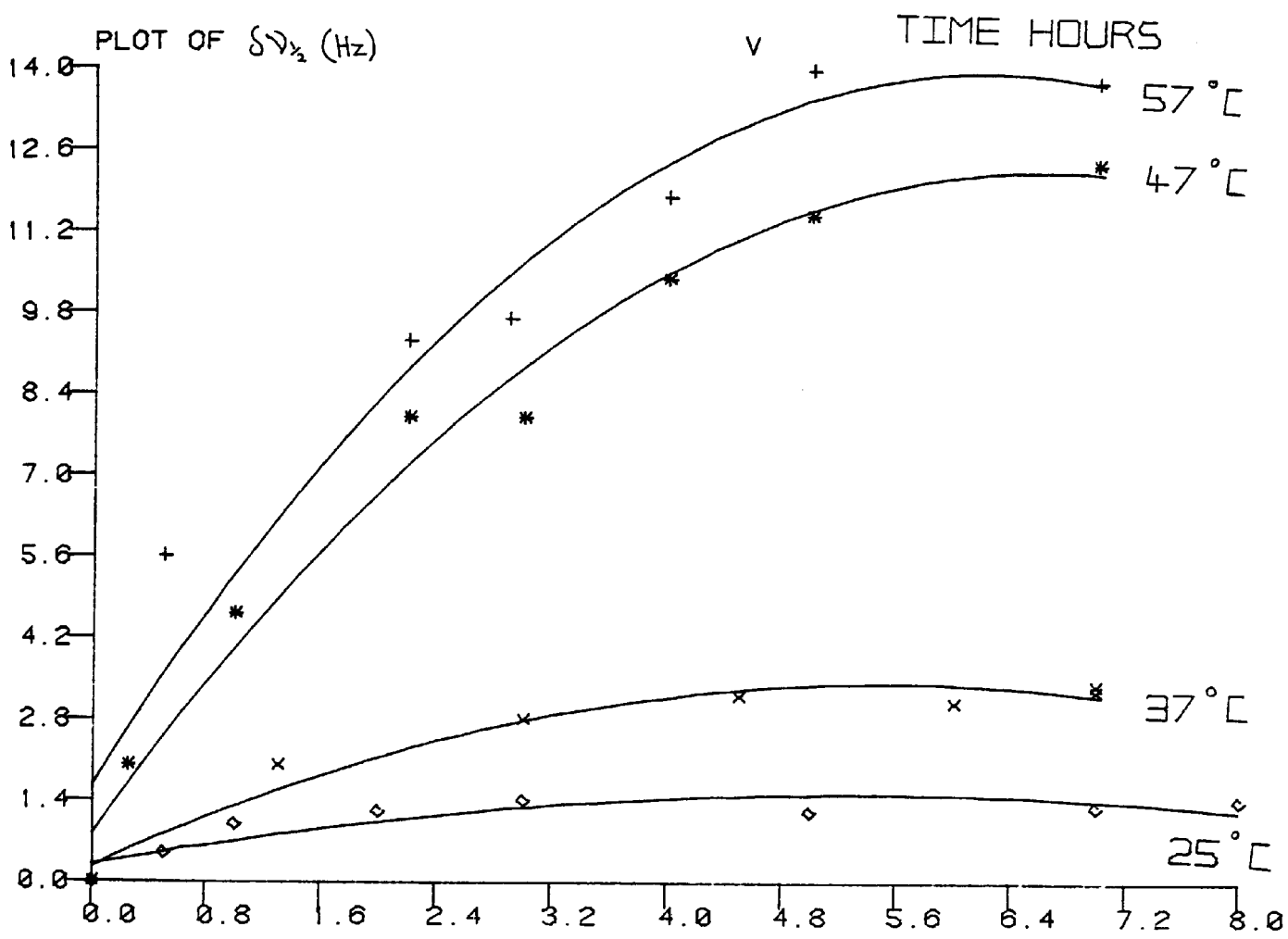

FIG. IV. 14 SHOWS THAT EGG PC/40 MOLE% PE VESICLES EXHIBIT HIGH RATES OF FUSION AT THE TRANSITION TEMPERATURE (47°C AND 57°C). BELOW THIS TEMPERATURE (AT 25°C AND 37°C) THE FUSION RATE IS SLOW.

IV.3.7. The polymorphic phase behaviour of *Micrococcus cryophilus* extracted phospholipids

The 24.15 MHz ^{31}P-nmr spectrum of the liposomes prepared from *Micrococcus cryophilus* extracted phospholipids at room temperature (21°C) is shown in Fig. IV.15.(b). The broad asymmetric lineshape with a small lowfield shoulder is similar to the ^{31}P-nmr spectra obtained for liquid crystalline phosphatidylcholines [204] and phosphatidylethanolamines [190] in the bilayer configuration. The size of the lowfield shoulder shown in spectrum (Fig. IV.15.(b)) is somewhat smaller than that shown by liposome dispersions of single phospholipids. At 4°C the ^{31}P-nmr spectrum (Fig. IV.15.(d)) has a highfield shoulder and reversed asymmetry as compared with the bilayer spectrum in addition a small spectral component superimposed on the ^{31}P-nmr spectrum indicating isotropic motional averaging was observed. This asymmetric spectrum has previously been identified with the hexagonal (H_{II}) phase [11]. Increasing the temperature to 22°C then decreasing it to 4°C (Fig. IV.15.(e)) showsthat the hexagonal H_{II} structure is reversible. However, the small spectral component in Fig. IV.15. (d) has now disappeared indicating that slight hysteresis may have occurred[205]. Figs. IV.15.(a) and (b) show that the bilayer structure dominates at higher temperatures.

Addition of 2 mM Ca^{2+} to the liposomes caused slight precipitation of the phospholipid and produced a ^{31}P-nmr spectrum (Fig. IV.15.(g)) consistent with the hexagonal H_{II}phase. Increasing Ca^{2+} concentration to 10 mM caused the complete precipitation of the phospholipid and microscopic structures which had the appearance of small polystyrene beads were observed. The ^{31}P-nmr spectrum of these structures (Fig. IV.15.(h)) contains a single sharp signal

Fig.IV.15 ^{31}P NMR LINE-SHAPES OF LIPOSOMES PREPARED FROM MICROCOCCUS CRYOPHILUS EXTRACTED PHOSPHOLIPIDS

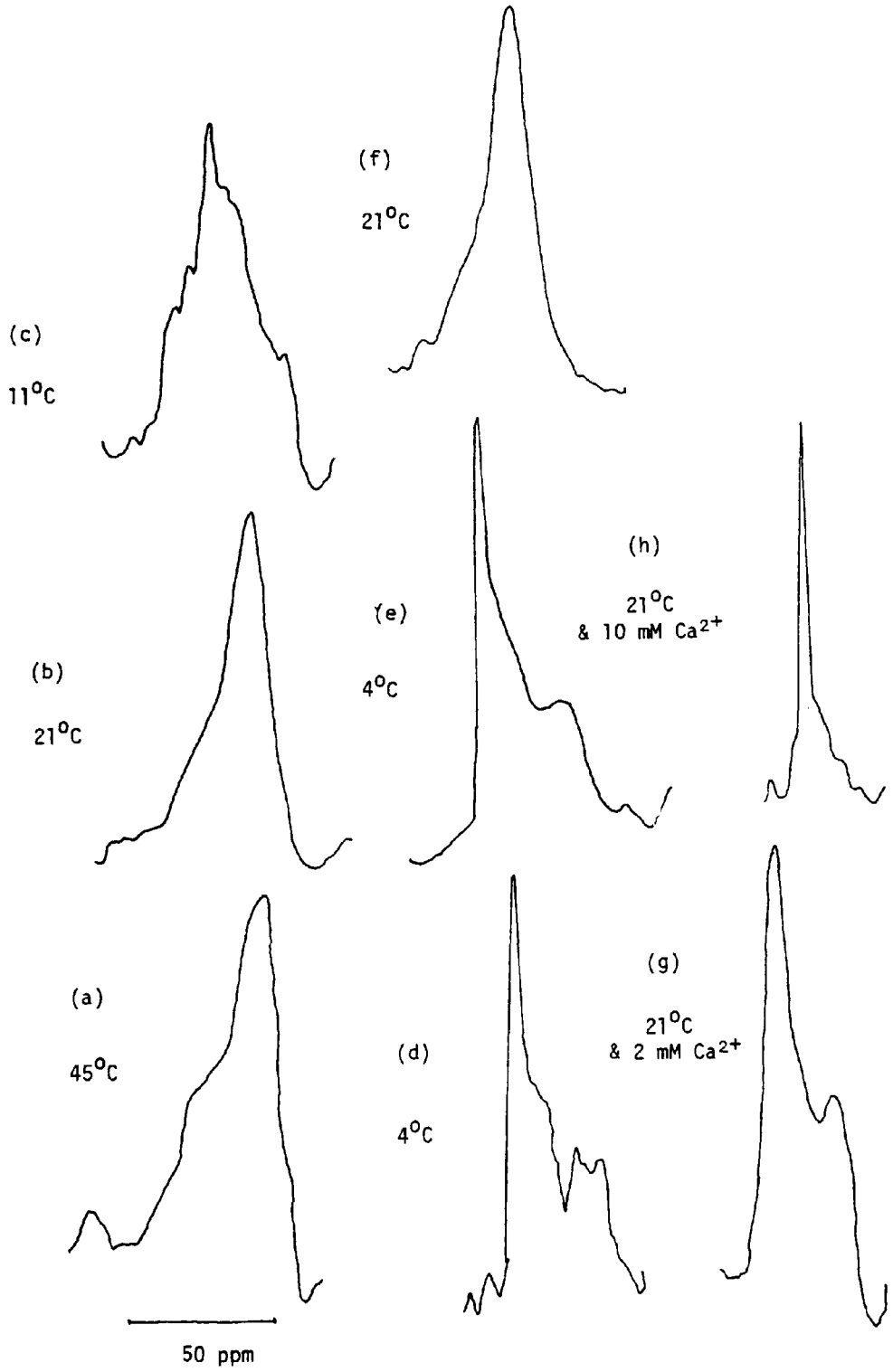

indicating that all the phospholipid experience isotropic motion.

IV.3.8 Lipid Peroxidation

During the transbilayer transport experiments (Section IV.3.5) egg PC/40 mole% PE vesicles incubated at 37°C, 47°C and 57°C (but not at 25°C) developed a yellow colour indicative of lipid peroxidation[103]. Because lipid peroxidation is associated with increased permeability the rate of cation permeability and the progress of peroxidation were measured simultaneously at 37°C. Fig. IV.16. shows that the vesicles incubated in air, those incubated under oxygen free nitrogen and those incubated with H_2O_2 show enhanced but comparable rates of transport. Therefore, the variation in vesicular environment does not seem to affect the rate of transport in these vesicles. The progress of lipid peroxidation, on the other hand, is sensitive to the vesicular environments (Bottom of Fig. IV.16). The peroxidation levels of the vesicles incubated with H_2O_2 are higher than those incubated in air or those incubated under oxygen free nitrogen. Hence, the progress of lipid peroxidation and transbilayer transport do not seem to be directly related.

However, a distinct feature of the transport occurring in the vesicles under all types of environments is the fact that a lag period of about three days during which minimal transport occurs (Fig. IV.16), this is followed by increased vesicular permeability during days 4 to 12. During this lag period the initial peroxidation breakdown products such as peroxides would be expected to react with free radicals to give further breakdown products such as short chain fatty acids, ketones, aldehydes and alcohols (Scheme I.1).

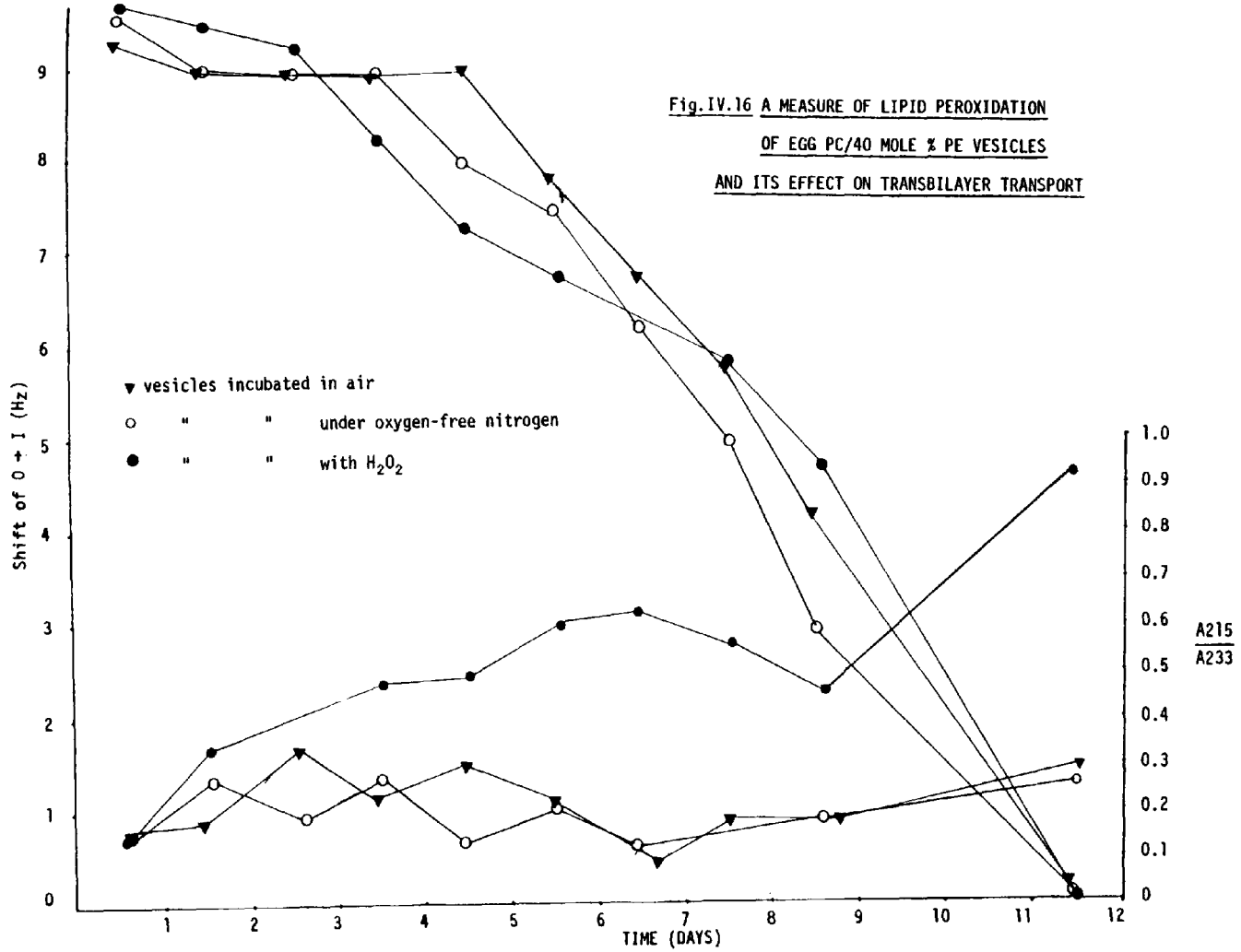

TOP: All types of vesicles (ie. under all extravesicular environments) show the same rate of transport.

BOTTOM: The vesicles incubated with H_2O_2 show higher degree of peroxidation compared with those incubated in air or under oxygen-free nitrogen.

IV.4 Discussion

IV.4.1 Transbilayer transport

At 37°C egg PC/10 mole% CL vesicles show (Fig. IV.2) that slow but appreciable amount of transport occurs. However, on addition of extra-vesicular calcium (5 mM) transbilayer transport increases rapidly (Fig. IV.2) particularly during the initial 5 to 10 minutes. Higher concentrations of calcium bring further change in the permeability of these vesicles. The almost instantaneous permeability enhancement occurring in these vesicles suggests that Ca^{2+} ions interact with cardiolipin (and phosphatidyl choline) headgroups; and such interaction may lead to certain bilayer instability causing vesicle permeability to increase. In fact, preliminary investigations conducted at the initial stages of this work have shown that cardiolipin concentrations as low as 1 mole% (Egg PC/1 mole% CL) cause enhanced (measurable) permeability changes compared with their counterparts containing pure egg PC (Fig. IV.3). Both Figs. IV.2 and IV.3 show that the cardiolipin component of the vesicles causes enhanced permeability which is dependant on the concentration of extravesicular calcium. The role of cardiolipin (and other acidic lipids) as cation-ionophores has been demonstrated by Tyson et al. [94] and Green et al;[206] these workers estimated the activity of this lipid to be comparable with that of the calcium ionophore X537A. However, for this lipid to act as an ionophore in this system (sonicated vesicles) it must be capable of conformational re-arrangements which permit the entry of lanthanide ions inside the interior aqueous space. Such structural re-arrangements are encouraged by the neutralization of cardiolipin negative charge by Ca^{2+}.[11] Model membrane studies of other workers have shown that the addition of calcium ions to cardiolipin containing

systems results in the formation of inverted micelles[207]. The occurrence of such micelles inside the hydrocarbon region of the bilayer (Fig. I.13) has been claimed to be demonstrated by the appearance of "lipid particles" [18] in freeze fracture replicas and by the prevalence of isotropic ^{31}P-nmr signals which indicate motional averaging in the nmr spectrum [11]. These inverted micelles are drawn approximately to scale with respect to the bilayer thickness (Fig. I.13) and it is clear that no geometrical constraints, or other topological problems are presented to the remaining bilayer. Hence, it is practically feasible to assume that the transitory formation of such inverted micelles provides a mechanism for lanthanide ion transport, in which net cation transfer is envisaged to occur providing that the lipid carrier is able to return to its original monolayer to initiate another transport cycle (Fig.IV.17).

Mandersloot et al.[208] reported that the addition of high concentrations of calcium (3.0 mM) to cardiolipin-phosphatidylcholine (1:1) liposomes results in the immediate precipitation of the lipid; and the complete loss of the permeability barrier. The extravesicular addition of 10 mM and 20 mM calcium (5:1 and 10:1 with respect to CL negative charge) to egg PC/10 mole% CL vesicles did not cause visible aggregation of the vesicle; nor caused destruction of the permeability barrier as shown in Fig. IV.2. This suggests that the relatively high concentration of the phosphatidylcholine component (90%) stabilized the vesicular bilayer. This stabilising property of PC is shared by other lipids such as PI and PS which are shown by ^{31}P-nmr to adopt the bilayer configurations when present separately[209][210], or in mixtures with cardiolipin[192][11].

Fig.IV.17

FACILITATED TRANSPORT OF IONS VIA FORMATION

OF INTRABILAYER INVERTED MICELLES

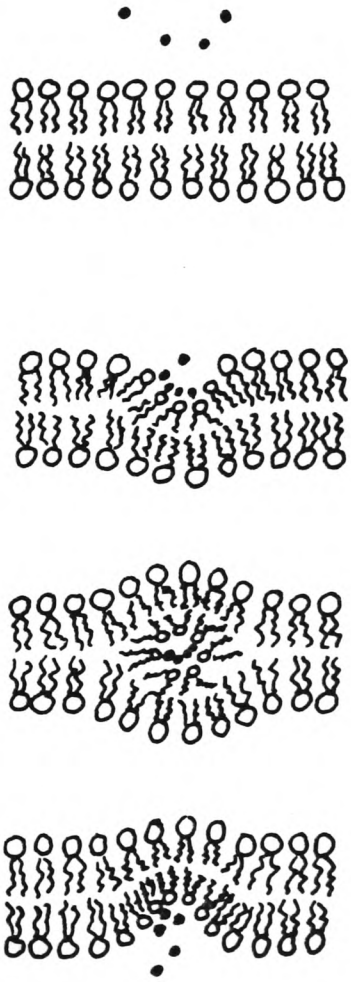

IV.4.2 Transbilayer flipflop

Monitoring transbilayer transport of lanthanide ions by the ^{1}H-nmr method involves the measuring of the lanthanide-induced shift of the inner choline signal with respect to an internal standard or with respect to the unshifted outer choline signal. However, the extravesicular addition of the lanthanide probe (Dy^{3+}) to egg PC/10 mole% PA vesicles caused the upfield shift of signal "O"; whilst signal "I" remained unshifted. In addition the ^{1}H-nmr spectrum of the vesicles shows that the outer choline resonance has a low-field shoulder, probably caused by the enhanced lanthanide binding due to the negative charge of phosphatidate . The extravesicular addition of the Ln^{3+} and Ca^{2+} caused the following time dependent changes on the ^{1}H-nmr spectrum of the vesicles(Fig. IV.4):

(i) The low field shoulder on the outer choline resonance gradually disappeared.

(ii) Signal I lost intensity but remained unshifted, whilst signal O shifted upfield.

(iii) Signal O enhanced in intensity and became more symmetrical as the down-field shoulder disappeared.

The only obvious explanation for this sequence of events is the migration of phosphatidate from the outer to the inner monolayer; hence the gradual disappearance of the lowfield shoulder. The simultaneous migration of phosphatidylcholine from the inner to the outer monolayer will cause the

gradual decrease of intensity of signal I and the increase of signal O intensity. Furthermore, the migration of PA from the outer to the inner leaflet decreases Ln^{3+} binding to the outer surface of the bilayer leading to the upfield shift of signal O. However, signal I remains unshifted suggesting that lanthanide ion transport does not occur. The above phospholipid exchange (flipflop) does not result in an increased number of lipid molecules in either of the two monolayers, and approximately equal number of PC have to move from the inner to the outer monolayer at a rate which is comparable to the appearance of PA in the inner monolayer.

These flipflop results are in agreement with those reported by De-Kruijff etal [188] who used ^{31}P-nmr to demonstrate that the conversion of PC to PA by phospholipase D causes the migration of PA formed in the outer monolayer to the inner leaflet; such migration is accompanied by an equally fast migration of PC from the inner to the outer monolayer. This group also reported that the flipflop process is not accompanied by transmembrane transport; a fact which is demonstrated here by the unshifting of the inner choline signal "I".

The agreement of these results suggests that a common mechanism of flipflop prevails; and it is suggested that inverted micelle intermediates serving in the re-distribution of phospholipids across the bilayer are involved (Fig. IV.18). However it is important to mention that the lack of transport in this system suggests that the inverted micelles mediating transmembrane flipflop (unlike those mediating transmembrane transport) do not open at either the extra-vesicular or the inter-vesicular aqueous spaces; but remain in lateral diffusion along the horizontal axis of the bilayer. The intermediary role of calcium in this process is to increase the exchange rate which is already initiated by the partial neutralization of PA negative charge by the trivalent lanthanide(Fig.IV.5).

Fig.IV.18 POSSIBLE MECHANISM OF FLIP-FLOP IN BIOMEMBRANES

(a)

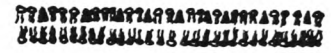

(b)

(c)

(d)

(a) Non-bilayer lipid is induced in one monolayer and subsequently redistributed across the membrane via formation of an intermediate inverted micell as in (b) and (c).

IV.4.3 Phospholipid distribution monitored by ^{31}P-nmr

The ^{31}P-nmr experiments were used to confirm the structural preference of PA and PC to the inner and outer monolayers, respectively. The structural preferences of PA and PC was demonstrated by the ^{31}P-nmr spectrum of egg PC/10 mole% PA vesicles (Fig. IV.6) which show that the ratio of the inner/outer PA is approximately 20:1 whilst that of inner/outer PC is approximately 1:2. This is consistent with the molecular shapes of these lipids (Fig. I.3) which show that the smaller headgroup size of PA (compared to that of PC) allows closer packing of PA molecules in the inner monolayer, and vice versa for PC. Barsukov and co-workers[201] investigated the transbilayer asymmetry of three negative phospholipids (PI,PG and PS) using two different shift probes and found that these negatively charged lipids distribute with a higher surface concentration in the inner vesicular shell than in the outer one. This finding is in agreement with the results of Berden et al.[146] who used shift reagent nmr, and those of Litman[211] who used chemical modification with impermeant reagents. However, recently Massari et al.[212] using a technique based on interaction of negative phospholipids with positive metachromic dyes arrived at an opposite conclusion that negative phospholipids prefer the external layer when their content in the vesicle is low and tend to distribute in the internal layer at high negative lipid to phosphatidylcholine ratios.

The reason for this discrepancy is not clear. One possibility is that the experiments with metachromic dyes were done at pH values which were 2 - 2.5 pH units higher than in the experiments reported here. (The acidity of the medium has been shown[146] to affect the distribution of negatively charged

phospholipids). Another possibility is that cationic dyes bind differently to the outer and inner surfaces of the vesicle bilayer. Although Massari etal discussed such a possibility they did not compare the binding capacities of the two surfaces. It is also possible that the presence of polyvalent metal cations or positive dyes may influence the transverse distribution of the negative phospholipids in a different way.

The phospholipid distribution of egg PC/10 mole% PA vesicles is altered dramatically on addition of low concentrations of calcium (1 mM) (Fig. IV.8). The outer PC signal intensity increases suggesting that PC is migrating to this monolayer, supporting the ^{1}H-nmr results discussed previously. The internal PA signal intensity does not increase suggesting, perhaps, that PA is removed from this monolayer to form inverted micelles inside the hydrocarbon region. Finally, the outer choline resonance shifts slightly upfield indicating that PA is removed from this monolayer.

IV.4.4. Phase behaviour of unsaturated PE

It may be argued, however, that the behaviour of charged lipids (i.e. PA and CL) is not relevant to the behaviour of the majority of biological membranes; cardiolipin and phosphatidic acid being usuallyonly minor components. It is in this context, therefore, that the behaviour of systems containing unsaturated phosphatidylethanolamines (which comprises 30% of erythrocyte phospholipids [213] and at least 50% of micro-organisms phospholipids) was investigated.

The bilayer → hexagonal (H_{II}) transition temperature exhibited by unsaturated

phosphatidylethanolamines is sensitive to fatty acid composition; occurring for example in the region of -10°C for unsaturated PE derived from soya and[214] in the region of 54°C for more saturated species derived from *Escherichia Coli*.[188] Sonicated egg PC vesicles containing 40 mole% PE derived from egg yolk show an abrupt increase in permeability at 47°C which suggests that the bilayer $\rightarrow H_{II}$ transition temperature occurs at about 47°C. It has been reported[11] that the transformation from bilayer to H_{II} configuration (or vice versa) occurs over a 5°C temperature range. It is also of interest that the bilayer $\rightarrow H_{II}$ transitions of synthetic species of PE with homogeneous fatty acid composition occur over a temperature range which is similar to that observed for naturally occurring species. This contrasts with the gel→liquid crystalline transition which is markedly broader in naturally occurring lipids as opposed to synthetic lipid systems. Egg PC/40 mole% PE vesicles show very slow rates of transport at 25°C and 37°C suggesting that the bilayer $\rightarrow H_{II}$ transition of this system occurs above 37°C.

Cullis et al.[11] reported that the bilayer $\rightarrow H_{II}$ transition temperature of <u>pure</u> egg PE system occurs at about 30°C i.e. approximately 17°C lower than the transition temperature of the above system PC/PE. This suggests that the phosphatidylcholine component of these vesicles is responsible for the maintenance of the bilayer configuration below 47°C. The substantial increase in permeability at 47°C and 57°C is attributed to the formation of inverted micellar intermediates induced by temperature. Finally the faster rate of transport occurring in egg PC/40 mole% PE vesicles compared to that measured in egg PC/10 mole% CL containing vesicles is due to the relatively high concentration of non-bilayer lipid in the former vesicles.

IV.4.5 Vesicle-vesicle fusion mediated by inverted micelles

In the absence of calcium ions egg PC/10 mole% CL vesicles are seen to remain unfused throughout the experiment (Fig. IV.11). The lack of fusion at this concentration is in contrast to the appreciable transport occurring in these vesicles (Fig. IV.2). This indicates that transbilayer transport and vesicle-vesicle fusion are mediated by two distinct mechanisms and this can be explained in terms of the two types of inverted micelles.

However, vesicle-vesicle fusion occurring in response to extravesicular calcium (Fig. IV.11) can only occur if the bilayer structure at the fusion sites is "violated". It is therefore suggested that a mechanism involving inverted micelles formed between the outer monolayers of two vesicular bilayers mediates such fusion processes (Fig. I.13). Evidence for the disposition of such micelles between the exterior monolayers of two fusing bilayers comes from the freeze fracture studies of Verkleij et al.[18] who reported that "lipidic particles" (100Å in diameter) of dimpled appearance, appear to be preferentially located in regions corresponding to the fusion interface. However, Miller[98] gave a different interpretation to the appearance of lipidic particles in freeze fracture replicas, and claimed that such structures serve as intermembrane attachment sites (IMAS); a view shared also by Hui et al.[101]. Sen et al.[97] and Verkelij et al.[215] however, challenge this view and point to the crucial results ignored by the IMAS model: they suggest that the appearance of isotropic ^{31}P-nmr signals can best be explained by a model in which inverted micelles are located in rows at the fusion sites of two bilayers. Furthermore, "lipidic particles" have only been observed in lipid systems in which at least one of the lipid species prefer the hexagonal H_{II} structure.

However, in agreement with the suggestion that vesicle-vesicle fusion is mediated by inverted micelles it has been possible to explain the rate of fusion occurring in sonicated vesicles containing very low concentrations of cardiolipin (1 mole%) (Fig. IV.12). In the absence, and in the presence of extravesicular calcium the rate of fusion is slightly higher than the controls containing pure eggPC. The rate of vesicle-vesicle fusion at this cardiolipin concentration is much lower than that occurring in the vesicles containing 10 mole% CL (Fig. IV.11). These results suggest that vesicle-vesicle fusion occurring in sonicated vesicles containing negatively charged phospholipids (e.g. CL) is mediated by inverted micelles, and these inverted micelles are distinctly different from those occurring inside the bilayer mediating transbilayer transport. In general, the fusion seen to occur in egg PC/10 mole% PA vesicles is more extensive than that shown to occur in egg PC/10 mole% CL vesicles over a range of experimental conditions (i.e. concentration of lipids, and calcium); this would seem to suggest that the difference in fusion is attributable to the differences in net charge, (between PA and CL). On the other hand, egg PC/40 mole% PE vesicles show considerable fusion rates at 47°C and 57°C; i.e. in the region of bilayer $\rightarrow H_{II}$ transition temperature previously discussed.

A particular extension of the fusion model occurring in these vesicles may apply to the behaviour of the erythrocyte membranes on ATP depletion[218]. Pronounced morphological changes are observed and membrane bound vesicles are "blebbed off"[216]; events that appear to be related to higher intercellular concentrations of calcium. The effect of calcium in the inner monolayer (which has a composition of 49% PE, 25% PS and 12% PC[217]) may be to induce a certain instability, and cause PE to adopt a preferred H_{II} configuration at physiological temperatures. The instability of the inner monolayer allows a

molecular model of the "blebbing off" process to be proposed. Such a model involving inverted micelles may be applied in general to processes of exocytosis and endocytosis occurring in biological membranes[19].

IV.4.6 The Phase Behaviour of *Micrococcus cryophilus* extracted Phospholipids

The polymorphic phase behaviour of liposome systems containing synthetic and naturally occurring phospholipids has been extensively studied in recent years, however, the behaviour of systems containing phospholipid composition of *Micrococcus cryophilus* (45% PE, 45% PG and 10% CL) provides a simple but interesting system for studying the polymorphic phase behaviour of phospholipid mixtures. Such study may help in the understanding of the relationship between the activity of Δ9 - desaturase enzyme which synthesises double bonds and the physical state of the membrane of the bacterium when grown at different temperatures [199][219]. The ^{31}P-nmr spectrum of liposomes prepared from the extracted phospholipids at room temperature (22°C) displays a broad peak (50 ppm wide) with a small low field shoulder indicating the structural preference for the bilayer configuration at the growth temperature (21 ± 1°C). Stabilization of the bilayer structure at this temperature is attributed to the phosphatidylglycerol and cardiolipin components which are shown by ^{31}P-nmr to adopt the bilayer configuration when present separately or in mixtures with phosphatidylethanolamine[220]. Such net stabilization of the bilayer structure for an H_{II} phase preferring lipid (i.e. PE) is well documented; occurring for unsaturated PE's in the presence of PC[209], PS[210][191], SM[221] and CL[192].

Noordam et al.[222] compared the barrier properties of $18:1_c/18:1_c$ phosphatidylcholine with $18:1_c/18:1_c$ phosphatidylethanolamine (the latter constitutes 70 to 75% of unsaturated PE of *Micrococcus cryophilus*). Both phospholipids formed bilayers which are highly permeable to K^+ and glucose; but with increasing temperature (40°C) only those prepared from the latter phospholipid lost their barrier function, as a consequence of a transition from a lamellar to hexagonal orientation. *Micrococcus cryophilus* phospholipids exhibit similar bilayer to H_{II} transformation at a much lower temperature (4°C) which demonstrates the influence of the bilayer - phase - preferring - components (i.e. PG and CL) on the transition temperature. However, the adoption of the hexagonal H_{II} configuration at this temperature shows that the cardiolipin and phosphatidylglycerol components (actually) enter the H_{II} phase matrix. Such behaviour is fully consistent with the previous suggestions[11] that the dynamic molecular shape of lipids such as unsaturated phosphatidylethanolamines dictates the preferred structure; in particular, at a given temperature unsaturated PE would be expected to give large cross-sectional area subtended by the acyl chains, thereby imparting a more pronounced 'cone' shape to the molecule. Such molecular shapes give rise to configurational rearrangements which can be distinguished by ^{31}P and ^{31}C-nmr[188][202], by X-ray diffraction[193][223], and by high magnification electron microscopy[16].

Fig. IV.15.(d) shows a narrow spectral component superimposed on the hexagonal H_{II} lineshape suggesting that a portion of the phospholipid experience isotropic motional averaging. The prevalence of these isotropic signals, as suggested previously[19][205] can not be unambiguously attributed to any one structure. However, the phospholipid dispersion consisted of large visible aggregates which suggests that the presence of small vesicles

which normally give rise to more translucent dispersion is unlikely. A more likely explanation for the source of this isotropic signal is the presence of inverted micelles occurring between the various bilayers in the liposomes structure [99]. Such an hypothesis agrees with that proposed by Gerritsen et al. [207] although, as yet, a final agreement on the relative contributions of inverted micelles and that of small vesicles to the appearance of these isotropic signals is not reached. However, the results obtained from freeze fracture [18] and X-ray [224] studies suggest that inverted micelles can occur in similar systems under certain conditions; and the use of similar techniques (none of which employed in this study) may give a better understanding of their occurrence in this system.

Allowing the liposomes to warm up to R.T. followed by cooling to 4°C produced a similar spectrum; i.e. consistent with the hexagonal structure suggesting that the bilayer → H_{II} transformation is reversible. However, the small spectral features present on the low field shoulder (Fig.IV.15.(d)) have now disappeared, probably due to the presence of slight hysteresis which is known to occur in mixtures with phosphatidylethanolamines [205]; especially that the protocol employed in this work (i.e. starting at R.T. then cooling to 4°C) favours the occurrence of such phenomenon [205]. Phospholipid hysteresis however, is shown to affect the bilayer → H_{II} transition temperature ($T_{B-H_{II}}$); and depressions by some 5 to 15°C can occur depending upon the composition of the sample. It should be noted that such temperature variations were not detected in this system as evident from the ^{31}P-nmr spectra presented in Figs. IV.15.(d) and (e).

At 11°C a broad (50 ppm) complex spectrum with signs of bilayer as well as hexagonal structure was observed (Fig.IV.15.(c)) which suggests that the

phase transition of this phospholipid mixture is rather broad. This is in contrast to the sharp transitions shown to occur in pure phosphatidylethanolamines[190]; and which might by explained by the structural preference of cardiolipin and phosphatidylglycerol components to the bilayer phase and the phosphatidylethanolamine component to the H_{II} phase. The existence of a broad transition is in agreement with the results of Noordam et al.[222] who reported a broad transition of $18:1_c/18:1_c$ phosphatidylethanolamine/phosphatidic acid liposome systems; (the former lipid constituting up to 75% of the unsaturation in *Micrococcus cryophilus* PE). Increasing the temperature above 30°C shows (Fig.IV.15.(a)) that the bilayer configuration dominates.

Having allowed the liposome dispersion to cool to R.T. and 2 mM calcium introduced, the ^{31}P-nmr spectrum (Fig.IV.15.(g)) is consistent with the hexagonal H_{II} configuration; perhaps due to the preference of the cardiolipin/Ca^{2+} component to the hexagonal H_{II} phase under these conditions[189]. However, because cardiolipin amounts to only 10% of the phospholipid mixture, and because PG (45%) and PE (45%) (i.e. the majority components) prefer the bilayer configuration at R.T., the suggestion that the CL/Ca^{2+} component is responsible for the hexagonal H_{II} structure was regarded an improbable. However, it has been reported[220] that phosphatidylglycerol reflects low affinity for Ca^{2+} at low concentrations, but at high concentrations calcium induces the hexagonal H_{II} phase and all signs of bilayer completely disappear. It is in this context, therefore, an explanation for the appearance of the hexagonal structure is given. Increasing calcium concentration from 2 mM to 10 mM resulted in the immediate precipitation of the lipid, and the ^{31}P-nmr spectrum consisted of a single sharp signal demonstrating that (virtually) all the phospholipid molecules undergo isotropic motion. It is tempting to

ascribe this narrow signal to the occurrence of small vesicles, or, a honeycomb structure[19], however; the phospholipid dispersion consisted of large visible aggregates which tumble very slowly with respect to the nmr timescale (10^{-5} s); thus causing line broadening. Therefore; the appearance of isotropic peak due to small vesicles, or a honeycomb structure is considered unlikely. It is suggested that the appearance of this narrow signal is probably due to the presence of a different phase, probably cubic. Cubic phases are formed by a network of hexagon-shaped lamellar bilayer units, but other molecular arrangements have also been described as cubic [225][226][227]. Wieslander et al.[228] reported that high degree of cis unsaturation (which comprises 70 to 75% of the phospholipid unsaturation in this system) favours the formation of cubic phases in the membranes of *Acholeplasma laidlawii*. Their ^{1}H, ^{2}H and diffusion nuclear magnetic resonance measurements have shown that mixtures of mono - and diglucosyl diglycerides form reversed cubic phases composed of large aggregates where the lipid can diffuse over macroscopical distances. The ^{31}P-nmr results (Fig. IV.15.(h))are consistent with the adoption of cubic phases, but further work is needed to support this preliminary study.

IV.4.7 Lipid Peroxidation

Vesicle preparation is extremely sensitive to autoxidation of lipids, both before and after dispersion, and stringent anaerobic procedures are required to ensure reproducible results concerning permeability studies. While autoxidation is not a severe problem with synthetic lipids or purified lecithin containing mostly saturated or mono-unsaturated fatty acids, the

increase use of complex lipid mixtures of biological origin is accompanied by greater hazards in this respect. It has been mentioned earlier (See results section) that a yellow colour, indicative of lipid peroxidation has been observed during the non-bilayer experiments discussed in this chapter. However, since it is known that lipid peroxidation is associated with increased bilayer permeability [195] an investigation of the effect of lipid oxidation on transbilayer transport was investigated using egg PC/40 mole% PE vesicles.

Phospholipid peroxidation and transbilayer transport were monitored simultaneously (See Materials and Methods), and the results are presented in Fig. IV.16 . The vesicles incubated in air and those stored under oxygen-free nitrogen are seen to exhibit a small degree of peroxidation, whilst those incubated with H_2O_2 exhibit high levels of peroxidation. On the other hand, lanthanide ion transport into all types of vesicles (i.e. under all three extravesicular environments) show similar permeability behaviour; a lag period of 4 days during which minimal transport occurs, followed by enhanced rate of transport during days 5 to 12. It must be mentioned, however, that this enhanced permeability is not caused by the temperature - induced conformational changes (i.e. Bilayer → H_{II}) occurring in the bilayer, because the incubation temperature of these vesicles (37°C) is well below the transition temperature previously discussed (See Section IV.4.4). Fig. IV.16 shows that the progress of lipid peroxidation as measured by the decrease in unsaturation (Klein index) is not related to the changes in permeability occurring in these vesicles which suggests that other peroxidation breakdown products beyond the changes in unsaturation may be responsible for this behaviour (See later). Furthermore, cation permeability increases rapidly during days 5 to 12, but only after a lag period of 4 days which indicates that the initial peroxidation breakdown

products such a conjugated dienes may have reacted with peroxide free radicals (or molecular oxygen) to give further degredation end-products such as short chain fatty acids, alcohol, ketones and aldehydes (Scheme I.1). ^{13}C-nmr spectra recorded before and after peroxidation took place (Fig.IV.19) show various spectral changes including a decrease in unsaturation. Therefore, it is suggested that oxidized phospholipid breakdown end-products accumulated during the lag period may reach critical levels leading to "structural changes" in the bilayer, thus enhancing the permeability. Shaw et al. [198] reported that single lamellar phosphatidyl [methyl - ^{2}H] choline vesicles incubated with isotopically labelled phosphatidylcholine vesicles did not exhibit phospholipid exchange for at least 5 days when incubated in air. Between days 5 and 7, extensive transbilayer movement occurred leading to an outer/inner phosphatidylcholine ratio of 2:1 by day 7. These workers suggested that the Klein index lost its usefulness at about day 6 since the apparent variety of carbonyls and peroxides produce a rather broad peak at 230 nm which distorts the ester-linked carbonyls which absorb at 215 nm.

However, autoxidation of long chain unsaturated fatty acids leads to the formation of short acyl fragments [103], and liposomes prepared from the latter were shown to be significantly more permeable than those containing long chain unsaturated fatty acids [230]. Therefore, it could be that the accumlation of short chain fatty acids during the lag period causes certain topological changes in the bilayer which increases permeability. Barsukov et al. [201] have recently found that lipid peroxidation can promote transbilayer movement in phospholipid vesicles, and presented ^{31}P-nmr data from oxidized vesicles that suggest non-bilayer structures, particularly highly isotropic inverted micellar intermediates, are produced upon oxidation of vesicles.

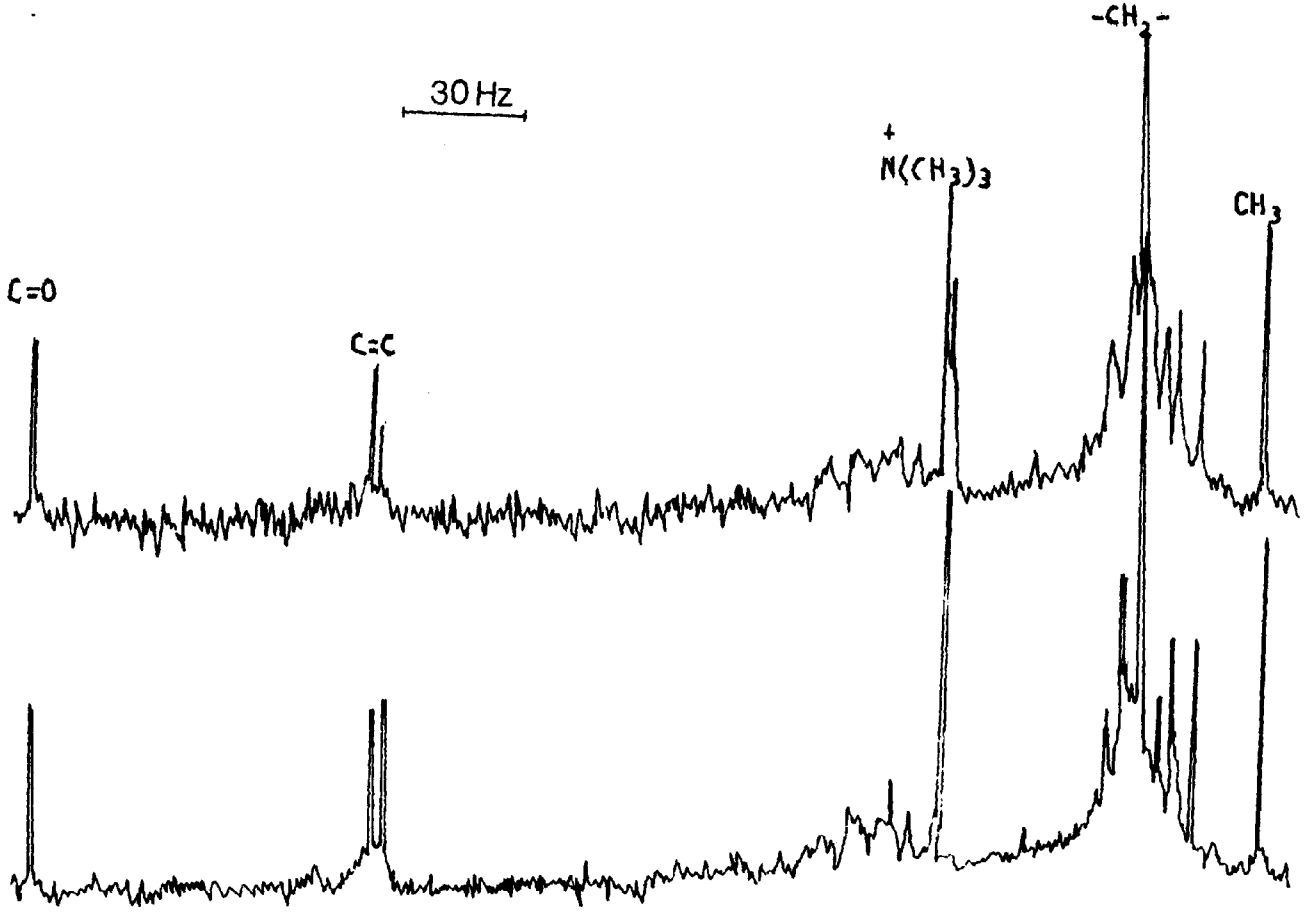

FIG.IV.19. ^{13}C-nmr spectra of Egg PC/10 mole % CL vesicles before and after peroxidation took place. The spectrum shows a decrease in C=C signal intensity as well as major alterations in the methylene envelope region.

And the results discussed in this chapter outline a mechanism of transbilayer transport via inverted micelles occurring in phospholipid containing non-bilayer lipids. The suggestion that short chain fatty acids produced by peroxidation are responsible for the formation of non-bilayer phases is not in agreement with the hypothesis of Gast et al.[106] who claimed that phospholipid hydroperoxides resuting from peroxidation of lipids are responsible for triggering non-bilayer phase configurations. However, lipid autoxidation is known to occur very rapidly[103] and initial peroxidation products such as hydroperoxides (and conjugated dienes) would be expected to react further giving short chain fatty acids, alcohols and ketones (See above). Therefore, the observed lag period before permeability changes occur is consistent with the suggestion that accumulation of peroxidation breakdown end-products is responsible for the configurational changes occurring inside the bilayer. However, more work is needed to resolve this point.

It is of interest to briefly mention the effect of phospholipid oxidation on vesicle-vesicle fusion. Fig.IV.20. show that the line-width of the acyl chain resonance increases with time suggesting that vesicle-vesicle fusion is taking place; probably via inverted micelle intermediate (Fig. I.13). Fusion processes occurring as a result of lipid autoxidation were reported previously; Gast et al.[106] measured the size changes of vesicles occurring due to air peroxidation, using the non-invasive quasi-elastic light scattering (QELS) techniques.[231]

A recent publication[171] suggested that autoxidation of multibilayer liposomes results in severe disruption of the membrane structure; and the resulting membrane fragments anneal to form vesicles of small diameter. Extensive peroxidation such as this would be expected to occur in unsatured monoenoic

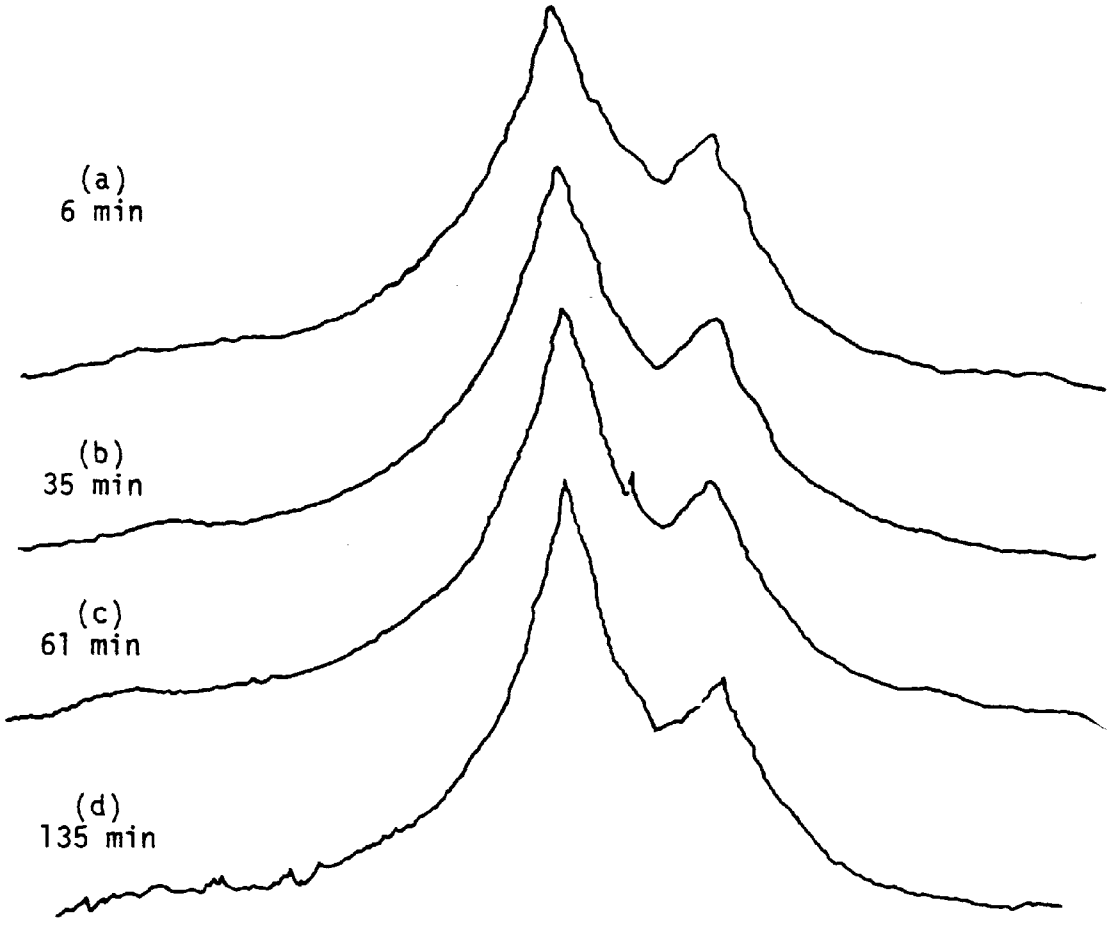

FIG.IV.20. The acyl chain signal of Egg PC/40 mole % PE vesicles increases, which indicates that vesicle-vesicle fusion is taking place.

fatty acid residues present in detergents such as Tween 80.[105] Complete peroxidation of multibilayer liposomes, however, is unlikely because peroxide free radicals present in the bulk water are inaccessible to the inner bilayers[105]. Transbilayer transport results discussed above show that complete loss of permeability barrier does not occur even after 12 days; the latter being the expected outcome if severe disruption of the membrane took place. Furthermore, the vesicle-vesicle fusion shown to occur in egg PC/40 mole% PE vesicles is in contrast with the observations of Kunimoto et al.[171] who reported that their electron micrographs gave evidence to the formation of small vesicles from disrupted membrane fragments. The use of the electron microscope involves air drying procedures and adsorption on coated grids, i.e. methods which make interpretation of the electron micrographs rather uncertain. Also, phospholipid dispersion in aqueous media leads to the formation of large multibilayer liposomes, but contamination with small multibilayer structures is frequently observed[232]. Hence, the presence of small size liposomes (vesicles) detected by this technique can not be decided unambiguously.

IV.4.8 Conclusion

The NMR/Ln^{3+} method has been successfully applied to the study of non-bilayer phase - induced transport, flipflop and membranes fusion processes. The results indicate how a clear distinction can be made between the types of inverted micelles which form the proposed mechanisms for each of the above processes. An extension of the methods using ^{31}P-nmr allowed preliminary conclusions to be made on the polymorphic phase behaviour

of phospholipids extracted from *Micrococcus cryophilus*. The relationship between non bilayer phase - mediated transport and the enhancement of bilayer permeability due to lipid peroxidation was discussed. The use of large vesicles and ^{31}P-nmr to monitor the polymorphic phase changes that are induced by lipid peroxidation breakdown products would be particularly useful.

CHAPTER V

CALCIUM ANTAGONISTS

CHAPTER V

Calcium Antagonists

V.1 Introduction

In this chapter the effect of three calcium antagonists on carrier mediated, pore mediated and non-bilayer mediated transbilayer transport of calcium probes across pure and mixed lipid vesicles is discussed. The use of ^{1}H, ^{13}C and ^{31}P-nmr and model building to determine the possible conformation and binding sites of these drugs is described.

Recently, several compounds with similar pharmacological effects, although with various chemical structures have been grouped together as calcium antagonistic drugs (Fleckenstein 1977) [117]. The main representatives of these so called "calcium antagonists", Verapamil, D600, Nephidipine and Diltiazem interfere with the normal functions of Ca^{2+} in the body. Thus Verapamil reduces the work-load on the heart by reducing the oxygen requirement of the myocardium[233], Nephidipine induces a potent vasodilating and antihypertensive effect in man and D600 is frequently used for the treatment of varient angina[234].

Several of these drugs have already been used clinically, particularly in Europe and Japan but are not available on demand in North America[235][118]. The reported side effects are nausea and dizziness after oral administration and flushing and dizziness after intravenous use. The injection may cause transient heart block, especially after rapid administration and, rarely ventricular fibrillation may be precipitated[233].

The mechanism of action of calcium antagonists, more precisely their exact site of action is not yet determined [235][119]. Experiments to investigate the mechanism of "calcium blocking" by these drugs have usually been carried out in complicated systems such as the heart muscle strip [109], or on the other hand oversimplified systems which bear somewhat tenuous resemblance to biological membranes such as the Pressman cell [20]. Single bilayer vesicular membranes containing single or mixed lipid systems offer a simple but biologically relevant alternative; and these are used in this study.

It is suggested that calcium antagonists affect only the slow inward calcium channels and the entry of calcium from extracellular pools [114], - however, other experiments show these drugs interfere with the release and binding of Ca^{2+} in intracellular pools [118].

Calcium ions play an important physiological role in the body - such as muscle contraction, glandular secretion at postsynaptic nerve terminals [236], and the calcium antagonists have been shown to inhibit Ca^{2+} transport in smooth muscle, sarcolemmal preparation [119]. It is thus rather surprising that these drugs are used therapeutically without "serious" side effects being observed. Clearly their mode of action requires further study.

In a recent editorial in Annals of Internal Medicine [237] the author uses the terms "calcium antagonists", "calcium blockers" and "slow-channel blockers" to mean the same thing. Other authors use equally confused nomenclature [115]. Critics in the field strongly object to this irregularity or looseness in using these terms. The reason for this confusion is twofold. Firstly: the fact that calcium antagonists have various chemical structures (Fig. V.1), and secondly: because the exact mechanism i.e. whether by blocking the slow "calcium channel" or by competitive binding with calcium still has to be elucidated.

Fig.V.1.

VERAPAMIL

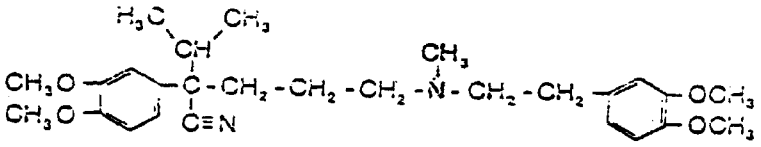

D600

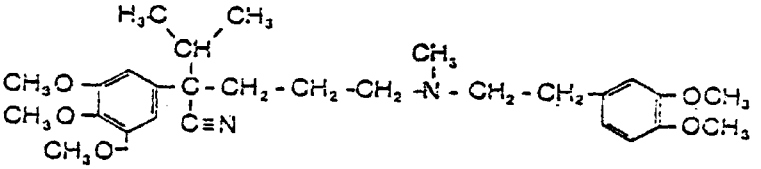

NEPHIDIPINE

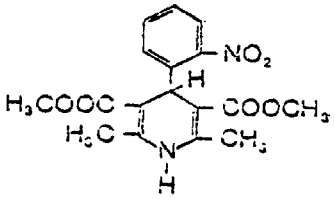

DILTIAZEM

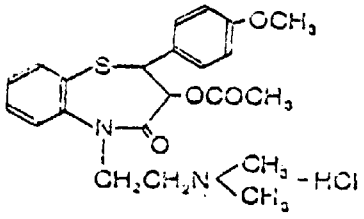

CALCIUM ANTAGONISTIC DRUGS AND THEIR STRUCTURES

However, these drugs have different therapeutic uses in cardiology and[238] their classification according to their physiological role may be serviceable in the meanwhile. In our laboratory we are currently investigating the effect of calcium antagonists on channel formation mediated by Alamethicin 30, and the results obtained so far suggest that low concentrations of the antagonists inhibit cation transport through this channel, but at high concentrations the antagonists potentiates the transport rate.

Chemical abstracts and "On Line" computer search (as well as private communications with Bayer, the manufacturers of Verapamil and D600) have shown that no nmr data were available for either Verapamil or D600. The work presented in this thesis describes the ^{1}H and ^{13}C-nmr spectra of Verapamil and Nephidipine, and assigns all resolvable signals using the "INEPT" pulse sequence (see Materials and Methods). The possible interactions of these drugs with the transported metal ions is investigated using lanthanide shift reagents/ ^{1}H-nmr techniques. Ultraviolet and fluorescence spectroscopy is employed to investigate the hypothesis of ionophore - antagonist interactions, (Malaisse et al.).[239] The antagonism property of these drugs is demonstrated using sonicated vesicles containing pure or mixed phospholipids. A possible site of action and mechanism of inhibition of these drugs has been suggested.

V.2 Materials and Methods

Chemicals:

Nephidipine (MW.346) was a gift from Bayer U.K. Limited (Haywards Heath, England). Nephidipine is insoluble in hydrophilic solvents, therefore stock solution was prepared from 17.6 mg/1 ml $CHCl_3$/MeOH. Because this antagonist disintegrates to ineffective degradation products on exposure to light the stock flask was covered with silver paper and stored in the dark. Verapamil (M.W.491) and its methoxy derivitive D600 (M.W.506) were gifts from Abbot (England) and Dr. B. Gomperts (University College Hospital Medical School, London) respectively. Stock solutions of these antagonists were prepared from 25 mg Verapamil/1 ml $CHCl_3$–MeOH and 25.7 mg D600/1 ml $CHCl_3$ - MeOH and stored at room temperature. D_2O solutions of these antagonists were also prepared.

The channel former ionophore Alamethicin 30 was obtained from PHLS (Porton Down, England). Stock solution of this ionophore was prepared from 1 mg/ml D_2O and the stock flask was kept at +5°C. Other ionophores used in this section were already described.

Experimental Methods:

V.2.1 Preparation of the Vesicles

The preparation of single and mixed lipid vesicles was already described.

However, the experiments involving the channel former Alamethicin were carried out using vesicle dispersion at a concentration of 10 mg/ml. These experiments were performed in the F.T. nmr instrument and therefore saves on the amount of lipid used (see section V.2.3)

V.2.2. Methods of addition of the antagonists

Three methods were used to introduce the antagonist:

(a) The required amount of the antagonist (in D_2O) was added to the nmr tube containing 0.5 ml of vesicle dispersion and 5 mM Pr^{3+}. Transport of ions was initiated by the addition of the required concentration of the D_2O solution of the ionophore.

(b) Chloroform solutions of the antagonist and the ionophore were added to the empty nmr tube, and the solvent was evaporated with N_2. Traces of the solvent were removed for 10 minutes using a water pump. 0.5 ml of the vesicle solution was added and the nmr tube was placed in a thermostated bath set at the required temperature (usually 37°C or 50°C, see text). The contents of the tube were shaken occasionally by hand to aid the partitioning of the antagonist and the ionophore. The transport of ions was initiated by the addition of lanthanide.

(c) The required volumes of the chloroform solutions of the ionophore, the antagonist and the lipid were pipetted in the empty sonicating

tube. The contents were mixed briefly, and the solvent was evaporated with nitrogen. Traces of the solvent were removed using an electric pump. The required volume of D_2O was added and the contents were shaken for 30 minutes using a flask shaker. The milky liposomes then formed were sonicated as previously described. This method allows the ionophore (A23187) and the antagonist (Nephidipine) to enter the hydrophobic region of the bilayer - an environment which is preferred by both reagents (see chemicals section). The transport of ions was initiated by the addition of the lanthanide.

V.2.3 NMR

The transport of ions was followed by the ^1H-nmr method already described. The FX60Q - FT nmr instrument was used to follow the transport of ions mediated by the channel former ionophore Alamethicin 30. All other experiments were performed using the C60 HL nmr instrument. As mentioned earlier, the vesicle concentration used in conjunction with Alamethicin was only 10 mg/ml.

Some of the results involving the transport of Dy^{3+} shown in this chapter are presented as the measured nmr shift (in hertz) against time - i.e. the calibration graphs were not used (See Chapter IV).

V.2.4 ^1H and ^{13}C spectra of the antagonists, and shift reagent studies:

Chloroform solutions of Nephidipine and Verapamil were prepared separately

in the 10 mm nmr tube. ^{1}H and ^{13}C-nmr spectra of these were recorded at room temperature using the FX60Q nmr instrument. Assignment of some of the ^{13}C-nmr signals was made using the "INEPT" pulse sequence program provided by the JEOL Company (JEOL News)[240]. This pulse sequence allows the transfer of the polarization (magnetization) of ^{1}H to ^{13}C nuclei through coupling. Identification of the coupled ^{13}C nuclei is made easier because this pulse sequence inverts primary and quaternary carbon atoms by 180° with respect to secondary and tertary carbon atoms. Other conditions used to obtain the spectra are shown. Interactions between the antagonists and the metal ions were investigated by ^{1}H-nmr shift reagent techniques[64]. This involved the titration of microlitre amounts of low concentrations of Pr $(Fod)_3$ or Yb $(Fod)_3$ to the chloroform solution of the antagonists, and measurement of the chemical shifts of the antagonist signals after each addition with respect to the unshifted internal standard. TMS or $CHCl_3$ nmr signals were used as the internal standard. The complexing (or binding) sites of the antagonist molecule were decided on the basis of the ^{1}H-nmr signals which show the largest nmr shifts. Space filling models of the antagonists were built to help interpreting the above nmr results.

V.2.5 Fluorescence Spectrophotometry

Fluorescence techniques were used to investigate the possible interactions of the ionophore (A23187 the only ionophore used which has fluorescence properties) and the antagonist.

Absorption and fluorescence spectra of 25 mg A23187/1.5 ml $CHCl_3$ were measured using (BAIRD - ATOMIC) Fluoripoint spectrofluorimeter. Successive microlitre

amounts of the chloroform solution of the antagonist were added to the same cuvette and the mixture was stirred by means of a small glass paddle. Absorption and fluorescence scans were recorded after each addition. The fluorescence quenching and wavelength shifts were noted.

V.2.6 UV Spectrophotometry

This technique was nominated to investigate the above interactions a little further and to help interpreting some of the fluorescence results obtained.

Absolute ethanol was found to be a better solvent than $CHCl_3$ at the wavelengths measured. 1.5 ml absolute ethanol containing 25 mg A23187 was pipetted in the cuvette, and absorption spectra were recorded. Successive microlitre amounts of the antagonist was added and the uv spectra were scanned at the same wavelengths. Any changes in the spectra were noted. Absorption spectra of the antagonists alone in absolute ethanol were also measured.

V.3 Experimental Results

V.3.1 Calcium antagonists interactions with A23187 investigated by ultraviolet and fluorescence spectroscopy

(a) Fluorescence:

The excitation and fluorescence spectra of A23187 as the free acid in chloroform are shown in (Fig. V.2.(a)). The fluorescence spectrum displays a single peak centred at 430 nm, and the excitation spectrum displays two maxima centred at 310 nm and 380 nm. The energy level diagram (Fig.V.2.(b)) shows the respective transition wavelengths λ_1, λ_2, and λ_3. The effect of adding microlitre amounts of the chloroform solution of verapamil on the excitation and fluorescence spectra of A23187 is shown in Figs. V.3.(a) and (b). Apart from slight decrease in the fluorescence probably caused by the dilution due to the addition of verapamil the ionophore spectra remain unchanged. Similar effects are shown (Fig.V.3.(c) and (d)) by D600 when employed at similar concentrations to verapamil (10:1 with respect to the ionophore). The calcium antagonist nephidipine caused substantial quenching of A23187 spectra at both excitation and fluorescence wavelengths (Fig.V.4.(a)). In order to investigate the causes of the quenching the ultraviolet spectrum of nephidipine in ethanol was recorded. Fig. V.4.(b) shows that this antagonist exhibits two maxima centred at 315 nm and 430 nm which overlap with the A23187 excitation and fluorescence wavelengths. This indicates that both A23187 and the antagonist absorb at similar wavelengths. Furthermore, the antagonist did not cause a wavelength shift (Stokes' shift) of the ionophore spectrum which shows that specific electronic interactions between these chemicals did not occur.

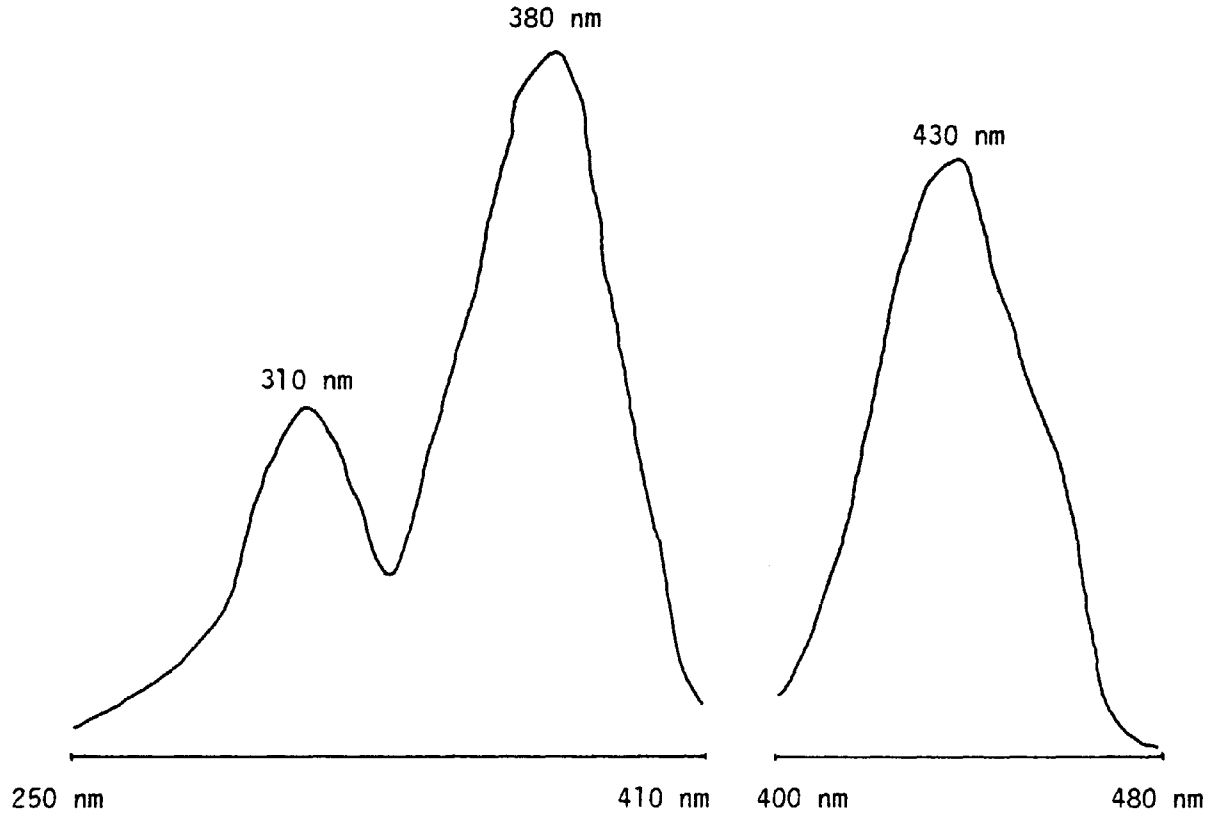

Fig.V.2(a) EXCITATION AND FLUORESCENCE SPECTRA OF A23187 IN CHLOROFORM

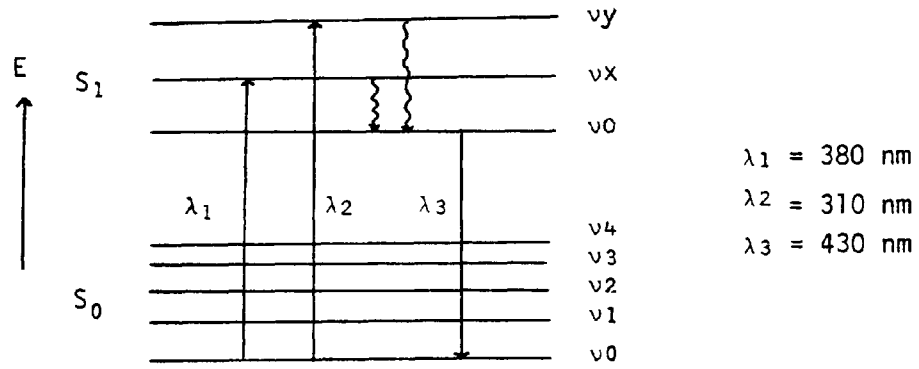

Fig.V.2.(b) ENERGY LEVEL DIAGRAM OF A23187 FLUORESCENCE

Fig.V.3 QUENCHING OF A23187 FLUORESCENCE BY VERAPAMIL AND D600

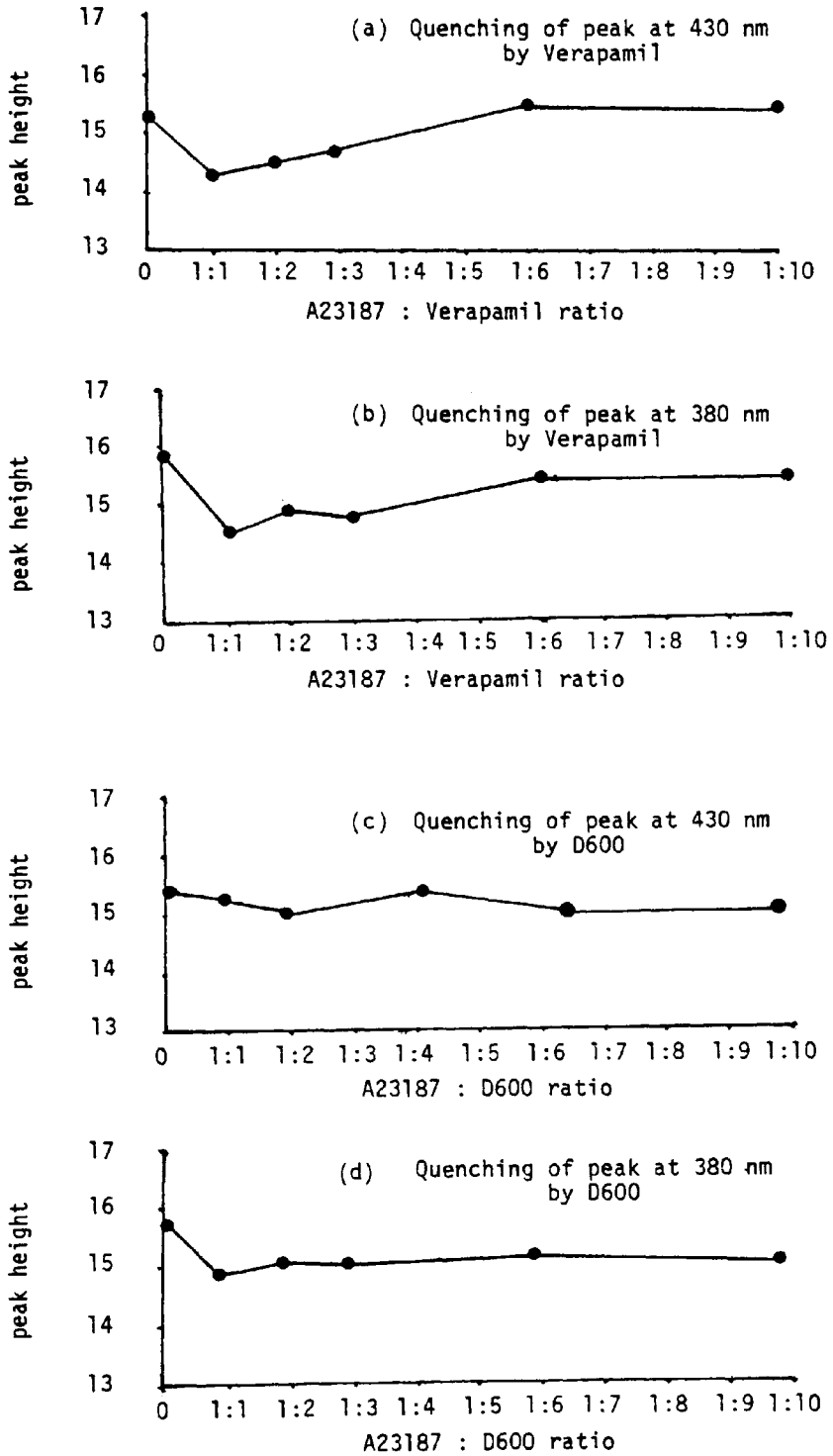

Verapamil and D600 cause minimal effects on the excitation and fluorescence wavelengths of A23187.

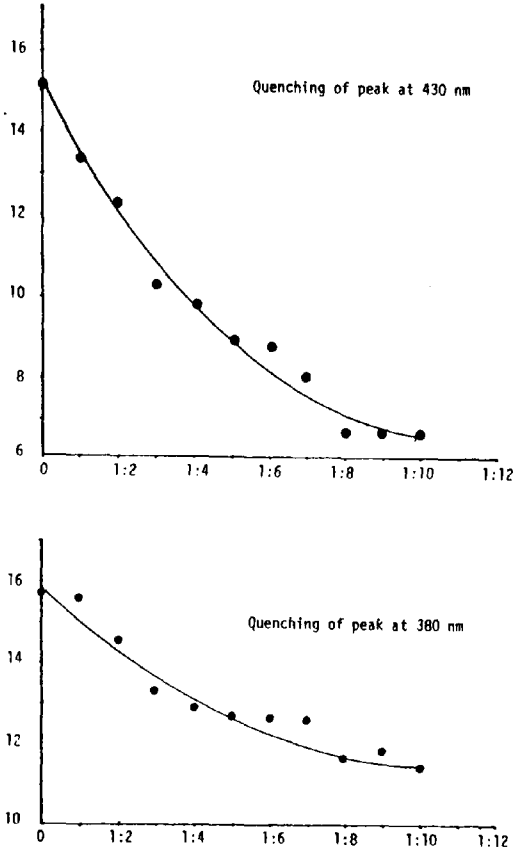

Fig.V.4. (a) QUENCHING OF A23187 FLUORESCENCE BY NEPHIDIPINE

Fig.V.4. (b) ULTRAVIOLET ABSORPTION SPECTRA OF NEPHIDIPINE IN ETHANOL

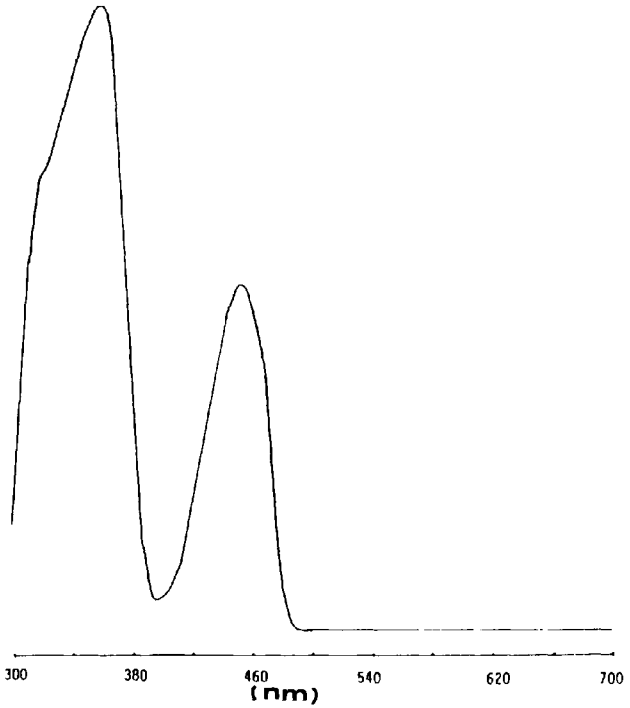

(b) Ultraviolet:

The ultraviolet spectrum of A23187 in ethanol (Fig. V.5.(b)) displays four main peaks centred at 204, 225, 278 and 378 nms. The peak centred at 278 nm has a prominant shoulder at 290 nm. The addition of the chloroform solution of verapamil to the ionophore caused the enhancement of the major absorption peaks (Fig. V.6.), and in addition a peak centred at 200 nm has developed. The ultraviolet absorption spectrum of verapamil alone (Fig.V.5.(a)) exhibits two broad bands centred at 230 nm and 278 nm and a broad shoulder at ~ 202 nm. The similarity between the uv spectra of A23187 and verapamil suggests that verapamil absorption bands are primarily responsible for the enhancement of the absorptions in Fig. V.6. and also responsible for the emergence of the new peak centred at ~ 200 nm. Investigation of the effect of the other antagonists D600 and nephidipine on the ultraviolet spectrum of A23187 have shown that only negligible changes were observed.

V.3.2 Interactions of the antagonists with the metal ion investigated by lanthanide shift reagents:

The nmr spectra of verapamil and nephidipine have not been published previously (see Introduction). Figs. V.7.(a) and (b) and V.8.(a) and (b) show the ^{1}H and ^{13}C-nmr spectra of verapamil and nephidipine respectively. The assignment of the resolved ^{13}C-nmr signals is carried out using the pulse sequence (INEPT) (see Materials and Methods).

Fig.V.5.

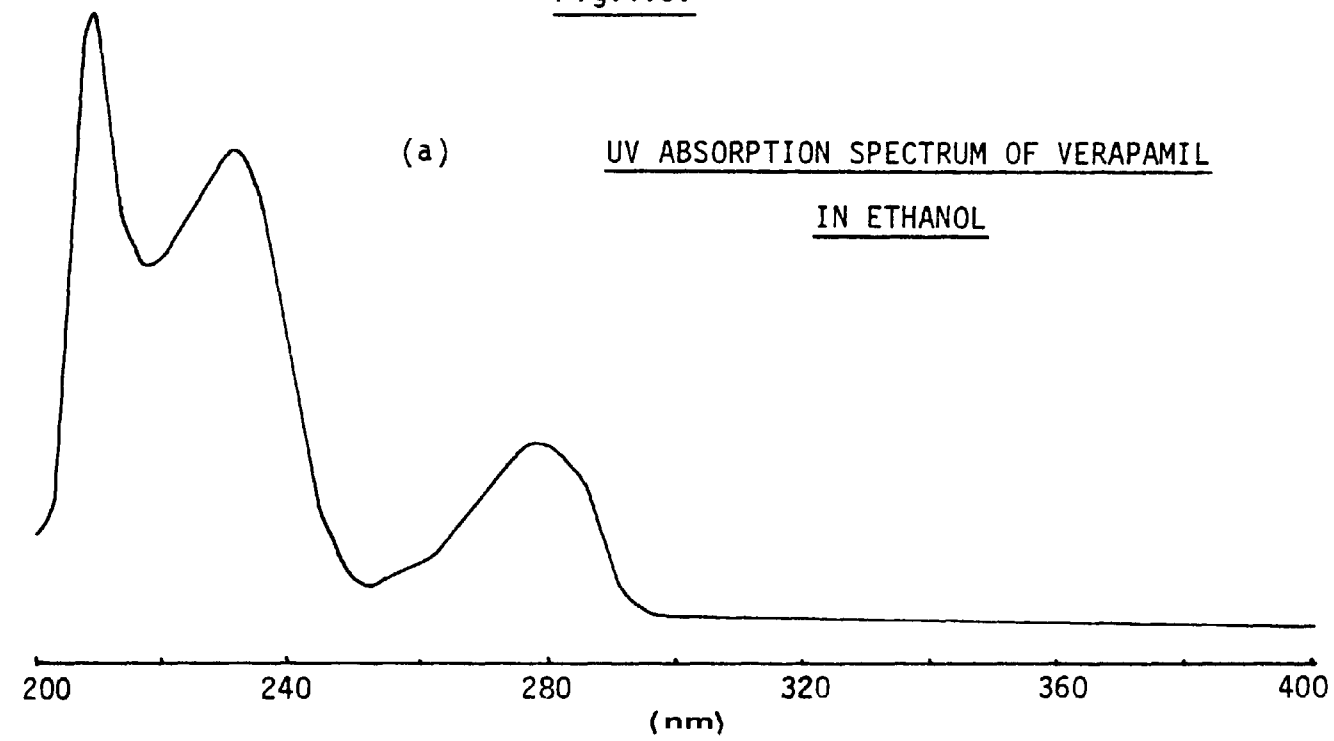

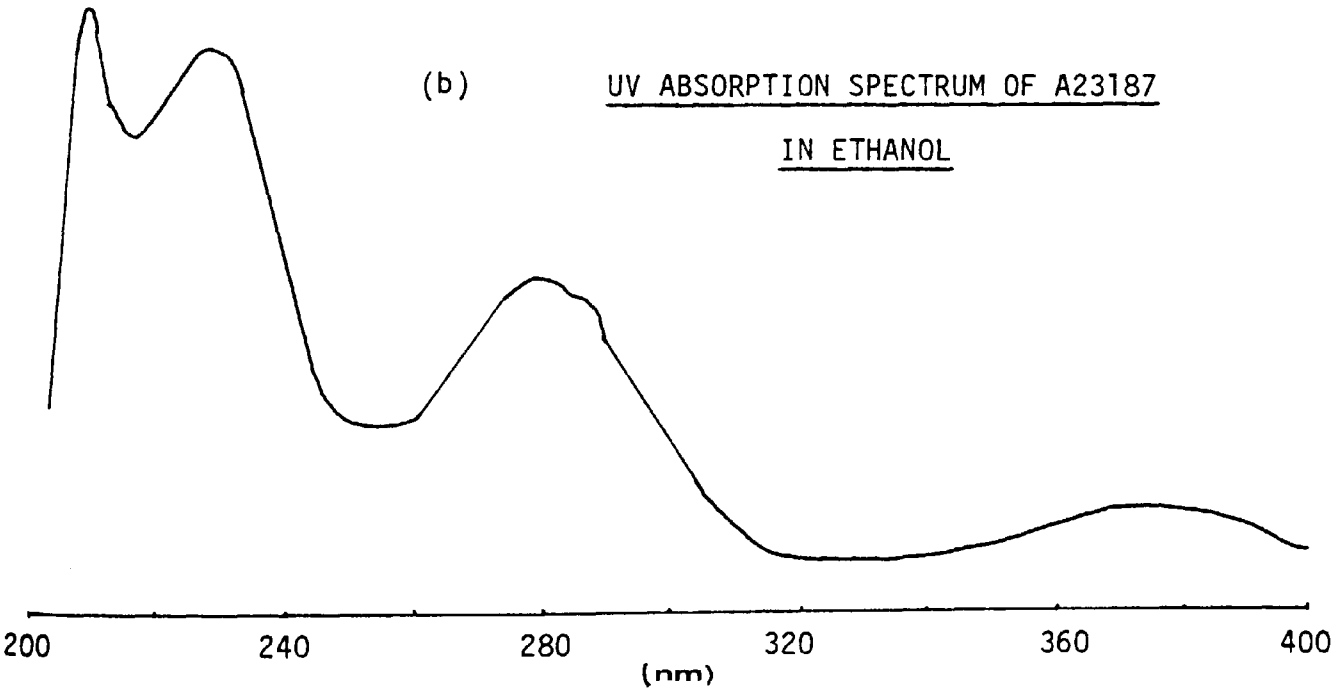

Ultraviolet absorption spectra of Verapamil and A23187 in ethanol.
Three of the absorption bands of these compounds overlap.

Fig.V.6. THE AFFECT OF VERAPAMIL ON THE UV ABSORPTION SPECTRUM OF A23187

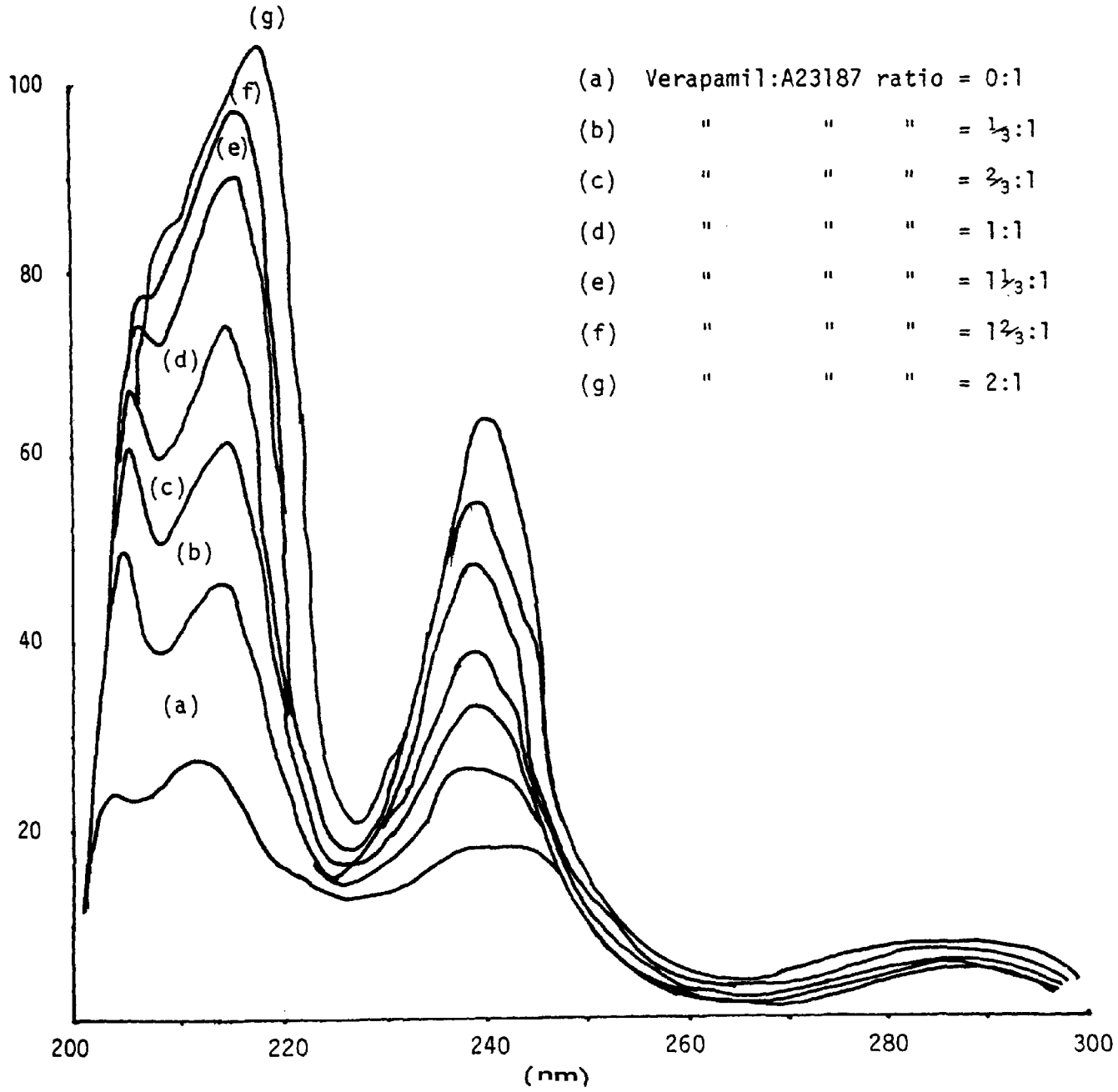

Increasing the Verapamil:A23187 molar ratio increases the intensity of the UV absorption peaks of A23187.

FIG. V.7.(a)

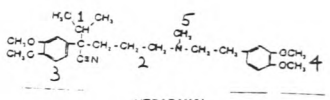

VERAPAMIL

35 μG PR (FOD)$_3$

20 μG PR (FOD)$_3$

12 μG PR (FOD)$_3$

5 μG PR (FOD)$_3$

$CHCL_3$ 3 5 4 2 1

^1H NMR SPECTRUM OF VERAPAMIL

FIG. V.7.(b)

^{13}C NMR SPECTRUM OF VERAPAMIL WITH INEPT

1,2,3,4,5,6

16,17,18,19

16

8

9

7

21 22 20

12,13,14,15

10,11

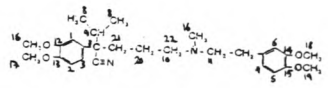

^{13}C NMR SPECTRUM OF VERAPAMIL

TMS

FIG. V. 8. (a)

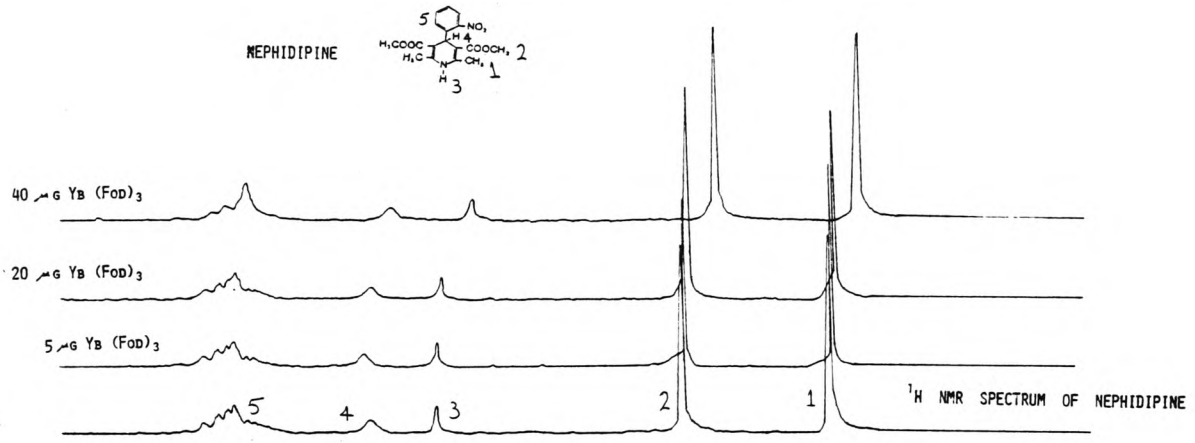

FIG. V. 8. (b)

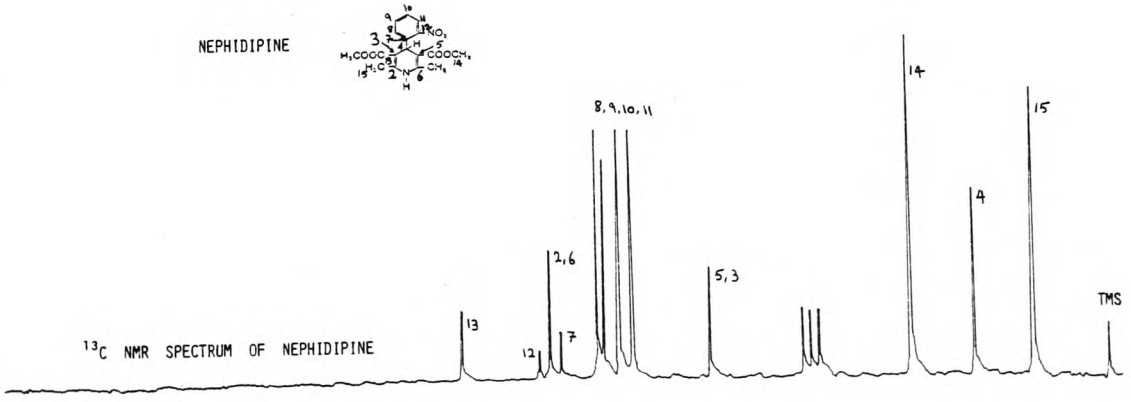

The antagonist/metal ion interactions are investigated by measuring the ^{1}H-nmr shift produced upon the addition of the lanthanide shift reagent. The successive addition of the chloroform solution of $Pr(Fod)_3$ to the chloroform solution of verapamil (Fig. V.7.(a)) caused the downfield shift of the ^{1}H-nmr signals due to the $-OCH_3$, NCH_3 and $-CH_2$ groups and the shift and broadening of the benzene resonance. The effect of adding the lanthanide reagent $Yb(Fod)_3$ on the ^{1}H-nmr spectrum of nephidipine is shown in Fig. V.8.(a). The resonance due to CO_2CH_3 and CH_3 groups are shifted downfield, and those due to the NH and NO_2 are also shifted but to a much lesser extent.

V.3.3 Effect of calcium antagonists on lanthanide ions transport across egg PC vesicles mediated by carrier type ionophores:

Equal amounts (40 µg) of the chloroform solutions of the ionophores A23187, Ionomycin and Nafod were added separately to three nmr tubes each containing 250 µg of the calcium antagonist verapamil. After evaporation of the solvent, 0.5 ml of the PC vesicles were added and the nmr tubes were placed in a thermostated water bath (at 50°C) for 30 minutes (see Materials and Methods). Transport was initiated by the addition of Pr^{3+} ions. The results in Figs. V.9.(a) (b) and (c) show that the transport rates mediated by the two antibiotic ionophores (A23187 and Ionomycin) is uninhibited, and this is different from the inhibited transport rate shown by the synthetic ionophore Nafod. Therefore, controlled experiments were then set up to investigate this difference in behaviour shown by natural and synthetic ionophores.

(a)

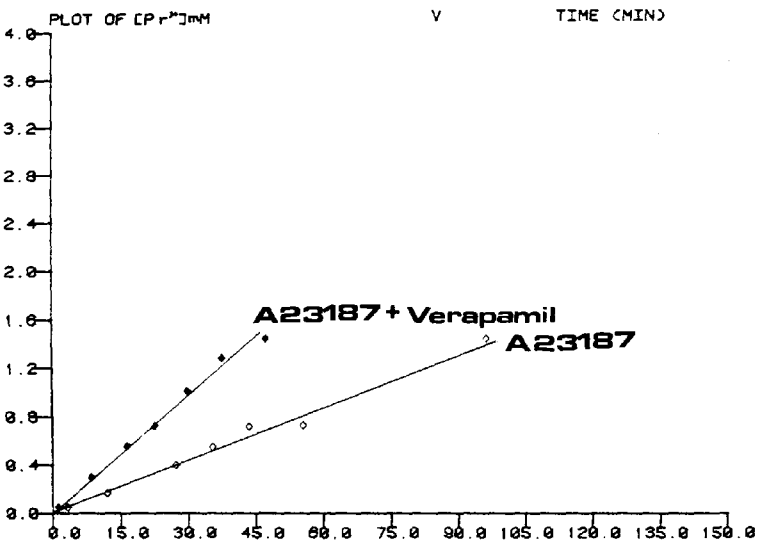

(b)

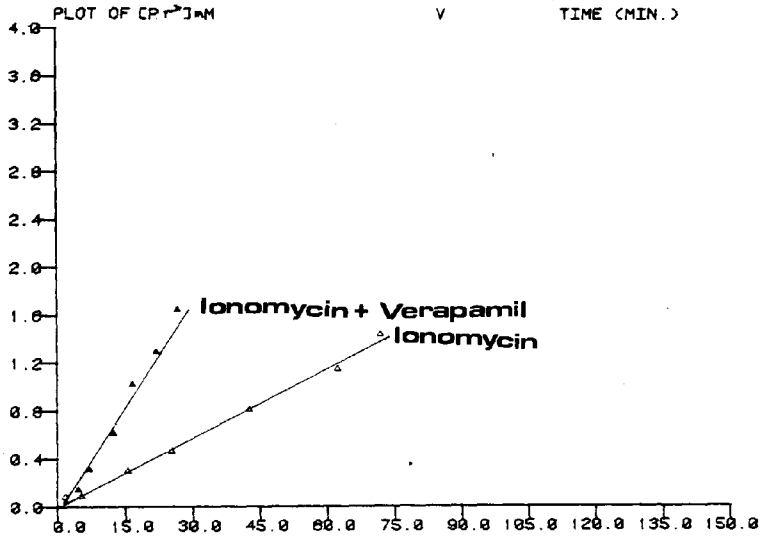

(c)

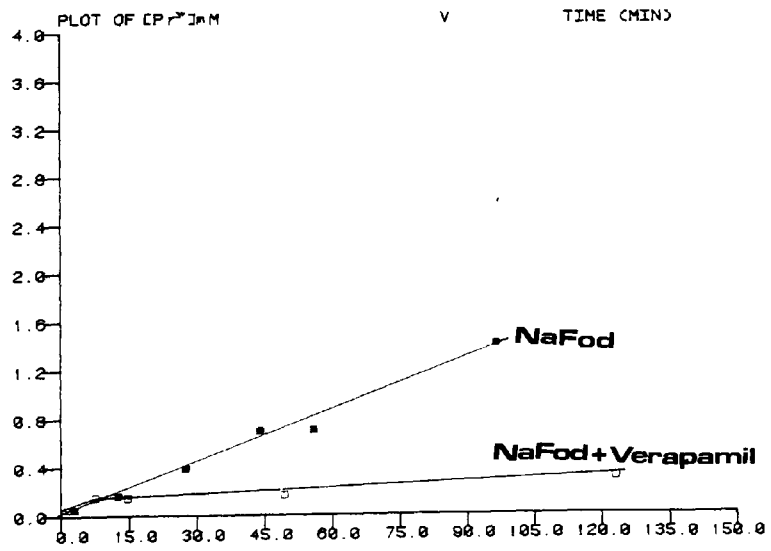

Fig.V.9 shows that Verapamil inhibits the transport mediated by NaFod but promotes the transport mediated by equimolar concentrations of A23187 and Ionomycin.

Equimolar concentrations of the ionophores A23187 (20 μg), Ionomycin (27 μg) and Nafod (12.5 μg) were added to three separate nmr tubes each containing 20 μg Verapamil (equimolar w.r.t. the ionophores), - and after the addition of the vesicles the rate of cation transport was initiated as described (see Materials and Methods). The results of the above experiments, and others where the antagonist verapamil is substituted with nephidipine or D600 are shown in Figs. V.10 and V.11. It can be seen that regardless of which antagonist is used, the rates of transport mediated by A23187 and Ionomycin are enhanced while the rate of transport mediated by Nafod is inhibited.

The following experiment shows the effect of various concentrations of Verapamil on the transport rate mediated by Nafod. The results in Fig. V.12. (a) shows that all concentrations of Verapamil (Between 50 μg and 250μg) inhibit the transport mediated by Nafod, and the degree of inhibition is proportional to the concentration of verapamil added. However, in a similar experiment using D600 a remarkably different result is obtained. Fig. V.12.(b) shows that using 15 μg or 50 μg, D600 inhibits the rate of transport but, unexpectedly, 150 μg or 250 μg D600 promotes rather than inhibits the rate. Because of this unexpected result the effect of a third antagonist, 176 μg nephidipine (Equimolar to 250 μg D600 or 250 μg Verapamil) on the transport rate mediated by the same ionophore (40 μg Nafod) is investigated. The results in Fig. V.13.(a) show that no inhibition was observed. In a further experiment, it was found that the extravesicular addition of 250 μg Verapamil to an nmr tube containing 176 μg nephidipine plus 40 μg Nafod promotes the rate of transport (Fig. V.13.(b)).

The experiments so far described show that using any of the three antagonists, the two natural ionophores (A23187 - Ionomycin) show a different behaviour

(a)

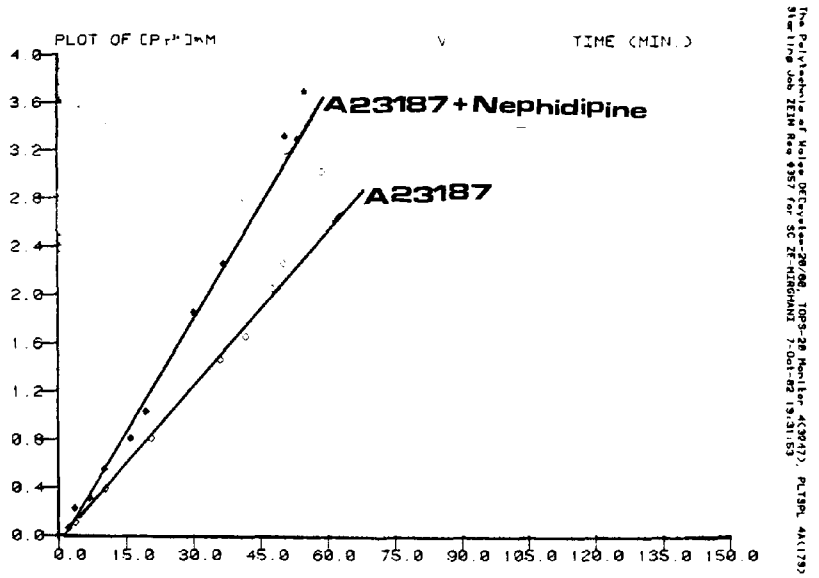

(b)

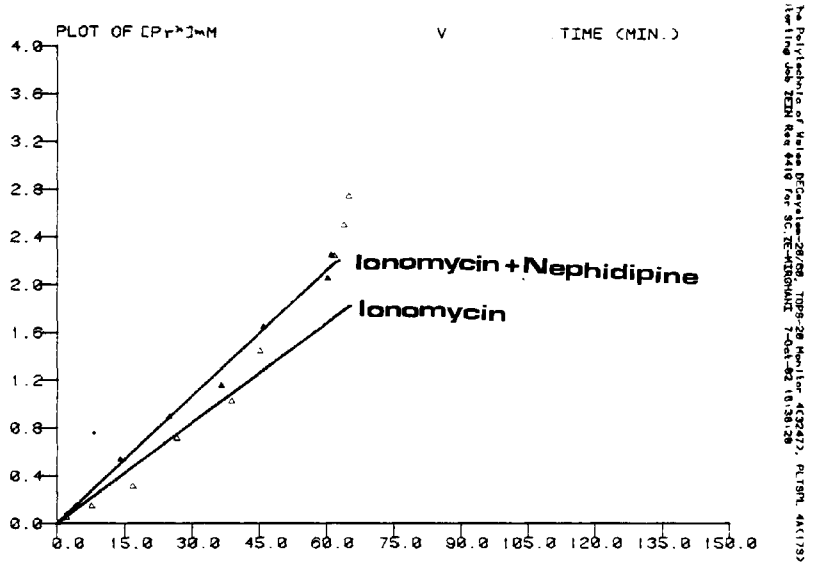

(c)

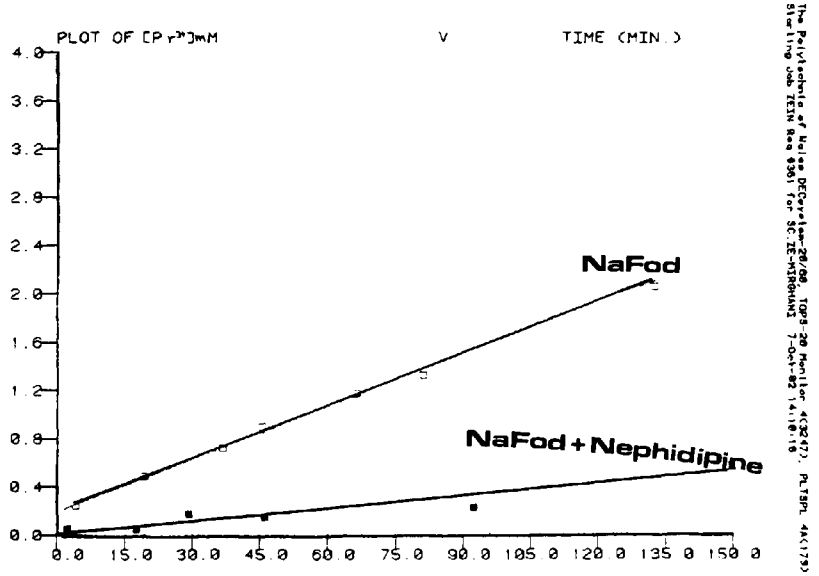

Fig.V.10 shows that Nephidipine inhibits the transport mediated by NaFod but promotes the transport mediated by equimolar concentrations of A23187 and Ionomycin.

(a)

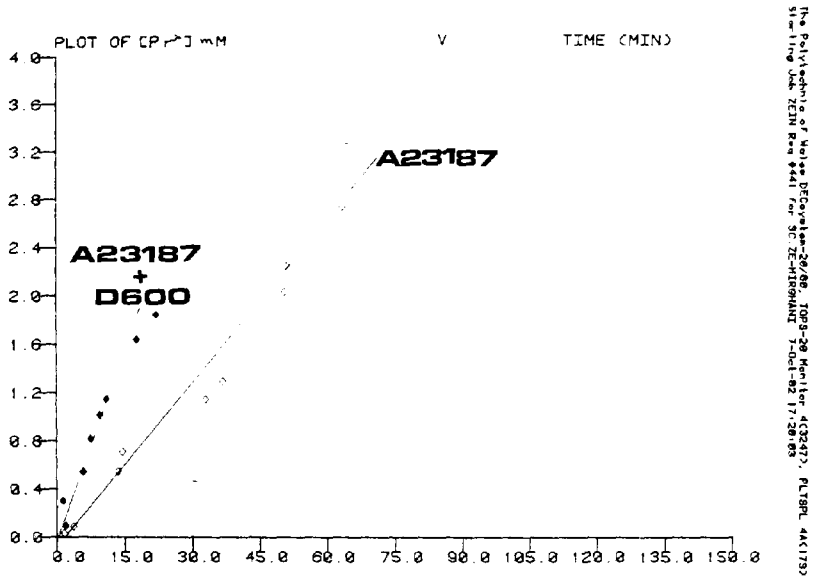

(b)

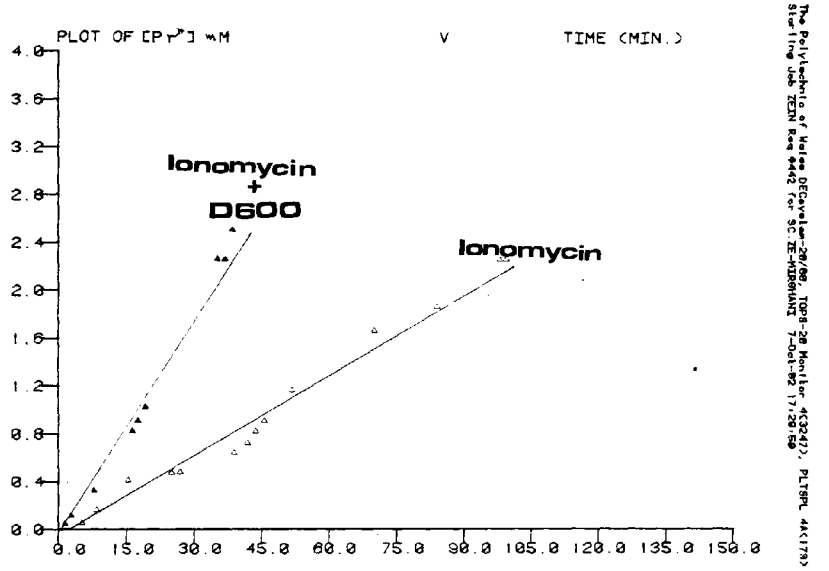

(c)

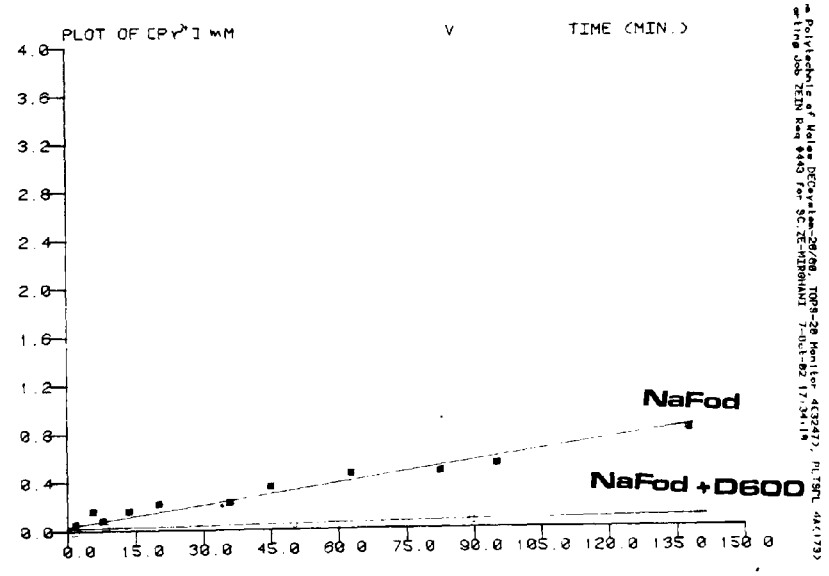

Fig.V.11 shows that D600 inhibits the transport mediated by NaFod but promotes the transport mediated by equimolar concentrations of A23187 and Ionomycin.

FIG. V. 12. A

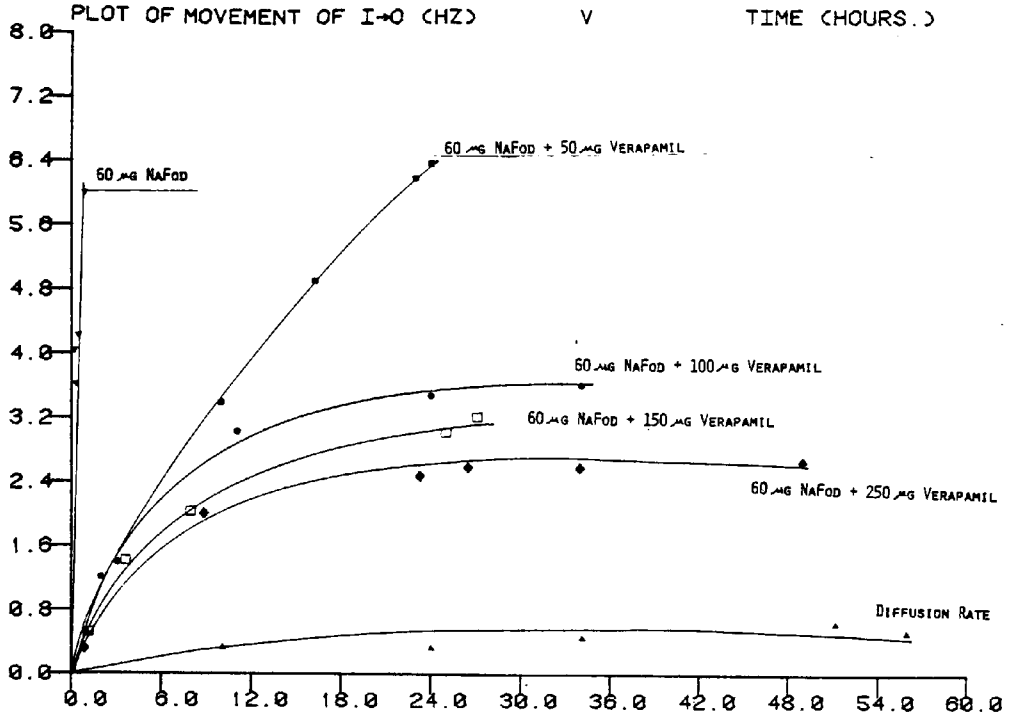

FIG. V. 12. B

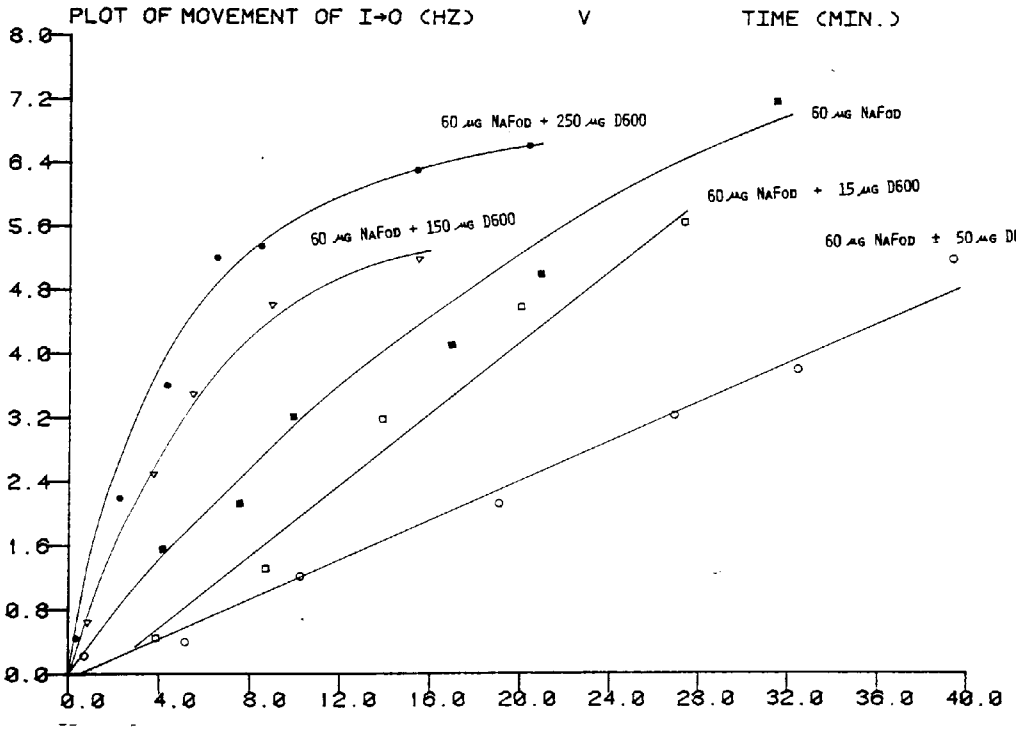

FIG. 12. A SHOWS THAT VARIOUS CONCENTRATIONS OF VERAPAMIL (50→250UG) INHIBITS THE TRANSPORT OF IONS MEDIATED BY 60 UG NAFOD. THE DEGREE OF INHIBITION IS PROPORTIONAL TO THE AMOUNT OF VERAPAMIL ADDED.

FIG. 12. B SHOWS THAT LOW CONCENTRATIONS OF D600 (15 AND 50UG) INHIBIT ION TRANSPORT MEDIATED BY NAFOD, WHILST AT HIGH CONCENTRATIONS (150 AND 250) D600 POTENTIATES THE RATE.

FIG. V. 13. A

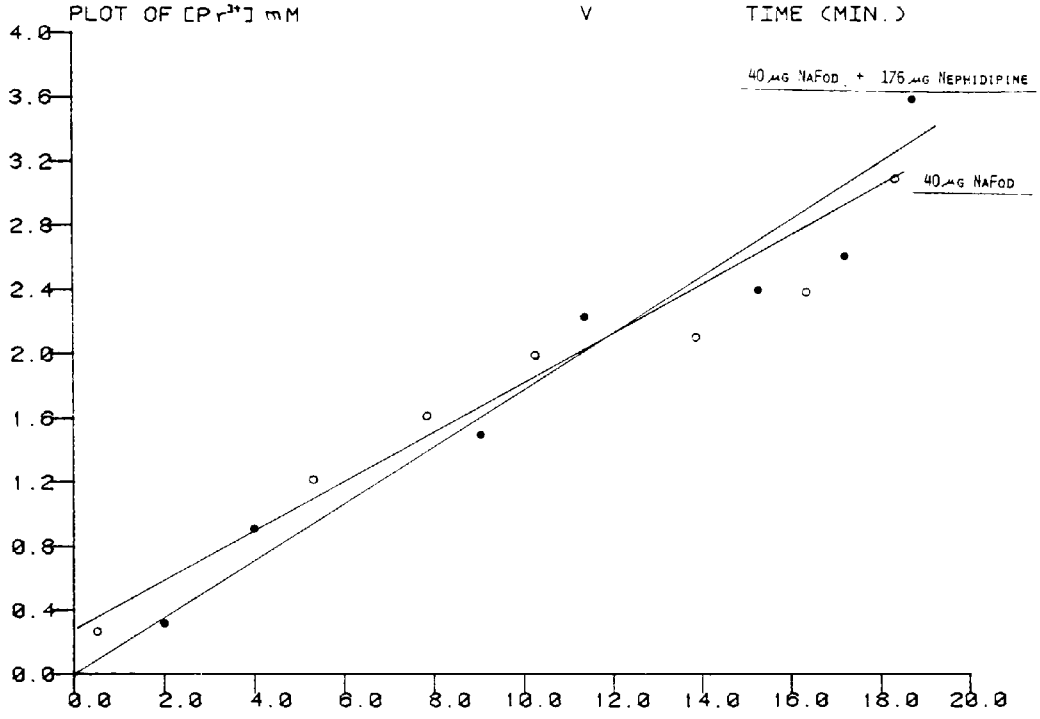

FIG. V. 13. B

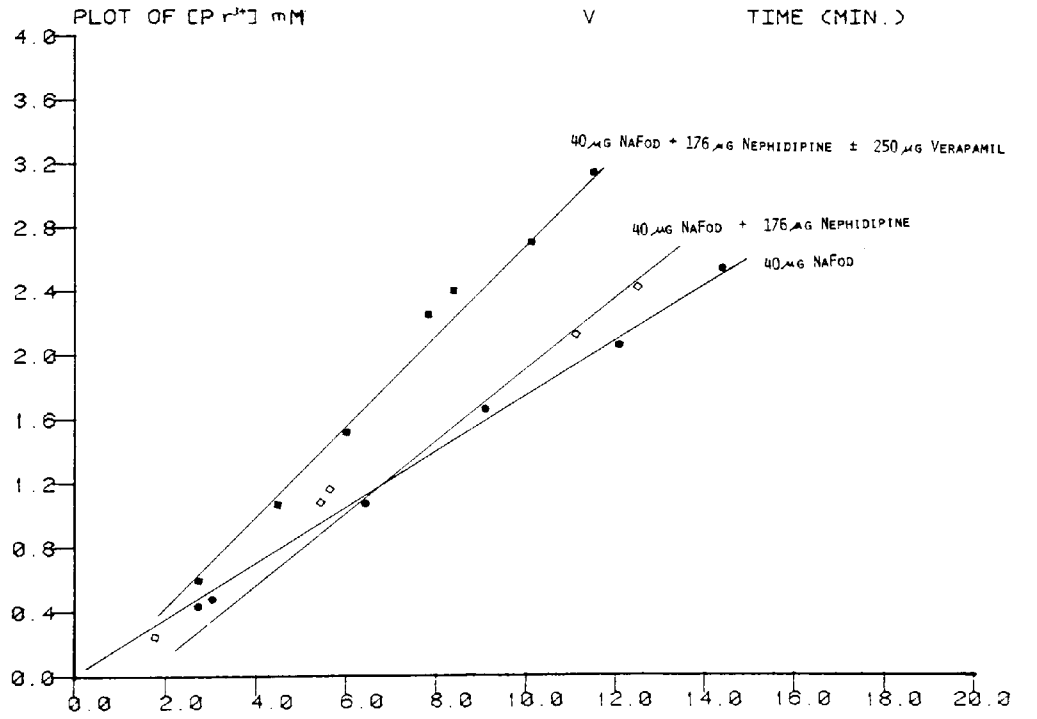

when compared with the synthetic ionophore Nafod. Secondly, the nature and relative concentration of the antagonist with respect to the ionophore are important factors determining whether a promotion or an inhibition of transport is observed.

In the light of these results the effect of "small" concentrations of the antagonist on ion transport mediated by antibiotic ionophores is investigated. Fig. V.14 shows that all concentrations between 5μg and 50 μg Verapamil inhibit the transport mediated by 50 μg Ionomycin. And consistent with previous results (see above), the degree of inhibition is proportional to the concentration of Verapamil added. Fig. V.14 also shows that the lower limit of inhibition by Verapamil is slightly lower than 5 μg.

The disposition of the antagonist with respect to the vesicular bilayer has important effects on the transport mechanisms mediated by carrier ionophores as shown below. The antagonist in the above experiments was added extravesicularly but two other methods were adopted to include the antagonist within the hydrocarbon core. In the first method the antagonist was added to the chloroform solution of the lipid, and after the necessary steps (see Materials and Methods), the ionophore was added extravesicularly from a D_2O solution. The second method involved the mixing of chloroform solutions of the antagonist, the ionophore and the lipid - followed by evaporation of the solvent. Calculated volumes of D_2O was then added to the dry lipid and the liposomes were sonicated (see Materials and Methods). As shown in Figs. V.15.(a) and (b) the results of both methods produced an "ineffective" inhibition as compared to the previous method where the antagonist was added extravesicularly. Moreover, it can be seen in Fig. V.16 that the inclusion of the antagonist in the bilayer "masks" the effect of another antagonist which may be

FIG. V. 14

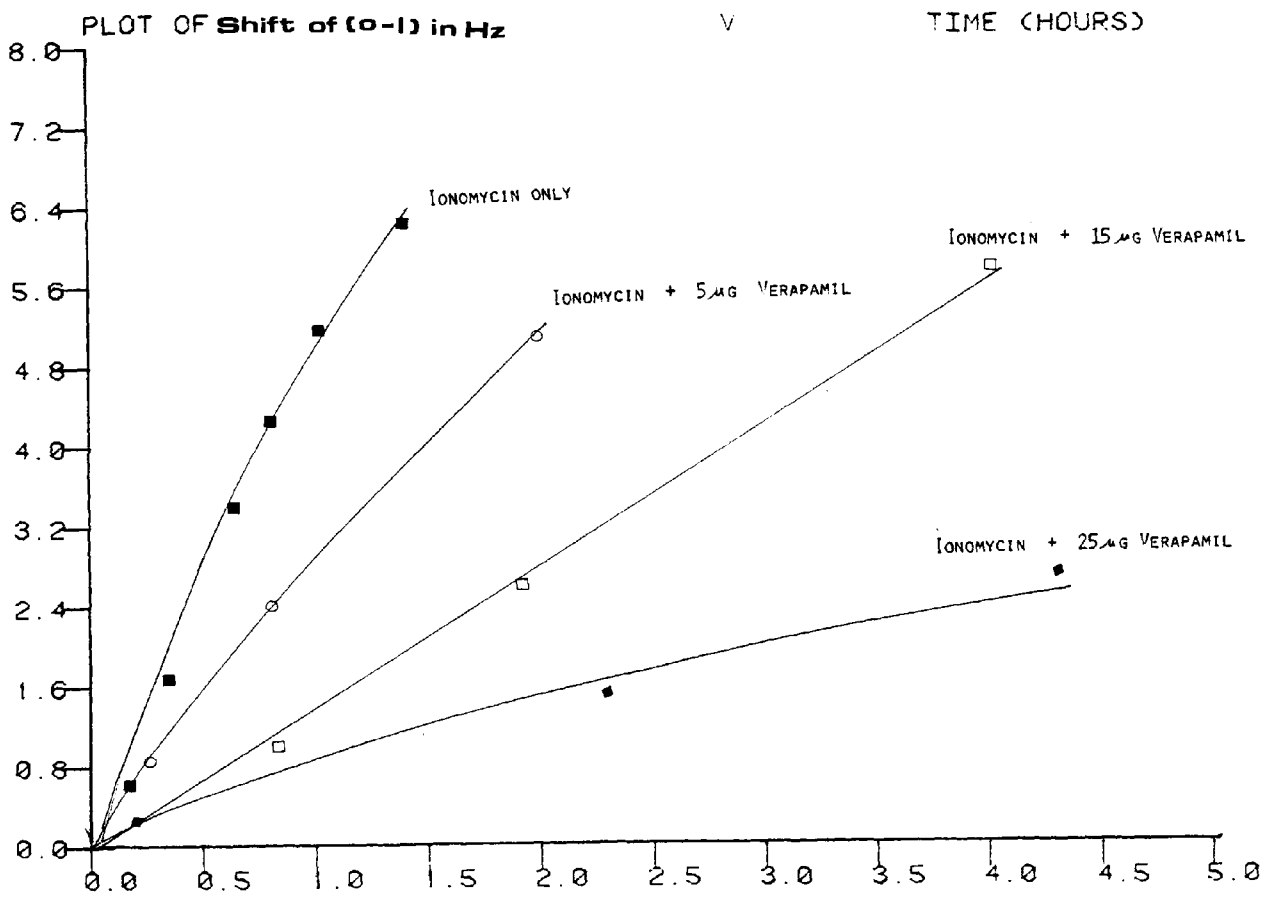

FIG. V. 14 SHOWS THAT LOW CONCENTRATIONS OF THE ANTAGONIST (5,15 AND 25UG VERAPAMIL) INHIBIT THE RATE OF ION TRANSPORT MEDIATED BY IONOMYCIN. THE LOWER LIMIT OF INHIBITION IS SLIGHTLY LESS THAN 5UG.

FIG.V.15. A

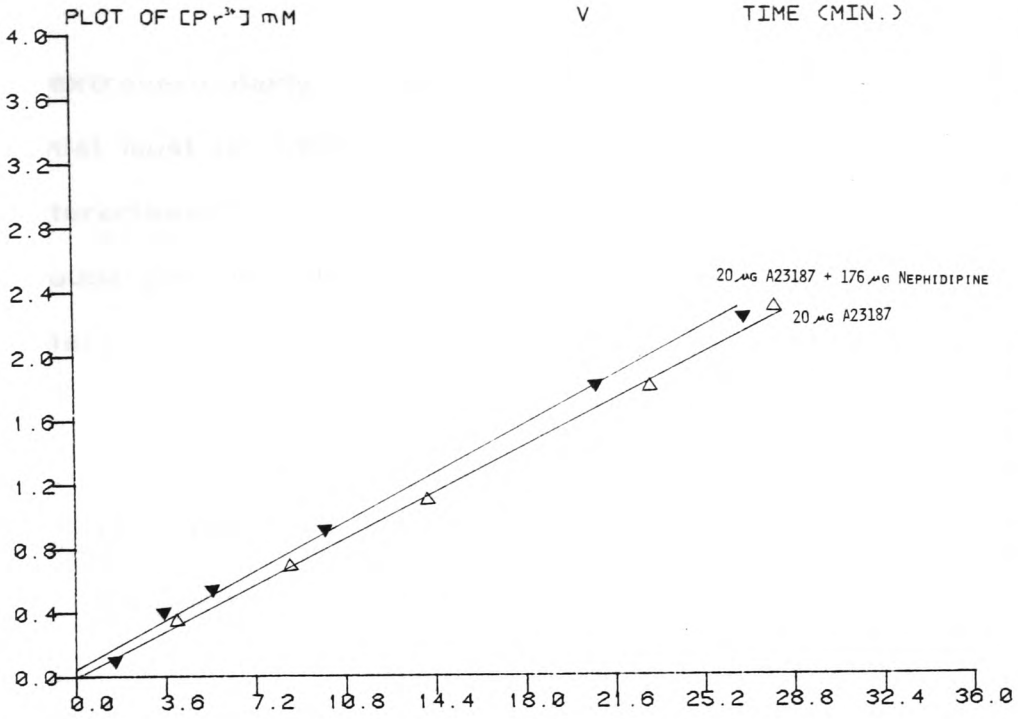

FIG.V.15. B

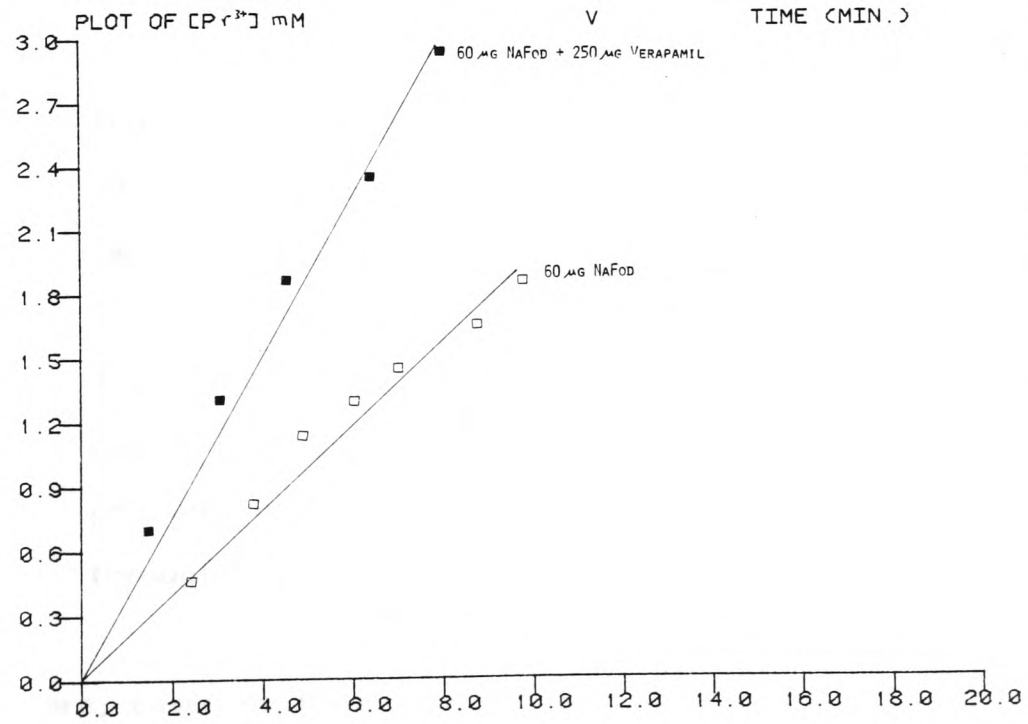

FIG. 15. A BOTH THE IONOPHORE (A23187) AND THE ANTAGONIST (NEPHIDIPINE) ARE INSIDE THE BILAYER. THE ANTAGONIST IS SEEN NOT TO INHIBIT ION TRANSPORT. IN FIG. V.15. B BOTH THE IONOPHORE NAFOD AND THE ANTAGONIST VERAPAMIL ARE INSIDE THE BILAYER. THE ANTAGONIST PROMOTED ION TRANSPORT.

added extravesicularly. Therefore, for an "effective" inhibition; the antagonist must be added to the extravesicular space, and this may indicate that interactions with the metal ion, with the ionophore or with the outer headgroups are possible hypothesis for mechanisms of action of the antagonist (see later).

V.3.4 The effect of calcium antagonists on ion transport mediated by the channel former alamethicin 30:

The experimental results in this section are based on the following suggestions abstracted from the literature survey:

(i) It is suggested that the calcium antagonists affect the entry of calcium through the voltage gated calcium channel i.e. the so called "slow calcium channel" (see introduction to this chapter).

(ii) The use of high concentrations of the calcium antagonists (i.e. higher than that required to block the voltage sensitive channel) promotes rather than inhibits the rate of conduction of ions through this type of channel (see introduction).

Therefore, based on these suggestions the effect of "high" and "low" concentrations of the antagonists verapamil and nephidipine on the voltage sensitive channel formed by alamethicin 30 were investigated. The results in Fig. V.17 (a) shows the effect of various concentrations of verapamil on ion transport mediated by 20 μg alamethicin. It can be seen that 50 μg of

FIG. V. 16

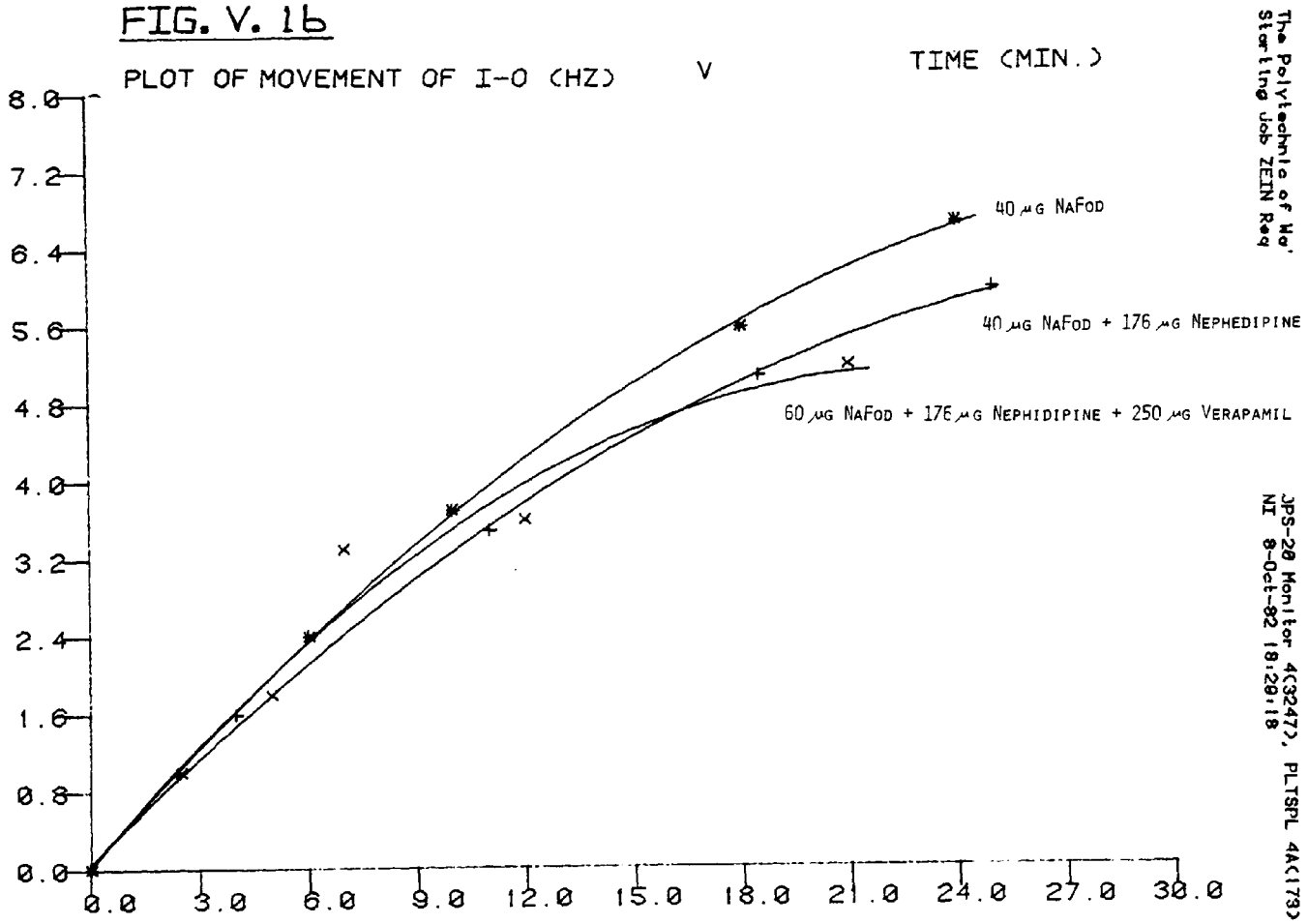

FIG. V. 16 SHOWS THAT THE PRESENCE OF AN ANTAGONIST (NEPHIDIPINE) INSIDE THE BILAYER MASKS THE EFFECT OF ANOTHER ANTAGONIST (VERAPAMIL) WHICH MAY BE ADDED EXTRAVESICULARLY.

verapamil "slightly" inhibits the rate of transport while higher concentrations (150 μg and 250 μg verapamil) promotes the transport rate as expected (See V.3.3.). The effect of very small concentrations of nephidipine on alamethicin mediated transport is shown in Fig. V.17.(b).

It is clear that a few microgramme difference in nephidipine concentration can either inhibit or promote the transport rate. These results are consistent with the above mentioned slow Ca^{++} channel mechanism of ion conduction.

V.3.5 The effect of calcium antagonists on membrane processes in vesicles containing non-bilayer lipids:

Malaisse suggested that the antagonist inhibits ion translocation by binding to the complexing sites of the ionophore thus preventing the ions from binding to the ionophore, but the results imparted above are not in agreement with this. However, this hypothesis suggested experiments using vesicles containing non-bilayer lipids, hence eliminating the requirement of an ionophore. The effect of the antagonist, therefore, would be on the mechanism of formation of two types of inverted micelles, i.e. those which mediate transmembrane transport/Flip-flop and vesicle-vesicle fusion respectively (Fig. I.13).

The effect of 250 μg verapamil on the rate of transport of Dy^{3+} ions across egg PC/10 mole% CL vesicles is shown in Fig. V.18.(a). Note that the addition of calcium ions promotes the transport rate considerably, but the addition of verapamil has no effect on the transport rate once calcium is added.

On the other hand verapamil reduces the fusion rate in these vesicles

FIG. V. 17. A

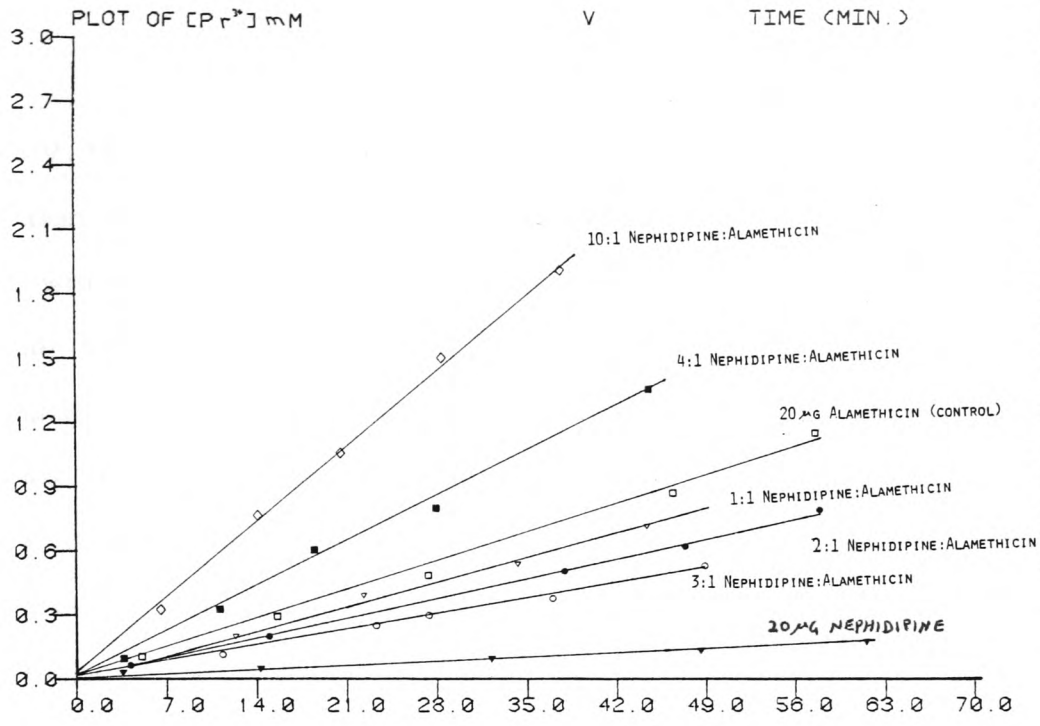

FIG. V. 17. B

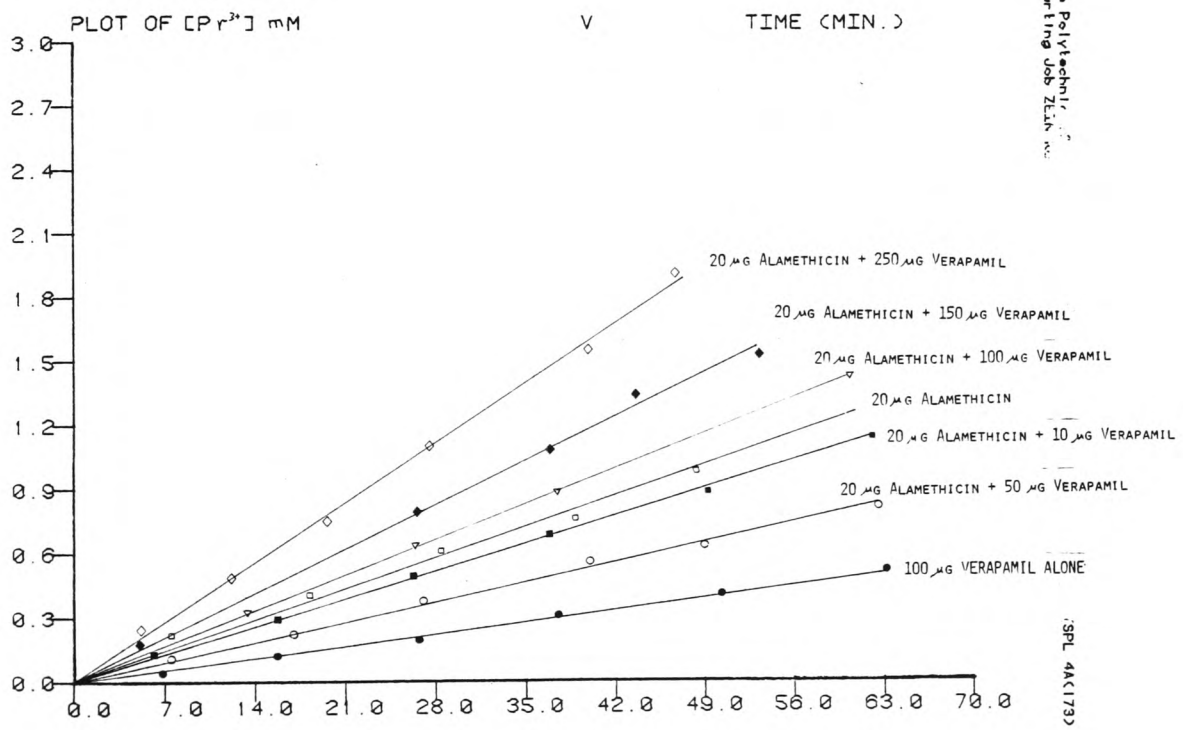

FIG. V. 17. B SHOWS THAT LOW CONCENTRATIONS OF VERAPAMIL (50 AND 100UG) INHIBIT ION TRANSPORT MEDIATED BY THE CHANNEL FORMER ALAMETHICIN 30 WHILST AT HIGH CONCENTRATIONS (150, 250UG) VERAPAMIL POTENTIATES THE RATE OF ION TRANSPORT.

FIG. V. 17. A SHOWS THAT LOW CONCENTRATIONS OF NEPHIDIPINE (1:1, 2:1 AND 3:1) INHIBIT ION TRANSPORT MEDIATED BY ALAMETHICIN WHILST AT HIGH CONCENTRATIONS (4:1 AND 10:1) NEPHIDIPINE POTENTIATES THE RATE.

(Fig. V.18.(b)) which indicates that this chemical interferes with the formation of the inverted micelles mediating vesicle-vesicle fusion but not those which mediate transbilayer transport and flip flop (Fig. I.13). Further evidence to this result is given in Fig. V.19 (a) which shows that verapamil has minimal effect on the rate of Flip-Flop in egg PC/10 mole% PA vesicles, but it inhibits the rate of vesicle-vesicle fusion (Fig. V.19.(b)). The above mentioned membrane processes occurring in mixed lipid vesicles are discussed in the previous chapter, but with reference to the effect of the antagonist on non-bilayer mediated processes see the following discussion section.

FIG. V. 18. A

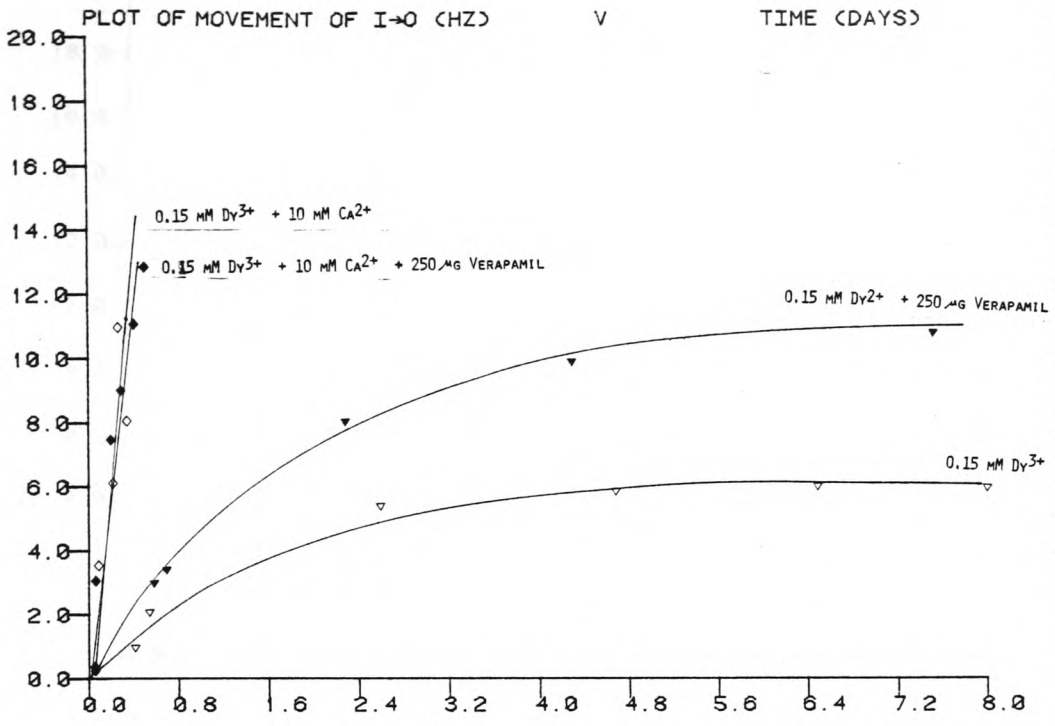

FIG. V. 18. B

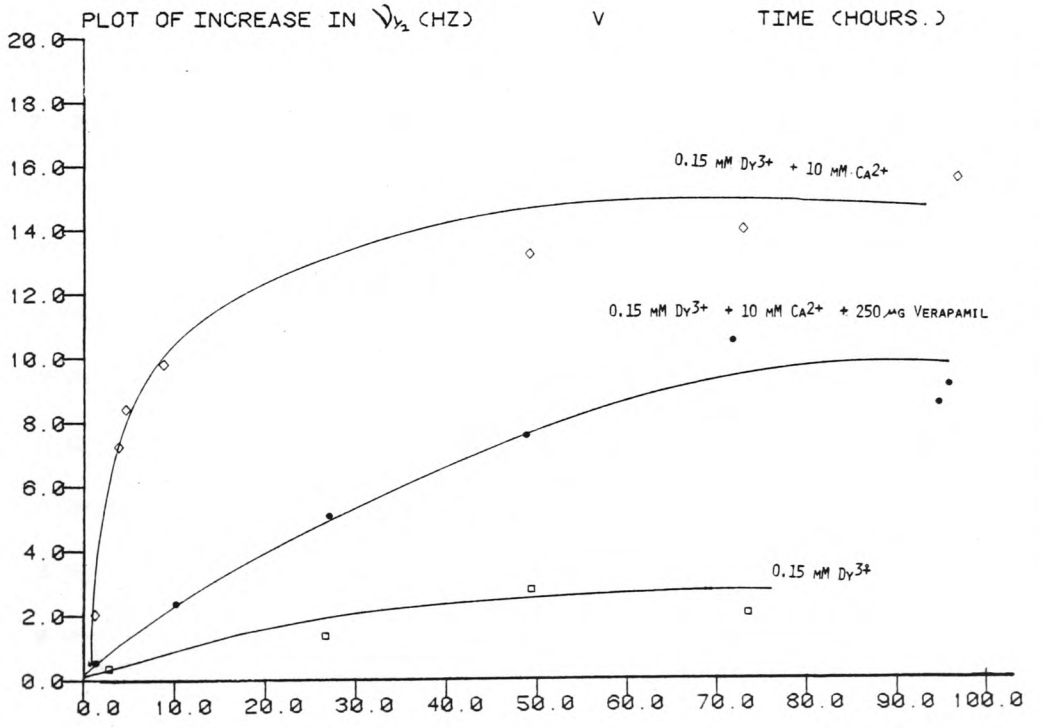

FIG. V. 18. A SHOWS THAT CALCIUM IONS TRIGGER NON BILAYER PHASES IN EGG PC/10 MOLE% CL VESICLES. VERAPAMIL IS SEEN NOT TO INHIBIT ION TRANSPORT MEDIATED VIA INVERTED MICELLAR INTERMEDIATES. HOWEVER, VERAPAMIL SUBSTANTIALLY INHIBITS MEMBRANES FUSION OCCURING IN THESE VESICLES (FIG. V. 18. B).

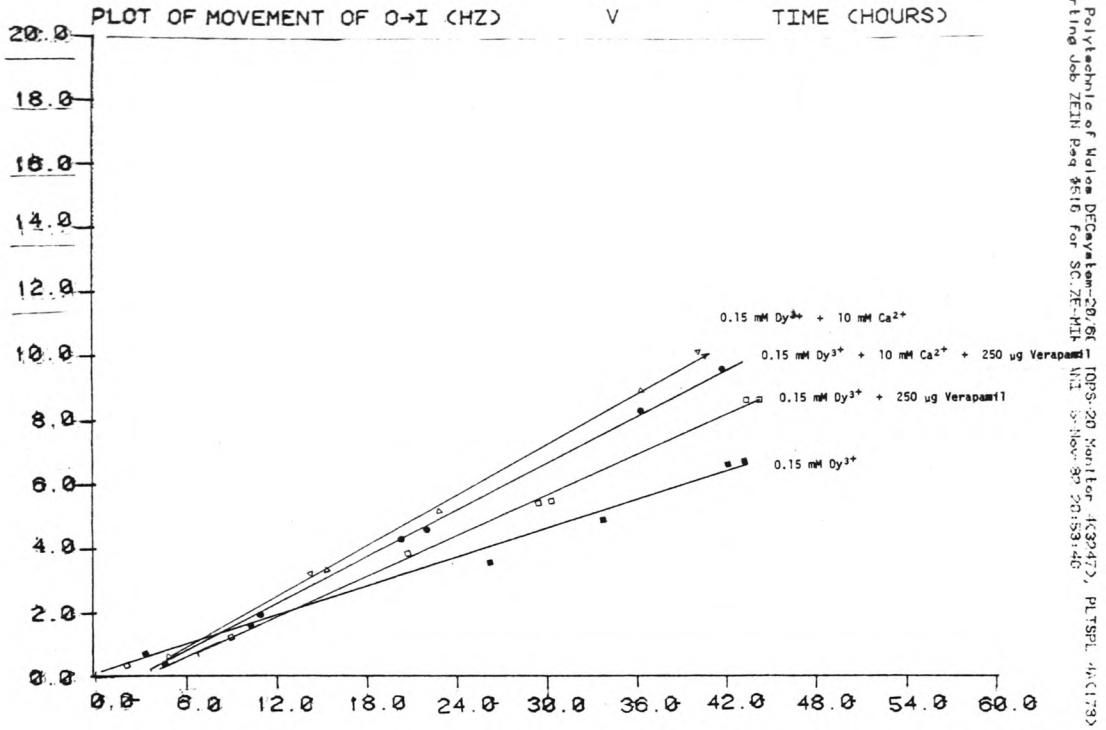

FIG. V. 19. B

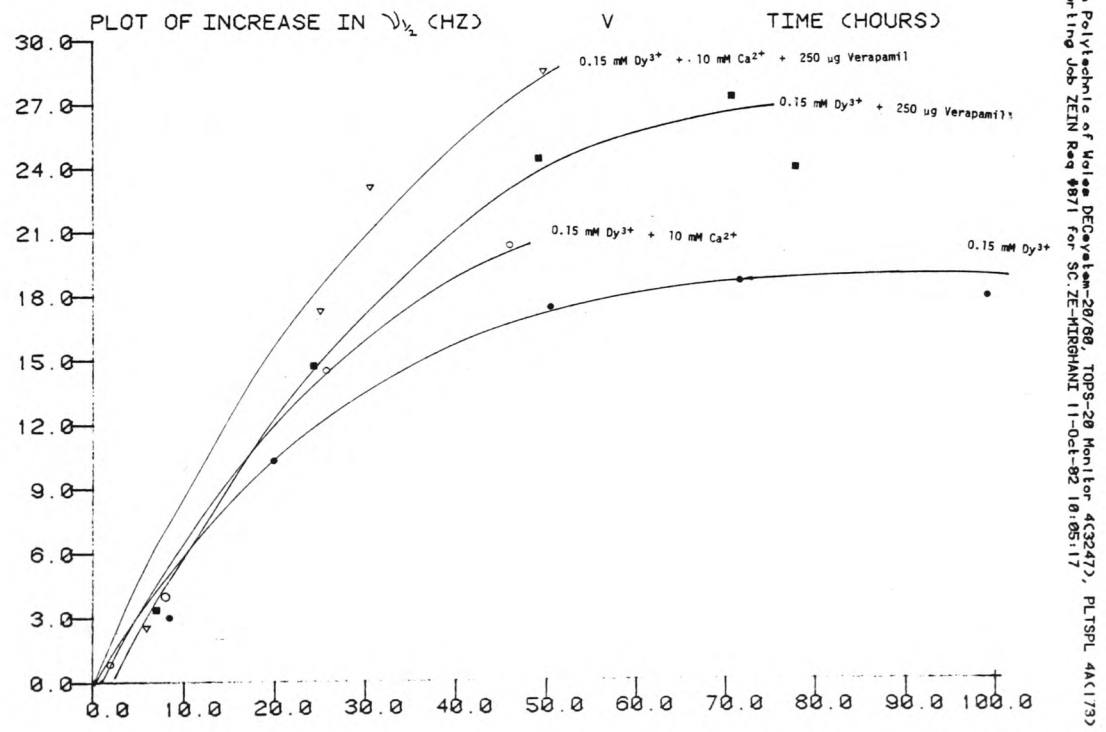

FIG. V. 19. A SHOWS THAT VERAPAMIL HAS MINIMAL EFFECT ON TRANSBILAYER FLIPFLOP OCCURING IN EGG PC/10 MOLE% PA VESICLES. MEMBRANES FUSION, HOWEVER, IS SEEN TO BE INHIBITED (FIG. V. 19. B).

V.4 Discussion

V.4.1 Calcium antagonist - ionophore interactions investigated by UV and fluorescence spectroscopy

The excitation and fluorescence spectra of A23187 as the free acid in chloroform (Fig. V.2.(a)) exhibit two maxima centred at 310 nm (due to the ketopyrole group) and 380 nm (due to the benzoazole ring) [241] - corresponding to the transition wavelenths λ_1 and λ_2 as shown in the energy level diagram presented in Fig. V.2.(b). The titration of microlitre amounts of the chloroform solution of Verapamil (up to 10:1 w.r.t. ionophore concentration) is seen (Fig.V.3.(a) and (b)) not to quench A23187 fluorescence or produce any observable wavelength shift. Similar concentrations of D600 were equally ineffective. Nephidipine, however, caused the quenching at both excitation and fluorescence wavelengths (Fig. V.4.(a)), but, similar to verapamil and D600 no wavelength shift was detected. The fluorescence quenching caused by nephidipine is due to the competition between the ionophore and the antagonist for photons (i.e. internal filter effect) [242]; and evidence to support this is given in Fig. V.4.(b) which shows the uv absorption spectrum of nephidipine in absolute ethanol displaying two absorption bands at 315 nm and 430 nm overlapping with A23187 excitation and fluorescence wavelengths, respectively.

These fluorescence data suggest that the relative affinity binding of the antagonist by the ionophore is too weak to account for the specific and sensitive behaviour of these drugs. Furthermore, the absence of a wavelength shift (Stokes shift) suggest that electronic interactions between the ionophore and the antagonists are quite unlikely [242]. However, these suggestions were re-affirmed by the uv results discussed below.

The ultraviolet absorption spectrum of A23187 in absolute ethanol displays four resolvable maxima located at 204, 225, 278 and 378 nms (Fig. V.5.(b)) with respective extinction coefficients 28200, 26200, 18200 and 8200 [243]. In addition the peak located at 278 has a prominant shoulder at about 290 nm. Of the three antagonists investigated, only verapamil caused measurable effects on the absorption spectrum of A23187. Increasing the verapamil: A23187 concentration (up to 3:1) caused an increase in the absorption of the bands centred at 278 nm and 225 nm; and in addition, a new peak centred at 200 nm has developed. The ultraviolet spectra of A23187 and verapamil at the scanned wavelength (200-400 nm) are in fact very similar (Fig. V.5.(a) and (b)), and the enhancement of the absorption wavelength at 278 nm and 225 nm, as well as the emergence of the peak at 200 nm are caused by the antagonist's absorptions alone. Hence, these uv results are in agreement with the fluorescence data; both suggesting that Malaisse's hypothesis of ionophore/antagonists interactions are an unlikely explanation for the mechanism of action of these drugs.

V.4.2 The antagonists' interactions with the metal ion investigated by shift reagent nmr

The antagonists' interactions with the metal ion was investigated using the nmr shift reagents Yb $(Fod)_3$ and Pr $(Fod)_3$ with verapamil and nephidipine, respectively. At the time this study was initiated the nmr spectra of the calcium antagonists were not reported (see introduction). The results presented in Fig. V.7 and V.8 show the ^{1}H and ^{13}C-nmr spectra of verapamil and nephidipine in chloroform. Assignment of all resolvable resonances was made possible by the "INEPT" pulse sequence provided by the JEOL Company

(see Materials and Methods).

The addition of the nmr shift reagent Yb $(Fod)_3$ caused the upfield shift of the signals due to the methoxy and nitryl groups of verapamil, and slight shifting and extensive broadening of the benzene resonance. Other effects observed at high concentrations of the shift reagent were the broadening of the resonance due to the methoxy group, and the downfield shift of the bridging methylene groups. These changes occurring in the ^1H-nmr spectrum of verapamil are due to the alteration of the magnetic environment of the antagonist caused by lanthanide ion binding to the antagonist. The space filling models of verapamil (Fig. V.20) show a "bridge" structure; the methylene groups at the "roof", and the methoxy and benzene groups at each side (Fig. V.20). The binding of the lanthanide ion to the methoxy groups (which show the largest nmr shift) may effectively pull the two sides of the bridge, particularly the benzene rings, thus causing the nmr shift of the benzene resonance. The downfield shift of the bridging methylene groups may be due to the bending of the molecule caused by lanthanide binding. The slight shift of the nitro group indicate that this site may offer a weaker binding; the methoxy group being the stronger binding site.

The effect of the nmr shift reagent Yb $(Fod)_3$ on the ^1H-nmr spectrum of nephidipine (Fig. V.8.(a)) is seen to cause the downfield shift of the signals due to the NH, CO_2CH_3, CH_3 and CH groups. The possible binding sites of nephidipines are easily identifiable because of the equivalence of the substituents on the ortho and meta positions which gave an approximately C_2 axis of symmetry along the vertical axis of the molecule (Fig. V.21). The space filling models of nephidipine (Fig.V.21) revealed that 180° rotation of the

FIG.V.20. SPACE-FILLING MODELS OF VERAPAMIL

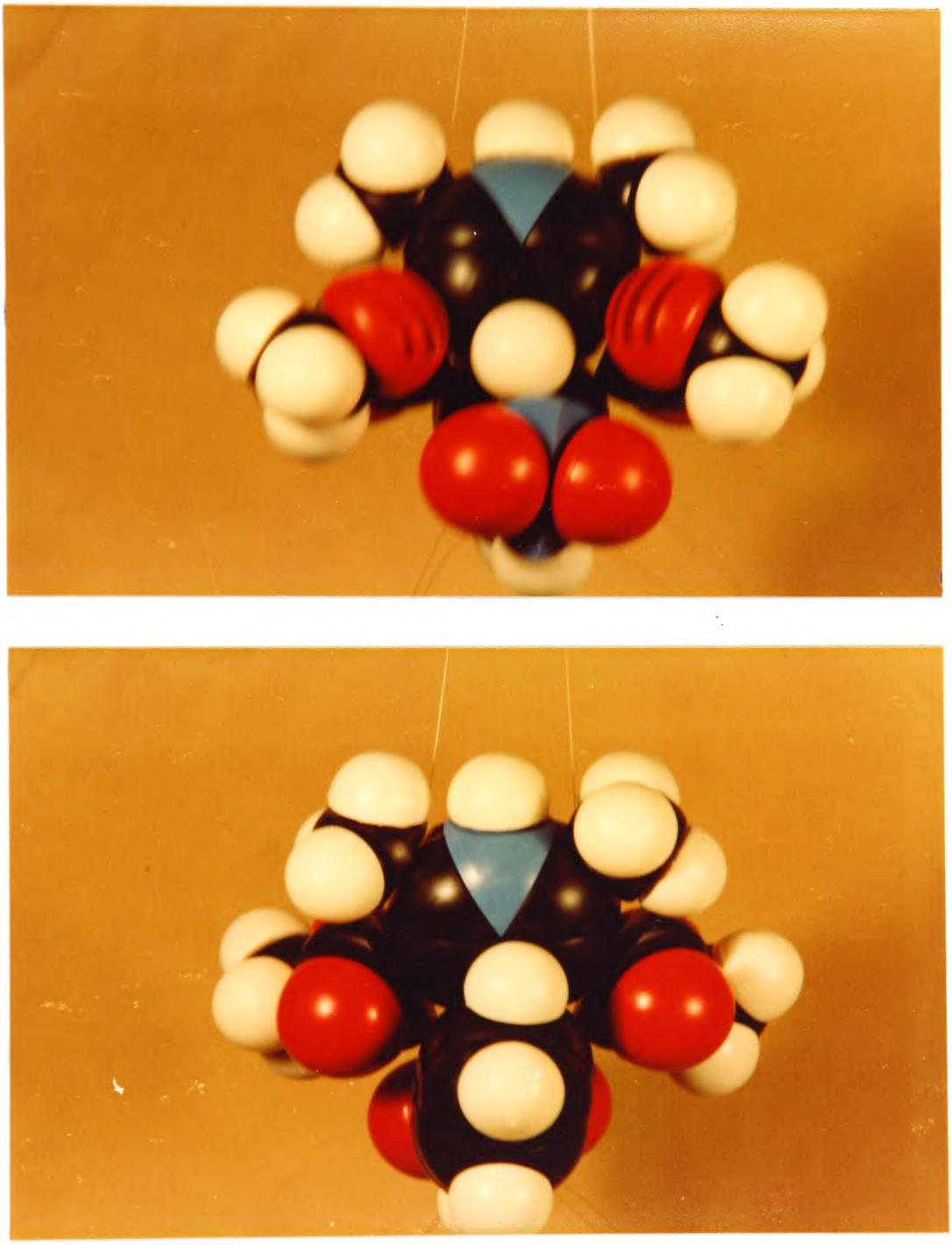

The front (above) and back (below) views of Verapamil show the molecule has a bridge structure with the benzene and methoxy groups at the sides and the bridging methylene groups at the root.

FIG.V.21. SPACE-FILLING MODELS OF NEPHIDIPINE

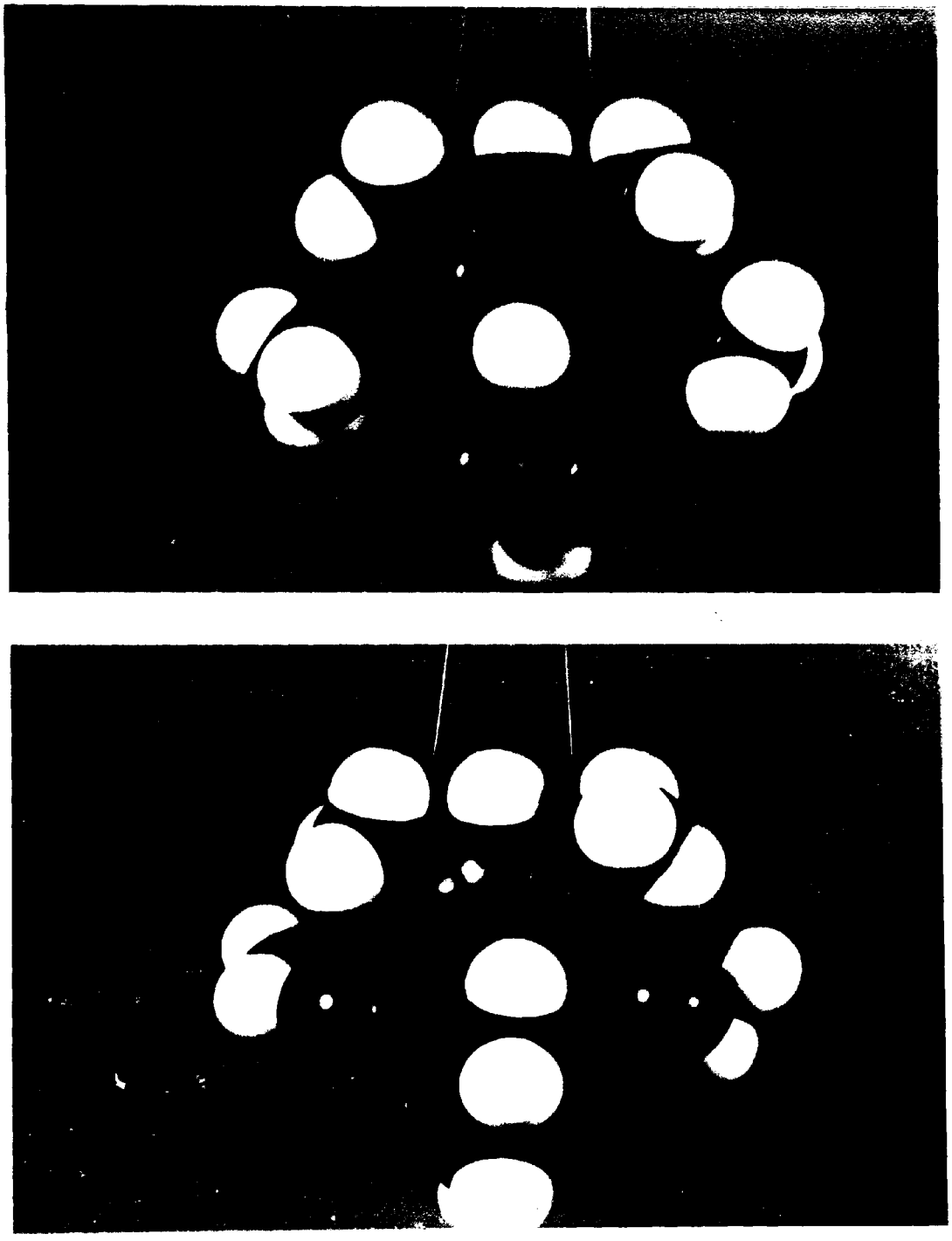

The front (above) and back (below) views of Nephidipine show that the molecule is symmetrical and a vertical C_2-axis (if drawn) bisect the molecule in equal halves.

upper benzene ring with respect to the lower pyridine ring is restricted due to the proximity of the nitro substituent in the benzene ring and the bulky CO_2CH_3 group on both ortho positions of the pyridine ring. This suggests that the downfield shift of the CH group present between the two rings is mainly due to the steric hinderance between the rings. The main binding sites of nephidipine seem to be the CO_2CH_3 with the CH_3 group brought close the Ln^{3+}shown by the largest nmr shift; the NH group, similarly to the NO_2 of verapamil, offer a secondary weaker site.

These nmr shift results suggest that the calcium antagonists bind the metal cations to such an extent that it might be possible to explain the inhibition property of these drugs reported by many workers[110][121]. The above hypothesis was further investigated using ionophore mediated transport of lanthanide ions across sonicated vesicles (see V.4.3).

V.4.3. Inhibition of ionophore mediated Ln^{3+} transport across egg PC vesicles by the calcium antagonists

The effect of the calcium antagonist verapamil on carrier mediated transport of lanthanide ions across sonicated egg PC vesicles was demonstrated, (Fig. V.12.(a)) . The degree of inhibition of Pr^{3+} transport mediated by NaFod is proportional to the extravesicular concentration of the antagonist. Low concentrations of this antagonists were also found to inhibit cation transport mediated by the naturally occurring ionophore ionomycin (Fig. V.14). However, differences in the antagonism behaviour of these drugs had emerged when equimolar concentrations of the synthetic ionophore NaFod and the antibiotic ionophores (A23187 and ionomycin) were used to transport the

lanthanide. Equimolar extravesicular concentration of verapamil inhibited NaFod mediated transport but promoted the transport mediated by A23187 and ionomycin (Fig. V.9.). Similar results were obtained with two further antagonists (nephidipine and D600) at equal concentrations to verapamil (Fig. V.10 and V.11). It has been previously suggested (see above) that the inhibitory property of these drugs is probably due to the metal ion - antagonist interactions, however, in the light of these results it appears that interactions between the antagonist and the metal ion ionophore complex may occur.

In order to investigate these possible interactions, the nature of the ionophore metal ion complexes were closely examined. The two antibiotic ionophores (A23187 and ionomycin) are known to undergo certain conformational changes when complexing the metal ion; thus adopting an hydrophobic exterior resulting in enclosing the hydrophilic binding sites on the interior of the molecule. On the other hand, the synthetic ionophore Nafod requires comparatively less conformational changes on complexing the metal ion; thus the complexing sites of this ionophore are relatively exposed (vulnerable) to the antagonist attack. Therefore, a competition between the antagonist and the ionophores for the transportable metal ion is likely to inhibit Nafod mediated transport more effectively than A23187 or ionomycin mediated transport. Such reasoning may explain the inhibition of Nafod mediated transport. However, it does not explain the promotion of ionophore mediated transport occurring with A23187 and ionomycin. Various workers [244] have reported the inactivity of the calcium antagonists when employed at high concentrations. Middleton and coworkers [244] have demonstrated the inactivity of verapamil, D600 and nephidipine in vascular smooth muscle when employed at concentrations significantly higher than those required to block the voltage sensitive channel. A similar conclusion has been reached for a number of other stimuli-

secretion coupling systems including mast cells[107], salivary glands[245] and the exocrine pancreas[246]. However, non of these workers reported an explanation which may account for the difference in the antagonistic behaviour of these drugs when used at extreme concentrations. However, a reasonable explanation for the enhancement of ionophore mediated (A23187 and ionomycin) transport may be that at high concentrations of the antagonist, mixed complexes between the metal ion, the ionophore and the antagonist may form, and such a complex may behave as a polyionophore. However, it is essential for the validity of this hypothesis to show that: (i) the antagonist alone act (by some mechanism) as a metal ion ionophore, and (ii) that the use of a mixture of ionophores to transport the same metal ion results in higher rate of transport than if only one of the ionophores in question was used for transport.

With regard to the first of these points, it was found that (Fig.V.22) various extravesicular concentrations of verapamil transport the lanthanide ion Pr^{3+} into sonicated vesicles at a rate which is considerably higher than the normal diffusion rate but lower than that shown by equal concentrations of an ionophore. Furthermore, these antagonists show appreciable solubility in organic solvents, and the addition of nmr shift reagents to these have shown strong affinity for metal ion - antagonist binding. These are properties common to natural ionophores. With regard to the ionophoretic property of these antagonists Grandjean and Lazlo[247] have recently shown that the transport of Pr^{3+} with X537A - etheromycin (1:1) mixtures, or by etheromycin - monensin (1:1) mixtures is faster than with each ionophore alone.

This group also reported that the effect on the transport with the ionophore mixtures are not merely additive, but a remarkable synergistic effect is set up. Hence, the ionophore, metal ion - antagonist complex may interact

FIG. V. 22

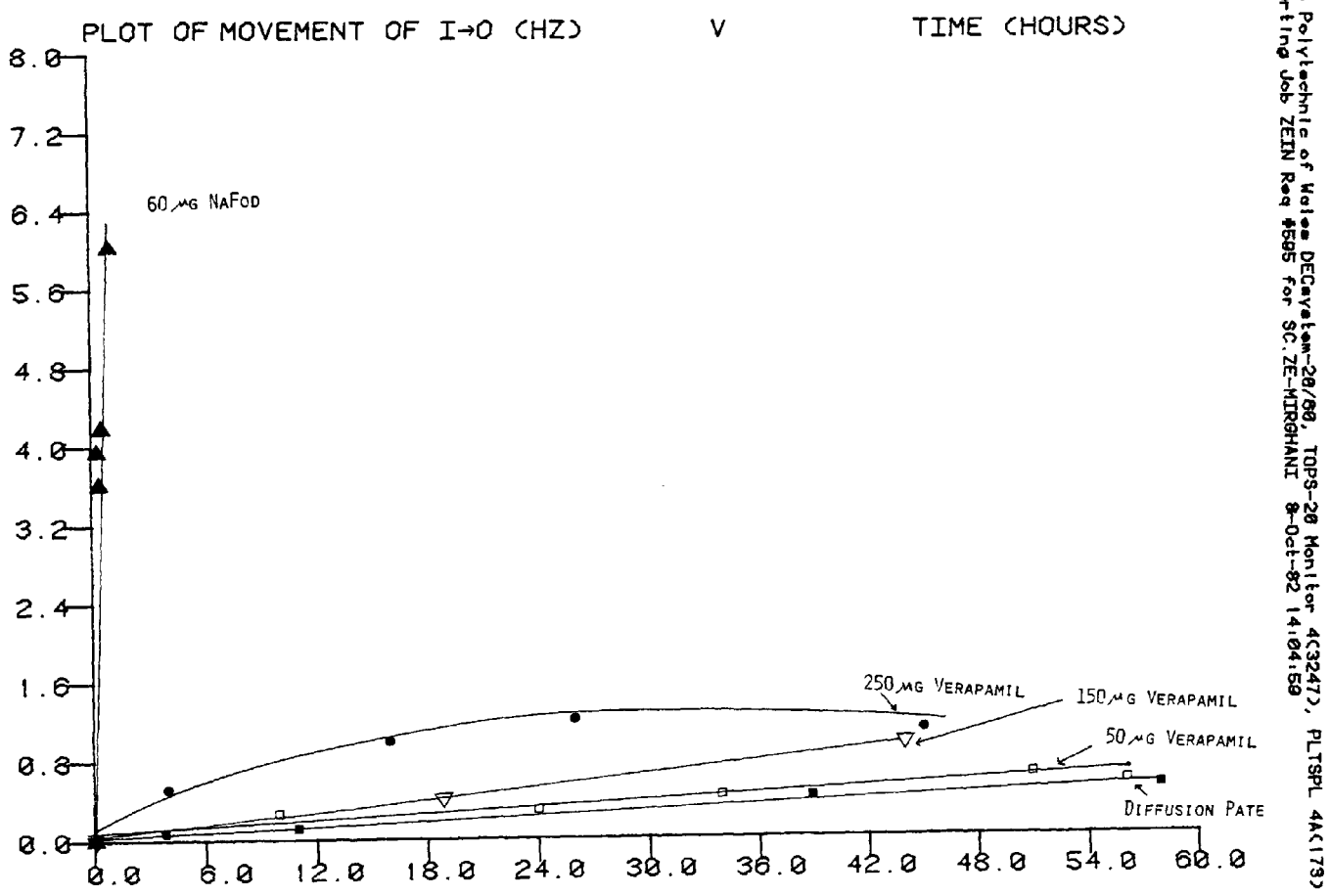

FIG. V. 22 SHOWS THAT VERAPAMIL ALONE EXHIBITS SLIGHT IONOPHORETIC PROPERTY BY TRANSPORTING Pr^{3+} AT A RATE WHICH IS SLIGHTLY GREATER THAN THE DIFFUSION RATE.

synergistically causing enhanced transport of the lathanide. However, the relative efficiency of transport by this suggested mechanism depends upon several factors: the stability constants of the complexes which may be involved in the rate determining step, and the rate constant for cation release from the complex; these are dependent on the flexibility of the ionophore and the antagonist [248]. None of these parameters are known yet for ionophores, and more work is needed to support the above transport hypothesis (also see later).

V.4.4 Site of Action

The experiments so far discussed involved the addition of the D_2O solution of the antagonist (verapamil, D600) to the extravesicular D_2O medium; except in the case of nephidipine where the solid antagonist was allowed to equilibriate with the pre-formed vesicles (see Materials and Methods). However, due to the hydrophobic nature of these drugs, and the possibility of their diffusion inside the bilayer, the exact (final) disposition of the antagonist with respect to the bilayer is not known. Other methods (see Materials and Methods) whereby the disposition of the antagonist is insured to be inside the hydrocarbon region - were used to identify the exact site of action of these drugs (i.e. whether at the vesicle surface, or inside the hydrocarbon region).

The inclusion of 176 µg nephidipine inside the bilayer (Fig. V.15.(a)) failed to inhibit A23187 mediated transport, and in a similar experiment (Fig. V.15.(b)) 250 µg verapamil showed inefficient inhibition of Nafod mediated transport. Comparable solvent extraction experiments by Malaisse et al. [239] have shown that antagonistic reactions occur when both the antagonist and the

ionophore were present in the organic phase and the metal ion in the aqueous phase. The results of an experiment (Fig. V.15.(a)) where 20 μg A23187 and 176 μg nephidipine were included in the lipid phase by sonication, and the lanthanide probe ions added extravesicularly have shown that minimal inhibition took place. Perhaps more interesting the extravesicular addition of sufficient concentrations of verapamil (250 μg)(which normally inhibits transbilayer transport) to the vesicle dispersion containing 176 μg nephidipine and 20 μg A23187 inside the bilayer resulted in minimal inhibition of transbilayer transport. It seems that these drugs inhibit cation transport only if they were present extravesicularly, and the hydrocarbon region of the bilayer is "free" of other chemicals (e.g. ionophore). The insertion of the antagonist inside the bilayer lowers the Van derWaals interactions and substantially expands the headgroup region which may interfere with the membrane surface activity of these drugs. Hwang et al. [249] reported that nonsteroidal antiinflammatry drugs (NSAIDS), for example indomethacin, partition inside purple membranes and DPPC liposomes, and their DSC measurements suggest that depression of the phase transition temperature occurs, perhaps as a result of decreasing chain and headgroup co-operativity.

However, the hypothesis of surface activity of the antagonists was also demonstrated using vesicles containing non-bilayer lipids. In agreement with previous findings (see chapter IV), calcium ions increase transbilayer transport in egg PC/10 mole% CL vesicles and transbilayer flipflop in egg PC/10 mole% PA vesicles (Figs. V.18.(a) and V.19.(a)). The extravesicular addition of verapamil (250 μg) to these vesicles shows no effect on transbilayer transport and minimal effect on transbilayer flipflop (Figs. V.18.(a) and V.19.(a)). In contrast, the rates of fusion in both types of vesicles is inhibited substan-

tially (Fig.V.18.(b) and V.19.(b)). It is previously mentioned that the mechanisms of transbilayer transport and flipflop and vesicle-vesicle fusion are mediated by two distinct types of inverted micelles; the former occurring inside the bilayer while the latter occurs between the outer monolayers of two fusing bilayers. These antagonists, therefore seem to interfere with the formation of the micelles mediating vesicle-vesicle fusion without affecting the micelles mediating transbilayer transport and flipflop. This suggests that the antagonists partition in the headgroup region (perhaps in close proximity to PA and CL headgroups), and inhibits the formation of the inverted micelles mediating vesicle-vesicle fusion, without partitioning deeply inside the hydrocarbon region thus not affecting the micelles mediating transmembrane transport and flipflop.

It may be argued that these drugs are appreciably hydrophobic, and it is commonly believed that the permeability of a given class of molecules is correlated with their solubility in organic liquids. However, it should be recognised that phospholipids and some other biomembrane constituents are amphipathic molecules; the polar headgroups and a few methylenes down the lipid chain constitute a hydrophilic region which shields the hydrophobic centre of the bilayer. Therefore, the hydrophobicity of a drug molecule alone does not ensure partitioning into the bilayer. Because of this amphipathic nature of the membrane there may be high activation energy for the partitioning of a given drug molecule; or the molecule may take up a conformation more in keeping with this 'intermediate' nature of the headgroup region. This may account for the fact that although these drugs are quite soluble in organic liquids their diffusion into the hydrocarbon region of the bilayer does not necessarily occur, and, their antagonism property is mainly due

to surface activity. These suggestions are in agreement with those reported by Mas-oliva et al.[119] They found that verapamil binds to high and low affinity sites of the cardiac sarcolemma; but the removal of the low affinity site i.e. N-acetyl glucosamine residues and the polar headgroups of phospholipids decreases the verapamil binding, which suggests, that the presence of these groups contribute to the binding of this drug.

V.4.5 Inhibition of channel mediated transport

The effect of the calcium antagonists on channel mediated transport was investigated using alamethicin 30. The mechanism of transport of this ionophore has been shown by Hunt and Jones[86] to depend on the aggregation of four alamethicin 30 monomers in a structure similar to staves in a barrel forming a channel which has a short lifetime. Low concentrations of verapamil (up to 100 μg - 20:1 verapamil: alamethicin) inhibit Pr^{3+} transport mediated by alamethicin, with maximum inhibition occurring at 30:1 and 20:1. Above this at 30:1 and 50:1 verapamil potentiates the rate. The calcium antagonist nephidipine is substantially more hydrophobic than verapamil, and at low concentrations (1:1 and 3:1) nephidipine inhibits the transport rate. Higher concentrations (4:1 - 10:1 nephidipine: alamethicin) nephidipine potentiates the rate.

Compounds of differing structures such as verapamil and nephidipine exerting similar effects on both channel mediated and carrier mediated transport must suggest that the inhibition by these drugs is controlled through the interaction at a common site. Therefore, a similar mechanism to

that discussed in carrier ionophore may operate, thus, inhibition may be due to the probability that the metal ion does not bind to the phosphate sites for sufficient time before the channel "decays". Promotion of the rate, on the other hand, may be due to the formation of a polyionophore (e.g. three monomers of alamethicin and one molecule of antagonist) forming the channel which produce synergistic effects on the rate of transport.

Conclusion

The NMR/Ln^{3+} method has been successfully applied to the study of the mechanism of action of the calcium antagonists. The results indicate the importance of the membrane surface in the activity of these substances and demonstrates clearly the concentration - depend nt effects on the antagonism process.

CHAPTER VI

GENERAL CONCLUSION

CHAPTER VI

General Conclusion

Nuclear magnetic resonance methods using Lanthanide ions as probes have been used in the study of a number of phospholipid vesicular membrane systems. The experimental results obtained and the conclusions reached have shown that the method can be successfully applied to these systems.

The potential of the method has been demonstrated in each of the areas studied so that several developments of the work can be readily envisaged. These would include the use of (a) large unilamellar vesicles to the study of non-bilayer phase effects, and reconstituted functional membrane proteins; (b) multinuclear NMR applied to monitor the diffusion of biologically important cations (e.g. $^{23}Na^{+}$) or the ionophore species itself (e.g. $^{19}F^{-}$ in the study of NaFod); (c) further study of the action of the calcium antagonists on channel mediated transport by ionophores or in reconstituted systems.

MEETINGS:

The following posters were presented at the scientific meetings below:

Poster 1

"NMR studies of non-bilayer phase effects induced by physiological concentrations of negatively charged lipids and calcium ions".

Poster 1 was presented at the Federation of European Biochemical Societies, 14th Meeting, Edinburgh, Scotland, March-April 1981. The abstract was published in "Biochemical Society Transactions, Vol.9, No. 2 (1981) p.p. 281. (see next page).

Poster 2

"^{1}H-NMR of non-bilayer phase effects in phospholipid membranes containing negatively charged lipids". G.R.A. Hunt and Z-E.M. Mirghani.

Poster 2 was presented at the Fifth International Meeting on NMR Spectroscopy. University of Exeter. July 1981.

NMR STUDIES OF NON-BILAYER PHASE EFFECTS INDUCED BY PHYSIOLOGICAL CONCENTRATIONS OF NEGATIVELY CHARGED LIPIDS AND CALCIUM IONS

G.R.A. HUNT and Z-E.M. MIRGHANI.
Department of Science, The Polytechnic of Wales, Pontypridd, CF37 1DL, U.K.

Time-dependent changes are observed in the NMR spectra of phosphatidylcholine (PC) vesicular membranes containing physiological concentrations of cardiolipin (DPG) or phosphatidic acid (PA). Extravesicular 0.15 mM Dy^{3+} is used as a paramagnetic probe ion to monitor vesicle permeability. The changes in spectra indicate that transmembrane transport and fusion in the PC/DPG vesicles are fast and Ca^{++} dependent. The PC/PA vesicles show appreciable transport rates with concentrations of PA as low as 1 mol %, but fusion is negligible and dependence on Ca^{++} much less than for DPG.

The results are consistent with non-bilayer phase mechanisms for these processes at low concentrations of DPG and PA.

APPENDIX 1

^{31}P-NMR studies of oriented multi-layers give specific information concerning the restricted anisotropic motion of phospholipids in bilayer structures. This local motion averages the two dominant sources of line broadening - the 'chemical shift anisotropy' and the dipolar interactions with the protons of the two nearest neighbour methylene groups. The chemical shift anisotropy results from an uneven electron density around the phosphate phosphorus, which produces shielding effects such that the magnetic field experienced by the phosphorus depends on the orientation of the phosphate group with respect to the magnetic field. Thus the chemical shift anisotropy and dipolar interactions have distinctly different effects: the chemical shift anisotropy results in a dependence of the phosphorus chemical shift on the orientation of the phosphate group with the magnetic field, whereas the dipolar interactions determine the linewidth at particular orientations.

Motions may be characterised by a 'correlation time' (τ_c,) where τ_c gives an indication of the time scale during which the motion occurs. For phospholipids, if the (restricted) motion in the phosphate region is fast enough (i.e. $\tau_c \ll 10^{-5}$ s) the chemical shift anistropy is reduced according to the amount of solid angle that the motion extends over, and the chemical shift then depends on the average orientation of the phosphate group with respect to the magnetic field. For spectra of oriented bilayers it is easy to show that the average orientation is along an axis perpendicular to the plane of the bilayer. This result indicates that a primary component of the motion is a rapid rotation of the phosphodiester region about such an axis. Similar results are obtained for all liquid crystalline species of phospholipid. It is likely that this motion

reflects rapid axial rotation of the entire phospholipid molecule about its long axis (as well as more localized motion in the phosphate region) as rotational correlation times of $\tau_R \leq 10^{-7}$s would be expected for lateral diffusion rates of $D_t \geq 10^{-8}cm^2/s$. This would be sufficient to produce the observed effects.

REFERENCES

1. Gomperts, B.D, The Plasma Membrane (Acad.Press,1977).
2. Finean, J. and Michell, R.H, New Comprehensive Biochemistry, Vol.1 (Elsevier, 1981).
3. Singer, S.J, Hospital Practice (1973) 81-96.
4. Chapman, D (ed.), Biological Membranes, Vol.2, 5-64 (Acad. Press, 1968).
5. Sandermann, H. (1978) BBA 515, 209.
6. Chapman, D., Urbina, J. and Keough, K.M.(1974) J. Biol.Chem. 249,2512-2521.
7. Chapman, D. and Salsburg, N.J. (1966) Trans. Farad.Soc. 62,2607.
8. Lee, A.G. (1975) Prog. Biophys.Mol. Biol. 29,3.
9. Gordon, L.M., Sauerheber, R.D. and Esgate, J.A. (1978) J.Supramol.Struct. 9, 299-326.
10. Chapman, D. (1975) Quart.Rev.Biophys.8, 185-235.
11. Cullis, P.R. and DeKruijff (1979) BBA 559, 399-420.
12. Luzzati, V. and Tardieu (1974) Ann. Rev. phys. Chem. 25, 79-94.
13. Luzzati, V., Reiss-Husson, F., Rivas, E. and Gullik-Krzywkki, R. (1966) Ann. N.Y.Acad.Sci. 137, 409-413.
14. Harlos, K. and Eibl, H. (1981) Biochemistry 20, 2888-2892.
15. Tinker, D.O. and Pinteric, L. (1971) Biochemistry 10, 860-865.
16. Saha, J., Papahadjopoulos, D. and Wenner, C.E. (1970) BBA 196, 10-19.
17. DeKruijff, B., Cullis, P.R. and Verkleij, A.J. (1980) Trends. Biol. Sci.5, 79-81.
18. Verkleij, A.J., Van-Echteld, C.J.A., Gerritsen, W.J., Cullis, P.R. and DeKruijff, B. (1980) BBA 600, 620 - 624.
19. Cullis, P.R., DeKruijff, B., Hope, M.J., Nayer, R. and Schmid, S.L. (1980) Can.J. Biochem. 58, 1091-1100.

20. Van Venetie, R. and Verkleij, A.J. (1981) BBA 645, 262-269.

21. Verkleij, A.J., Mombers, C., Gerritson, W.J., Leunissen-Bijvelt, L. and Cullis, P.R. (1979) BBA 555, 358-361.

22. Cullis, P.R. and Mc Laughlin, S. (1977) TIBS, 196-199.

23. Singer, S.J. and Nicolson, G.L. (1972) science 175, 720-731.

24. Racker, E. (1972) J. Biol. Chem. 247, 8198 - 8200.

25. Racker, E. and Eytan, E. (1975) J. Biol. Chem. 250, 7533-7534.

26. Shamoo, A.E. and McLennan, D.H. (1974) PNAS 71, 3522-3526.

27. Gomez-Puyon, A. and Gomez-Lojero, C., Current Topics in Bioenergetics, Vol.C. (Acad. Press, 1977).

28. Hendler, R.W. (1971) 51, 66-96.

29. Harrison, R. and Lunt, G.G., Biological Membranes (Blackie, 1980).

30. Watt, A. (1981) Nature, 294, 512-513.

31. Bittar, E. (ed.) Membrane Structure and Function, Vol.1, (Wiley - Interscience, 1980).

32. Campbell, P.N. and Marshall, R.D. (eds.) Essays in Biochemistry, Vol.16 (Acad. Press, 1980).

33. Szoka, F. and Papahadjopoulos, D. (1980) Ann. Rev. Biophys. Bioeng. 9, 467-508.

34. Neher, E, Sandblom, J. and Eisenman, G. (1978) J.Memb.Biol.40, 97-116.

35. Apell, H.J., Bamberg, E., Alpes, H. and Lauger,P. (1977) J.Memb.Biol. 31, 171-188.

36. Mueller, P., Rudin, D.O., Tein, H.T. and Wescott, W.C. (1967) Recent Progress in Surface Science 1, 379-393.

37. Jain, M.K. The Biomelecular Lipid Membrane (Van Nostrand, 1972).

38. Saunders, L., Perrin, J. and Gammack, D.B. (1962) J. Pharm.pharmacol.14, 567-572.

39. Abramson, M.B., Katzmann, R. and Gregor, H.P. (1964) J.Biol.Chem. 239, 70-76.

40. Papahadjopoulos, D. and Miller, N. (1967) BBA 135, 639-678.

41. Papahadjopoulos, D. and Watikins, J.C. (1967) BBA 135, 639-52.

42. Huang, C.H. and Charlton, J.P. (1971) J. Biol. Chem. 246, 2555-2560.

43. Johnson, S.M., Bangham, A.D., Hill, M.W. and Korn, E.D. (1971) BBA 233, 820-826.

44. Lawaczek, R., Kainosho, M. and Chan, S.I. (1976) BBA 443, 313-330.

45. Barenholz,Y, Gibbs, D., Litman, B.J., Thompson, T.E. and Carlson, F.D. (1977) Biochemistry 16, 2806-2810.

46. Horwitz, A.F., Michaelson, D. and Klein, M.P. (1973) BBA,298,1.

47. Sheetz, M.P. and Chan, S.I. (1972) Biochemistry 11, 4573.

48. Chapman, D., Kamat, V.B., DeGier, J. and Penkett, S.A. (1968) J.Memb. Biol. 31, 101.

49. Hunt, G.R.A. and Tipping, L.R.H. (1978) BBA 507, 242.

50. Hunt, G.R.A. (1980) Chem.phys.Lipids, 27, 353-364.

51. Degani, H. (1978) BBA 509, 364-369.

52. Knowles, R.F., Marsh, D. and Rattle, H.W.E., Magnetic Resonance of Biomolecules (Wiley, 1976).

53. Levine, Y.K., Birdsall, N.J., Lee, A.G. and Metcalfe (1972) Biochemistry 11, 1416.

54. Metcalfe, J.C., Birdsall, N.J., Feeney, J., Lee, A.G., Levine, Y.K. and Partington, P. (1971) Nature 233, 199.

55. Seelig, J., Gally, H. and Wohlgemuth, R. (1977) BBA 467, 109.

56. Oldfield, E., Meadows, M. Rice, D. and Jacobs, R. (1978) Biochemistry 17, 2727.

57. Brown, M.F., Seelig, J. and Haberlen, U. (1979) J.Chem. Phys. 70, 5045.

58. Davis, J.H. (1979) Biophys. J. 27, 339.

59. De Kruijff, B., Verkley, A.J., Van Echteld, C.J.A., Gerristen, W.J., Mombers, C., Noordam, P.C. and DeGier, J. (1979) BBA 555, 200.

60. Sussman, M.V. and Chin, L. (1966) Science 151, 324.

61. Jenkinson, T.J., Kamat, V.B. and Chapman, D. (1969) BBA 183, 427.

62. Keough, K.M., Oldfield, E., Chapman, D. and Peynon, P. (1973) Chem. Phys. Lipids 10, 37.

63. James, T.L., Nuclear Magnetic Resonance in Biochemistry (Acad. Press, 1975).

64. Mayo, B.C. (1973) Chemical Society Reviews 2, 49-74.

65. Hinckley, C.C. (1969) J.Am.Chem.Soc.91, 5160.

66. Lippard (ed.) Current Topics in Bioinorganic Chemistry, Vol.18 (Wiley).

67. Emsley, J.W., Feeney, J. and Sutcliffe, L.H, Progress in Nuclear Magnetic Resonance Spectroscopy, Vol.14, Part 2 (Pergamon, 1980).

68. Bl ney, B. (1972) J. Mag. Reson. 8, 91-100.

69. Emsley, J.W., Feeney, J. and Sutcliffe, L.H., Progress in NMR spectroscopy, Vol.14 (Pergman, 1981) 67-11.

* 80. Maniloff, J., Coleman, I.R., Miller, M.W. (eds.). Effects of Metals on Cells Subcellular Elements and Macromolecules (1970) 235.

81. Carafoli, E. and Semenza, G, Membrane Biochemistry (Springer - Verlag, 1979).

82. Pressman, B.C. (1965) PNAS 53, 1076.

83. Martell, A. E. (ed.) Inorganic Chemistry in Biology and Medicine (1980) 1-23.

84. Pressman, B.C. (1973) Fed. Proc. 32, 1698-1703.

85. Lau, A.L.T. and Chan,S.J. (1975) PNAS 76, 2170.

86. Hunt, G.R.A. and Jones, I.C. (1982) Bioscience Reports (in press).

87. Michell, R.H. (1975) BBA 415, 81-147.

88. Salmon, D.M. and Honeyman, T.W. (1980) Nature 284, 344-345.

89. Thorn, N.A. and Petersen, O.H, Secretory Membranes of Exocrine Gland (Munksagaad, 1974).

90. Lapetina, E.G. and Gatrecasas, P. (1979) 573, 402-573.

* for references 70-79 see end of list

91. Porcellati, G., Amducci, L. and Galli, C, Functions and Metabolism of Phospholipids in CNS and PNS (Plenum, 1976).

92. Putney, J.W., Weiss, S.J., Van De Walle, C.M. and Haddas, R.A. (1980). Nature 284, 345-347.

93. Serhan, C. Anderson, P., Goodman, E., Dunham, P. and Weissman, G. (1981) J. Biol. Chem. 256, 2736-2741.

94. Tyson, C., Vande-Zande, H. and Green, D.E. (1976) J.Biol. Chem. 251, 1326-1332.

95. Verkleij, A.J., Mombers, C., Leunissen - Bijvelt, L. Ververgaert, P.J.J.T. (1979) Nature 279, 162-163.

96. Vail, W.J. and Strollery, J.G. (1979) BBA 551, 74-84.

97. Sen, A., Williams, W.P., Brain, A.P.R., Dickins, M.J. and Quinn, P.J. (1981) Nature 293, 488-490.

98. Miller, R.G. (1980) Nature 287, 166-167.

99. De Kruijff, B., Verkleij, A.J., Van Echteld, C.J.A., Gerritsen, W.J. Mombers, C., Nordam, P.C. and De Gier, J. (1979) BBA 555, 200-209.

100. Ken-Chun-Lin, Weis, R.M. and Mc Connell, H.M. (1982) Nature 296, 164-165.

101. Hui, S.W., Stewart, T.P. (1981) Nature 290, 427-428.

102. Fleischer, S. and Packer, L. (eds.) Methods in Enzymology, Vol. L11., 302-306.

103. Valdimirov, Yu.A., Olenev, V.I., Suslova, T.B. and Cheremisina, Z.P., Advances in Lipid Research, Vol.17 (1980).

104. Valdimirov, Yu.A. and Cheremisina, Z.P. (1975) Studia. Biophys.49, 161.

105. Edwards, J.C. and Quinn, P.J. (1982) BBA 710, 502-505.

106. Gast, K., Zirwer, D., Ladhoff, A.M., Schreiber, J., Koelsch, R., Kretschmer, K. and Lasch, J. (1982) BBA 686, 99-109.

107. Weiss, G.B. Calcium in Drug Action (Plenum Press., 1978).

108. Mullins, L.J, Ion Transport in Heart (Raven Press, 1981).

109. Katz, A.M. and Messineo, F.C. (1981). Am.Heart.J. 102, 491-500.

110. Katz, A.M. and Messineo, F.C. (1981) Am.Heart J. 102, part 32, 491.

111. Biochemical Society Transactions, (June 1980) Vol.8, No. 3.

112. Finean, J.B., Coleman, R. and Michell, R.H, Membranes and Their Cellular Functions (Wiley, 1978).

113. Michell, B. (1982) TIBS 7, 123-124.

114. Fleckenstein, A. (1972) Drug Research 22, 2019.

115. BMJ (Jan 1981) 282, 89-90.

116. Stone, P.H., Elliott, M.A., Jones, E, Muller, J.E. and Eugene, B. Ann.of Internal Medicine 93, 875-885.

117. Fleckenstein, A. (1977) Ann. Rev. Pharmacol. Texicol. 17, 149-166.

118. Church, J. and Zoster, T.T. (1980) Can.J. Physiol. Pharmacol.58, 254.

119. Mas-Oliva. J. and Nayer, W.G. (1980) Br.J. pharmacol.70, 617-624.

120. Malaisse, W.J. (1979) Experiments 35, 1578.

121. Opie, L.H.(1980) Lancet 12, 806-809.

122. Bergelson, L.D. ; Barsukov, L.I. ; Dubrovina, N.I. and Bystrov, V.F. (1970) Dokl.Akad.Nauk.SSSR 194, 708.

123. Bystrov, V.F., Dubrovina, N.I., Barsukov, L.I. and Bergelson, L.D. (1972) FEBS Lett. 25, 337.

124. Papahadjopoulos, D., Poste, G., Schaeffer, B.E. and Vail, W.J. (1974) BBA 352, 10-28.

125. Hauser, H., Phillips, M.C., Levine, B.A. and Williams, R.J.P. (1975) Eur.J.Biochem.58, 133-144.

126. Grasdalen, H., Eriksson, L.E.G., Westman, J. and Ehrenberg, A. (1977) BBA 469, 151-162.

127. Hauser, H., Hinckley, C.C., Krebs, J., Levine, B.A., Phillips, M.C. and Williams, R.J.P. (1977) BBA 468, 364-377.

128. Westman, J. and Eriksson, L.E.G. (1979) BBA 557, 62-78.

129. Mc Laughlin, A., Garistoph, C. and Mc Laughlin, S. (1978) BBA 513, 338-357.

130. Barsukov, L.I., Volkova, V.I., Shapiro, Yu.E., Vikotrov, A.V., Bystrov, V.F. and Bergelson, L.D. (1977) Bioorg. Khim. 3, 1355-1361.

131. Chrzeszczyk, A., Wishnia, A., Springer, C.S. Jr. (1981) BBA 648, 28-48.

132. Cohen, J.A. and Cohen, M. (1981) Biophys. J. 36, 623-651.

133. Hunt, G.R.A. and Tipping, L.R.H. (1980) J. Inorg. Biochem. 12, 17-36.

134. Pike, M.M., Simon, S.R., Balschi, J.A. and Springer, C.S.Jr. (1982) PNAS 79, 810-814.

135. Korn, E.D. (ed.) Methods in Membrane Biology, Vol.2 (Plenum Press).

136. Finer, E.G., Flook, A.G. and Hauser, H. (1972) BBA 260, 59.

137. Berden, J.A., Cullis, P.R., Hoult, D.I. Mc Laughlin,A.C., Radda, G.K. and Richards, R.E. (1974) FEBS lett.46, 55 - 58.

138. Brunell, E.E., Cullis, P.R. and De Kruijff, B. (1980) BBA 603, 63-69.

139. Dwek, R.A., Campbell,I.D., Richards, R.E. and Williams,R.J.P., NMR in Biology (Acad. Press, 1977).

140. Korn, E.D. (ed.) Methods in Membrane Biology, Vol.10 (Plenum Press) 1-121.

141. Mc Laughlin, S.G.A., Szabo, G. and Eisenman, G. (1971) J. Gen. Physiol. 58, 667-687.

142. Barsukov, L.I., Shapiro, Yu.E, Viktrov, V.F. and Bergelson (1976) Bioorg. Khim 2, 1404-1415.

143. Hutton, W.C., Yeagle, P.L. and Martin, R.B. (1977) Chem. Phys. Lipids 9, 255-265.

144. Korn, E.D. (ed.) Methods in Membrane Biology, Vol.9, (Plenum Press).

145. Hauser, H., Phillips, M.C., Levine, B.A. and Williams, R.J.P. (1976) Nature 261, 390-394.

146. Berden, J.A., Baker, R.W. and Radda, G.K. (1975) BBA 375, 186-208.

147. Michaelson, D.M., Horwitz, A.F. and Klein, M.P. (1973) Biochemistry 12, 2673.

148. Barsukov, L.I., Shapiro, Y.E., Viktrotov,A.V., Volkova,V.F., Bystrov, V.F. and Bergelson, L.D. (1974). Biochem. Biophys. Res. Commun. 60, 196.

149. Bystrov, V.F., Dubrovina, N.I., Barsukov, L.J. and Bergelson, L.D. (1971) Chem.Phys.lipids 6, 343.

150. Andrews, S.B., Faller, J.W., Gillian, J.M. and Barnett, R.J. PNAS 70, 1814.

151. Michaelson, D.M., Horwitz, A.F. and Klein, M.P. (1974) Biochemistry 13, 2605.

152. Kostelnik, R.J. and Castellano, S.M. (1973) J.Mag.Res.9, 291.

153. Hauser, H. and Barnett, M.D. (1973) Biochem. Biophys. Res. Commun. 53, 399.

154. Hunt, G.R.A. (1975) FEBS lett. 58, 194-196.

155. Sears, B., Hutton, W.C. and Thompson, T.E. (1976) Biochemistry 15, 1635.

156. Shapiro, Y.E., Viktrotov, A.V., Voikova, V.I., Barsokov,L.I., Bystrov, V.F. and Bergelson, L.S. (1975) Chem.Phys.lipids 14, 227.

157. Yeagle, P.L. Hutton, W.C., Martin, R.B., Sears, B. and Huang.C. (1976) J. Biol. Chem. 251, 2110.

158. De Kruijff, B., Cullis, P.R. and Radda, G.K. (1975) 275, 6.

159. Huang, C., Sipe, J.S., Chow, S.T. and Martin, R.B. (1974) PNAS 71, 359.

160. Koch-Light Catalogue. Koch-Light Lab. Limited, England, 1973.

161. Mimms, L.T., Zampighi, G., Nozaki, Y., Tanford, C. and Reynolds, J.A. (1981) Biochemistry 20, 833-840.

162. Ting, D.Z., Hagan, P.S., Chan, S.I., Doll, J.D. and Springer, C.S. (1981) Biophys.J.34, 189-216.

163. Hokin, L.E. (1981) J.Memb. Biol.60, 77-93.

164. Pressman, B.C. (1968) Fed.Proc. 27, 1283-1288.

165. Gomparts, B.D, Bennett, J.P. and Allan, D. (1981) 117, 559-562.

166. Hunt, G.R.A., Tipping, L.R.H. and Belmont, M.R. (1978) Biophys. Chem.8, 341-355.

167. Krasne, S., Eisenman, G. and Szabo, G. (1971) Science 174, 412-415.

168. Martin, D.R. and Williams, R.J.P. (1976) Biochem.J.153, 181-190.

169. Chen, S.T. (1978) Ph.D. Dissertation State University of New York, Stony Brook. N.Y.

170. Degani, H., Simon, S. and Mc Laughlin, A. (1981) BBA 646, 320-328.

171. Kunimoto, M., Inoue, K. and Nojima, S. (1981) BBA 646, 169-178.

172. Bennett, J.P., Cockcroft, S. and Gomperts, B.D. (1979) Nature 282, 851-853.

173. Massini, P. and Naf, U. (1980) BBA 598, 575-587.

174. Shaw, D, Fourier Transform N.M.R. Spectroscopy (Elsevier,1979).

175. Wulf, J. and Pohl, W.C. (1977) BBA 465, 471.

176. Bangham, J.A. and Lea, E.J.A. (1978) BBA 511, 388.

177. Barrow, G.M., Physical Chemistry, Third Edition (Mc Graw-Hill Limited 1973).

178. Donis, J., Grandjean, J., Grosjean, A. and Laszlo, P. (1981). Biochem. Biophys. Res. Commun. 102, 690-696.

179. Papahadjopoulos, D., Vail, W.J., Pangborn, W.A. and Poste,G. (1976) BBA 448, 265-283.

180. Fiskum, G. and Lehninger, A.L. (1979) J. Biol.Chem. 254, 6236-6239.

181. Nicholls, D. (1981) TIBS, 36-81.

182. Mitchell, P. (1961) Nature 191, 144 148.

183. Mitchell, P, (1968) Chemiosmotic Coupling and Energy Transduction, Glynn Research Bodmin.

184. Niggli, V., Sigel, E. and Carafoli, E. (1982) J. Biol.Chem. 257, 2350-2356.

185. Waisman, D.M., Gimble, J.M., Goodman, D.B.P. and Rasmussen, H. (1981) J.Biol.Chem. 256, 415-419.

186. Waisman, D.M., Gimble, J.M., Goodman, D.B.P. and Rasmussen, H. (1981) 256, 420-424.

187. De Kruijff, B. and Baken, P. (1978) 507, 38-47.

188. Cullis, P.R. and De Kruijff, B. (1978) BBA 507, 207-218.

189. Cullis, P.R., Verkleij, A.J. and Ververgaert, P.H.J.Th. (1978) BBA 513, 11-20.

190. Cullis, P.R. and De Kruijff, B. (1978) BBA 513, 31-42.

191. Tilcock, C.P.S. and Cullis, P.R. (1981) BBA 641, 189-201.

192. Sen, A., Williams, W.P., Brain, A.P.R. and Quinn (1982) BBA 685, 297-306.

193. Feguson, K.A., Hui, S.W., Stewart, T.P. and Yeagle, P.L. (1982) BBA 684, 179-186.

194. Barclay, L.R.C. and Ingold, K.U. (1980) J.Am.Chem.Soc. 102, 7792-7794.

195. Smolen, J.E. and Shohet, S.B. (1974) J. of Lipid Research 15, 273-280.

196. Dobrestov, G.E., Borshevskaya, V.A., Petrov, V.A. and Vladimirov, Y.A (1977) FEBS lett. 84,125.

197. Hunter, F.E., Gebkki, J.M., Hoffslen, P.E., Weinstein, J. and Scott, A. (1963) J.Biol.Chem.238,828.

198. Shaw, J.M. and Thompson, T.E. (1982) Biochemistry 21, 920-927.

199. Russell, N.J.(1977) Biochem.Soc.Trans. 5, 1492-1494.

200. Klein, R.A. (1970) BBA 210, 486-489.

201. Barsukov, L.I., Victrov, A.V., Vasilenko, I.A., Evstigneeva, R.P. and Bergelson, L.D.(1980) BBA 598, 153-168.

202. De Kruijff, B., Rietveld, A. and Van Echteld, C.J.A. (1980) BBA 600, 597-606.

203. Hunt, G.R.A. and Tipping, L.R.H. (1978) BBA 507, 242-261.

204. Arnold, K., Losche, A. and Gawrisch, K. (1981) BBA 645, 143-148.

205. Tilcook, C.P.S. and Cullis, P.R. (1982) BBA 684, 212-218.

206. Green, D.E., Fry, M. and Blondin, G.A. (1980) PNAS 77, 257-261.

207. Gerritsen, W.J., De Kruijff, B., Verkleij, A.J., De Geir, J. and Van Deenen, L.L.M. (1980) BBA 598, 554-560.

208. Mandersloot, J.G., Gerritsen, W.J., Leunissen Bijvelt, J., Van Etchelds, C.J.A., Noordam, P.C. and De Geir, J. (1981) BBA 640, 106-113.

209. Cullis, P.R., Van Dijck, P.W.M., De Kruijff, B. and De Geir, J. (1978) BBA 513, 21-30.

210. Cullis, P.R. and Verkleij, A.J. (1979) BBA 552, 546-551.

211. Litman, B.J. (1973) Biochemistry 12, 2545-2554.

212. Massari, S., Pascolini, D. and Gradenigo, G. (1978) Biochemistry 17, 4465-4469.

213. Bishop, C. and Surgenor, D.M. (eds.) The Red Blood Cell (Acad.Press, 1964).

214. Cullis, P.R. and De Kruijff, B. (1976) BBA 436, 523-540.

215. Verkleij, A.J. and De Kruijff, B. (1981) Nature 290, 427-428.

216. Lutz, H.A., Shih-Chun, L. and Palek, J. (1977) J. Cell Biol. 72, 548-560.

217. Zwaal, R.F.A., Roelofson, B. and Colley, C.M. (1973) BBA 300, 159-170.

218. Sheetz, M.P. and Singer, S.J. (1977) J. Cell. Biol. 73, 638-646.

219. Russell, N.J. (1978) BBA 513, 179-186.

220. Farren, S.B. and Cullis, P.R. (1980) Biochem. Biophys. Res. Commun. 97, 182-191.

221. Cullis, P.R. and Hope, M.J. (1980) BBA 597, 533-542.

222. Noordam, P.C., Van Etcheld, C.J.A. De Kruijff, B, Verkleij, A.J. and De Geir, J. (1980) Chem.Phys.lipids 27, 221,232.

223. Rand, R.P. and Sengupta, S. (1972) BBA 255, 484-492.

224. Hui, S.W., Stewart, T.P., Yeagle, P.L. and Albert, A.D. (1981) Arch. BioChem. Biophys. 207, 227-240.

225. Lindblom, G., Larsson, K., Johansson, L.B.A., Fontell, K. and Forsen, S. (1979) J.Am.Chem.Soc., 101, 5465.

226. Luzzati, V. and Spegt, P.A. (1967) Nature 215, 701.

227. Fontell, K. (1978) Prog.Chem.Fats and other lipids 16, 145.

228. Wieslander, A., Rilfors, L., Johnsson, L.B.A. and Lindblom,G. (1981) Biochemistry 20, 730-735.

229. Dahle, L.K. Hill, E.G. and Holman, R.T. (1962) Arch. Biochem. Biophys. 98, 253-261.

230. De Gier, J., Mandersloot, G. and Van Deenen, L.L.M. (1968) BBA 150, 666-675.

231. Dang, Q.Q., Dedieu, J.C. and Blazy, B. (1980) BBA 597, 464-476.

232. Korn, E.D. (ed) Methods in Membrane Biology, Vol.1 (Plenum Press, 1974).

233. Information Sheet received from the Knoll Research Institute, Ludwigshafen/Rhein (F.R. Germany).

234. Guazzi, M, Fiorentini, C., Olivari, M., Bartorelli, A., Necchi, G. and Polese, A. (1980) Circulation 61, 913-919.

235. Zoster, T.T. (1980) Am. Heart J. 99, 805-810.

236. Blaustein, M.P., Ratzlaff, R.W. and Chweitzer, E.S. (1980) Fed.Proc.39, 2790-2795.

237. Lazzara, R., Scherlag, B. (1980) Ann.of Internal Medicine 39, 919-921.

238. Elliott, M.A., Peter, H.S., Muller, J.E., Braunwald, E. (1980). Ann. of Internal Medicine 93, 875-885.

239. Malaisse, W.J., Davis, G. and Somers, G. (1977) Experimenta 33, 1035-1036.

240. JEOL News (1982) 18A, 3(23)-5(25).

241. Puskin, J.S., Vistnes, A.I. and Coene, M.T. (1981) Arch. Biochem. Biophys. 206, 164-172.

242. Peters, D.G., Hayes, J.M. and Hieftje, G.M. Chemical Separation and Measurement (Saunders, 1974).

243. Pfeiffer, D.R., Reed, P.W. and Lardy, H.A. (1974) Biochemistry 13, 4007-4014.

244. Middleton, E., Drzewiecki, G. and Triggle, D. (1981) Biochem.pharmacol.30, 2867-2869.

245. Putney, J.W. (1978) Pharmac.Rev.30, 209.

246. Foreman, J.C., Mongar, J.L. and Gomperts, B.D. (1973) Nature 245, 249.

247. Grandjean, J. and Laszlo, P. (1982) Biochem. Biophys.Res. Commun. 104, 1293-1297.

248. Burgemeister, W. and Winkler-Oswatisch, R. (1977) Top.Curr. Chem. 69, 93-196.

249. Huang, S.B. and Shen,T.Y. (1981) J.Med. Chem. 24, 1202-1211.

70. Dos Remedios, C.G. (1981) Cell Calcium 2, 29-51.

71. Chapman, D. and Wallach, D.F.H. (eds.) Lanthanides as Calcium Probes in Biomembranes, Vol.3 (Acad. Press, 1976).

72. Williams, R.S.P. (1970) Quarterly Reviews 24, 331-365.

73. Long, C. and Mount, B. (1971) Biochemistry 123, 829.

74. Takata, M., Pickard, W.R., Lettvin, J.Y. and Moore, J.W. (1966) J. Gen. Physiol, 50, 461-471.

75. Blanstein, M.P. and Goldman, D.E. (1968) J. Gen. Physiol. 51, 279.

76. Hagiwara, S. and Takahashi, K. (1967) J. Gen. Physiol. 50, 583-601

77. Weis, G.B. and Goodman, F.R. (1969) J. Pharm. Exp. Ther. 169, 46.

78. Hodgson, B.J., Kidwai, A.M. and Daniel, E.E. (1972) Can. J. Physiol. Pharm. 50, 730.

79. Mela, L. (1969) Biochemistry 8, 2481.